PREDICTION OF OPERATIONAL ENVELOPE

MANEUVERABILITY EFFECTS ON ROTORCRAFT DESIGN

A Thesis
Presented to
The Academic Faculty

by

Kevin Lee Johnson

In Partial Fulfillment
of the Requirements for the Degree
Doctor of Philosophy in the
School of Aerospace Engineering

Georgia Institute of Technology
May 2013

PREDICTION OF OPERATIONAL ENVELOPE

MANEUVERABILITY EFFECTS ON ROTORCRAFT DESIGN

Approved by:

Prof. Dimitri Mavris, Advisor
School of Aerospace Engineering
Georgia Institute of Technology

Prof. Vitali Volovoi
School of Aerospace Engineering
Georgia Institute of Technology

Prof. Mark Costello
School of Aerospace Engineering
Georgia Institute of Technology

Prof. George Vachtsevanos
School of Electrical and Computer Engineering
Georgia Institute of Technology

Prof. Daniel Schrage
School of Aerospace Engineering
Georgia Institute of Technology

Date Approved: 4 March 2013

ACKNOWLEDGEMENTS

There are multiple people who I owe gratitude due to their support during my PhD work at Georgia Institute of Technology. First and foremost, I wish to thank my advisor, Prof. Dimitri Mavris for his guidance and support throughout my graduate studies. This effort would not be what it is today without his unique ability to provide both critical thought-provoking questions and encouragement simultaneously. I would also like to extend my thanks to my Ph.D. committee: Prof. Mark Costello, Prof. Daniel Schrage, Prof. George Vachtsevanos, and Prof. Vitali Volovoi. I thank them for the encouragement and technical expertise that enabled this dissertation to come to fruition. Their guidance through the Ph.D. process has been invaluable in helping me learn how to conduct research and approach real-world engineering problems.

I would also like to thank my fellow aerospace graduate students, particularly Bryan Boling, Kemp Kernstine, Katlyn Sullivan, and Grant Whittington. Your support in reviewing slides, discussing important problem areas, and editing the document has been important to the successful completion of the program. Support from my family over the years has been instrumental and for your aid I am indebted. Finally, I would like to thank anyone that I have missed.

TABLE OF CONTENTS

LIST OF TABLES

Page

LIST OF FIGURES

Page

LIST OF SYMBOLS, ABBREVIATIONS, AND ACRONYMS

Accel	Acceleration
ADS	Aeronautical Design Standard
AHS	American Helicopter Society
Alt	Altitude
C	Main Rotor Blade Chord
CBA	Constrained Bifurcation Analysis
CG	Center of Gravity
DCFC	Design Constraining Flight Condition
EoM	Equations of Motion
FMC	Filtered Monte Carlo
IA	Interval Analysis
LSQ	Least Squares
MA	Maneuver Automation
Mass	Vehicle Weight
MC	Monte Carlo
NM	Nelder-Mead
NOE	Nap-of-the-Earth
ODE	Ordinary Differential Equations
RK4	4^{th} Order Runge-Kutta
RFP	Request for Proposal
ST	Horizontal Tail Area
T0	Main Rotor Collective Angle
T0D	Main Rotor Collective Rate
Tlat	Lateral Cyclic Angle
TlatD	Lateral Cyclic Rate
Tlong	Longitudinal Cyclic Angle
TlongD	Longitudinal Cyclic Rate

Tt	Tail Rotor Collective Angle
TtD	Tail Rotor Collective Rate
TFN	Triangular Fuzzy Numbers
TPP	Tip-Path Plane
TrFN	Trapezoidal Fuzzy Numbers
TRSTA	Tail Rotor Moment Arm
Vel	Velocity
A	Rotor Disk Area
A1	Longitudinal Flapping Angle
B1	Lateral Flapping Angle
$\bar{C}$	Characteristic Length
C_{df}	Drag Coefficient for Reference Area
C_{d0}	Profile Drag Coefficient
CL	Lift Coefficient
CT	Thrust Coefficient
CTT	Tail Thrust Coefficient
DMR	Diameter of Main Rotor
F	Force
K_β	Coupling Coefficient
M	Moment
P	Roll Rate
P	Power
PI	Induced Power
PP	Profile Power
PPAR	Parasitic Power
Q	Pitch Rate
Q	Dynamic Pressure
R	Yaw Rate
R	Rotor Radius
R/C	Rate of Climb

S_{ref}	Drag Reference Area
T	Thrust
tf	Final Time
U	Resultant Velocity a Discrete Element
$V\infty$	Freestream Velocity
VT	Rotor Tip Velocity
W	Weight
a_{0inc}	Zero Lift Curve Slope
β_0	Coning Angle
γ	Lock Number
ε	Efficiency Coefficient
Θ	Pitch Angle
Θ_0	Main Rotor Collective
Θ_1	Lateral Cyclic
Θ_2	Longitudinal Cyclic
Θ_t	Tail Rotor Collective
κ	Empirical Correction
λ	Tip-Path Plane Inflow Ratio
μ	Inflow Velocity
ρ	Air Density
σ	Rotor Solidity
τ	Blade Mass Centrifugal Force Ratio
νi	Induced Velocity
Ø	Roll Angle
Ψ	Heading Angle
Ω	Rotor Rotational Speed

SUMMARY

If the implications of requirements and constraints are not adequately captured in the early stages of design, the result is often expensive and timely engineering changes. Traditionally, the early stages of design have focused on static performance analyses without considering the design impacts on dynamic maneuvers; however, typical military helicopter operation requires precise maneuverability performance for successful mission completion. Therefore, the focus of this work is to address the issues with integrating maneuverability analysis into a conceptual design process. The problem in this effort is decomposed into three major areas within this work: designing for maximum maneuverability, capturing controllability concerns, and defining the mission maneuvers.

In order to capture the impact of design variations on maneuverability, a model formulation that includes the necessary measures and captures the impact of changing requirements real-time is required. In order to overcome these challenges, the integration of a parametric helicopter model into a dynamic simulation environment is presented. The parametric rigid body formulation is shown to offer a more conservative estimate of maneuverability than traditional energy-based formulations through quantitative analysis of a typical pop-up maneuver. The maneuverability limits are captured in multiple dimensions such that the variability in design parameter values can be directly traced to maneuver performance attributes. Additionally, the dynamic motion is simulated independent of the control system due to human-interaction and dimensionality constraints associated with conceptual design.

Although the control system design is not directly integrated into the conceptual design process, it is important to capture control constraint and requirement information as early as possible. Without this knowledge, infeasible dynamic maneuvers are deemed feasible. Hence, control related measures are required to relate the control system design constraints to the vehicle maneuver limits. These measures must account for a multitude of control design decisions, while remaining at the appropriate level of detail for conceptual design. Two measures are integrated in this work, which include control deflection rate and trajectory divergence rate. Both of these measures are general enough to be applied to any control architecture, while at the same time provide quantitative measures that relate overall vehicle maneuverability to control system requirements. It is demonstrated that the control constraints offer a more conservative and robust solution due to the elimination of infeasible designs.

These maneuverability trades must be conducted for the entire helicopter flight envelope, which is unaffordable at the conceptual stage. As a result, a maneuver taxonomy is developed such that the immense maneuver space can be expressed through a subset of maneuvers. However, the complexity of the maneuver mathematical formulation presents difficulties when integrating into a design framework. Therefore, the mathematical formulation is modified to reduce the number of variables required. The combination of the maneuver model and the taxonomy allow for the performance of individual maneuvers to be analyzed such that the impact of design constraints or changes in the maneuver definition can be fully explored real-time.

Addressing the three major needs yielded a methodology termed GT-RISE, which stands for Georgia Tech Rotorcraft Inverse Simulation Environment. The methodology enables the impact of design choices on maneuverability to be assessed for the entire helicopter flight envelope, while enabling constraints from control system design to be assessed real-time. A canonical example from helicopter literature that emphasizes the need to perform Nap-of-the-Earth flight analyses and conceptual design simultaneously is analyzed using the GT-RISE methodology. The process is shown to provide the systematic and traceable real-time analysis trades required to elevate knowledge in the conceptual design stages through quantitative maneuverability analysis, which mitigates cost, risk, and uncertainty.

CHAPTER 1

INTRODUCTION AND PROBLEM FORMULATION

The majority of the product cost is committed by the end of the conceptual design phase [1-3]. As a result, a greater focus on conceptual design is essential in meeting the new and specialized requirements of the customer. Traditionally, the early stages of helicopter design have focused on static performance analyses, such as excess power techniques, without considering the impacts of maneuvering flight [4]. This approach has been implemented mainly due to the combinatorial limitations posed by design and the incomplete knowledge of constraints and requirements [3, 5]. However, military helicopter operations require precise maneuverability characteristics for successful Nap-of-the-Earth (NOE) flight maneuvers. NOE flight consists of precise maneuvering in and around obstacles, which the helicopter uses for cover, thus, enabling completion of missions unique to helicopter platforms. Many military helicopter NOE flight scenarios and problems are classified; therefore, a literature search was performed to find an unclassified canonical example that could be used as a surrogate for formulating the problem. The classified problems are indirectly assessed through determining the necessary requirements and solving the unclassified example.

Figure 1.1: AHS Design Competition 2012

Sikorsky [6] has recently introduced the 2012 American Helicopter Society (AHS) design competition that forces the designer to consider effects on maneuverability characteristics resulting from design decisions. The top-view of the mission is shown in Figure 1.1. The importance of capturing the impacts on performance, cost, and safety using maneuverability analyses has been discussed since the 1970s [7]. However, due to the combinatorial problems of integrating maneuverability analyses with design, this integration has not been completed. As a result, flight dynamics and control implications are not considered until the preliminary design stages, which often results in costly design modifications later in the design process [8, 9]. Maneuverability analyses provide many valuable insights into the helicopter NOE operational envelope [8, 10], which directly impacts important design decisions [11] related to maneuverability, agility, and control.

This information is of great interest, which is demonstrated by recent focus on multi-role type design efforts such as the Joint Multi-role Rotorcraft [12]. In order to incorporate maneuverability analysis capabilities into the helicopter design framework, a thorough literature review must be conducted to uncover all of the hurdles that must be addressed.

The AHS design problem is an unclassified example of NOE flight operations that must be addressed by the helicopter design community. In order to provide the most traceability and understanding, the problem is decomposed into three major areas: designing for maximum maneuverability, capturing controllability concerns, and defining the mission maneuvers. This decomposition is represented in Figure 1.2. These three research areas relate directly to NOE flight requirements. The first area, which is designing for maximum maneuverability, is important for both military NOE operations and the AHS design competition because the design that can outperform the other helicopter designs will win in NOE combat scenarios. The 'maximum maneuverability' is defined by the minimum mission time although other measures, such as blade loading, could be considered simultaneously. The second research area specifies the need to capture the controllability concerns. This requirement is stated because during NOE flight operations a precise maneuver path must be followed. Any divergence from the path can be catastrophic because the helicopter is flying in and around obstacles. Similarly, the AHS design competition requires the helicopter to follow a specific mission path, while considering the implications of traveling into a pylon or the spectators. The third research area deals with the mission maneuver specifications since there are an immense number of NOE flight operations that must be analyzed. Additionally, the maneuver

specifications are dynamic in nature and cannot be analyzed with only steady-state analysis techniques. These problem areas require a shift in design and maneuver analysis capabilities [13-15], which are discussed in more detail in the following sections. The objective is to determine all of the requirements that must be addressed to enable successful design for helicopter NOE flight.

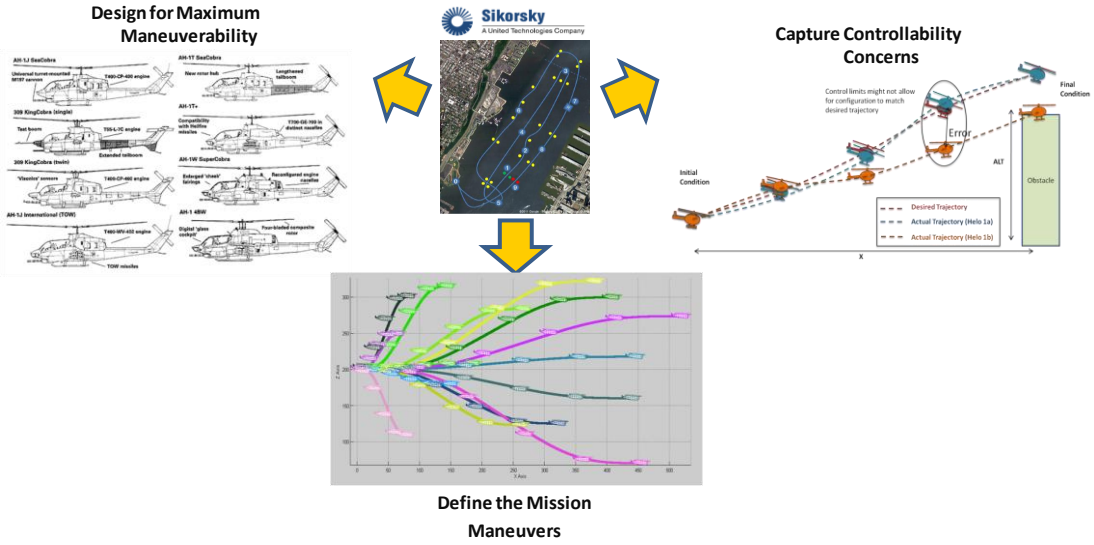

Figure 1.2: Decomposition of the Problem

1.1 Designing for Maximum Maneuverability

As previously mentioned, the first category of the decomposition is designing for maximum maneuverability, which consists of determining design parameters that produce minimum maneuver time. Historically, design methods have employed the use of static based analyses to make important design decisions regarding performance; however, the 2012 AHS design competition requires simultaneous design and analysis of dynamic NOE maneuvers. A summary of the literature review is presented in this section

to aid in defining the needs of the problem. A more complete literature review is presented in Chapter 2 when the remaining questions are addressed.

The objective of the design process is to make important design decisions such that the minimum time mission is achieved. This goal is consistent for both the 2012 AHS design competition and typical military helicopter NOE flight procedures. In order to accomplish this task, the method employed must determine the impact on maneuverability due to the design variations for dynamic operations. This requires appropriate model formulation to capture the necessary measures and apply the required constraints. Additionally, the capability to capture variability in the design parameters independent of controller design is essential. Finally, the manner in which the maneuverability information is collected and presented must be systematic, traceable, and real-time to allow for the greatest amount of knowledge to be gained. These requirements for design for maximum maneuverability are discussed in the following sections.

A notional example of capturing the required performance constraints for dynamic operation is demonstrated in Figure 1.3 where the time histories are shown for both main rotor collective and power required when performing a 10.6 second pop-up maneuver. The yellow constraints represent the design requirements on the system. The bottom portion of the figure shows the power required during the maneuver, which is obtained using an energy-based design approach. The top portion of the figure displays the main rotor collective time history with the maximum control deflection constraint imposed. This kinematic constraint represents one of the many constraints that can be implemented with the rigid body formulation. If only the energy-based formulation is

applied, the main rotor collective constraint could not be imposed or analyzed. As a result, infeasible solutions may be missed and selected as the optimum design, which will not be uncovered until later stages when the rigid body formulation is applied. Avanzini [16] notes that, "mechanical limitations of control travel or control rates" are just a few of the constraints that lead to poor predictions using the energy-based formulation alone.

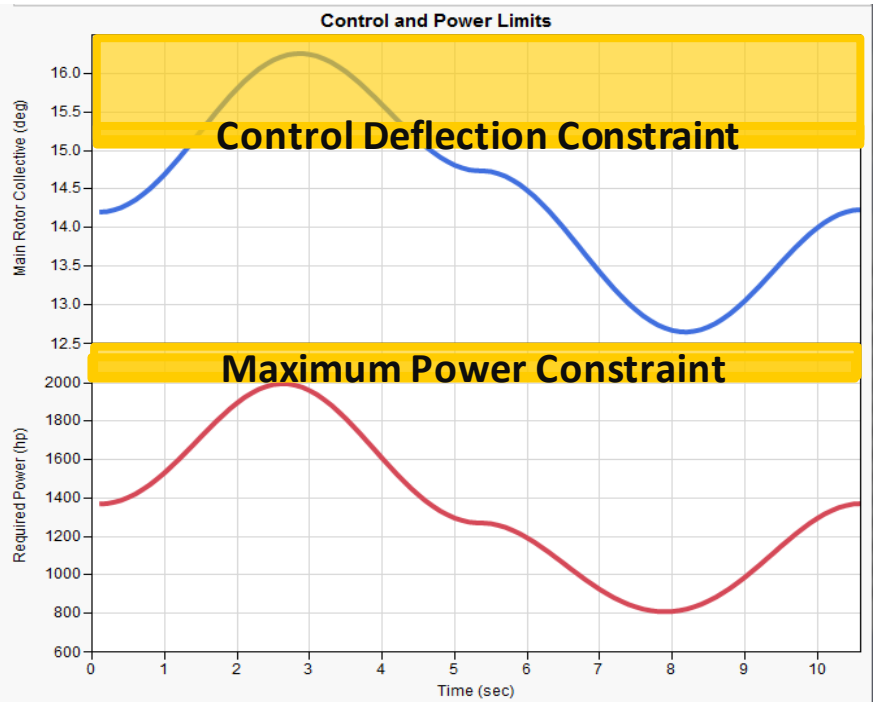

Figure 1.3: Model Fidelity Related Constraints

Additionally, various assumptions can be applied when forming the rigid body helicopter model and the previous example only represents a notional case. Hence, a more thorough down selection from the various fidelity approaches in literature must be completed. This investigation is presented in Chapter 2 of this thesis; the findings are summarized here in order to provide a clear scope for the present work. Avanzini [17]

analyzed 13 various fidelity rigid body models and the results are summarized in Figure 1.4.

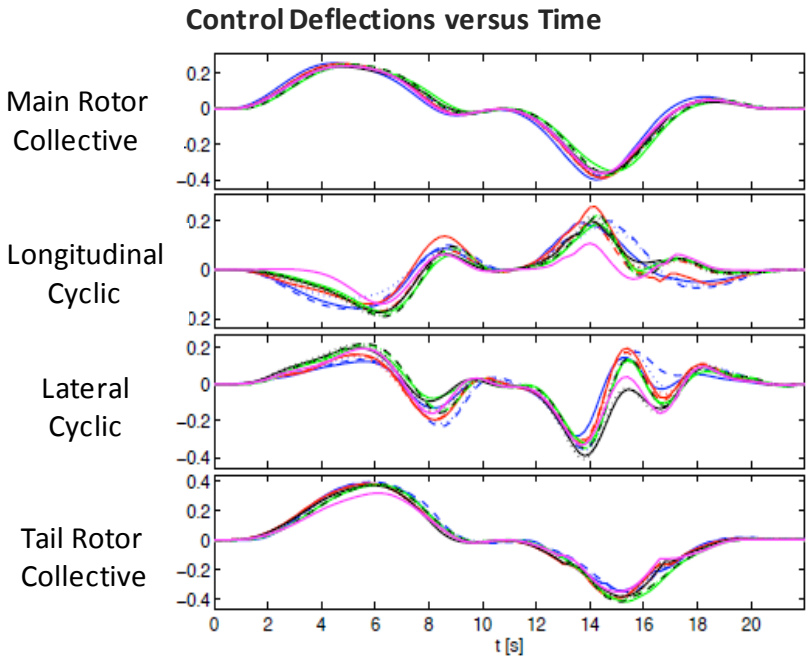

Figure 1.4: Various Fidelity Rigid Body Formulations

The results demonstrate that the most simple rigid body formulation, which is shown as the blue dashed line, closely approximates the control time histories of higher fidelity formulations when performing a smooth maneuver. Design space exploration is the major focus in the early design stages, which means that many different designs must be investigated. The computational time increase for the small increase in accuracy obtained from the higher fidelity rigid body formulation is not beneficial in the early stages of design; hence, a simple rigid body helicopter model is sufficient. Additionally, the information that is required to populate the parameters of the higher fidelity models is unknown in this stage. Often times, even if the information is available, the combinatorial

nature of the problem prevents adequate sampling of the space due to computational limits. The simplifying assumptions and the resulting limitations of the simple rigid body model are discussed during mathematical model development.

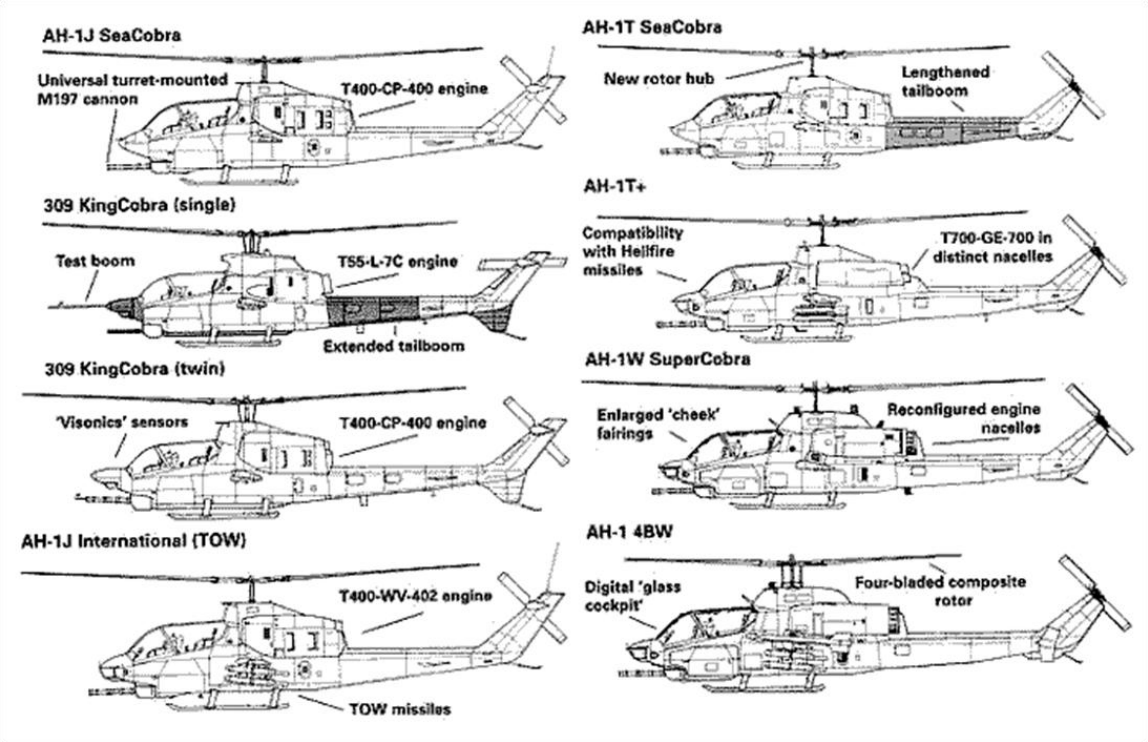

Figure 1.5: AH-1 SeaCobra Variants

The second attribute of the problem to take into account when designing for maximum maneuverability is the impact of design parameter variations on maneuverability characteristics. For this exercise, assume that the AH-1 SeaCobra is selected as the appropriate starting point for design since commonly design starts from a previous design exercise [3]. It turns out that multiple variants of the AH-1 exist that alter the weight, center of gravity, tailboom length, and engine properties as displayed in Figure 1.5 [18]. The implications of these various alterations must be quantitatively

captured, in addition to other parameters, in a systematic and traceable manner. Additionally, much benefit is gained if these trades can be conducted in a real-time parametric sense, rather than sequential one point at a time trade studies. Both of these characteristics enable faster iterations and more transparent results, which result in a decrease in time, risk, and overall cost.

The final requirement for addressing design for maximum maneuverability is the presentation of maneuverability information. In order for the most knowledge to be gained during trade studies, the data must be analyzed systematically and real-time. Additionally, the data must include the quantitative time history data to enable determination of the sources for constraint violation. Some previous studies have summarized the maneuverability results in tabular form with little information provided from the time history analyses [19, 20]. However, Celi [21] shows that the entire maneuverability time histories can be used to analyze the impact from the various constraints and requirements through analysis of a fixed design for a slalom maneuver. This becomes even more important for analyzing maneuverability during design because the maneuver performance for each configuration is going to be dictated by different constraints. Hence, the ability to filter down through the results to determine the constraints that are impacting the maneuverability limits is necessary. The differences in displaying the time history information versus only summarizing the data is demonstrated in Figure 1.6, where the top portion of the figure is the time history and the bottom portion is only summarizes the characteristics of the maneuver.

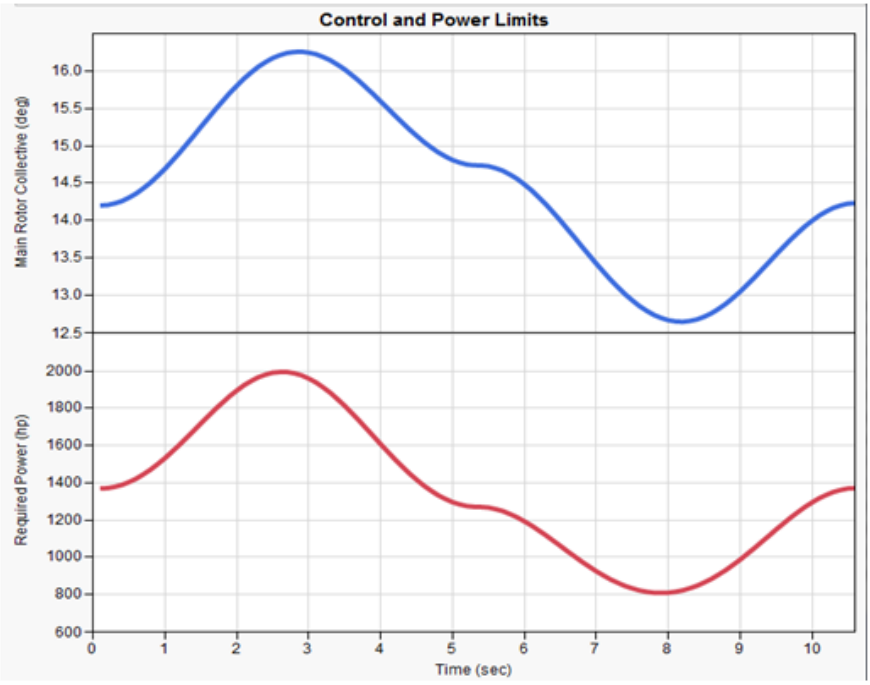

Performance Parameter	Value
Time	10.6 sec
Maximum Main Rotor Colllective	16.25 deg
Maximum Power Required	2000 hp

Figure 1.6: Performance Summary versus Time Histories

Determining the appropriate techniques necessary to form a method that can address all of the needs simultaneously requires careful analysis of literature. It is shown in Chapter 2 that no single reference addresses all of the necessary attributes of the 2012 AHS design problem. As a result, the first research objective of this work is established. It must be kept in mind that only the requirements related to designing for maximum maneuverability have been introduced. The remaining two areas of the problem, which include capturing controllability concerns and defining the mission maneuvers are introduced separately. The final objective of this work is determining a methodology that

addresses all of the requirements of the problem simultaneously. The requirements associated with designing for maximum maneuverability, which have been discussed in this section, are summarized in the following bulleted list and are used later in this work to develop an overall research objective and form research questions.

Designing for Maximum Maneuverability Requirements

- Capture the maneuverability for dynamic NOE operations
- Measure the maneuverability independent of control design
- Include quantitative impact of appropriate fidelity constraints
- Capture the effect from variability in multiple design parameters
- Provide traceable and real-time design tradeoff capabilities

1.2 Capturing Controllability Concerns

The second component of the decomposition is capturing controllability concerns that stem from control design and integration decisions. Control system design decisions, both hardware and software, have a major impact on maneuverability of the system. Chipperfield [22] states, "these include, but are not limited to, the type and location of sensor and actuator devices, the sensed parameters used to close control loops, the form of control to be employed and the size of design margins for stability, robustness, and degradation." All of these decisions have a major impact on the integration of the controller into the system, which can substantially degrade the performance capabilities from that of the ideally controlled system.

It is important to capture this information as early in the design as possible; however, difficulties arise because of the quantity and quality of data required for these types of trades. For example, the moment that a control architecture is chosen for the

system, a large number of controller specific tuning parameters are introduced. The curse of dimensionality arises as the parameters are added to the design process. Furthermore, two or more different control architectures may need to be compared quantitatively to choose the correct scheme. As a result, there must be a tradeoff in the amount of control information in the design process and the capability to make quantitative trades that aid in controller development.

The importance of capturing the performance degradation due to these control selection decisions is presented in the notional example in Figure 1.7. As stated previously, the performance measure is minimum time to complete the mission. The horizontal axis in Figure 1.7 displays four different maneuvers. This number varies depending on the number of maneuvers within the mission definition. The figure demonstrates the impact on maneuver capabilities from fixing the control decisions early in the design process. The blue curve in the figure represents the helicopter design parameters resulting in the maximum maneuverability. This design is integrated with a perfect controller such that the maneuverability is dictated by the design parameters rather than the controller. Since a perfect controller is implemented the maximum theoretical maneuverability is achieved. The other two curves represent the performance degradation from integrating a non-perfect controller with the same helicopter design. The orange curve represents a notional nonlinear controller, while the green curve displays a notional linear controller with fixed gains. The main point of this figure is to show that some degradation in performance occurs during integration of any non-perfect controller.

With the wider availability of sensor and actuator components, and more engine parameters becoming measurable and controllable, more detailed models are necessary to include all of these control parameters into the maneuverability analyses, which pose problems for conceptual design due to the combinatorial nature. Chipperfield [22] states that "the task of selecting a suitable control configuration is thus further complicated by the number of possible, but perhaps undesirable, configurations." Hence, the curse of dimensionality prevents inclusion of all the various architectures and trades in the early stages of design.

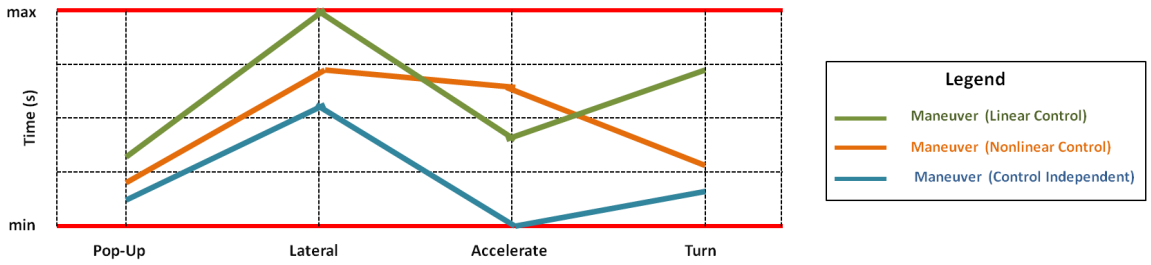

Figure 1.7: Notional Example of Control Integration

The previous example demonstrates that the vehicle maneuverability must be evaluated separate from the maneuverability of the control integrated system; however, the quantitative degradation in maneuverability due to control decisions cannot be ignored. This hurdle is addressed by reviewing the control integration and design process, which is displayed in Figure 1.8. The control integrated maneuverability process begins with control system design, which involves detailed control decisions regarding processing, actuator, and sensor types/locations. These decisions cannot be made during the conceptual design process because the detailed nature of such decisions. The second step of the process is the characterization of the control system. This involves developing

an understanding of how the various control system design decisions propagate to the overall controller characteristics. These characteristics can vary greatly depending on the stage of the design and the amount of information available. Finally, these characteristics directly impact the control integrated system maneuverability.

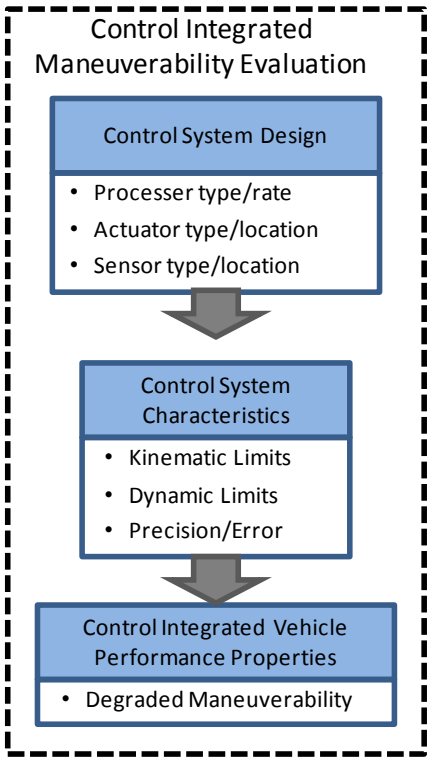

Figure 1.8: Control Integrated Maneuverability Evaluation Process

Commonly, the control system design problem consists of the specification of a plant and a few operating points of interest, and the control designer is required to meet some performance criteria [23]. This process involves a compromise in order to meet the performance requirements at the various points within the envelope. As determined through literature review, the link between the control integrated maneuverability and the

control design appears through the control system characteristics, which is displayed in Figure 1.8. The approach of analyzing maneuverability independent of controller characteristics has been common in recent years; however, none have bridged the gap of coupling maneuverability and design [24-27].

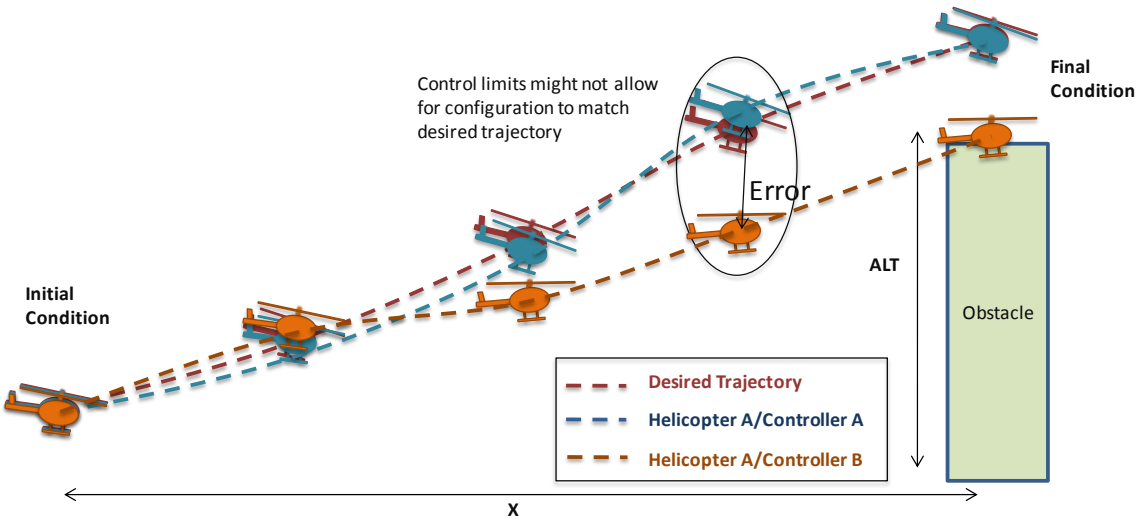

Figure 1.9: Trajectory Error Resulting from Controller Integration

Additionally, the NOE flight operations require the tracking of precise flight paths for safe and successful mission completion. The control system design decisions directly impact the capabilities for a control integrated system in performing these NOE operations. It is essential to capture the impact from control system errors that result in the path following divergence when performing NOE maneuvers. For a fixed helicopter design, the various control designs may result in vastly different maneuverability capabilities as indicated in Figure 1.9. The figure shows the maneuver capabilities for two different controllers for the same design. Hence, the integrated vehicle may not be able to follow the desired trajectory depending on the control decisions. The requirements

determined through the literature review are summarized below and are discussed in detail in Chapter 3. These needs are the motivation for the second research objective of this work.

Capturing Controllability Concerns Requirements

- Capture impact of control system degradations on maneuverability independent of control system design
- Account for error propagation using appropriate measures

1.3 Defining the Mission Maneuvers

The third and final decomposition area of the AHS design problem is defining the dynamic NOE mission maneuvers. The competition is unique from previous design problems because the maneuvers cannot be defined by only steady-state points. Rather, the mission consists of multiple dynamic maneuvers that represent military helicopter NOE flight, which are combined in a sequential manner. Analyzing dynamic operation is more computationally challenging than analyzing steady-state operation. Further expanding on this issue, the dynamic maneuver operational envelope is immense as indicated by Figure 1.10, which shows just 15 of the possible pop-up trajectories for a fixed altitude and time frame. This notional pop-up maneuver space represents the numerous trajectories for a simple planar motion of two variables. Once the other parameters and planes of motion are introduced, analyzing the entire maneuver space quickly becomes intractable in conceptual design.

Multiple problems arise when trying to analyze the entire mission space for all axes motion. As stated by Perez [8], “The number of analyses required to cover the entire envelope becomes unaffordable at the conceptual stage.” Hence, a literature review must

be conducted to determine how to handle the entire helicopter operational space during conceptual design. This literature review, which is fully discussed in Chapter 4, includes approaches from the spacecraft design, the path planning, and the helicopter performance analysis communities.

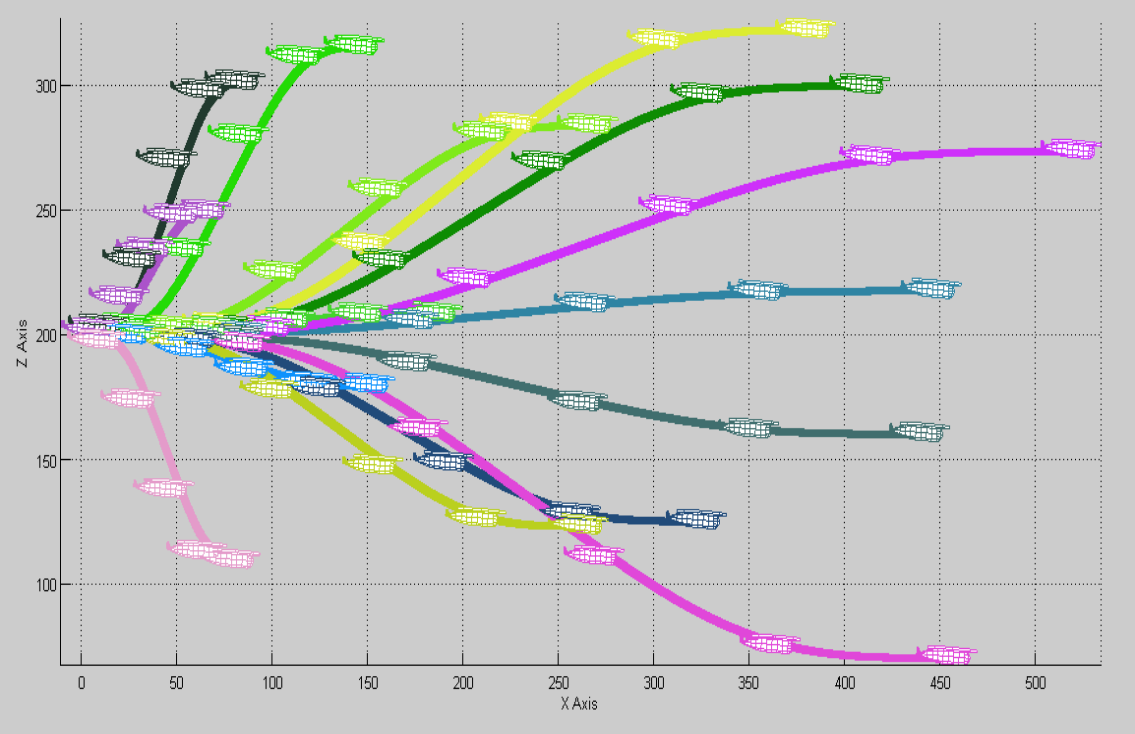

Figure 1.10: Various Pop-Up Maneuvers

Although, flight dynamics and controllability concerns in aircraft design have been considered since the 1970s [28] most of the integration has occurred in the later stages of design. Another major challenge posed by the competition is that the maneuvers are under-constrained. As a result, multiple paths exist that offer potential solutions to each of the maneuvers within the overall mission. This is demonstrated in Figure 1.11 where three different pop-up maneuvers produce the same end result. The optimum path

is the path that requires the least amount of time to complete without violating any design or maneuver constraints.

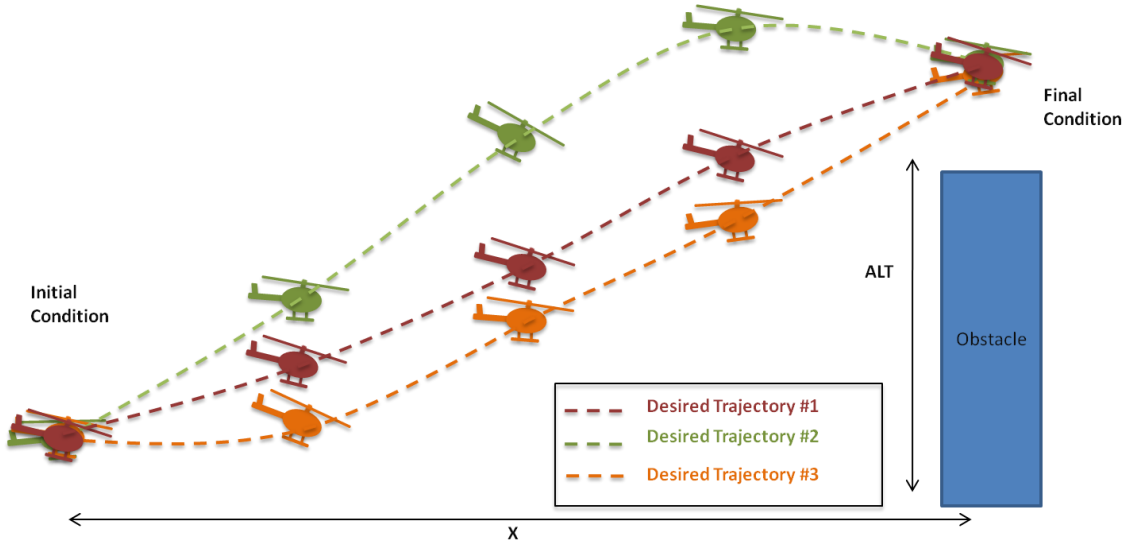

Figure 1.11: Multiple Paths for Single Maneuver Definition

As the number of maneuvers within the mission increases, the combinatorial issues grow exponentially. Additionally, the results from one maneuver dictate constraints on the subsequent maneuver because of the sequential mission definition. An optimization algorithm for determining the fastest mission can be easily integrated; however, without a human driving the constraints, the impact from the various constraints on each of the maneuvers within the mission cannot be adequately captured and analyzed. Furthermore, these trades must be conducted in real-time and the ability to analyze any maneuver within the helicopter operational envelope is essential. These observations result in the third and final set of requirements.

Defining the Mission Maneuvers Requirements

- Analyze the maneuverability over the immense helicopter operational envelope
- Enable human-driven real-time trades for both missions and individual maneuvers

1.4 Thesis Structure

The research presented is not intended to provide all the modeling capabilities of the early stages of design; consequently, the role is addressing important areas of research that enable design for helicopter NOE flight to be completed. This is accomplished by using the AHS design competition as a surrogate to the military helicopter problem since many aspects of military problem are classified. The objective of this work is to provide the designer with an understanding of the impacts of design decisions on the maneuverability characteristics, while offering control requirements to be passed to the control design engineer. Additionally, the process developed in this work captures the quantitative dynamic helicopter maneuverability in the entire operational envelope, which enables use for any future design problems with NOE design goals.

Three major areas of the problem decomposition were introduced in the previous sections and the requirements within each area are summarized in Figure 1.12. All three areas must be addressed in order to completely address the NOE helicopter design problem; additionally, each of the issues is dependent upon selection of the methods used in the other areas. The chapters are presented such that each area contains the literature review necessary to address the posed questions, while at the same time building from previous steps. The problem is decomposed in order to make incremental changes to the process, which results in a more clear and traceable presentation. Each of the research

areas is presented in a separate chapter and upon conclusion of the final question; the motivating problem is fully addressed.

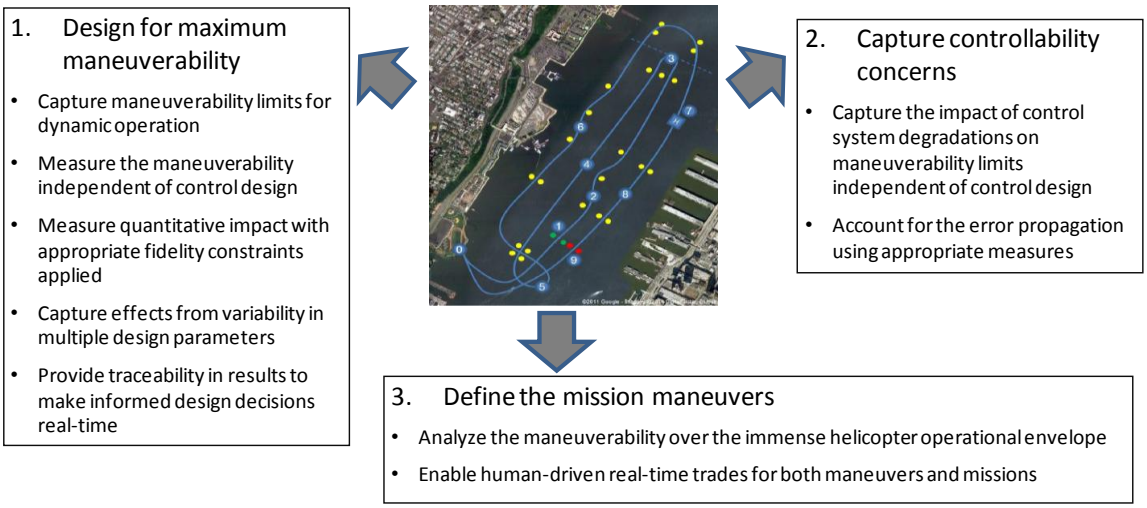

Figure 1.12: Summary of Problem Requirements

Chapter 1 presented the motivating problem and the research areas necessary to fully address the needs. Additionally, the problem decomposition was presented that divided the problem into three categories, which is shown in Figure 1.12. These categories separate the contributions into three separate but dependent chapters, which when combined enable a methodology for solution of the motivating problem.

Chapter 2 reintroduces the aspects of the AHS motivating problem from the design for maneuverability perspective. Considerations for the maneuver space and controllability are made at this point; however, these problems are not addressed until the later chapters. The necessary adjustments to include design assessment into the dynamic maneuverability analysis are presented through a literature review. A process is presented for enabling parametric design trades in the early stages of design using maneuverability

characteristics. Emphasis is placed on the capability to systematically perform real-time trades that provide improved and traceable results over traditional methods.

Chapter 3 expands upon the framework developed in Chapter 2 by including controllability measures into the systematic and traceable process. Control integration literature is reviewed and a method for control integration into early design without detailed control system development is presented. The method is then integrated, thus, enabling controllability concerns to be included in the analysis framework.

The dynamic maneuver space is addressed in Chapter 4, which requires a literature search of methods for defining and capturing the helicopter operational envelope. The flight envelope for helicopters is immense. Multiple sources for defining this space are presented and the most thorough technique for the helicopter problem is selected. Additionally, several methods are reviewed for systematically decomposing the maneuver and mission space into a subset of maneuvers in order to overcome combinatorial issues. A modified taxonomy approach for conceptual design is developed that uses multiple sources in literature.

The AHS design problem can be addressed after all of the research questions are discussed and methods for solving the problems are presented. A methodology for using the tools developed in Chapters 2, 3, and 4 is summarized that includes all of the essential characteristics. Finally, possible areas of future work are presented to show various ways that the presented method and tools can be expanded upon.

CHAPTER 2

DESIGNING FOR MAXIMUM MANEUVERABILITY

2.1 Introduction

As defined in the AHS 2012 design competition [6], there is a need in rotorcraft literature to analyze the maneuverability characteristics of rotorcraft for dynamic maneuvers, while accounting for changing constraints as knowledge of the problem progresses. Additionally, the rotorcraft community has noted the importance of capturing impacts resulting from configuration variability, which introduces additional difficulties in dealing with maneuverability analyses [29]. Third, the quantitative real-time maneuverability analyses must provide traceability through application of appropriate fidelity modeling and constraints. Finally, control design and tuning has a major impact on maneuverability of the final design; hence, in order to determine the vehicle design parameters for maximum maneuverability, the vehicle maneuverability limits must be decoupled from the maneuverability degradations of the control system [21]. In order to better understand the direction of this chapter, the overall research objective is first presented. and then supporting literature on the first aspect of the objective is reviewed.

Overall Research Objective: Develop a methodology that enables real-time and traceable assessment of:

- **Design parameter impacts on maneuverability characteristics**
- **Maneuverability degradations due to control system characteristics**
- **Entire helicopter operational envelope maneuverability**

The focus of Chapter 2 is addressing the first aspect of the overall research objective, which is capturing design parameter impacts on maneuverability characteristics. Recently, rotorcraft mission definitions have expanded to include requirements associated with dynamic maneuvers in order to capture requirements related to NOE flight. The dynamic maneuver requirements directly impact the vehicle definition by dictating design parameter values and configuration choices. The difficulty of capturing these constraints stems from the fact that NOE flight cannot be defined by steady-state operations. Hence, the performance of dynamic maneuvers is required, which was not included in previous conceptual design analyses because of complexity and combinatorial limitations. Examples of dynamic maneuver requirements are stipulated in the AHS design competition [6] and include such tasks as slalom, pop-up, and 180-degree turn maneuvers. Figure 2.1 summarizes the mission and maneuver requirements.

Additional difficulties arise because of the design-related knowledge gap, which forces researchers to investigate the effects of design parameter variability on maneuverability characteristics [30]. The dynamic nature of the maneuvers forces the process to account for design parameters associated with controllability in addition to the geometric, propulsive, and aerodynamic related parameters, which furthers dimensionality and model fidelity considerations. Moreover, mathematical modeling of the actual system requires various levels of assumptions depending on the formulation employed. Due to the number and type of assumptions made, the best design according to the analysis may drastically over-predict maneuverability estimates of the real system.

Through literature review, it is shown that the some assumptions must be removed in order to capture the measures necessary for a design for maneuverability framework.

Segment	0	1	2	3	4	5	6	7	8	9
Maneuver	Staging	Start	Slalom	Short Stop	Straight Away	Quad Pylon	Slalom	Hover, Pirouette, Pickup	Side Flight	Finish
Altitude	<200 ft AGL	< 200 ft AGL	<200 ft AGL	<500 ft AGL	< 200 ft AGL	< 200 ft AGL	< 200 ft AGL	Sea Level	<200 ft AGL	< 200 ft AGL
Temp	80°F	80°F	80°F	80°F	80°F	80°F	80°F	80°F	80°F	80°F

Figure 2.1: 2012 AHS Design Competition Mission Requirements

The final requirements to consider when assessing the impact of vehicle design variables on maneuverability characteristics are related to control system design and integration decisions. The objective of this chapter is not to address the controller design, but to understand the maneuverability limits of the vehicle independent from the controller. Control design cannot be included in the conceptual design phase because of the combinatorial nature of the design problem and the inability to include the detailed

information necessary for adequate control system development. Hence, it is necessary to analyze methods that decouple the controller when analyzing vehicle maneuverability characteristics. In the next section, the requirements associated with designing for maximum maneuverability are investigated through literature review, which is presented in three categories: model fidelity considerations, inclusion of design parameter variability, and separation of control design and vehicle design during maneuverability assessment.

2.2 Literature Review

The problems associated with selecting the appropriate model fidelity for maneuverability analysis, capturing changes in maneuverability characteristics due to design parameter variability, and decoupling the control and vehicle maneuverability contributions are investigated. First, the issues associated with selecting the fidelity of model necessary for inclusion of maneuverability measures are explored. Various methods of dynamic analysis as related to maneuverability calculations and inclusion of constraints are introduced. Second, the process of relating maneuverability characteristics to variability in design parameters for changing constraints and requirements is discussed. A plethora of techniques exist in literature for capturing variability; however, properties of the rotorcraft problem limit the applicability of some of the methods, which is examined and documented. Third, the impact of control integration on the overall system maneuverability is presented and a method is uncovered that allows the user to decouple these contributions.

2.2.1 Model Fidelity Considerations

Determining if a design is dynamically capable of performing a required maneuver is key knowledge that will limit rework, increase safety, and decrease risk and cost [31]. Flight mechanics analysis provides this necessary information, which is defined by Phillips [32] as "the science of predicting and controlling aircraft motion." For nonlinear dynamic systems, such as helicopters, developing a technique for analyzing maneuvering flight is one of the most complex and challenging problems in applied flight mechanics [33]. As early as the 1970s, flight mechanics analysis programs have focused on capturing the kinematic characteristics of maneuvering flight [34, 35]. Although greatly simplified, these programs offer necessary insight into the improvements required for integrating maneuverability analyses with design [36].

Fidelity of the rotorcraft mathematical model has a major impact on accuracy of results, as well as computational cost and time. Additionally, the fidelity has large implication on whether a particular maneuver is feasible or not. The feasibility of a maneuver, subject to the vehicle dynamics and limited control authority (control saturation), is typically ensured by proper constraints placed on the state and control variable limits. Hence, appropriate model fidelity is required in order to account for these constraints [37-39]. Understanding what information is to be extracted from the experiment and the corresponding computational effects are essential in selecting the appropriate fidelity method. For example, assume that a design requirement is that a helicopter must perform a specified pop-up maneuver within a constrained time interval. It may be the case that the feasibility of this maneuver depends on the control surface

effectiveness and corresponding kinematic limits rather than traditional static performance measures such as power available or blade loading.

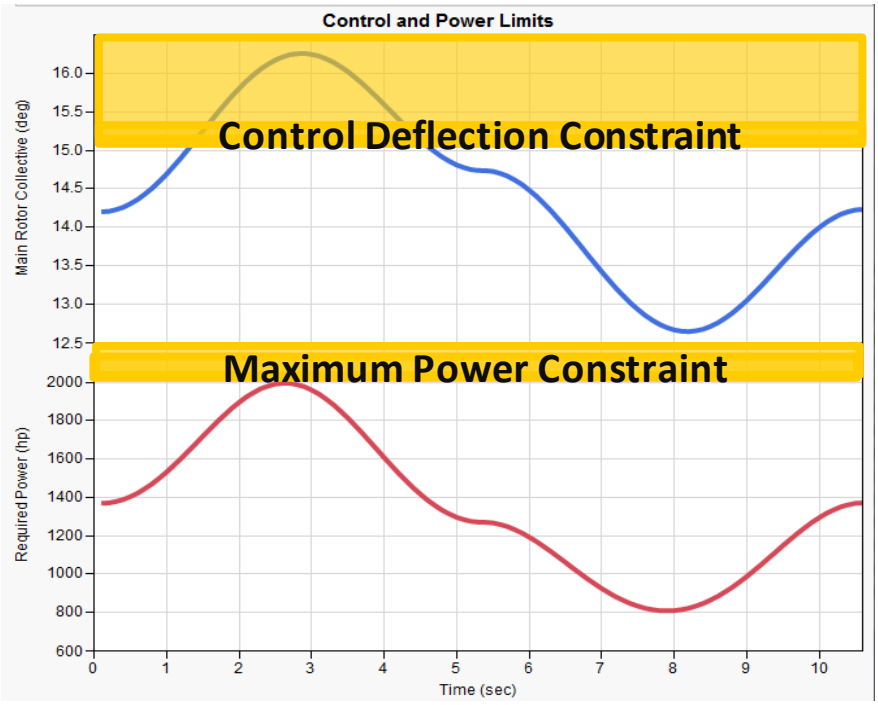

Figure 2.2: Control Time Histories

Figure 2.2 is a notional representation of this scenario where the collective kinematic limit of 15 degrees is reached prior to reaching the maximum power limit of 2000 hp. This example demonstrates that the helicopter modeling environment must provide the capability to acquire the necessary information to capture these limits such that design decisions can be systematically made. Assumptions are required within any modeling framework and the validity of such arguments must be investigated. The fidelity of modeling methods are organized into three major groups in this work; energy-based methods, rigid body methods, and higher fidelity methods.

2.2.1.1 Energy-Based Formulation

The energy-based approach applies multiple assumptions, which results in a formulation that ignores body properties such as inertias and control settings. With these limitations, the analysis breaks down when applied to some accelerated maneuvers [21, 40, 41]. This energy-based formulation is an extension of the common power balance used in rotorcraft analysis studies that is based on power available and power required. Power available is the result of engine properties at speed and altitude; however, depending on the configuration, power available can also include a component of lift. Power required is based on drag of the vehicle and is dependent upon altitude, speed, and attitude of the vehicle [42, 43]. A standard power required curve is presented in Figure 2.3 [44].

The attribute that allows the energy-based method to expand analysis capabilities to dynamic maneuvers rather than static operating points stems from the process of velocity integration. As the velocity increases, the point on the power required curve is shifted to the right and the corresponding excess power is changed. Excess power is directly correlated with capability to accelerate. The method obtains a quasi-dynamic maneuverability estimate by interpolating and integrating between steady operating points. As a result, this method is not capturing any of the transients, which is why the method is termed quasi-dynamic [19].

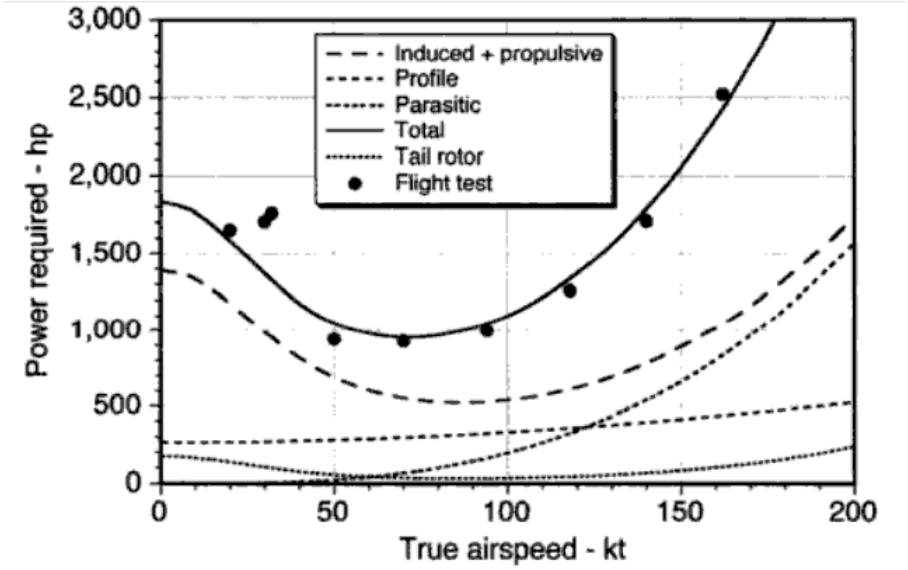

Figure 2.3: Power Required Diagram

One major concern is that energy-based methods may predict values which exceed the physical limits of the real vehicle as noted by Avanzini [16], "which might include mechanical limitations of control travel or control rates, limitations of rotor and tail rotor torque, and even structural limits of critical components." Moreover, it should be noted that the method determines that a maneuver is successful if the power available is larger than the power required. It does not account for any measure of controllability, which limits the method's ability to adequately capture the necessary performance measures required [19].

2.2.1.2 Rigid Body Formulation

The goal in mathematical modeling is to find a technique that is powerful enough to adequately represent the helicopter maneuverability characteristics over the entire operational envelope, but at the same time is efficient enough for conducting design

analysis trades. This means that part of the accuracy obtained through complex models must, often times, be sacrificed in the early stages of design. Frazzoli [45] states that "such a model can be derived by physical intuition and first principles: at the basis of the model we have the rigid body dynamics, coupled with momentum theory and basic aerodynamics for the computation of forces acting on the helicopter." In recent work, Avanzini [46] addresses short term agility, which is defined by the time derivative of acceleration vector in [47], using the rigid body Equations of Motion (EoM) with good correlation with flight data.

Equation 2.1: EoM General Functional Form

$$\dot{state} = function\ (state, controls, time)$$

The nonlinear rigid body EoM for dynamic analysis has been applied to many research efforts in recent years [48]. Usually, the EoM are not time dependent; however, for rotating subsystems such as helicopter rotors, the equations may be periodic in time [49]. Many of the earliest works assumed linearized dynamics and small angle approximation, which were found to be too limiting when applied to helicopter maneuver simulation [33].

As with the energy-based approach, the rigid body formulation requires assumptions; however, the assumptions are much less limiting. One important simplifying assumption as expressed by Anderson [50] is that the dynamics of the "main rotor coupled lead/lag and rotorspeed degrees of freedom" are often ignored. Additionally, rigid body rotorcraft models are usually confined to quasi-steady

aerodynamics through a uniform induced velocity distribution assumption [51-53]. The various assumptions limit applicability to analysis involving specific types of maneuvers; hence, there is a tradeoff between higher fidelity modeling techniques and design space exploration capabilities.

2.2.1.3 Higher Fidelity Formulations

Much rotorcraft design literature calls for higher fidelity analysis methods, which is confirmed when considering the complex problem of rotorcraft maneuverability analysis for a well-defined vehicle. However, the applicability of the various methods in conducting maneuverability in early design, when much of the detailed aspects of the vehicle are unknown, must be examined. Avanzini [17] analyzed the reliability in predicting the required control action using 13 models of varying fidelity for a set of three rotorcraft maneuvers: hurdle-hop, slalom, and lateral repositioning. Results from the analysis indicate minor loss of fidelity for much less computational complexity when the simple rigid body EoM are used.

Figure 2.4 [17] shows the command time histories for a pop-up maneuver via showing control displacement from the initial trim position. All 13 models are shown on the figure, which demonstrates that there is little difference between the various fidelity methods. Hence, although the higher fidelity methods may provide slightly more accurate results, they require many more variables to approximate the response and exponentially more time for computation. Avanvini's [17] work provides quantitative evidence supporting application of the lower fidelity rigid body model rather than higher fidelity

formulations for early design purposes when analyzing smooth maneuvers. Additional rationale for using the simple rigid body formulation is presented by Anderson and Bottasso. Anderson [50] shows that simple modifications to the process alone can recover performance that is often lost with much simpler models. Consequently, Botasso [37] investigates the implications of forcing smooth control histories, which essentially approximates the effects of modeling a higher fidelity system model when studying the trajectory problem.

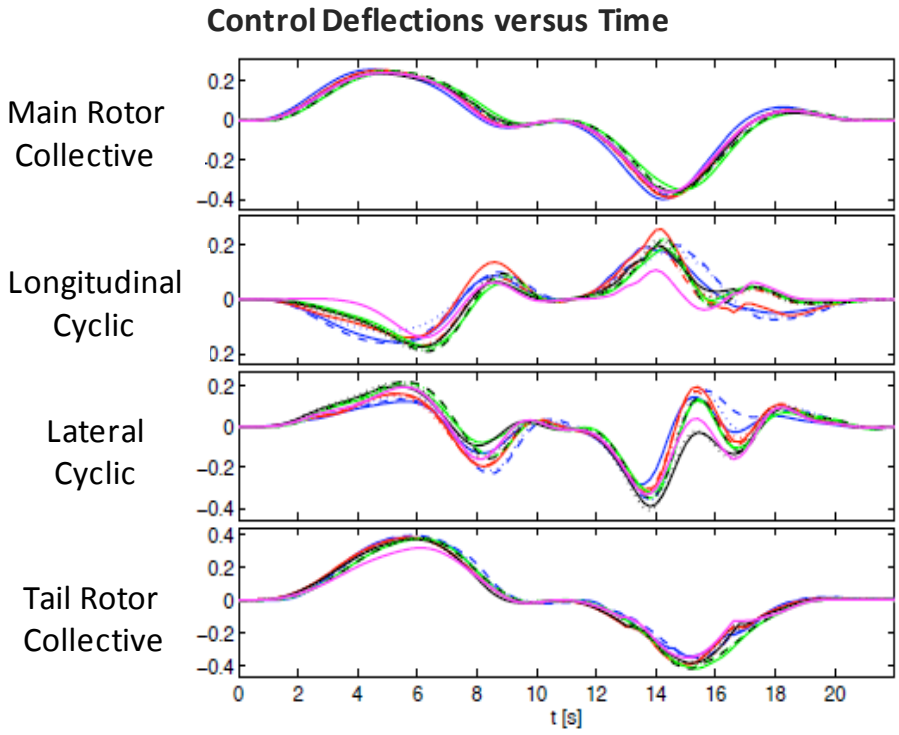

Figure 2.4: Control Time Histories for Multiple Fidelities

As complexity of the model increases so does the level of knowledge that is required to populate the model. Much information is unknown during early design and some of the more detailed parameters are difficult to predict. Even if all of the parameter

ranges could be drastically reduced, the curse of dimensionality prevents adequate searching of the design space due to computational limitations. Therefore, a simplified rigid body model is selected over the higher fidelity formulations because of the complexity, marginal increase in accuracy, dimensionality concerns, and computational requirements associated with complex formulations.

2.2.2 Capturing Variability in Design Parameters

Previous rotorcraft design studies have had little integration of configuration variability effects on maneuverability analysis. This section introduces the differences between variability and uncertainty and discusses the applications to aerospace engineering in recent years. Once variability and uncertainty are introduced, a few of the most common analyses methods in aerospace engineering design are presented. The complex nature of the rotorcraft problem and the required ability to quickly adjust constraints greatly limits the application of some variability and uncertainty inclusion techniques. Through literature review, it is determined that a probability distribution based method that utilizes data filtering techniques provides the necessary attributes to address all aspects of the problem. The other mathematical techniques that are investigated do not allow for easy recalculation of design space as requirements and constraints are changed.

2.2.2.1 Variability versus Uncertainty

Only recently has an effort been made of classifying and defining variability and uncertainty in aerospace engineering. Uncertainty and variability are philosophically different and are commonly separated for risk analysis design studies. Variability is defined as the effect of chance, which cannot be reduced through further study or measurement because it is a function of the system. Hence, variability analysis captures the helicopter configuration design space of alternatives, which has been a major focus in recent years. Bivens [54] and Dooley [55] address maneuverability with inclusion of a few design variable impacts for NOE operation, but do so based on handling qualities rather than by analyzing maneuverability limits. This analysis was expanded upon by Kim [20] where a control architecture was assumed to be linear so it is unknown whether the vehicle or the controller is the limiting case. Cao [56] analyzes one helicopter versus another helicopter but does not link the performance differences to design variables. Celi [57] calculates the sensitivities of the quickness with respect to rotor/fuselage design parameters and achieves max quickness through design value selection; however, the author notes that the method generates too aggressive maneuvers and analyzes the effects one variable at a time.

DeLaurentis [30] defines uncertainty as "the incompleteness in knowledge, that causes model-based predictions to differ from reality in a manner described by some distribution function." Although more detailed hierarchical taxonomies exist [58], the most basic grouping of aleatory and epistemic [59-62] is sufficient for understanding the uncertainty in design parameters required in this work. Aleatory uncertainty is the

intrinsic variation associated with a physical system or environment. Epistemic uncertainty is any lack of knowledge during formulation of the modeling process, which occurs due to incomplete information of some characteristic of the system or the environment [58]. The next few sections introduce various analysis techniques used in aerospace literature, which can be implemented to capture either variability or uncertainty depending on how the technique is applied.

2.2.2.2 Convex Underestimates

Convex underestimating algorithms account for variability in function value over a range of inputs by developing multipolynomials that bound the function space. These multipolynomials, termed underestimators, are convex polynomial expressions that are guaranteed to bound actual function values over the entire range of inputs. The function bounds are indicative of variability within the function approximation. These methods have been mainly applied to find global optimum solutions [63] in nonconvex spaces. The determination of proper underestimators is a major computational expense and a new set of underestimtors must be determined each time that the design variable ranges change. Moreover, for large input variable ranges, the underestimators can drastically over predict the true function bounds.

The development of guaranteed underestimators requires much knowledge about the function. To guarantee proper underestimation requires function second derivative information [63-65]. This type of information is difficult to guarantee for many problems, especially functions without analytic forms [66, 67]. In many cases the helicopter EoM

do not have an analytic derivative [68], which causes undesired error to occur when numeric derivatives are calculated [69]. The theoretical guarantee of global optimality when determining proper underestimating functions is discussed in [70-72]. Failure to achieve optimality guarantees is presented by Singer [73], where the solutions are determined by using standard numerical methods. As a result of the numerical errors, there is no guarantee that the solution bounds are valid [63]. See [74-78] for a thorough review of recent advances in convex underestimating algorithm development. Efficient recalculation of the feasible space is required in order to conduct design trades, unfortunately, both convex underestimating algorithms and interval analysis methods fail to meet this requirement.

2.2.2.3 Interval Analysis

Interval mathematics is derived in R.E. Moore's Ph.D. thesis from the 1960s [79, 80]. Moreover, this mathematical framework was implemented on a digital computer as early as 1970 [81]. Van Kampen [82] states that "interval arithmetic can cope with the inherent problems related to the limited precision of numbers in digital computers." Interval analysis (IA) is used as a global optimization technique for determining global maximums, minimums, or zeros of rational functions over a rectangular search region [83]. Interval algorithms solve for global solutions of equations by decomposing the function into basic mathematical operations and using logic to bound each operation. By bounding each operation, the variability of the entire function is bounded [84]. The major benefit of interval methods is that they are capable of operating on the actual function rather than requiring the generation of underestimators. As noted by Manetsch [85], "the

efficient solution of global optimization problems requires methods that do not require analytical expressions for the objective function or its derivatives."

One problem with IA is that the computation time tends to grow exponentially with the dimension. Even for small problems, enormous computation time is required if the problem is highly nonlinear or ill-conditioned [86]. Although interval methods are mathematically proven to guarantee solution bounds for a rational function, they can suffer computationally due to dependency issues, which stem from interval logic and the additive nature of terms. See [87] for a thorough discussion on the theory and application of interval analysis mathematics.

2.2.2.4 Fuzzy Logic

Fuzzy numbers and fuzzy arithmetic have been studied in recent years as a way to model the variability and uncertainty in engineering design problems [88]. Fuzzy set theory stems from the need for a more complete model of uncertainty [89] . Similar to interval method, implementation of extended arithmetic operators on fuzzy numbers is computationally complex [90]. Many applications overcome this difficulty by limiting the membership functions to certain shapes, usually either triangular fuzzy numbers (TFN) or trapezoidal fuzzy numbers (TrFN). Unfortunately the TFN shape is not closed under multiplication and division [91]; hence, the resulting shape is only approximated and can lead to incorrect results when used in engineering applications [92, 93]. Although developed separately, recent literature shows the relationship between fuzzy set theory and interval methods, with regards to their topological properties [94, 95]. The real-time

analysis requirements limit applicability of both Fuzzy Logic and Interval Analysis. Additional implementation difficulties arise due to the complex iterative nature of the helicopter EoM.

2.2.2.5 Monte Carlo Methods

The Monte Carlo (MC) method was developed in the 1940s by John von Neumann, Stanislaw Ulam, and Nicholas Metropolis at the Los Alamos National Laboratory. As stated by Stuckman [96],"the Monte Carlo method of global optimization is strictly a uniform random search technique." The method has been expanded to allow various types of probability distributions to represent an input [97]. The method works by randomly selecting each input variable from its respective distribution and then evaluating the function with the chosen inputs [98]. Advantages of the method were realized when studying systems of particles, which had complicated interaction effects [99]. The mathematical representation most commonly used for uncertainty analysis is a probability distribution coupled with Monte Carlo analysis because of the robustness and the simplicity of the method [100].

Filtered Monte Carlo (FMC) is an extension of the MC method, which first computes function values over a random probability distribution of input parameters. The distribution of each parameter can be selected independently of other parameter distributions. The results are collected and a resulting response distribution is created. Kuhn [97] states that then "post-processing of the output occurs through a series of filters to ensure constraints are met." This process can also be applied to stochastic optimization

problems with sequential filtering and sampling techniques [101]. FMC techniques have been applied to a wide range of optimization and requirements analysis problems [102]. Unlike the other methods reviewed, the filtered data method provides the capability to systematically add and change requirements and view the resulting feasible design space in real-time; therefore, it is selected as the appropriate variability analysis technique to capture the impact from variability in the design variables.

2.2.3 Separation of Vehicle and Control Maneuverability Effects

Controllability measures must be included in the design process because rotorcraft platforms are inherently unstable and control integration is becoming increasingly important with highly maneuverable and autonomous configurations [8, 11, 13, 103-108]. One major point of contention is that the control decisions directly impact the maneuverability characteristics of the system. For example, assume that the system under analysis is to be integrated with a linear gain-scheduled controller. It is well documented that linear gain-scheduled controllers are limited to scheduling variables with slow dynamics. This design choice may pose performance limitations when comparing a system with faster dynamics to a system with more slowly varying parameters. As a result, it may be the case that the slow varying system will outperform the fast varying system when integrated with a linear gain-scheduled controller because the choice of controller is not adequate for stability of the fast varying system. However, if a different controller architecture is integrated, the fast varying system may have more potential to outperform the slow varying system [109-113].

Figure 2.5 summarizes these observations by displaying the same helicopter design with a notional linear, nonlinear, and a perfect controller. The nonlinear controller is shown to outperform the linear controller for three of the four maneuvers tested; the only maneuver for which the linear controller has better maneuver performance is the notional acceleration maneuver. Further analysis of the figure shows an additional curve that demonstrates the absolute best performance that can be achieved with an ideal controller; this curve is termed controller independent analysis. The helicopter and controller combination that results in the optimum performance depends on the maneuver under investigation; however, if a perfect controller is integrated, the maximum theoretical maneuverability due to design parameters is obtained for all maneuvers.

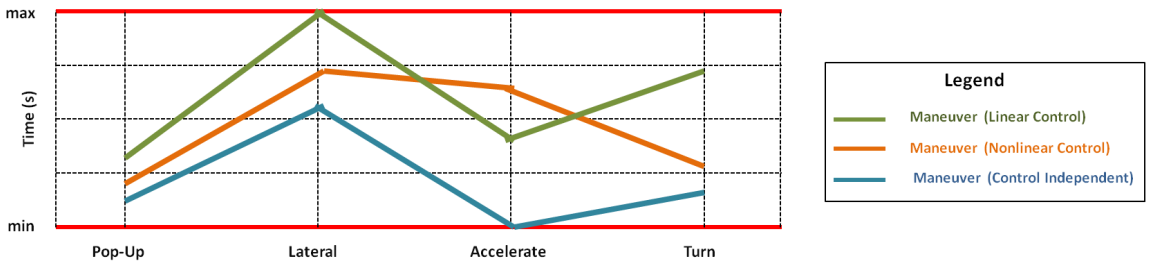

Figure 2.5: Importance of Control Architecture on Dynamic Performance

Additionally, control design is an iterative and human driven process and in order to assess the true maneuverability of the vehicle, the control architecture cannot be fixed. In past design efforts, the controller selection and tuning was typically performed prior to or during dynamic simulation [103]. The previous example shows that it is essential to obtain dynamic maneuver limits independent of controller design in order to capture the true design limits. Fortunately, a technique has been provided in literature that addresses this need and has received much attention in recent years.

This method, which is termed inverse simulation [48], uses an optimization routine to calculate the controls necessary to follow a prescribed path through time integration. This is opposite to the original line of thought, which consisted of perturbing the controls and recording the resulting motion. As a result of the mathematical formulation, inverse simulation has been found to provide a better format to validate against actual flight test data than traditional methods, which are based on bifurcation and continuation theory. Furthermore, Murray-Smith [48] mentions that inverse methods are well-formulated for capturing the performance effects of configuration changes, such as the mass or the position of the centre of gravity, in a straightforward fashion. Moreover, the results are based in the time domain, which makes for easy interpretation. Both bifurcation and inverse simulation methods are reviewed in the next sections to demonstrate the benefit of inverse simulation compared to the traditional method. Additional literature is also included that addresses some of the fundamental considerations and concerns that must be addressed when applying inverse simulation techniques.

2.2.3.1 Bifurcation and Continuation Techniques

Bifurcation has been used since the early 1980s and is a standard tool in use today for the analysis of nonlinear phenomena in aircraft flight dynamics [114, 115]. Bifurcation analysis is very useful when studying systems of smooth and continuous nonlinear ordinary differential equations (ODE), especially in those regimes where nonlinear phenomena are dominant [116]. Bifurcation analysis is a mathematical technique that determines the steady-state equilibrium conditions and trim settings for a

given set of continuous nonlinear equations [117]. A bifurcation occurs when the system exhibits a qualitative transition in local stability [118]. Iqbal [117] comments that "mathematically the occurrence of a bifurcation exists whenever the eigenvalues migrate from the stable region of the complex s-plane across the imaginary axis into the unstable region or vice versa." For an introduction to bifurcation theory see Crawford [119] and Strogatz [120].

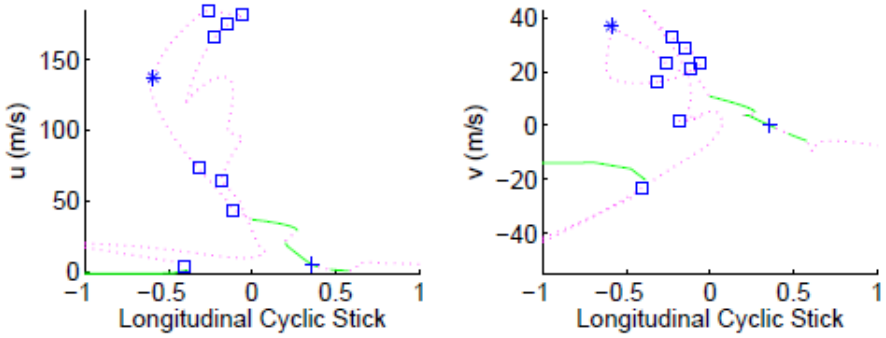

Figure 2.6: Bifurcation Diagrams Helilink Helicopter

During analysis, the technique records all of the critical points in the state-control space in which equilibrium solutions are created, destroyed, or undergo a change in stability [121]. A global picture of the steady-states and stability characteristics may be generated over a wide range of conditions by recording the critical points. After completing the analysis and recording the data, the results are displayed in bifurcation diagrams for examination similar to that shown in Figure 2.6 [115, 122-124]. If conducting maneuverability analysis and design simultaneously, all of these diagrams would need to be generated for each design. This results in a large amount of data that must be generated and stored. Additionally, when calculating the control settings required

to follow a prescribed path, these tables must be used for interpolation since there is no direct relationship. This step introduces more computational burden and a greater amount of error into the analysis.

Bifurcation analysis has been extended and manipulated over the years in order to provide the necessary tool set for various types of problems. Constrained bifurcation analysis (CBA) is a bifurcation method that is augmented with constraint equations to obtain desired flight conditions or operational scenarios. CBA is expected to correlate better with flight tests because maneuvers flown by pilots can be modeled more accurately using the constraints to obtain only the trim conditions of interest [114]. Extended bifurcation analysis provides the analyst with the ability to analyze non-steady state operational conditions by adding a set of kinematical constraint equations [125].

Bifurcation analysis techniques have been used to study numerous nonlinear flight dynamics problems for various platforms and operational scenarios. Poli [124, 126] used similar methods to study the influence of various design parameters in an undersling load helicopter model. Avanzini [127] applied the method to a highly augmented aircraft model, which is an actively controlled vehicle with negative or marginal static stability. These methods have also been used to determine control law parameters for gains in control design [128]. Critical flight regimes for helicopters and flexible aircraft problems have also been analyzed [118, 129]. For a review of bifurcation method applications to aircraft dynamics problems see Goman [130].

In order to achieve the benefits of bifurcation analysis in a well structured manner, continuation methods are utilized [131]. Continuation is a path-following algorithm that traces out a curve of steady-states while varying one parameter [118]. Sibilski [129] further elaborates on the origin by stating that "continuation methods are a direct result of the implicit function theorem, which proves that the steady-states of a system are continuous functions of the parameters of the system at all steady-states except for steady-states at which the linearized system is singular." Numerical continuation methods have been used for many years in aircraft nonlinear dynamics studies to track the equilibrium in nonlinear flight regimes [122]. Anathkrishnan [121] was able expand the method in order to generate complete bifurcation diagrams of multiple parameters with a single computation.

2.2.3.2 Inverse Simulation Methods

Inverse simulation techniques approach the aircraft maneuver problem using the opposite thought process, which involves defining a path and calculating the control histories [27]. Anderson [50] states that inverse simulation methods have been successfully employed for several years to analyze "the maneuverability, operational suitability, and conceptual design of helicopters." Although there is no standard way of taking into account control saturation or flight envelope constraints, even for differentially flat systems [132, 133], inverse simulation provides satisfactory approximations.

In practice, simulation models are more often used off-line to assess an aircraft's response to control stimuli or to examine its stability characteristics. Thomson [134] explains that "the crucial advantage of a helicopter is its ability to operate close to the ground tracking a precise flight path." Since the required control inputs are unknown a priori, this was impossible to replicate efficiently prior to the formulation of inverse simulation techniques. In addition to the advantages in path tracking, inverse simulation also provides much benefit when the complexity arising from coupling terms are included in the analysis.

The coupling problems associated with helicopter control can be appreciated by considering the example of forward acceleration without changing heading or altitude. The acceleration is achieved by application of forward longitudinal cyclic, which tilts the rotor disc forward and produces a forward pitch. The component of the thrust vector that balances the weight is reduced through this action; hence main rotor collective must be increased to account for this loss in thrust. As a result, tail rotor collective must increase to account for the added torque. Finally, lateral cyclic is required to balance out this side force that is created due to the increase in tail collective, which in turn has an impact on the other forces and moments [134]. When applying bifurcation, only one control is adjusted while the other variables are held constant; therefore, this situation could not be analyzed in a straightforward manner. On the other hand, the inverse simulation technique can solve for these required control inputs using numerical optimization algorithms. Additionally, the changes in control settings that result from design changes can be easily tracked and compared using inverse methods [48]. This application has

been demonstrated in Nannoni and Stabellini [135] for a helicopter design for takeoff maneuvers.

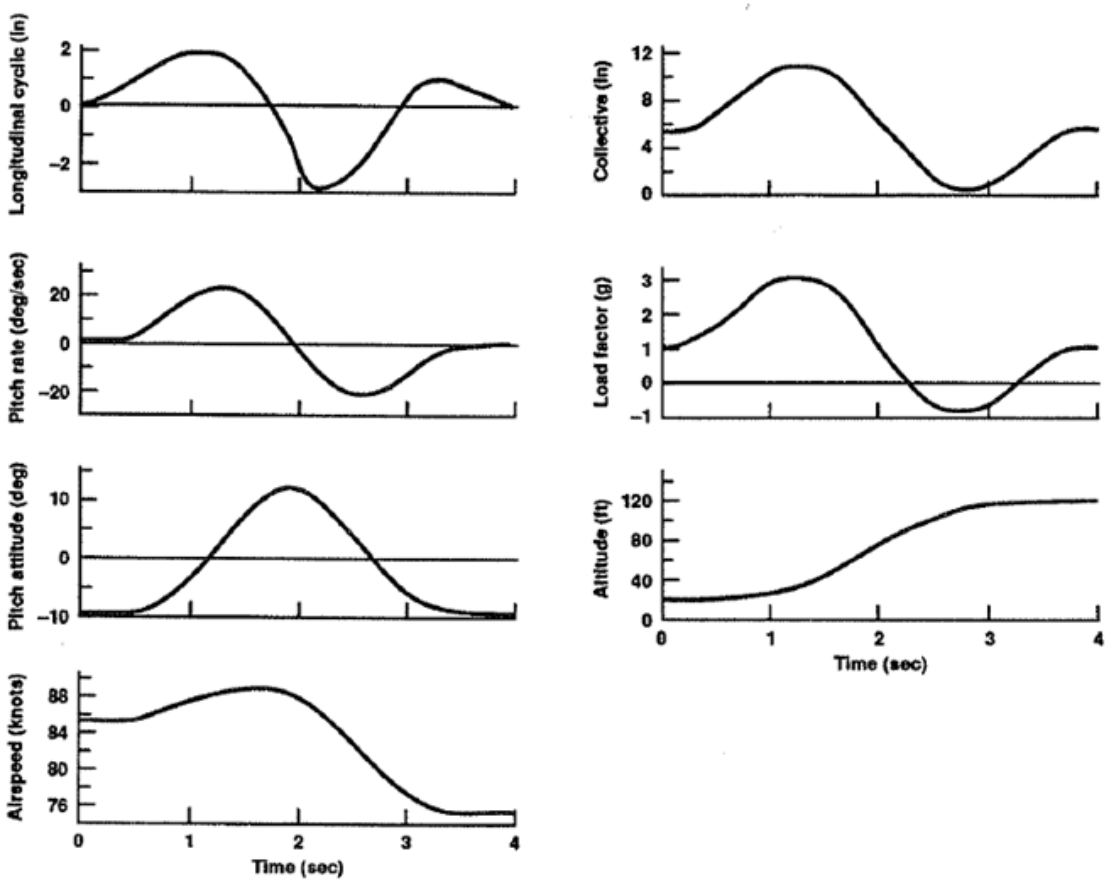

Figure 2.7: State and Control Time Histories

The validity of inverse simulation has been shown through comparisons of state and control histories against actual helicopter flight test data. Whalley [136] validated rotorcraft inverse simulation results through a series of piloted simulations by comparing state and control time histories [41]. Although, the maneuvers were not exactly identical, the state and control responses could be used to predict time histories of the actual

system. Figure 2.7 [136] shows typical time histories for a pop-up maneuver for a traditional single main rotor helicopter configuration.

Inverse simulation techniques use time-based analyses to determine responses to either control or state constraints. De Matteis [137] states that "time-based analysis is used rather than frequency based because it allows for the solution to have physical meaning." Throughout the years, the inverse simulation method has evolved in order to address many types of problems [138-140]. Cao [33, 56] expanded the method to model aerobatic maneuvers by dividing the flight envelope into longitudinal, lateral, and coupled maneuvers. Through this analysis, the authors were able to calculate state and control time histories for pop-up, lateral jink, and 180 degree turn maneuvers. Recently, Avanzini [46] has shown that analyzing short-term metrics using inverse simulation techniques can lead to determination of the max attainable agility components. This is accomplished by using the simplified rigid body EoM to simulate three common helicopter maneuvers: rapid deceleration, max performance turn, and a reverse turn. The control time histories to complete the maneuvers are displayed, which provide the maximum performance for each of the maneuvers tested for a fixed helicopter design. Su [141] furthered the research by investigating a coaxial helicopter using inverse simulation methods. Additionally, inverse methods have been applied to the control problem [142].

Inverse simulation techniques fall into three major categories: differential, integration, and global methods. Differential methods [143] are "suitable for nominal problems only, where the number of control inputs equals that of the tracked variables [16]." The solution of the inverse problem is a significantly more challenging for the

rotorcraft case than for a conventional airplane, especially when individual blade dynamics are incorporated in the model [21, 50]. Differential methods do not provide the necessary functionality for capturing the complexity associated with helicopter models [27]. Wood [34] treated the helicopter as a simple system and analyzed its ability to maneuver based on the energy balance approach, which utilized the differentiation inverse method. Differentiation consists of discretizing the flight path into a series of time steps, using numerical differentiation to obtain angular rates, and solving the equations of motion at each time step as a set of algebraic equations as presented in Kato [143]. The problem with this technique, as stated by Thomson [144] is that "even small changes to the mathematical model can require a significant effort in recasting the inverse solver."

Integration methods [26] are mathematically robust and can be applied to a broad spectrum of problems, even those with redundancies [137]. Among other methods, one advantage of integration methods is the capability of dealing with complex, high order mathematical models on the basis of a solution scheme that can be applied with only minor variations to the dynamical models of various order and complexity [16]. For helicopter application, the earliest study was the optimization of helicopter takeoff and landing performance [145]. At the same time, Thomson [146] investigated the inverse solution for a prescribed flight path based on a set of linearized equations of motion. As the nonlinear EoM are applied, additional concerns regarding algorithm stability are introduced. For example, constraint oscillations are induced in certain unconstrained states whenever an inverse simulation is performed [147, 148]. The characteristics of these oscillations are a complex function of the model order, which are due to internal

zero dynamics [149]. Integration methods are the most commonly implemented because the computational concerns can be handled through appropriate constraint selection and maneuver definition [150].

Finally, global methods [151] determine the time-history of the control variables by means of a variational approach and the benefit is that this method can be used to track the control changes over the entire mission [16]. Recently, Avanzini [46] has shown that analyzing short-term metrics using inverse simulation techniques can lead to determination of the max attainable agility components. Hence, there is no need to analyze the entire mission at once but rather it can be analyzed in smaller subsets.

Inverse simulation is not the same as model inversion although they share similarities. Both use previously defined trajectories and mathematical optimizers to find proper control setting. Differences originate in where the inversion process is applied. Model inversion calculates the inverse model in advance and then performs forward simulation by feeding the defined trajectory with the corresponding derivatives of appropriate order [152-154]. On the other hand, inverse simulation uses the full nonlinear EoM to find optimized control settings at each time step to meet an objective function. This process forces the vehicle to follow a prescribed path, which is essential for analysis of NOE maneuvers.

2.2.3.3 Computational Considerations

The first consideration when applying inverse simulation techniques is specifying the correct number of constraints for the number of controls. In the inverse problem, if

both flight trajectory and flight attitude are given, there will be no solution because the problem will be over-constrained. If either flight trajectory or flight attitude alone is given, then there will be many solutions. This is because the degree of freedom of a controlled maneuver for an helicopter is between three and four [143]. For example, one constraint method presented by Sentoh [142] specifies the initial and final states, while an optimization technique minimizes an integral performance index that is based on the square deviation of the actual state from the desired one with constraints on the controls. Additional issues arise when implementing a minimization method because of nonconvexities within the maneuver space. As a result, it is possible that two solutions may exist in the same minimum neighborhood resulting in oscillation between the solutions for successive time steps in the simulation. Hess [26] recommended a high frequency filter technique to stabilize the results. Hess was matching states rather than accelerations, which are more affected by this oscillation phenomena.

The second consideration originates because solving the equations of motion of the vehicle in an inverse manner is not a trivial task. Avanzini [155] states that, "issues such as numerical stability and accuracy, computational time, and reliability of the algorithm are taken into consideration." Numerical errors result from machine error, which occur because computers can only retain a certain number of bits in the stored variables [69]. Integration errors are an outcome of using the linearized version of the Taylor Series to approximate the integration process. Various integration routines have been developed for particular problems to minimize the error. Betts [156] points out that less sophisticated, fixed-step ODE solvers can often be more efficient because they do

not introduce numerical noise in the gradients [21]. “In general, ode45 is the best function to apply as a first try for most problems [157].” The Fourth-Order Runge-Kutta (RK4) method was chosen because of the model prediction capabilities, robustness, integration time efficiency, and ease of implementation. The objective is to evaluate the dynamic performance for a pre-defined maneuver and relate the limits to the vehicle design parameters; hence, inverse simulation is chosen over the traditional approach.

2.3 Approach

The approach to the remaining problem, as determined through literature review, is presented in four parts. First, the research question is formulated based on findings from the literature review that includes several key needs that are provided in the 2012 AHS design competition. Secondly, the process is decomposed into a series of elements, each of which is explained. Third, the hypothesis is presented that address the research question using the formulated process components. Finally, a test plan is formulated that details what simulations are to be conducted and what information is to be extracted from the process when applied to the rotorcraft problem in order to substantiate the hypothesis.

2.3.1 Research Question

The focus of the first thesis contribution is to address all of the requirements necessary for design for maximum maneuverability. The requirements are summarized in the following research question, which is formulated based on extensive review of model fidelity considerations, design variability inclusion methods, and control design independent dynamic simulation techniques.

Research Question 1: How can the impact of design parameter variability on rotorcraft maneuverability limits be quantitatively captured independent of control design for changing requirements?

The research question has multiple characteristics that warrant further elaboration. First, the question specifies application to design of rotorcraft platforms, which are chosen because of the need presented in the 2012 AHS design competition. Second, the analysis methodology must provide quantitative results that are independent of control design such that the true maneuverability limits resulting from design parameter selection may be quantitatively captured. The third requirement is that the effects of configuration variability on maneuverability characteristics must be captured. Finally, this decision making framework must allow for easy manipulation of design, performance, and kinematic constraints because of the fluid nature of design requirements throughout the design process. In combination, these attributes create a very difficult problem that requires a well structured, traceable, and systematic process. Furthermore, due to the changing constraints and requirements throughout design, the method must enable real-time analysis such that the relationship between design parameters, maneuverability characteristics, and constraints may be captured.

2.3.2 The Process

A systematic and traceable process is required to formulate a hypothesis that addresses the first research question. The process, which is presented in Figure 2.8, has several important components that have been selected using the research presented in the

literature review section. The combination of these techniques offers unique attributes and capabilities not possible using previously developed approaches. Three major elements are integrated in order to fulfill the needs when provided with the initial design information from the problem description. The first element is the parametric rigid body rotorcraft model along with a novel parametric maneuver model that enable design integrated maneuver analysis. Secondly, inverse simulation techniques are included in the process to enable trajectory analysis for NOE flight maneuvers independent of control design. Finally, a filtered data technique is included in the post processing to provide systematic, traceable, and real-time design trade analysis capabilities. These elements are combined to form a four step process which consists of the problem formulation, mathematical model development, simulation, and post processing/data filtering.

The design information consists of the baseline design specification, upper and lower bounds on the variability of the design definition, and a baseline maneuver. All of which are assumed to be provided in order to begin the process. The mission definition is usually provided in the initial problem definition, while the baseline design may consist of a set of various designs that are being considered as potential solutions to the problem. Each design needs to be executed through the process separately unless the entire design space exploration is desired. If this is the case, then the design variability must cover the entire ranges of the designs. The initial configuration space is based on previous design for maneuverability literature in order to more fully mimic an actual design process. These ranges and variables are discussed more fully during implementation.

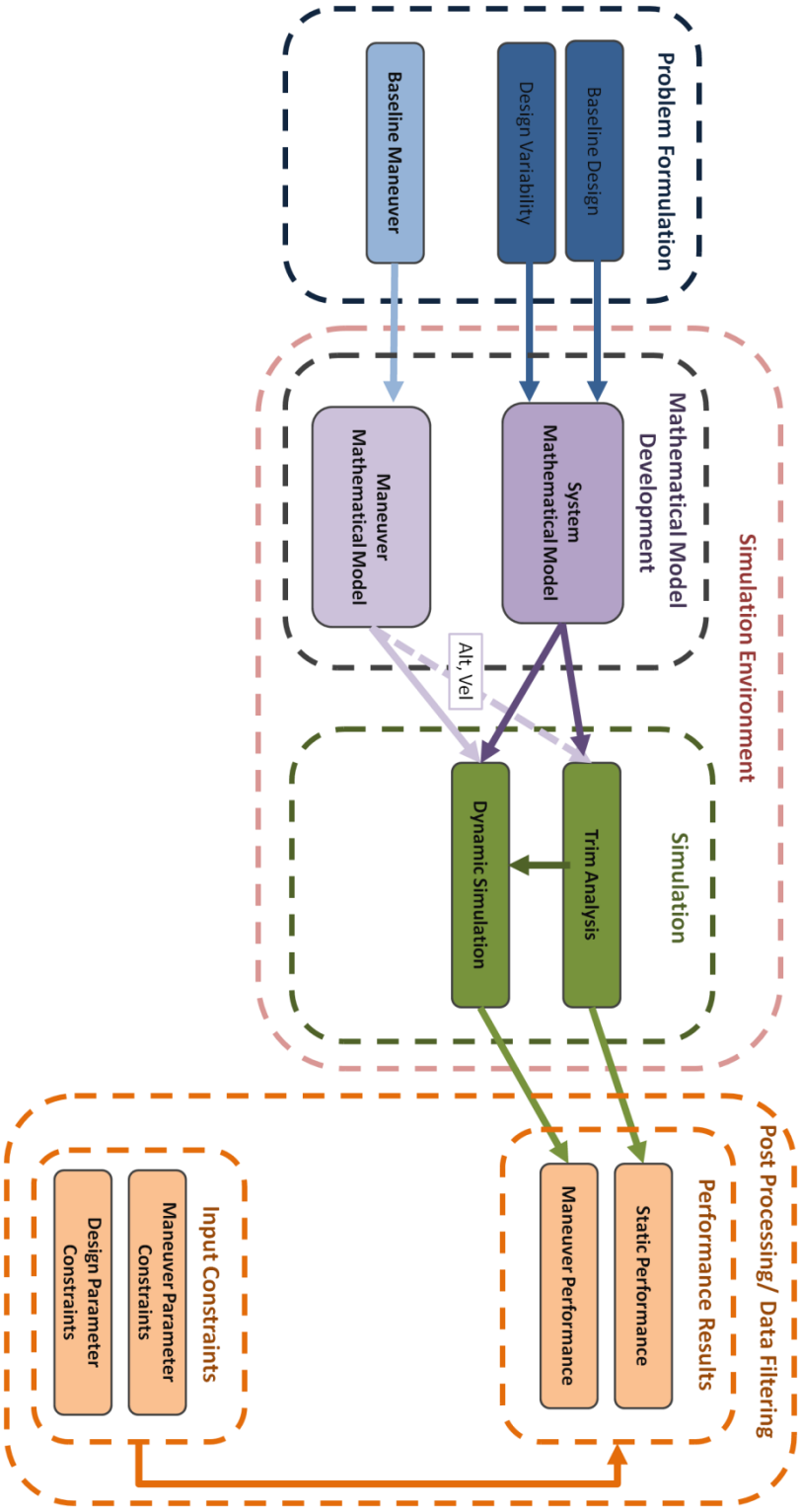

Figure 2.8: Process Flow

The second step of the process is to take the information provided and develop mathematical models of the system and the maneuver to be performed. The mathematical model of the system must be parametric such that design variations can be analyzed. Additionally, the system parameters must be maintained to a reasonable number to mitigate combinatorial issues, while at the same time offering the appropriate fidelity to include necessary constraints. The mathematical models must be structured for inclusion into the simulation environment, which requires careful selection of states and controls for the system definition. The system model development requires the second order ordinary differential equations of the system, which are the EoM of a helicopter in this analysis, to be described in a manner in which integration provides the next state when given the current state and control settings. The various assumptions of the selected rigid body model are discussed during implementation. The maneuver must also be modeled mathematically and can be specified by various mathematical representations. The selection and development of a parametric maneuver model for defining the conceptual design maneuver space is derived and discussed during implementation.

After the appropriate ranges are selected to encompass the design variability, the total number of simulations must also be determined. The number of runs is based on experience and knowledge of the problem and determining the appropriate number is commonly an iterative process. Previous literature notes that dynamic simulation is computational expensive, thus, it is essential to use as few experimental runs as possible to accurately describe the design space. The number of runs is selected using Design of Experiments, which is a structured methodology for selecting experimental runs such that

the most information can be gathered for the least number of runs. This enables much less computational burden than pure random sampling of the design space that is common among Monte Carlo techniques [158].

Once the models are generated and the inputs defined, the simulation environment is used to determine the trim solution. This portion of the analysis does not require the entire maneuver definition, only the initial steady-state conditions. The trim solutions are used to verify that the system model is closely approximating the actual system. Solver selection and constraint variable determination must be made during this step. The solver is the main contributor to the robustness, computational efficiency, and accuracy of the simulation.

The second step of the simulation environment performs dynamic analysis of the system attempting to perform the defined maneuver. The important technique enabling NOE maneuver analysis independent of control design is inverse simulation. The results of this simulation are then compared to actual helicopter flight test data. The simulation captures the change in maneuverability characteristics resulting from the variation in design parameters. The failed runs are not discarded because they represent the cutoff between the feasible and infeasible maneuver and design combinations, which allows for important design trades.

Additionally, inverse simulation requires constraints for satisfactory optimization of the solution. Depending on the application, the designer may wish to constrain any combination of position, velocity, acceleration, or orientation. These constraints can be

placed on any state or control variables; however, selection of the appropriate constraints should be done with extreme care. All of these issues are problem specific and are discussed during implementation.

The final element of the process is based on a Monte Carlo data filtering technique that permits real-time and traceable design space exploration with changing constraints and requirements. The Filtered Monte Carlo (FMC) method uses a database of previously computed maneuverability information. All prior rotorcraft dynamic analysis techniques applied constraints into the mathematical definition of the vehicle; however, this formulation allows constraints to be dynamically placed on design variables and performance measures. As a result, the designer can view the impact of these constraints real-time rather than being required to run an entirely new set of optimizations. Filtered data techniques allow for visual verification of trends in the data that can be helpful with validation purposes and provides traceability for developing understanding of the problem. Furthermore, FMC is robust and enables integration of the complex helicopter EoMs.

2.3.3 Hypothesis

The key components of the hypothesized method are discussed here briefly to show how the need is being addressed. The first characteristic is fulfilled by the combination of a mathematical rotorcraft model and inverse simulation techniques. By integrating these two components, the maneuverability of rotorcraft vehicle can be captured quantitatively. Additionally, by using a six degree-of-freedom rigid body rather

than only the energy-based formulation, which is implemented in previous design efforts, more conservative maneuverability estimates are captured. The rotorcraft model is parametric such that, the design variables can be easily adjusted to view the impact on maneuverability due to changing design variable settings. In addition to fulfilling the dynamic analysis requirement, inverse simulation also allows the maneuverability to be calculated independent of control architecture. Finally, by specifying parameter ranges on the design variables of the parametric rotorcraft model, variability in dynamic performance can be captured and the impact of changing constraints can be assessed using the filtered data approach. Through combination of these components, the first hypothesis of this thesis work is established.

Hypothesis 1: A six degree-of-freedom rigid body parametric rotorcraft inverse simulation model in combination with Filtered Monte Carlo provides improved quantitative maneuverability tradeoff capabilities over traditional design methods.

2.3.4 Test Plan

The question as to what information is to be gathered through experimentation and analyzed through data filtering has yet to be fully addressed. The experimental information consists of both inputs to the environment and outputs that indicate dynamic maneuver and system characteristics. Inputs to the simulation environment consist of design parameter ranges and the maneuver definitions. The combination of these two pieces of information completely defines the context of each experimental run. The

model outputs appear at two levels within the simulation environment: trim analysis determination and dynamic motion simulation. Conducting dynamic motion simulation is dependent on whether a trim solution is determined in the previous step.

The trim condition is defined as steady-level flight at a constant forward velocity, which is specified in the maneuver definition. Some design parameter combinations may not have a trim solution. The failure to determine a trim condition can result due to no solution existing or can result due to inability of the optimizer to determine the solution. The inability to converge on the solution results from nonlinearities and nonconvexities within the mathematical representation [159]. The optimizer's convergence properties are dependent on the algorithm. A failed trim case does not necessarily mean that no solution exists. This emphasizes the importance of selection of optimization algorithm on the simulation results. If a trim condition is determined, the state and controls that provide this solution are stored, while an additional variable tracks the experimental runs that failed.

Once the trim solution is determined, the dynamic simulation of the vehicle may be conducted for the specified maneuver. All the states, controls, and auxiliary variables, such as torques and powers, are calculated at each time step as the specified path is followed. As a result, a large amount of data is created during simulation. All of which is not necessary in the data analysis portion of the process. Hence, the parameters of interest are extracted from this data, which include maximum and minimum control deflections, states, torques, and required powers. Obtaining the control deflections and the required powers enables trades that demonstrate the benefits of including rigid body system

models for determining conservative maneuver limit estimates. Within this analysis framework, both time and maximum acceleration are specified as inputs. The feasibility of a maneuver is determined by whether a set design completes the entirety of the maneuver. If at any point during the maneuver, the system cannot follow the prescribed path due to system limits, the simulation is terminated. A failed run during simulation versus during trim calculation are very different and are tracked separately.

The experimentation is divided into four subparts. First, the maneuver success criterion is examined. This set of experiments are investigated to show that the established process is capable of determining the design and maneuver combinations that are feasible. This is essential in order to prune the design space for analysis of only the feasible simulations. Second, the energy-based filters are applied to the feasible design space and the impact on both the trim space and the maneuver space are investigated. Third, the rigid body filter is applied to the maneuver space to show that improved maneuverability estimates are achieved through application of the parametric rigid body equations into the maneuverability analysis framework. Finally, the pop-up maneuver is examined and the filtering process is applied to determine the minimum time maneuver. Further analysis is shown that relates the design and maneuver performance to the applied constraints to enable robust design down selection. Through completing the series of experiments, the hypothesis is substantiated.

2.4 Implementation

The proposed process consists of four major steps, which are presented with regards to the rotorcraft problem in this section. The first step of the process is the

gathering of the design information, which includes the baseline vehicle and maneuver. The model development is presented second, which includes the technical derivation of two different fidelity system models for conceptual design. The first model is based on the energy approach, while the second utilizes the rigid body equations of motion. The integration of the parametric rigid body six degree-of-freedom helicopter model into a design and maneuverability analysis framework is a contribution of this work. In addition to helicopter model development, the maneuver model is established for a common helicopter maneuver that is validated against literature and flight test data. Following the maneuver selection, an argument for mathematical formulation is discussed. The maneuver proposed in this work simplifies the maneuver definition such that it can be easily integrated into the design process, this is the second original development shown in this contribution. Third, important criteria regarding solver algorithm and constraint variables selection for the inverse simulation technique are presented. Differences in the trim algorithm and the dynamic simulation methods are discussed. Verification and validation of the algorithms is then provided. Finally, the FMC technique is introduced, which enables the designer to apply various constraints on the design space and view the impact of requirements on both input and output parameters real-time.

2.4.1 Problem Formulation

As stated by Chipperfield [23], “design problems seldom start completely from scratch” and many times the new design starts from the previous design exercise. Using this information, thirteen input parameters associated with the AH-1 helicopter, originally investigated in Kim [20], were selected for investigation within the helicopter modeling

framework, which are described in detail in Prouty [49, 160, 161]. One of the parameters that is defined in Kim's analysis was directly related to power available. This variable is removed from the analysis in this work by dynamically applying it as a constraint during post processing. The resulting twelve parameters of interest are presented in Table 2.1 with the ranges selected to represent the various AH-1 configurations. These ranges can be narrowed through the use of dynamic constraints as configurations are removed from the design space.

Table 2.1: Input Parameters and Ranges for Screening

Variable Name	Unit	Baseline	Lower	Upper
Main Rotor Diameter	ft	48	46	52
Main Rotor Chord	ft	2.75	2.4	2.8
Main Rotor Tip Speed	ft/s	780	770	790
Tail Rotor Diameter	ft	9.5	8.5	10.5
Tail Rotor Chord	ft	1	0.8	1.2
Tail Rotor Tip Speed	ft/s	740	730	750
Vertical Fin Area	ft^2	18.5	16.5	20.5
Horizontal Tail Area	ft^2	11	11	15
Vehicle Mass	lb	10000	10000	15000
Tail Rotor Moment Arm	ft	45.8	45	46.7
Main Rotor Hinge Offset	%R	0	0	0.1
Center of Gravity	ft	16.25	15	16.7

Often times in design many variables are included in the analysis, all of which are not essential to capturing the variability of the response. A common technique for pruning the design space to a few of the most important variables is through the implementation of a screening test. A screening test is a procedure in which a minimal set of experiments are defined using the ranges of the input variables [162]. In Kim [20] the results are run through the simulation environment and then analyzed through the use of

Paerto Analysis to determine the parameters that contribute the most variability to the response.

A summary of the results presented by Kim [20] are shown in Figure 2.9, which represents the variability impact of the input parameters on the dynamic response for the pop-up maneuver. The variable names are listed on the left of the plot and the bars represent the percent of the variability in response that results from each parameter. The variables are listed in terms of importance, with main rotor diameter being the most important parameter and accounting for over 20% of the variability. The top six parameters incorporate close to 90% of the variability in the performance. Common procedure is to select the parameters that account for close to 80% of the variability; however, since there is a clear cut-off at the top six parameters, 90% was used.

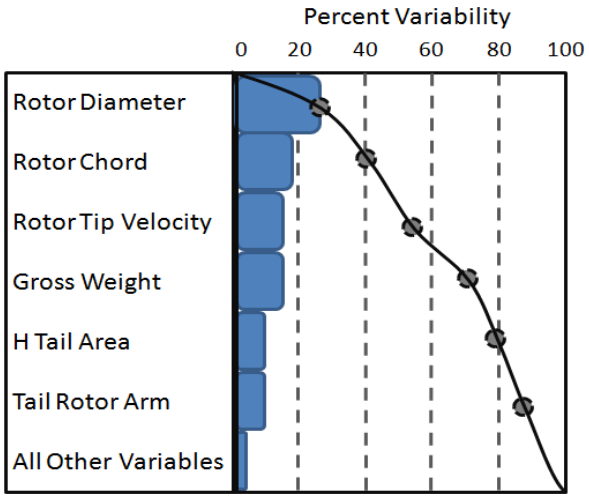

Figure 2.9: Summary of Paerto Analysis

The most important parameters determined through the implementation in Kim [20] are utilized in this work. The six design parameters that are important to capturing

the variability in maneuver performance are: main rotor diameter, main rotor chord, main rotor tip velocity, vehicle mass, and area of the horizontal tail. In addition to these parameters, this analysis also includes Center of Gravity (CG) location, which was not captured in the previous analysis effort by Kim but is known to be important to the response. The inputs and ranges selected are displayed in Table 2.2. One additional note is that the CG location and the tail rotor moment arm are specified in distance from the nose. Traditionally, the distance would be specified relative to the CG but since it is a variable in this analysis, this definition was more easily implemented.

Table 2.2: Design Parameters and Ranges

Variable Name	Symbol	Unit	Baseline	Lower	Upper
Main Rotor Diameter	DMR	ft	48	46	52
Main Rotor Chord	C	ft	2.75	2.4	2.8
Main Rotor Tip Speed	VT	ft/s	780	770	790
Vehicle Mass	MASS	lb	10000	10000	15000
Horizontal Tail Area	ST	ft^2	11	11	15
Tail Rotor Moment Arm	TRSTA	ft	45.8	45	46.7
Center of Gravity	CG	ft	16.25	15	16.7

2.4.2 Mathematical Model Development

Only two mathematical models are required in order to address the research objective: a vehicle model and a maneuver model. However, the model development stage consists of three separate tasks for this analysis. The first task is the development of the energy-based system model. This formulation is included to show that it does not provide the adequate fidelity to apply the necessary constraints; hence, requiring the rigid body formulation. After the energy-based model is derived, the rigid body formulation is

presented. The rigid body formulation includes all of the energy-based equations in addition to the equations of motion, which include the necessary states and controls. It is shown that although the rigid body model is considered a relatively simple model, the helicopter EoM are complex and require multiple optimization loops within the formulation. The assumptions are documented throughout derivation of the rigid body equations. Finally, the maneuver model is discussed, which includes a discussion on the selection of a maneuver that is validated using literature and flight test data. Derivation of the mathematical representation of this maneuver is presented and the velocity and path descriptions are shown.

2.4.2.1 Energy-Based Formulation

The energy-based model for the system is derived from the point mass assumption, which greatly reduces the complexity of the helicopter model. Because of this assumption, the problem reduces to an excess power calculation for each maneuver under consideration. The excess power is the difference between power available, which is based on the engine properties, and the power required, which is based on the helicopter drag properties. In the formulation applied in this work, the power required is decomposed into three major contributors: profile, induced, and parasitic. These powers correspond to different aerodynamic and geometric properties of the design, each of which is explained through decomposition of the variables within the mathematical approximation. Profile power includes the losses associated with the rotor properties and the theoretical relationship is developed from blade element theory by Glauert and

Bennett. The profile power coefficient with a uniform blade chord is expressed in Equation 2.2.

Equation 2.2: Profile Power Coefficient Equation

$$C_{Po} = \frac{\sigma C d_0}{4\pi} \int_0^{2\pi} \int_0^1 \left(\frac{U}{\Omega R}\right)^3 dr\, d\psi$$

The U represents the resultant velocity at the discrete element. The remaining parameters are properties of the rotor blade system where σ is the rotor solidity, Cd_0 is the profile drag coefficient of the airfoil, R is the radius of the rotor blade, and Ω is the rotational speed of the rotor blade. Through neglecting the radial component of velocity and integrating the expression, Equation 2.3 is derived. The variable K varies depending on the model assumptions and approximations; while a fixed value of 3 is a valid approximation for this analysis [44].

Equation 2.3: Profile Power Coefficient Approximation

$$C_{Po} = \frac{\sigma C d_0}{8}(1 + K\mu^2)$$

The profile power can then be determined from the profile power coefficient by re-dimensionalizing the problem. The formulation used for profile power in this work is presented in Equation 2.4, where ρ is the density of air, VT is the rotor tip velocity, A is the rotor disk area, and μ represents the inflow velocity. Inflow velocity is a function of rotor tip velocity and freestream velocity.

Equation 2.4: Profile Power

$$P_{profile} = \frac{\sigma C d_0}{8}(1 + K\mu^2)\rho(V_T)^3 A$$

The second power developed in this formulation is induced power. Induced power is derived from simple 1-D momentum theory and can be approximated using Equation 2.5. The variable κ is an empirical correction for tip losses and nonuniform inflow and it ranges in values from 1.15 to 1.25. The induced power is also a function of thrust, T, and induced velocity, v_i.

Equation 2.5: Induced Power

$$P_{induced} = \kappa T v_i$$

The third and final power component within the power required breakdown is parasitic power, which results from viscous shear effects and flow separation on the fuselage and rotor hub. The parasitic power is approximated by specifying the combination of rotor and airframe drags as a reference area, S_{ref}, and a corresponding drag coefficient, C_{df}. The equation for parasitic power is represented in Equation 2.6.

Equation 2.6: Parasitic Power

$$P_{parasitic} = \left(\frac{1}{2}\rho(V_\infty)^2 S_{ref} C_{df}\right) V_\infty$$

Power available is the result of engine properties at speed and altitude and sometimes includes a component of lift depending on the configuration. The lift component is ignored in most conventional helicopter conceptual and preliminary

analyses. Power available is relatively constant with altitude for conventional rotorcraft systems.

An example application of the energy-based method equations is shown by analyzing the rate of climb calculation. When the simulation is run, a corresponding acceleration is required at each time step in order to complete the specified maneuver. The ability of the system to accelerate is calculated in Equation 2.7, which uses the power required equations previously developed to determine the rate of climb. It may be observed that if either the power required or the weight is too large, then the power available will not permit acceleration and the maneuver cannot be completed. Due to the mass assumption, variables related to the controllability of the vehicle do not appear in the expression.

Equation 2.7: Rate of Climb Calculation

$$R/C = \varepsilon_{efficiency} \frac{\left(P_{available} - P_{required}\right)}{W}$$

2.4.2.2 Rigid Body Formulation

The rigid body formulation includes all of the previous power decomposition equations in addition to the helicopter EoM. The rigid body EoM are first order differential such that the state derivatives may be determined by the current state and control settings. The state vector is the minimum set of variables required to uniquely define the system motion throughout time. The number of states of the system can vary depending on the model fidelity, simplifying assumptions, and the number of subsystems

included in the analysis. Unlike the energy-based approach, the rigid body formulation includes the necessary control actuation information [163]. The EoM are derived in body frame coordinates in this work; however, conversion to a Newtonian frame is required in order to apply the laws of motion.

Although more complex than the energy-based approach, some assumptions, which are discussed during derivation of the EoM, are required in order to make the rigid body formulation tractable for conceptual design. Derivation of the rigid body EoM for the helicopter starts with Euler's equations; however, the buildup progresses more smoothly if the forces and moments corresponding to the various helicopter components is presented first. The formulation progresses by separating the helicopter into four components: main rotor, tail rotor, fuselage, and wing and tail. The main rotor is the primary force and moment generating component of the helicopter and is also the most complicated mathematically. The tail rotor equations follow which use similar techniques as the main rotor derivation. Third, the fuselage components are modeled and simplifications are provided. Finally, the wing and tail components contribution to forces and moments are presented. The wing and tail are lumped into one derivation since the forces and moments are calculated using the same procedures.

2.4.2.2.1 Main Rotor

An optimization needs to be performed in order to determine the forces and moments generated by the main rotor because of the coupling effects. This optimization loop generally starts with either an initial guess of thrust coefficient, CT, or tip-path plane

inflow ratio, λ. Inflow velocity ratio is defined as the ratio of induced velocity to rotor tip velocity. The specification of λ rather than CT was found to be more stable and offer faster convergence properties for the equations applied. Within the iteration loop, the inflow velocity is iterated upon in order to find a CT value for the main rotor. Equation 2.8 displays the relationship between inflow ratio and thrust coefficient. All of the rotor equations were developed by Hennis and McCormick [164] and are re-presented here for completeness. These equations have been used in several literature references and are commonly implemented in software packages for analyzing maneuverability for a fixed helicopter design.

Equation 2.8: Thrust Coefficient

$$CT = \frac{a_{0inc}\sigma}{2}(\lambda * T1 + \theta_0 * T2) + \left(\theta_2 - K_\beta * B1\right) * T4$$

The T1, T2, and T4 coefficients in Equation 2.8 are based on rotor properties, which are a function of freestream and rotor tip velocity. The other rotor variables are a_{0inc}, which is rotor lift curve slope at zero incidence, and rotor solidity, σ. The value of rotor solidity is dependent upon the number of rotor blades, the blade chord, and the rotor radius. The two control variables appear in this formulation of the CT equation: main rotor collective, Θ_0, and longitudinal cyclic, Θ_2. The lateral flapping, B1, comes into the equation through multiplication of K_β, which is a term that indicates the measure of coupling between the longitudinal and lateral modes. After a value for CT is obtained, a subsequent tip-path plane inflow velocity is calculated using Equation 2.9. At low speed

the tip-path plane inflow ratio is mainly due to induced velocity, while at higher speeds it is dominated by the helicopter parasitic drag.

Equation 2.9: Tip-Path Plane Inflow Ratio

$$\lambda_{new} = \frac{CT}{2 * \sqrt{(\mu^2 + \lambda^2)}} + \frac{\mu^3 S_{ref}}{2CT}$$

This iteration loop continues until λ_{new} is equal to λ_{old}. As mentioned previously, helicopters have a high degree of cross coupling due to rotor dynamics. Hence, it is not practical to simulate the longitudinal and lateral rigid body dynamics separately, but some of the higher order effects may be ignored [165]. For instance, the inertial coupling between the rotor and fuselage is very complicated. Fortunately, ignoring this coupling by assuming a first order-path-plane dynamic model that incorporates the first order longitudinal and lateral flapping coefficient dynamics with a quasi-steady inflow model has been shown to provide satisfactory results [166]. This limits the model's ability to capture aerodynamic properties associated with Mach number variation, three-dimensional blade tip effects, or retreating blade stall. Rutherford [167] states that although these assumptions are applied "this model has provided useful and valid results [168] for a wide range of applications." This formulation is applied by Celi [57], who indicates that "this is an acceptable assumption as firstly, blade flap motion is much more influential in terms of predicting blade loads and the blade dynamics are much faster than those of the body modes."

The physics of bladed flapping are relatively basic; however, when all the harmonics are combined, the resulting motion can be highly complex. Commonly, the blade motion is explained via decomposition into the major contributing analyses presented by Gessow and Myers [44]. In addition to the thrust coefficient and inflow ratio equations, the longitudinal flapping, lateral flapping, and coning angle equations are also included in the optimization loop due to the coupling. Equations 10-12 represent these calculations where again the A, F, and B variables are based on uniform inflow and linearly twisted blade assumptions. It can be observed that all of the equations are highly dependent upon one another, thus, making convergence to a solution a non-trivial exercise.

Equation 2.10: Rotor Coning Angle

$$\beta_0 = \gamma\left(\lambda * F1 + \left(\theta_0 + K_\beta * \beta_0\right) * F2 + \left(\theta_2 - K_\beta * B1\right) * F4\right) - \tau$$

The coning angle represents the average part of the flapping motion that is independent of time and blade azimuth angle. The coning angle equation results from the moment balance about the flapping hinge from a combination of aerodynamic and inertial forces. The centrifugal loads on the blade remain constant for a fixed rotor speed, while the aerodynamic relationship is much more complex and varies with lift distribution. The coning angle is proportional to the induced velocity, which is a function of forward velocity. The variable B1 represents the lateral flapping and τ represents the blade mass impact on the centrifugal force due to the rotating system. Lock number, γ represents the ratio of aerodynamic to inertial forces of the rotor system.

Equation 2.11: Longitudinal Flapping

$$A1 = \lambda * A11 + \left(\theta_0 + K_\beta * \beta_0\right) * A12 + \left(\theta_2 - K_\beta * B1\right) * A14$$

The longitudinal flapping equation, Equation 2.11, represents the amplitude of the pure cosine flapping motion, which may be viewed as the fore aft tilt of the rotor tip-path plane. Dissymmetry in the lift produced between the advancing and the retreating sides of the rotor disk are created during forward flight because the advancing blade confronts a larger dynamic pressure. The dynamic pressure on the retreating side of the blade causes the blade to flap downward, which increases the effective angle of attack that results in increased lift. Figure 2.10 [44] displays the effect on tip-path plane due to longitudinal tilt and coning together.

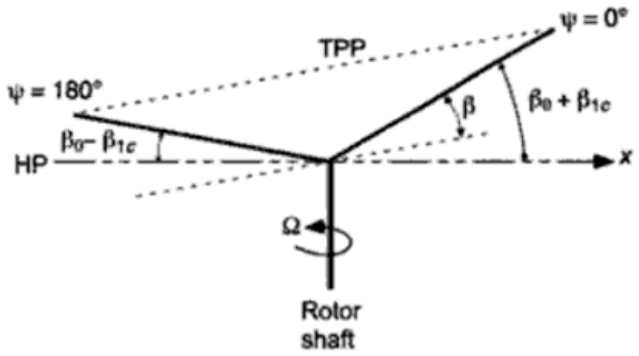

Figure 2.10: Longitudinal Flapping

The fourth equation within the optimization loop is the lateral flapping, which represents the amplitude of the pure sine motion. The resulting amplitude variation results in left-right tilt of the tip-path plane. During forward flight, the dynamics influence a tendency for the blade to tilt to the right when viewed from behind. With calculation of Equation 2.12 one loop through the optimization is complete.

Equation 2.12: Lateral Flapping

$$B1 = \beta_0 * B11 - \left(\theta_1 - K_\beta * A1\right)$$

When the optimization loop is converged, the values obtained can be used to calculate the total rotor thrust using Equation 2.13. The components of thrust in the various axis of the system can be determined by using the control setting and flapping results. Hence, the main rotor has force and moment contributions in all three axis of the body.

Equation 2.13: Rotor Thrust

$$T = \frac{1}{2}\rho A(VT)^2 CT$$

Some helicopter model formulations have applied assumptions that limit rotor maximum lift coefficient; however, as noted by Celi [41] "for typical current helicopter, actuator displacement and rate limits will be reached before the rotor max lift coefficient becomes the limiting factor." At the other extreme, including detail related with some of the actuator dynamics may be ignored for many flight mechanics applications. This is because the actuator time scale is much faster than the vehicle dynamics. This assumption results in the linear rotation of the control hinge being captured rather than the detailed electrical input to the valves/solenoid. This simplification is crucial since the fine scales of the actuator dynamics are not required at the early design stage, which results in great computational savings [37]. These assumptions can be viewed in the rotor flapping equations since the control rotational inputs are provided as inputs to the equations. Additionally, the rotor downwash can be calculated using the inflow ratio along with

geometric parameters that relate the location of the wing, fuselage, and tail relative to the rotor. The equations for these approximations may be viewed in Johnson [42].

2.4.2.2.2 Tail Rotor

The second component forces and moments that are derived are those relating to the tail rotor. Fortunately, all of the assumptions that applied to the main rotor calculations can be carried over into tail rotor analysis. In addition to following the same optimization process, the tail rotor flapping and coning can be ignored. Hence, the tail rotor thrust coefficient and inflow ratio are found by applying an optimization routine to Equation 2.14 and Equation 2.15. The forward velocity component of Equation 2.9 has been removed when applied to tail rotor analysis in Equation 2.15. The tail rotor thrust can then be calculated by using Equation 2.13, but replacing the rotor variables in the expression with the tail rotor properties.

Equation 2.14: Tail Rotor Thrust Coefficient

$$CTT = \frac{(a_{0incT}\ \sigma_T)}{2}(\lambda_T * T1T + \theta_T * T1T)$$

Equation 2.15: Tail Rotor Inflow Ratio

$$\lambda_{Tnew} = \frac{CTT}{2 * \sqrt{(\mu_T{}^2 + \lambda_T{}^2)}}$$

The tail thrust effects the forces and moments on the system through a couple methods due to its position relative to the center of gravity. The first and most straight forward effect of the tail thrust is a component of force in the y-axis of the body

coordinate system. In addition to this force, the tail is located a distance higher than the center of gravity location, which contributes to a rolling moment. Finally, the major contribution of the tail is the counter torque moment about the z-axis of the body that results due to being located a far distance aft of the CG location, which may be viewed in Figure 2.11 [169]. The engine torque is calculated using the power required equations and converting power to torque using the rotational rate of the main rotor.

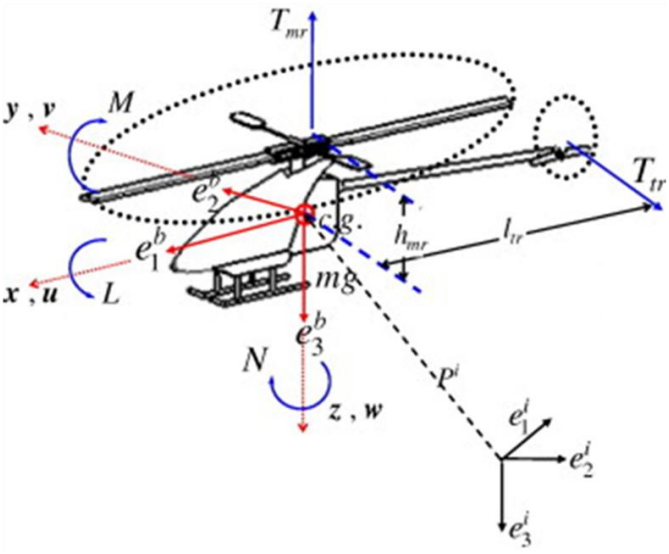

Figure 2.11: Tail Rotor Moment Contribution

2.4.2.2.3 Fuselage

The third component in the rigid body model development is the fuselage. It can be assumed that the only contribution of the fuselage is parasitic drag for conventional helicopter configurations. The other aerodynamic forces and moments are considered negligible due to the small magnitude in relation to other contributors. The fuselage drag equation is presented in Equation 2.16, where Q represents the dynamic pressure. Unlike

the energy-based formulation, the rigid body formulation requires this drag to be converted into vector quantities. This is done using state variables that are stored during each time step of the simulation. The transformation from the wind frame to the body frame is discussed in Etkin [163].

Equation 2.16: Fuselage Drag

$$Drag_{Fuselage} = Q * S_{ref}$$

2.4.2.2.4 Wing and Tail

The final components in the derivation of the EoM are the wing/tail forces and moments. Fortunately, the aerodynamic equations are simpler for non-rotating components, especially, for the flight maneuvers that are typically performed by helicopters. The tail lift and drag forces are assumed negligible compared to the forces produced by the fuselage and the rotor components. Therefore, the only contributions to the EoM from the tail are the moments resulting from the lift component of the tail, which produces a stabilizing moment in the pitch and the yaw axis because of the distance from the center of gravity. Equation 2.17 represents the formulation for calculating the lift and drag forces, while Equation 2.18 displays the moment equation. The moment equation is the equal to the force representation multiplied by the moment arm.

Equation 2.17: Wing and Tail Forces

$$Forces = Q * S_w * CL_w$$

Equation 2.18: Wing and Tail Moments

$$Moments = Q * S_w * CL_w * \bar{C}$$

Figure 2.12 displays the method for converting the aerodynamic forces on the wing and tail surfaces from the wind reference frame into the body reference frame. A similar method is applied to convert the fuselage forces. It may be observed that the angle of attack, α, is the only variable that is required for this conversion in the longitudinal, while side slip, β, is required in the lateral forces and moments conversion.

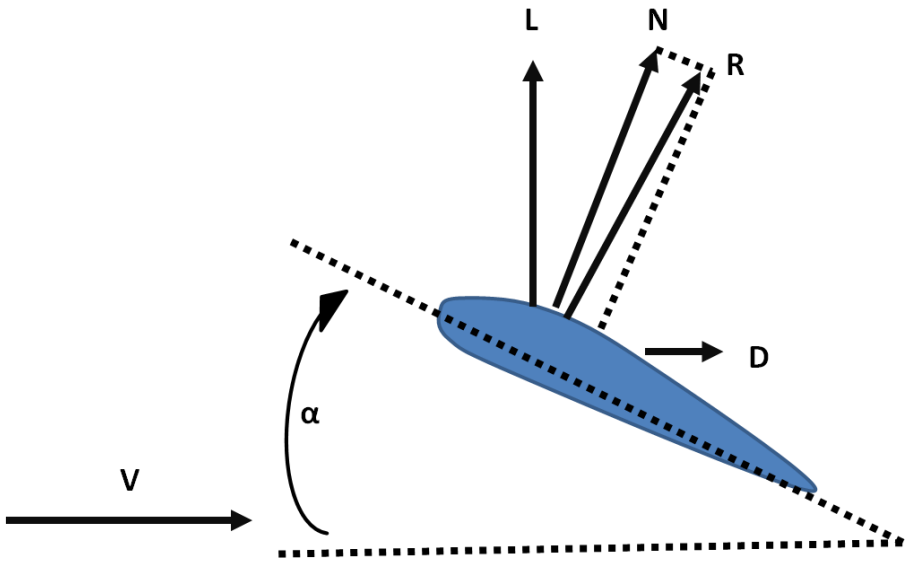

Figure 2.12: Wing and Tail Resultant

2.4.2.2.5 Integrated Components

The equations derived in this section are combined to form the EoM of the conventional helicopter. The resulting states of the system are position, linear velocity, angular velocity, and orientation. The controls are collective, longitudinal cyclic, lateral

cyclic, and tail collective. The equations derived are used to calculate the resulting accelerations of the system for given state and control combinations. By combining this model with an integration routine, the resulting motion can be calculated and observed, while the power information is also calculated during each time step. Hence, the energy-based approach results are included in the rigid body formulation.

The focus of this work is to develop a process that enables integration of maneuverability assessment with conceptual design. As a result, the elements of the process have been selected for conceptual design studies when higher fidelity modeling is sacrificed for design space exploration capabilities. The assumptions involved in the derivation of the simple rigid body helicopter limit maneuverability analysis to specific types of maneuvers. For example, the quasi-steady inflow assumption only applies to smooth maneuvers; hence, analysis breaks down when applied to aggressive maneuvers such as barrel rolls and transient maneuvers such as quick hops. Additionally, many of the characteristics associated with agility cannot be analyzed with the simple rigid body model. The various assumptions associated with the power equations provide further limitations regarding detailed lift distribution effects on the rotor blades, which hinders the model's ability in predicting loads resulting from Mach number and three dimensional effects. The elements of the process may be replaced with higher fidelity analysis techniques that enable analysis of both high speed and low speed transient maneuvers as computational capabilities increase or the design progresses into the later design stages.

2.4.2.3 Maneuver Model Formulation

Future autonomous vehicle operations in urban and battlefield environments will require extremely agile airborne platforms to perform their missions. Many authors consider model-based approaches for evaluating maneuvering performance [45, 170-172]. Remarkably, even for aggressive maneuvers such as barrel rolls, Piedmonte [173] shows that consistent paths are followed during piloted operation, hence mathematical modeling of NOE flight is a valid approach. In recent years an attempt has been made in developing a set of maneuver development and evaluation criteria that resulted in the Aeronautical Design Standards (ADS). The ADS-33 maneuver definitions are stated as a set of criteria that the helicopter must satisfy rather than a precise trajectory that the helicopter must follow [41]. The goal of the ADS-33 requirements is "to provide an overall assessment of the rotorcraft's ability to perform certain critical tasks [21]." One major concern for integration of the conceptual design is the manner in which the maneuvers are defined, as a result, multiple optimum solutions may exist for a single prescribed maneuver [24].

One of the major focuses of this research is to develop a relationship between design parameters and maneuver performance. As a method of controlling the size of the design space and removing some of the variability in the optimum solution path, the path must be defined directly rather than through constraints [36]. Cao [174, 175] was able to express the helicopter maneuver space by specifying flight motion conditions mathematically through a polynomial fit. It turns out that at least a fourth order polynomial is required to insure smoothness when defining the position. This means that

at least 5 parameters are required to define the path; furthermore, it is difficult to visualize the resulting path by seeing the coefficients alone. An example of a pop-up maneuver expressed through a fifth order polynomial is presented by Cao [33] and is shown in Equation 2.19.

Equation 2.19: Polynomial Maneuver Model

$$Position = 0.0064t^5 - 0.1249t^4 + 0.6452t^3 \qquad 0 \leq t \leq 7.7472$$

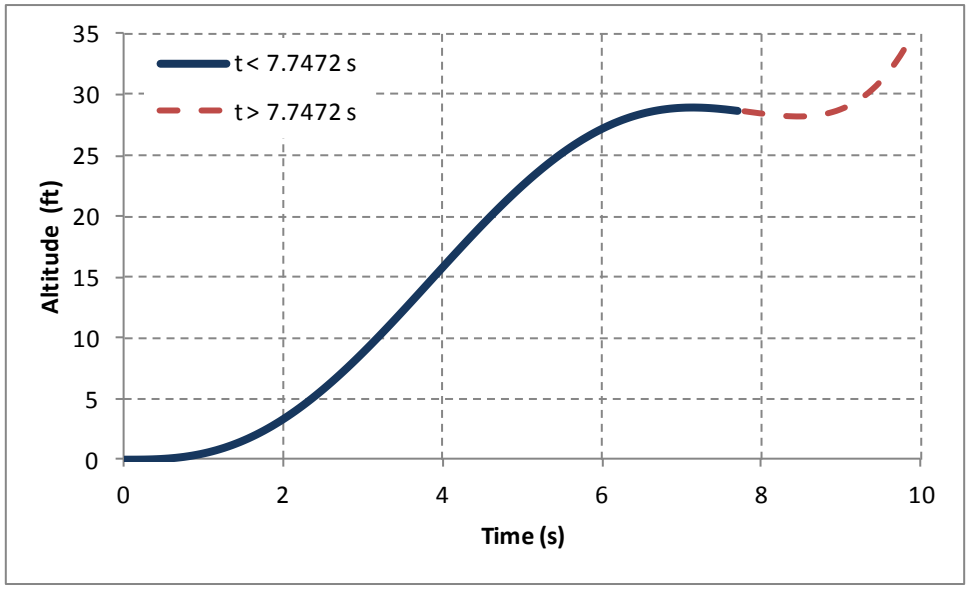

Figure 2.13: Resulting Polynomial Path

The polynomial function presented in Equation 2.19 is defined on the time interval from 0 seconds to 7.7472 seconds. The coefficients are selected such that the path is a smooth pop-up maneuver with an increase of 30 feet in altitude. The path may be observed as the smooth solid line in Figure 2.13. One difficulty in defining the maneuver using the polynomial representation is that the resulting path is very difficult to visualize by only viewing the coefficients. Additionally, beyond the final time of 7.7472

seconds the function doesn't have a well behaved form as indicated by the dashed line. This may create problems when attempting to stitch maneuvers together or when changing the total time for the maneuver.

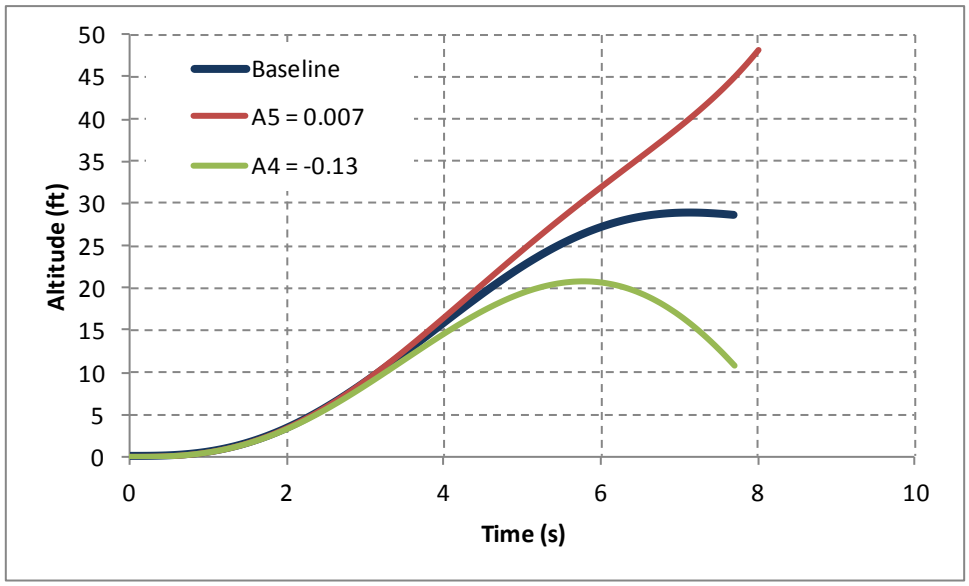

Figure 2.14: Polynomial Path Sensitivity

Another major issue when defining the maneuver through a polynomial representation is that the polynomial shape is very sensitive to the coefficients; thus, the resulting path can change significantly through small changes to the coefficients. Figure 2.14 presents these findings by showing the baseline maneuver compared to two other drastically different maneuvers that are defined by small changes from the baseline. Changing the A4 coefficient from -0.1249 to -0.13 maintains the appropriate pop-up path shape over the timeframe from 0 to 5.8 seconds. However, the maneuver shape drastically changes when the A5 coefficient is adjusted from 0.0064 to 0.007. This demonstrates the large sensitivity of the path characteristics through minor variations in

the definition, which is not a desired quality. Furthermore, using this formulation to describe a general pop-up maneuver description is extremely difficult.

Cao [33] developed a trigonometric function that is much easier to understand and provides the same level of smoothness that is required to eliminate numerical error associated with the zero order dynamics. This description uses the combination of two different cosine functions to describe the path. Two concerns are determined through analyzing this definition. By defining the maneuver by position rather than velocity a greater amount of numeric instability is introduced because an additional stage of differentiation is required. Also, the body frame velocities can change at the rate of the faster rotational dynamics; hence, much benefit is achieved by using navigation frame coordinate system for maneuver definition.

With the previous observations and assumptions a new maneuver model formulation is required for conceptual design and maneuver analysis. The maneuver model derived in this work is defined via a single trigonometric function of linear velocities in the navigation frame along with a yaw rate constraint. For more information on the navigational reference frame see Etkin [163]. An example mathematical maneuver for a pop-up is shown in Equation 2.20. The vertical velocity is defined as a function of current time, final time, and maximum velocity. As opposed to the polynomial representation that requires at least 5 input variables, this representation only requires two inputs: maximum velocity and final time. The pop-up maneuver is selected to show the usefulness of the proposed technique, while additional maneuvers are addressed in Chapter 4 of this dissertation.

Equation 2.20: Mathematical Model Representation

$$Velocity = \left(-1 * \cos\frac{t * 2\pi}{tf} + 1\right)\frac{V_{max}}{2}$$

The mathematical model representation using a single trigonometric function is presented in Equation 2.20, where the output velocity is in the vertical direction of the navigational frame. This is because the pop-up maneuver only requires a change in vertical velocity, while the lateral and forward velocities remain constant. Additionally, yaw rate is constrained to a zero value so that the helicopter is not rotating about the vertical axis while performing the maneuver. The velocity profile produced by Equation 2.20 is shown in Figure 2.15. The benefit of this functional representation is that the maximum velocity can be easily specified and the resulting motion is straightforward. For this example, the maximum velocity of the maneuver was specified to be 20 ft/s, which can be observed in Figure 2.15. Additionally, the simulation total time is specified as 10 seconds. Using this knowledge, it can be determined that the total altitude change of this pop-up will be 100 ft.

Figure 2.16 verifies these findings by displaying the resulting path of the defined maneuver. This model definition overcomes the detriments of the polynomial expression and requires fewer inputs than the trigonometric definition in Cao [33]. This novel maneuver function is derived because the curse of dimensionality is always a concern with aerospace design problems, especially with the integration of dynamic maneuverability assessment. The benefit of requiring fewer inputs is essential in

integrating the maneuverability analysis into a design framework since multiple designs and paths are analyzed during conceptual design space exploration.

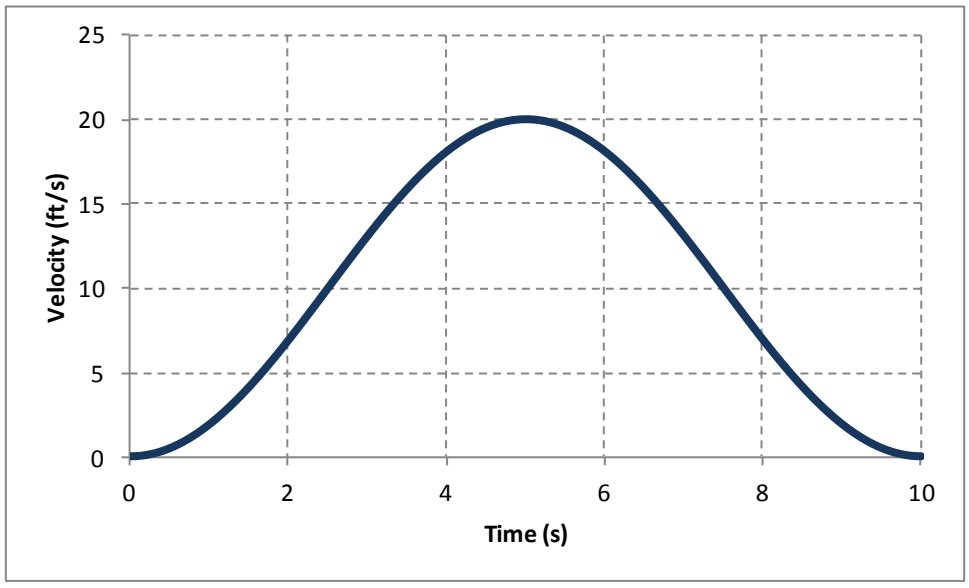

Figure 2.15: Velocity Profile

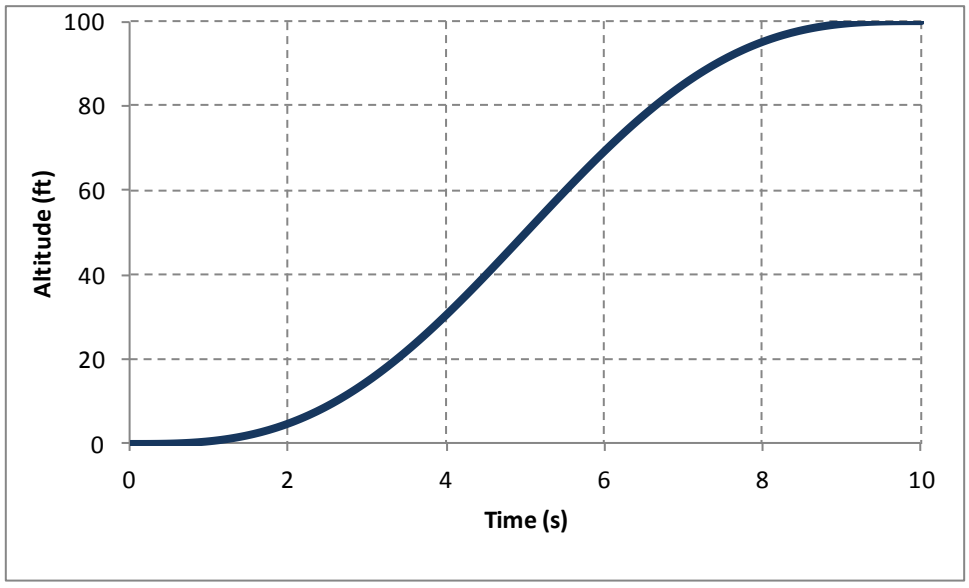

Figure 2.16: Pop-Up Maneuver Path

Figure 2.17 depicts the maneuver formulation's ability to easily model changes in velocity, which is accomplished by only changing V_{max} within Equation 2.20. In addition to the baseline maneuver, both a 15 ft/s and a 25 ft/s maneuver are shown. An additional benefit from this formulation is that the maximum velocity is defined independent from the maneuver time. Hence, V_{max} can be increased until the simulation fails for a given design and this velocity represents the maximum velocity maneuver that a design is capable of completing.

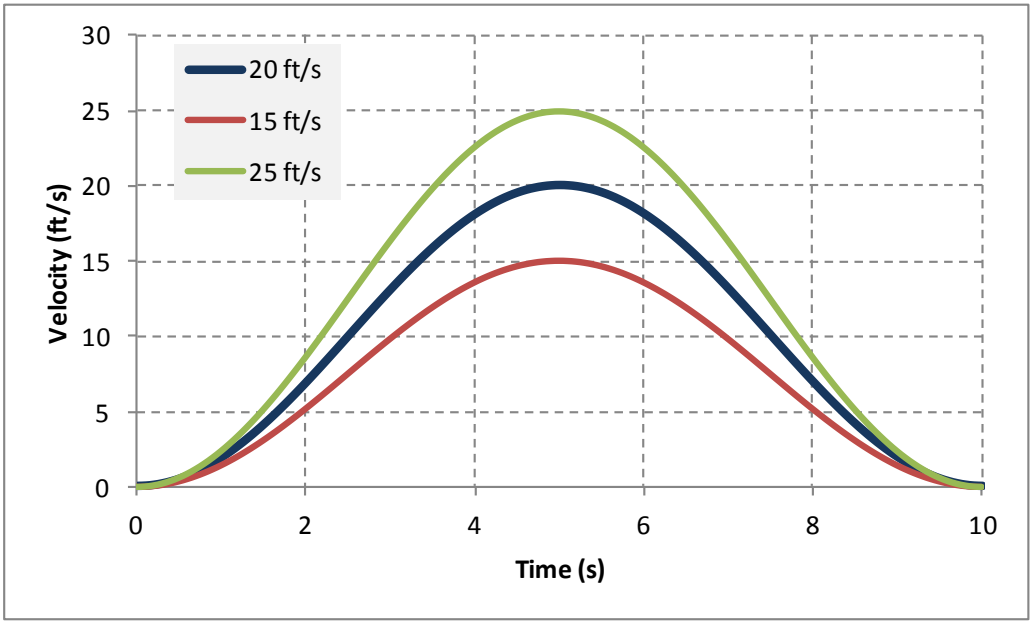

Figure 2.17: Trigonometric Definition – Velocity Variation

Conversely, the total time of the maneuver can be altered independently from the maximum velocity. Figure 2.18 displays the velocity function as the time is changed from 10 seconds to 12 seconds. It may be observed that the peak velocity of the maneuver is unchanged through this adjustment. This means that both final time and maximum velocity can be adjusted independently to easily define the maneuver that is required for

simulation. Determining the polynomial coefficients for previous maneuver definition techniques required more computational effort and expertise.

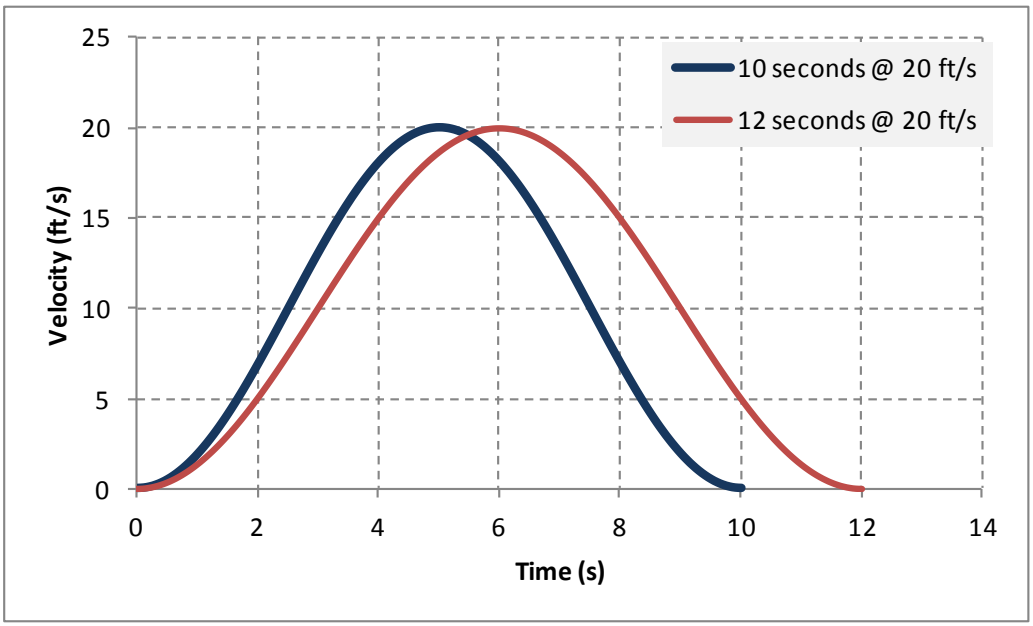

Figure 2.18: Trigonometric Definition - Time Variation

The combination of the maximum velocity and final time variables allow for the entire design space of pop-up maneuvers to be defined. For a fixed velocity and altitude, Figure 2.19 displays thirteen various pop-up maneuvers that can result by only varying the maximum velocity and the final time. With the variation in altitude and initial horizontal velocity, the entire pop-up maneuver space is captured, which was not possible with previous maneuver definitions.

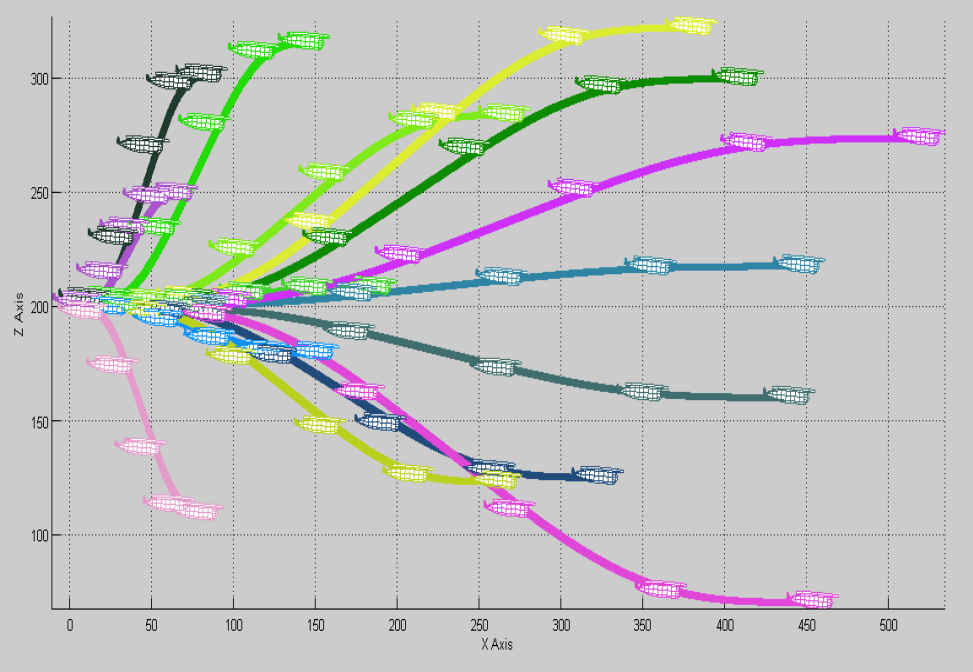

Figure 2.19: Pop-up Maneuver Space

2.4.3 Simulation

The setup of the simulation environment consists of two major tasks since integration based inverse simulation was selected as the appropriate method. The considerations stem directly from the process employed in basic flight mechanics formulations. First the trim analysis is conducted for the initial flight conditions, then inverse methods are applied to simulate the maneuver. Both of these steps require an optimization algorithm for solving for the states and controls required to either trim or follow the defined path, respectively. For this reason, the selection of the optimization algorithm is first discussed, which is followed by a detailed description of how the trim and maneuver analyses are conducted.

2.4.3.1 Optimization Algorithm Selection

As stated by Cox [176], "much research has been done to find computationally efficient methods to determine solutions within high dimensional, nonconvex design spaces." Both the trim solution problem and the path following problem are determining state and control combinations that result in a zero solution. In the trim case, the zero acceleration solution is determined, while the error in path is zeroed during path following. Deterministic optimization algorithms can be separated into two major categories when determining the zeros of a function: zero-order and first-order methods. Zero-order methods require only function evaluation knowledge and have a long history of successful application. Vanderplaats [177] states that "these methods are usually reliable and easy to program, often can deal effectively with nonconvex and discontinuous functions, and in many cases can work with discrete values of the design variables."

First-order methods require gradient information to be supplied, either by finite-difference computations or analytically, hence, first-order methods are termed gradient-based algorithms [177]. Aircraft trimming is often performed by gradient-based numerical algorithms originating from the field of nonlinear constrained optimization. Drawbacks to gradient-based methods result from the dependence on the function derivative calculation. As the number of variables and nonconvexity of the solution space increases, the computational expense of the derivative evaluations grows exponentially. Furthermore, local extrema points mitigate the algorithms' ability to find global optima. For this reason, multiple starting points are utilized; however, this does not guarantee that

the solution is found [68, 178]. Gradient-based algorithms have been applied to global optimization problems by utilizing various starting points [69]. Various journal articles have compared efficiencies for numerous multi-start global optimization algorithms [179].

The constraint oscillations that occurred during previous inverse simulation efforts were caused by the dynamic properties of the internal system and result from the optimizer jumping between solutions for each time step. Hence, both convergence tolerance and time step can have a large impact on the simulation results. Various techniques have been used in literature to mitigate these affects. Lu [180] uses the derivative-free Nelder-Mead optimization method to eliminate discontinuities associated with derivative-based methods. The author also suggests using sensitivity equation techniques [181] to remove singularities associated with the Jacobian matrix. De Matteis [137] uses a local optimization based on Sequential Quadratic Programming in combination with a global newton-raphson approach and Lee [182] applies equality constraints to optimization process. Celi [21] specifies a scalar minimization function and optimizes using the BFGS algorithm, while Cao [33] solves the path planning problem using nonlinear least squares optimization method.

The Nelder-Mead (NM) method, which is shown to be useful in inverse dynamics problems [183-185], and the nonlinear least squares (LSQ) method presented by Cao [33], which does not require a scalar minimization function, appear in research in recent years as the most effective optimization methods for determining trim solutions. The NM algorithm represents derivative free methods, while nonlinear LSQ represents derivative-

based optimizers. The effectiveness as applied to the helicopter simulation environment is tested in this section for both of these optimization algorithms.

The input variables and ranges in Table 2.2 are used to investigate each method's ability in determining trim solutions. The convergence criteria for each of the methods are slightly different because of the manner in which each optimizer operates; however, they have been selected to make the results comparable. Nelder-Mead optimization was set to exit the algorithm loop after reaching a maximum of 500 function evaluations or a function/input tolerance of 1e-17. On the other hand, the nonlinear LSQ method was set to exit when a maximum of 30 iterations or a function/input tolerance of 1e-17 was reached. Hence, both methods applied the same tolerance on function and input parameters. Because of the number of variables and the finite difference method used in the nonlinear LSQ algorithm, this resulted in a maximum of 500 function evaluations if all 30 iterations were performed. Each trim experiment was conducted for 200 different experimental design and pop-up maneuver combinations. Additionally, this was performed using an initial guess close to the solution and with only one starting point guess.

The nonlinear LSQ determined 199 trim solutions for the 200 runs meaning that the algorithm did not find the solution for only one case. The one non-converged run was rerun using multiple restarts and the trim solution was determined. The NM formulation did not determine any of the trim points within the optimizer option selected, although all points were converging to solution. The method is able to determine the trim solutions if this value is increased by approximately a multiple of five; however, the amount of time

for convergence is on the order of 1000 times slower than nonlinear LSQ method. Therefore, the nonlinear LSQ method was chosen as the optimizer in this work.

2.4.3.2 Trim Solution versus Path Simulation

Prior to performing inverse simulation, the initial trim conditions first need to be determined. Much work has been conducted in the area of developing general formulations for computing numerical trim values for a six-degree of freedom nonlinear models. Through analysis of the dynamic performance problem, a general approach to trim through minimization of a cost function as presented by DeMarco [186] is selected for this work. This method allows for integration of multiple models and provides the ability to both trim the vehicle in steady-state flight and calculate control settings to follow a prescribed path.

The process for determining the trim conditions for the simulation is shown in Figure 2.20. After the helicopter model parameters and the maneuver parameters are fully defined, the first step of the trim process is an initial guess for system states. Only nine states are included in this estimate, while the rotational rates (P, Q, R) and the heading (Ψ) are forced to be zero. The states relating to velocity components are provided in the body reference frame, while the maneuver definition specifies velocities in the navigational frame; therefore, these velocities are not the exactly the same and require a transformation. The transformation of the body frame velocities to navigation frame velocities is accomplished through knowledge of the orientation of the system.

Two variables from the maneuver model are used during the trim process: the altitude and the initial forward velocity in the navigation frame. The maneuver based parameters of final time and maximum velocity are ignored during trim. The states and controls are feed into the helicopter equations of motion, which calculates all 12 state derivatives. An optimization algorithm uses the state derivative information to iteratively change the state and control variables that drive the state derivatives to a zero value. The helicopter model contains two optimization loops within the EoM block, hence, as noted by Kato [187], "the solutions obtained from inverse simulation of the nonlinear EoM are not simple" [187]. Elgersma [188] comments on trimming the aircraft EoM: "When computing numerical trim solutions, it is difficult to know if all possible trim solutions have been found [188]." Additionally, the existence and number of trim solutions within the function space is not known a priori [186, 189].

The same process is applied during maneuver path following with two extensions, which are shown in Figure 2.21. The first extension is the inclusion of an integration routine within the analysis in order to track motion throughout time. The second issue that arises is due to the velocity information from the maneuver definition changing with time. The optimization algorithm depends on the function value for convergence, thus, the function value calculation must be updated as the maneuver progresses in time. The optimization algorithm no longer adjusts state information during path simulation and only has access to control changes. Additionally, the lesser number of degrees of freedom decreases the number of constraints that can be applied to only the three linear velocities and the yaw rate.

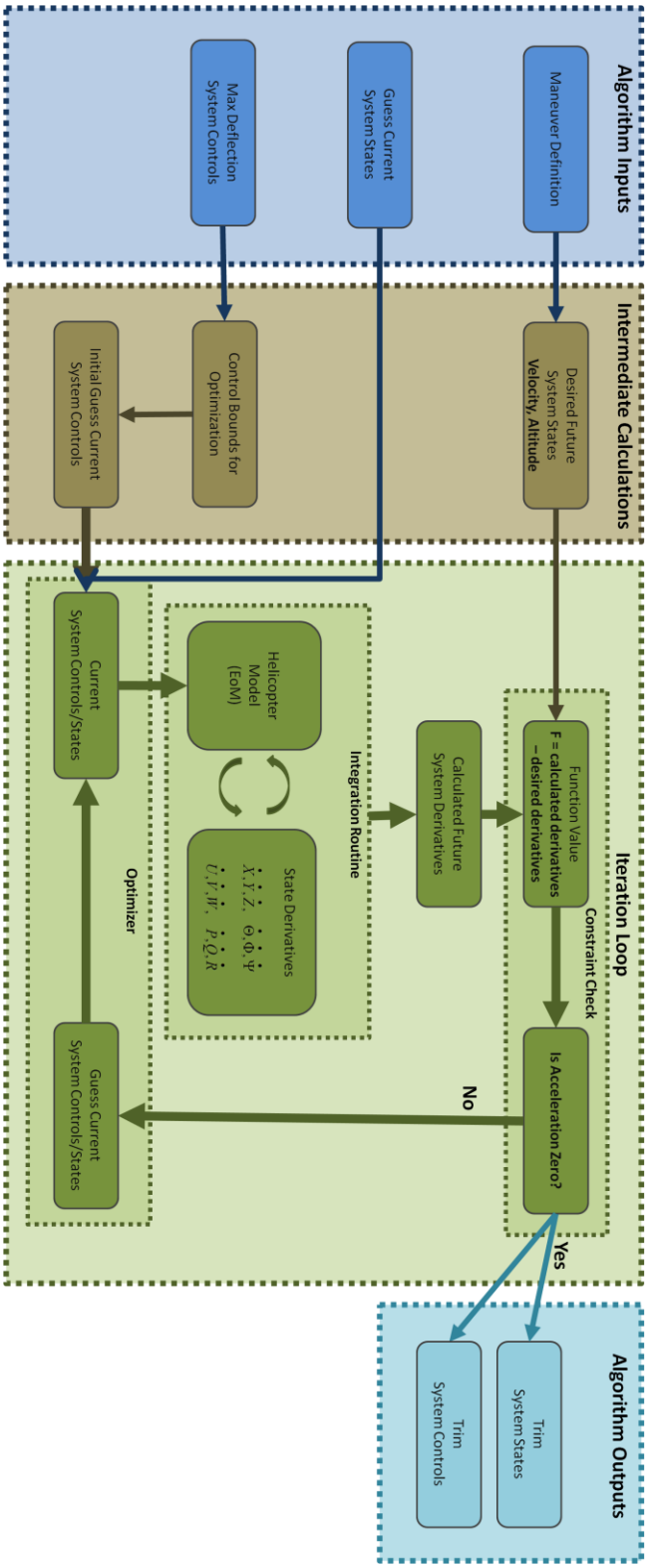

Figure 2.20: Trim Process Diagram

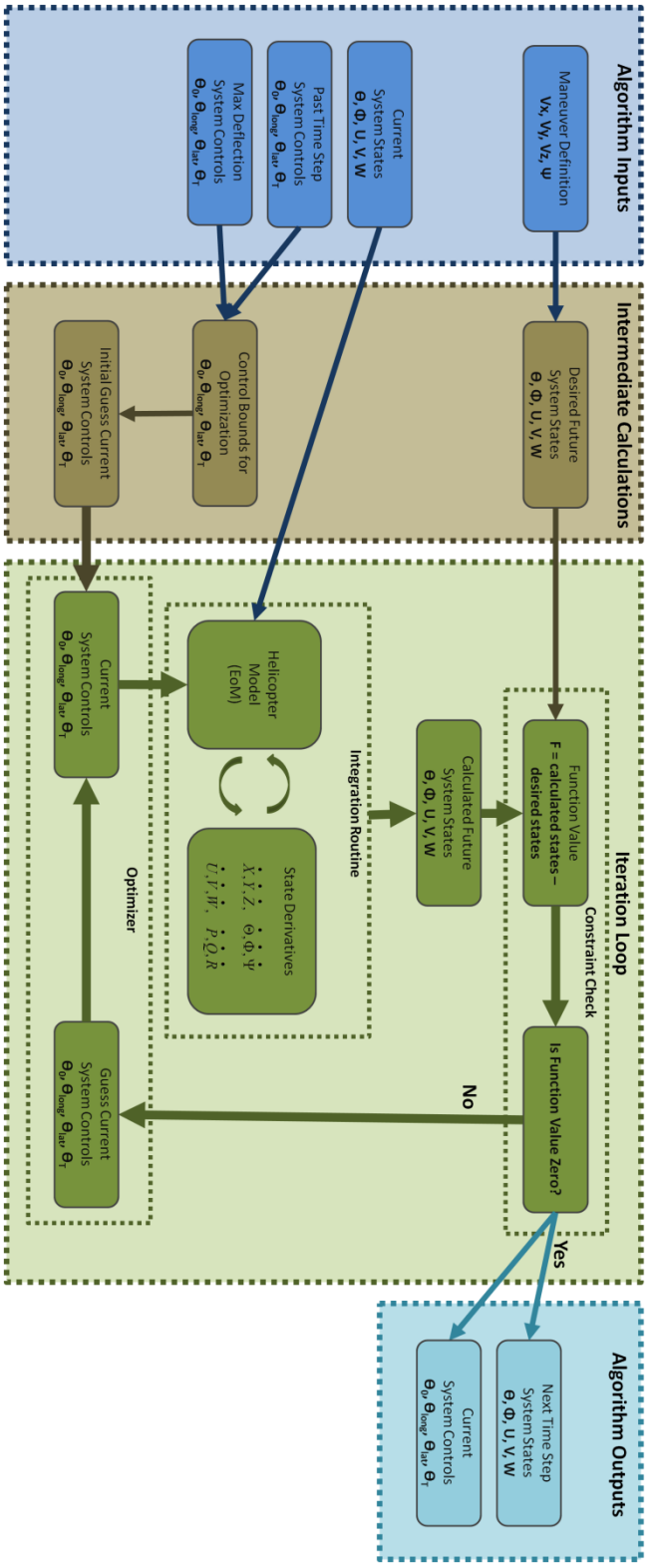

Figure 2.21: Path Following Process Diagram

2.4.3.3 Algorithm Additional Concerns

Another consideration within the environment is selecting the appropriate time step for simulation. Gao [24] observed the skipping of dynamics by having too large of time step. Lee [182] was able to remove the oscillations by decreasing the time step, while on the other hand, Isakov [190] documents the problems with specifying too small of time step. A time step of one-tenth of a second is chosen for this analysis because it provides the desired convergence properties, while remaining large enough to make the simulation time feasible. If the time step is made smaller, the convergence of the optimizer does not need to be specified as small; however, computational time is greatly increased for no informational benefit.

2.4.3.4 Algorithm Verification

While determining the trim conditions, it is understood that the trim space should be continuous and display trends with velocity as design parameters vary. The following discussion summarizes some of the trends within the design space and displays the algorithm's ability to determine the trim points for a wide range of inputs. The trends are not tight curves because of the variability in the design parameters required to model the numerous configurations. First, the x and z body velocities and pitch attitude are discussed. This is followed by an analysis of the trim orientation of the vehicle through a discussion of the attitude using the pitch, roll, and yaw angles. Finally, the impact of control settings for changing design parameters is discussed. All of these results are

shown for 9000 runs over the design space using a space filling Design of Experiments with the same variables and ranges as used in the trim algorithm selection experiment.

Traditionally the static flight conditions in design are evaluated prior to analyzing the maneuver performance. Hence, a thorough analysis of how the trim condition is impacted from design parameter variation is important to investigate at this stage of the analysis. The first step in the trim procedure is to view all of the simulations that did not converge to a steady-state solution. Once these runs are determined, the designer must determine why each of the failed simulations did not converge. Rerunning of the failed trim cases using a multi-start algorithm is sometimes necessary in order to show that a solution exists. Verification that the simulation achieved a trim solution is completed by viewing the minimum function value obtained from each simulation. The value was below 1e-8 for all of the 9000 simulation runs, which means that all of the runs achieved a trim solution.

The second step is to verify that the trends in the trim solutions are valid by analyzing all of the trim solutions together in a holistic manner. This is completed by viewing the various trim state and control variables versus velocity. The trim condition corresponds to five states of interest and four controls. The states consist of three linear velocity components, pitch angle, and roll angle. The angular rates and yaw angle are forced to be zero through the trim constraints so they are not included in the trim analysis.

Since the pop-up maneuver involves only longitudinal motion, the important states are those in the xz-plane. The top portion of Figure 2.22 shows that the vehicle velocity in the x-axis of the body frame is closely matching the defined velocity in the navigational frame. The experiment designs consist of specifying velocity and altitude of the maneuver in addition to the design parameters of interest. The relationship of body velocity components to the defined velocity is through the 2-norm. The magnitude of the combination of the body velocity components must form the defined velocity. The y-axis and z-axis velocities are adjusted in order to drive the accelerations to zero for trim. The pitch angle is necessary in producing the forward component of thrust necessary to achieve faster forward velocities. As a result, the magnitude of the pitch angle grows as the defined maneuver velocity increases. The pitch of the vehicle is defined as negative clockwise when viewed from the right side of the vehicle; hence, a negative pitch represents a forward tilt.

As the helicopter travels faster, the z-axis component of the body velocity increases in the negative direction. The vertical component of the velocity becomes more negative with forward flight because the vehicle must pitch the rotor toward the direction of flight and the positive z-axis is defined downward. The spread in the data results due to variability in the design parameters. For example, at hover condition (zero velocity), the pitch of the vehicle can either be positive or negative depending on whether the CG is fore or aft of the main rotor location.

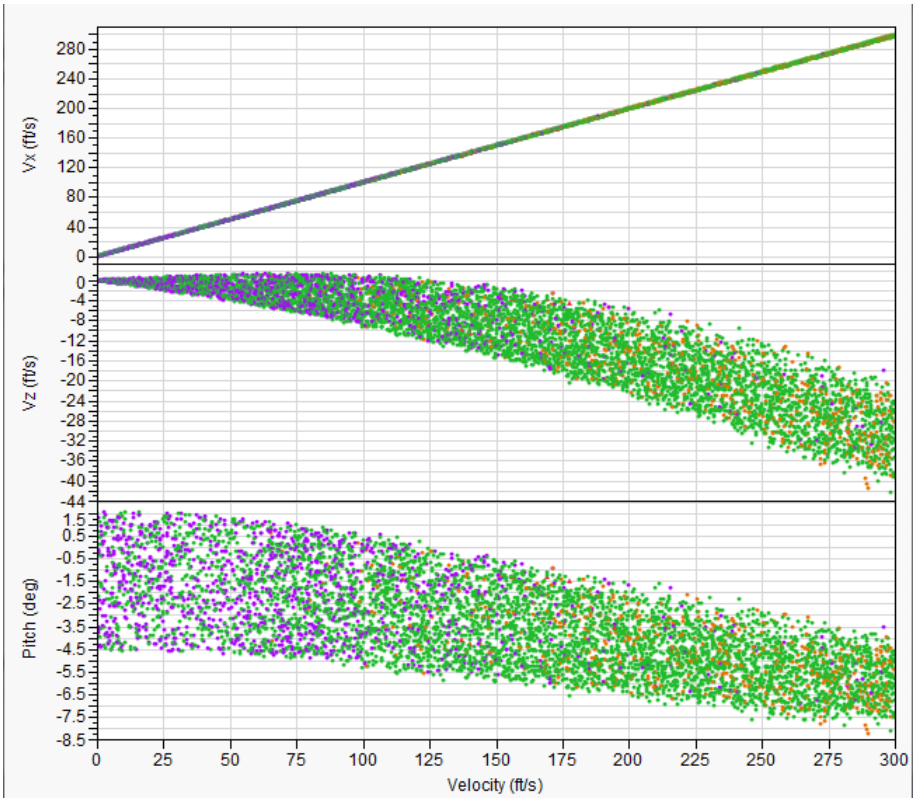

Figure 2.22: Longitudinal Velocity Decomposition

In addition to the longitudinal velocities, the vehicle attitude in trim is also important and highly impacted by design decisions. This is to ensure that the vehicle orientation relative to trim conditions is making logical sense. The yaw angle is constrained to be zero during trim calculation, which may be observed in Figure 2.23. The only remaining angle to fully define the vehicle attitude is the roll angle, which is a function of the amount of tail and lateral cyclic required to counteract the forces and moments caused by the main rotor. Hence, the magnitude of the roll angle is smallest when the required power is minimum, which appears in Figure 2.23 to occur between 150 and 175 ft/s. The best way to verify this observation is through analyzing the power

requirements for the various trim settings and checking to see if the minimum power occurs in this range.

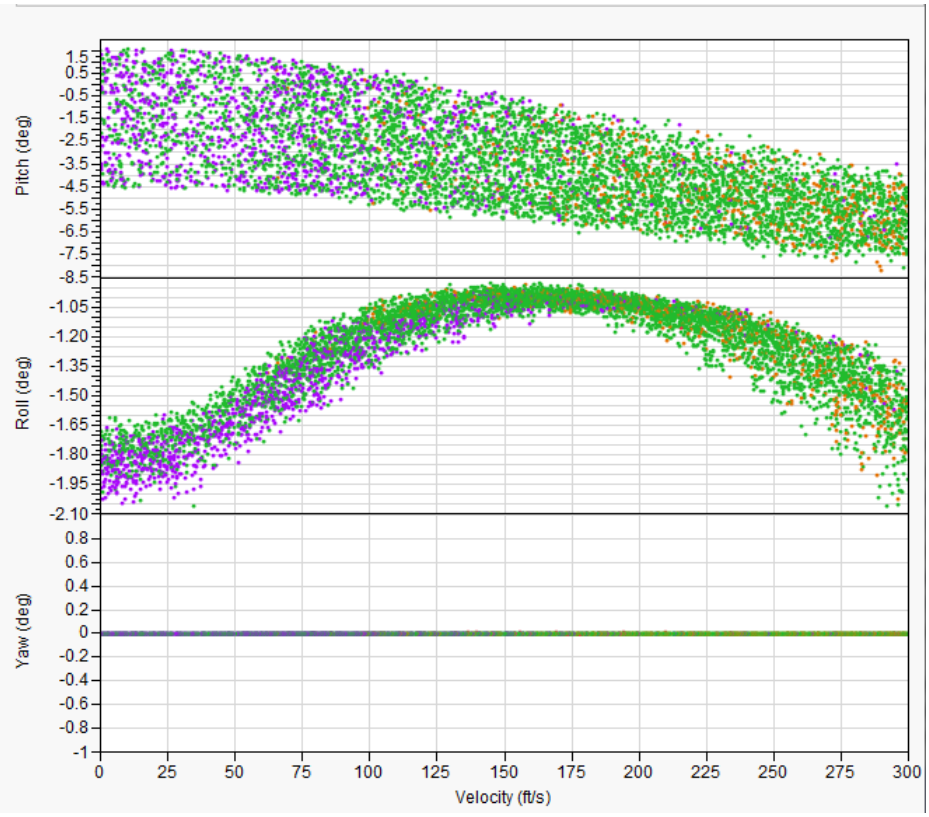

Figure 2.23: Attitude at Trim

Throughout this analysis a common theme is the importance of the control deflection predictions with changes in design parameters. The idea is to capture the changes in performance capabilities via variations in the design parameters and constraints. Therefore, it is important to be able to analyze the control deflections necessary for trim for the range of design variables. This is summarized in Figure 2.24, where it may be observed that the main rotor collective (T0) increases with velocity as expected. The design parameters create a spread in the data that reaches a maximum of

12 degrees in main rotor collective at trim for many designs between velocities of 150 to 250 ft/s. The tail collective (Tt) is used to counter the torque created by the main rotor; hence, the tail rotor collective increases with main rotor collective. The most variation occurs near hover and stems from the main rotor rotational rate and tail rotor moment arm design parameters. As velocity increases, other vehicle parameters start to impact the EoM in the form of aerodynamic forces and moments, as a result this variation reduces. Additionally, the lateral cyclic (Tlat) changes to account for the side force generated from an increase in the tail rotor collective. Finally, the longitudinal cyclic (Tlong) continues to provide forward tilt of the TPP as velocity increases.

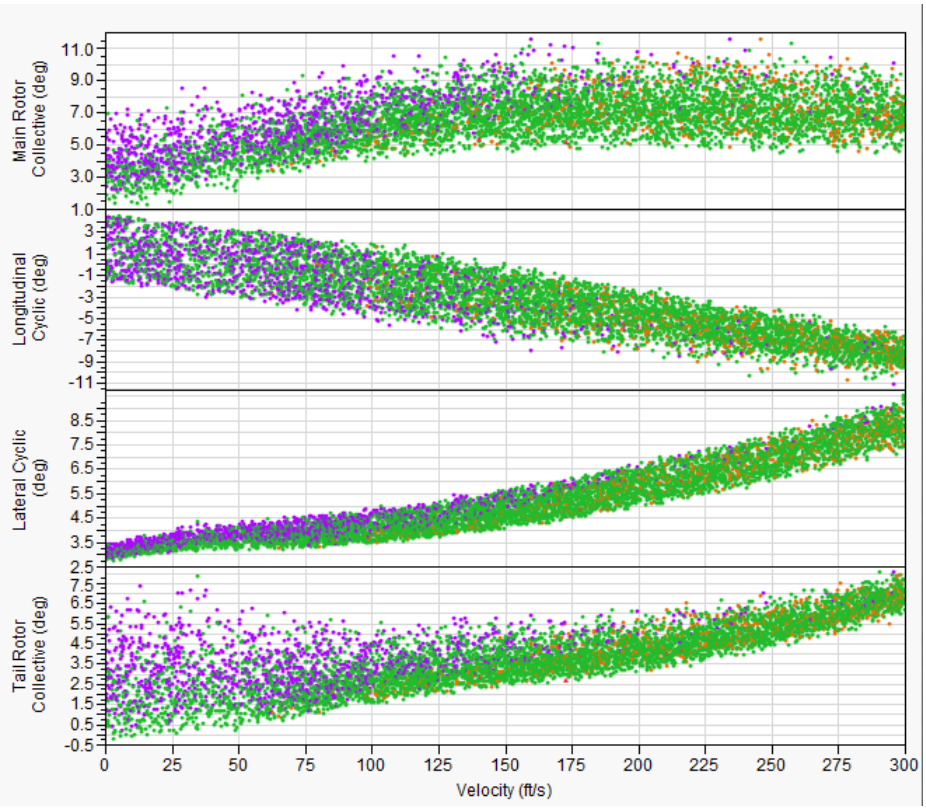

Figure 2.24: Control Deflections at Trim

By viewing the figure, it is observed that the longitudinal cyclic reaches a deflection of approximately -15 degrees at 300 ft/s (177 kts) for a few of the designs, which means that this velocity is not possible if a constraint of 12 degree kinematic deflection limit is imposed. In keeping with the same definition of positive and negative rotations, the longitudinal cyclic is defined as negative clockwise when viewed from the right of the vehicle, while lateral cyclic is defined as negative clockwise when viewing the vehicle from the front. At hover the value of longitudinal cyclic can be either positive or negative depending on several of the design parameters such as the CG location.

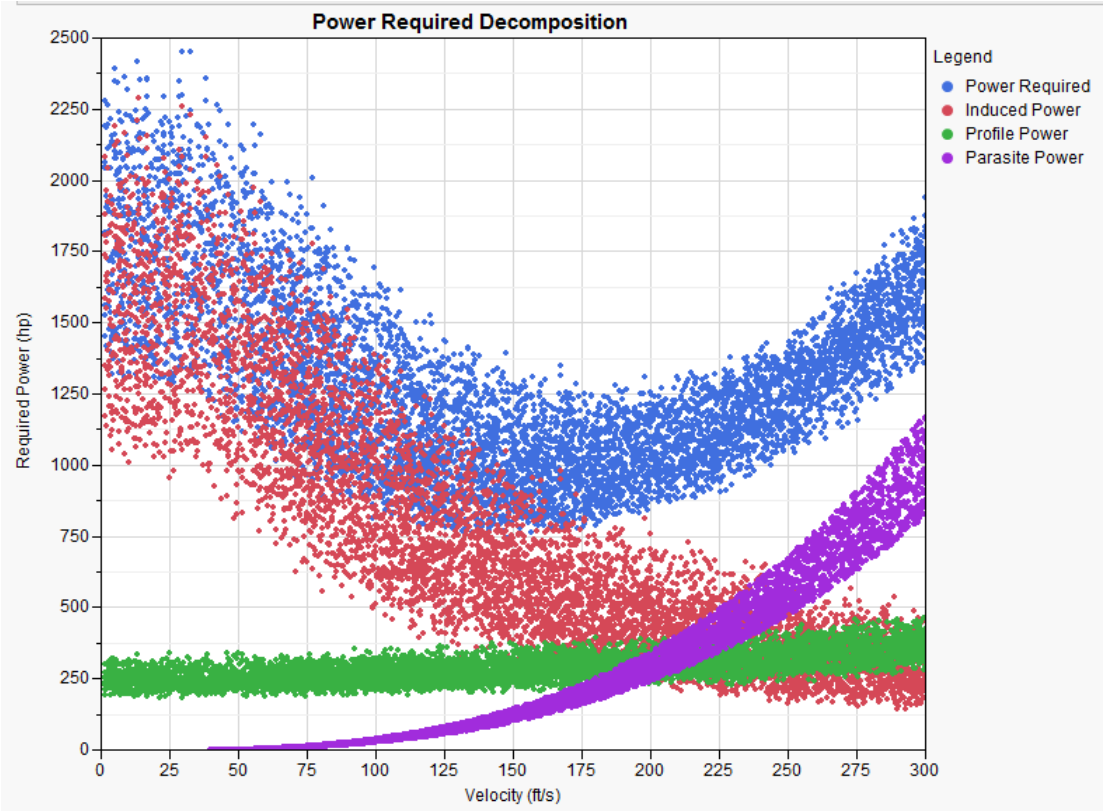

Figure 2.25: Trim Power Required - All Designs

The final set of outputs to discuss from the trim analysis is the power requirements. The power required is decomposed into induced, profile, and parasitic. The following is a summary of the power decomposition found from looking at all 9000 runs within the environment. It must be kept in mind is that this is a combination of all simulations so the power can vary drastically between run. The main point of Figure 2.26 is to show that for the range of all the design variables and maneuver ranges, the trends are correct for the trim power required as compared to Lieshman [44]. The minimum power occurs between 150 and 175 ft/s as expected from analyzing the roll angle.

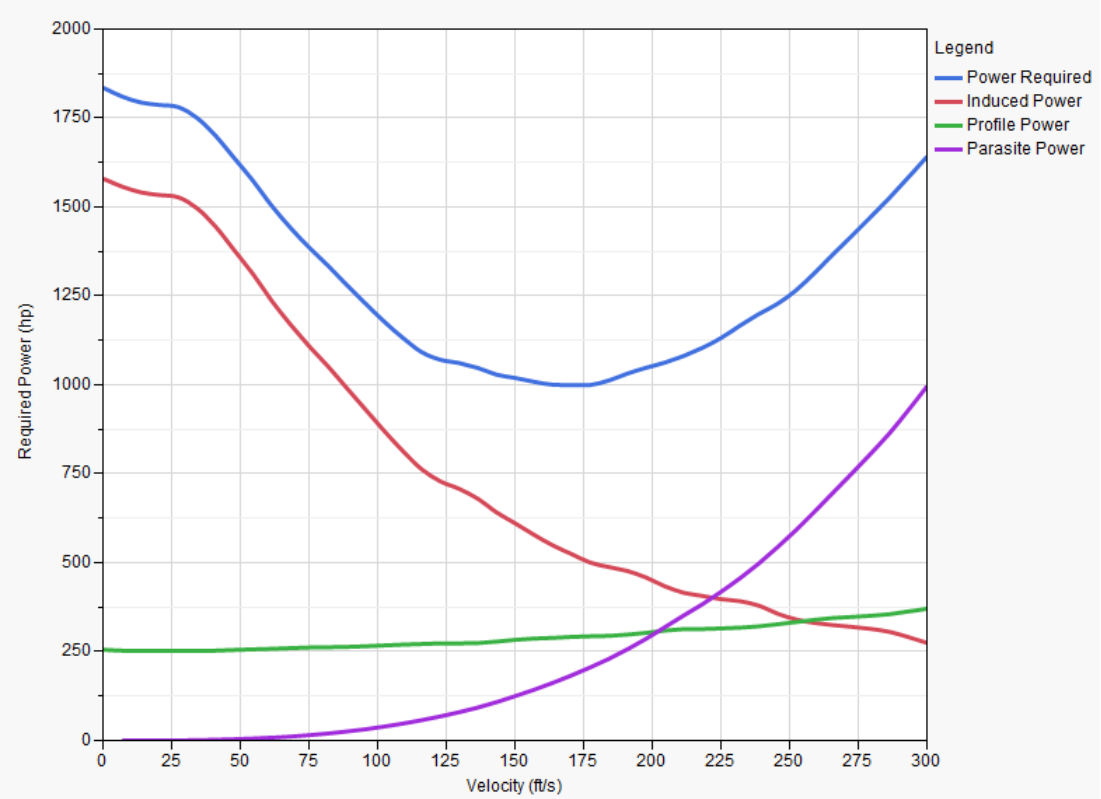

Figure 2.26: Trim Power Required - Trends

2.4.3.5 Algorithm Validation

The validation procedure achieves two tasks, verification that the rigid body model and inverse simulation procedure match previous research efforts and that the simulation results are consistent with actual flight test data. The pop-up maneuver defined by Hess and Gao [25] was chosen as a validation maneuver because of the large amount of previous literature on the maneuver. Even for a fixed time simulation, multiple pop-up paths exist. The pop-up consists of z-axis acceleration in the navigation frame as exhibited in Figure 2.27. Each of the eight paths shown in the figure represents a different maximum acceleration for a fixed initial altitude, velocity, and time. Although the broad spectrum of pop-up maneuvers is simulated in this work, it is important to select a single pop-up within this set for validation.

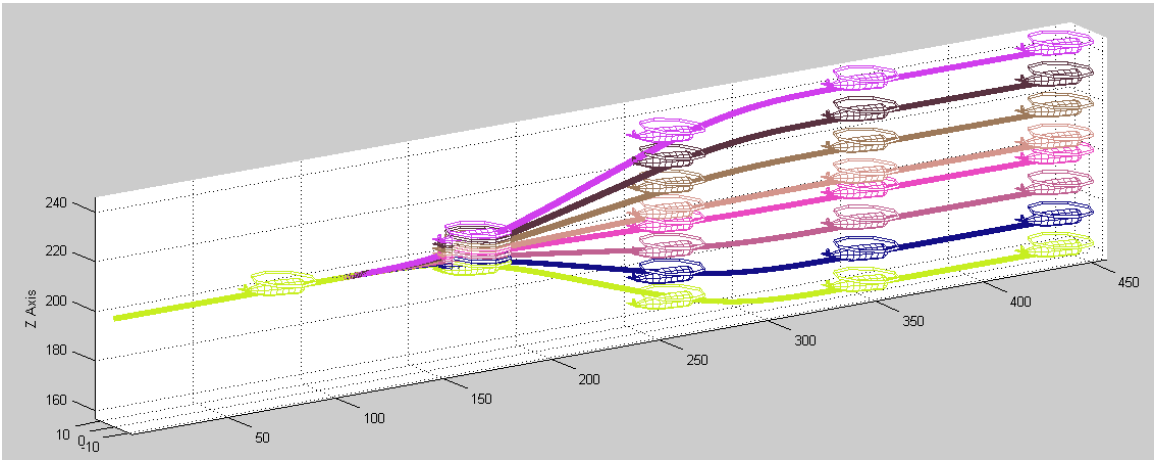

Figure 2.27: Multiple Pop-Up Trajectories

The pop-up maneuver chosen consists of a vertical displacement of 185 ft at approximately hovering conditions over a 10.6 second time frame, which is slightly

different than presented in Hess [25]. The reason for this is that all of the various references used different maneuver definitions so the maneuver model parameters were chosen such that the results in this work could be compared to multiple references. In addition to the vertical velocity constraint required to perform the pop-up maneuver, the zero heading, zero horizontal velocity change, and lateral position constraints are applied. This maneuver may be observed in Figure 2.28 through displaying time histories of vertical position, velocity, and acceleration.

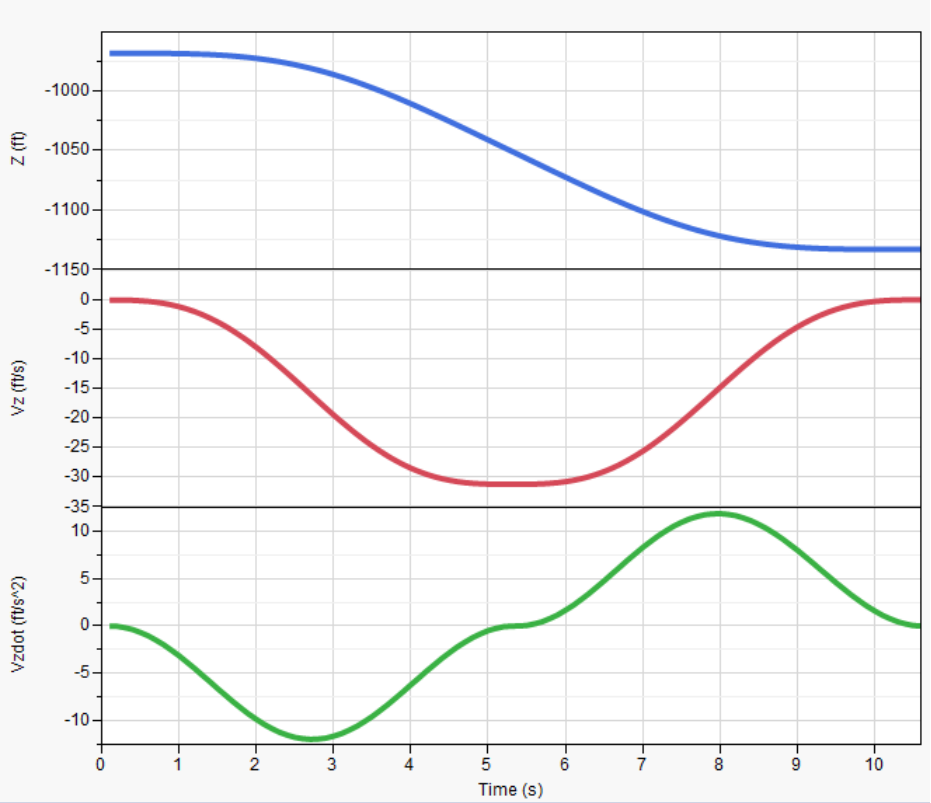

Figure 2.28: Simulated Pop-Up Maneuver

The maneuver is easily modeled through definition of the vertical velocity profile using the trigonometric representation derived earlier, which is slightly different than the

manner in which the maneuver is defined in other references. The maneuver starts at an altitude of 950 ft and through 10.6 seconds of simulation the helicopter reaches a height of 1135 ft via a smooth path. The positive z-axis is defined downward in the inertial reference frame; hence, larger negative values represent higher altitudes. The vertical velocity and vertical linear acceleration over the simulation are also displayed in the figure; however, these parameters are presented in the body frame of reference, while the maneuver is defined in the navigational frame. The maximum vertical velocity of 30 ft/s occurs 5.3 seconds into the simulation and gradually tapers off to a zero value according to the mathematical representation derived earlier in this work. The smooth velocity profile is provided in the maneuver definition, which results in the position and acceleration profiles remaining smooth throughout the simulation.

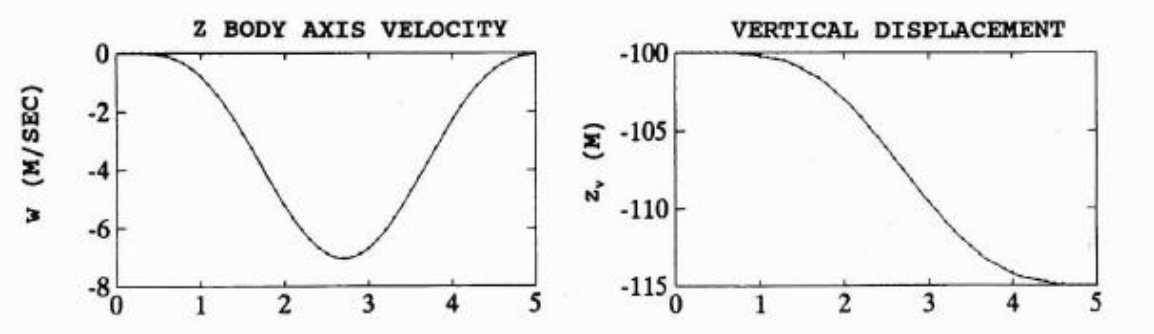

Figure 2.29: Vertical Position and Velocity

Validation consists of analyzing various state and control time histories from previous research efforts and comparing trends. The vertical position and velocity profiles from Hess [25] are displayed in Figure 2.29. A maximum velocity occurs half way into the maneuver with a magnitude of approximately 7.25 m/s or 24 ft/s. The shape of the velocity and the position are very similar despite the difference in time frame and

units. Because the time frame of this maneuver is only 5 seconds the final vertical displacement is about 50 ft.

Since the controls are calculated during inverse simulation, an important aspect for validation is comparison of the magnitude and the trends in control deflections. The control time histories corresponding to the velocity defined in Figure 2.29 are shown in Figure 2.30. The control deflections are shown relative to displacement from trim setting, hence, at time zero all of the controls are zero. Other references did not use this technique and displayed the actual displacement rather than the relative displacement. This is more informative so the actual displacement is used when presenting results from this work.

The main rotor collective is displayed in the upper left corner of the figure and increases during the initial period of the pop-up to provide the increase in lift necessary, while the collective decreases during the second half of the maneuver to allow the helicopter to decelerate to hover at the new altitude. The tail rotor collective (pedal) is displayed in the bottom right portion of Figure 2.30 where the pedal increases to account for the increase in torque that is generated due to main rotor collective increasing. The pedal value is negative because of the reference frame definition. The lateral cyclic is used during this maneuver to negate the side force created due to the increase in tail collective; therefore, the trend is similar to that of the pedal. This may be viewed in the bottom-left portion of Figure 2.30. The longitudinal cyclic may be observed in the top-right portion of the figure and follows the same general trend with slightly more deflection and time spent on one side of the zero line. The sign in deflection is dependent on the center of gravity and the main rotor position, as well as, the reference frame

definition. Through further analysis of Whalley [136] and Thomson [144] , it is observed that the longitudinal cyclic time history varies depending on the design parameters.

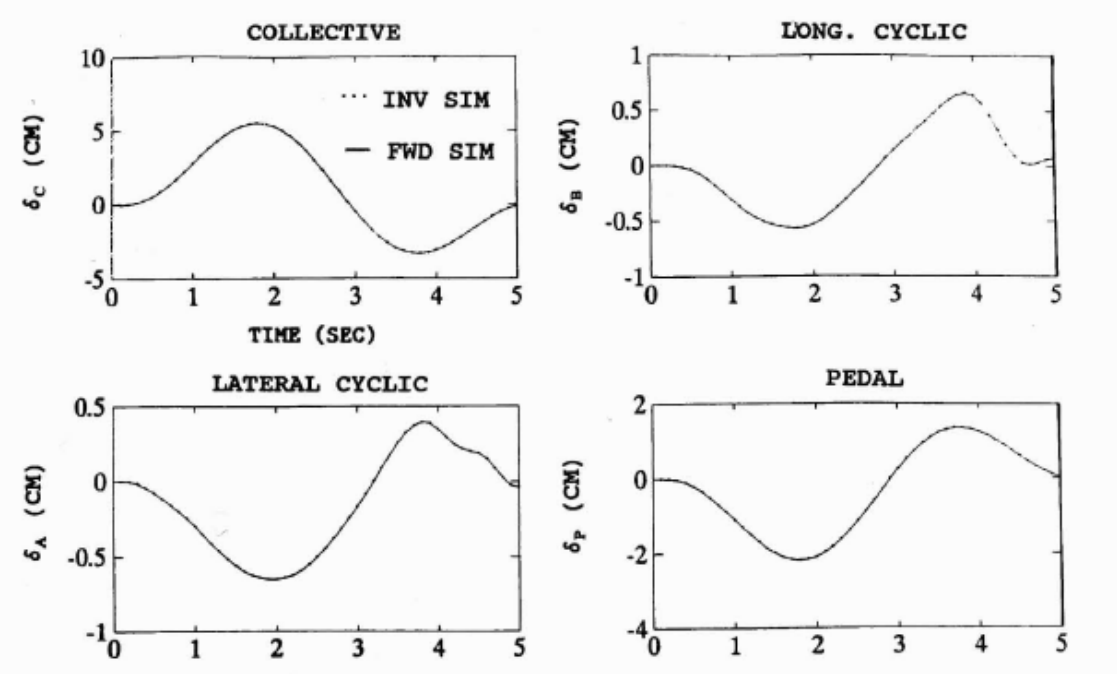

Figure 2.30: Control Time Histories

The vertical state and state derivatives for the pop-up maneuver have already been discussed and presented in Figure 2.28. The next step of the validation is to analyze the control deflection time histories and compare to the results from previous literature, which were verified through comparison to actual flight test data. The control deflection time histories are displayed in Figure 2.31. The trends for main rotor collective are very similar to those discussed previously. During the first half of the simulation the collective increases in order to increase acceleration in the vertical direction, while the collective decreases below the trim setting in the second half of the simulation to allow the helicopter to decelerate to hover.

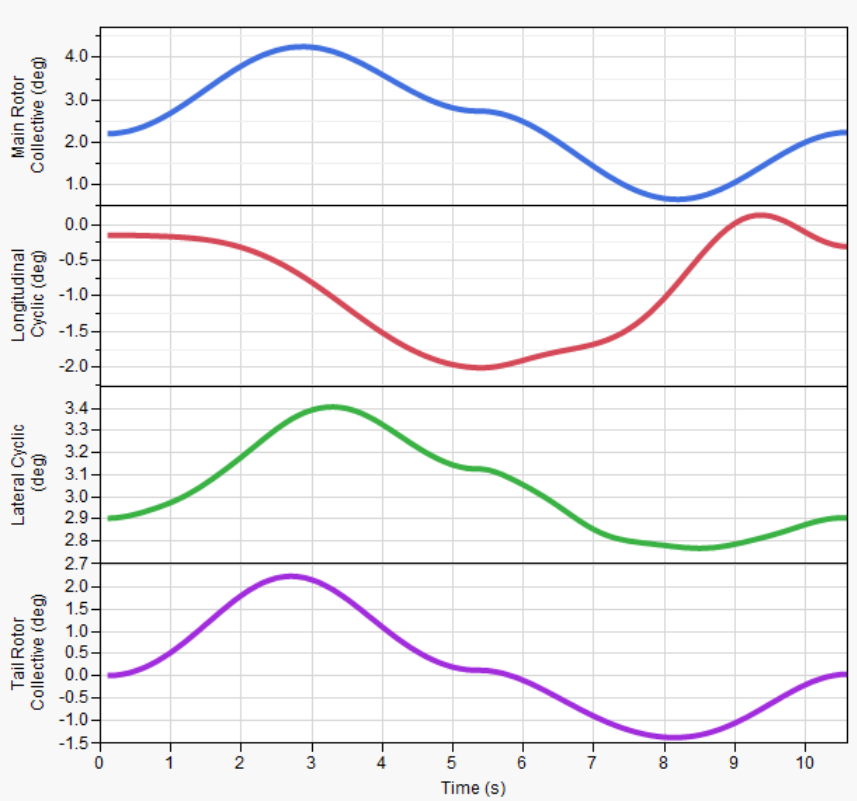

Figure 2.31: Control Deflection Time Histories

The tail rotor collective is used to balance out the torque produced by the main rotor, hence, the curve follows the same trend. As tail rotor force increases, lateral cyclic is required to balance this side force, which is observed in the control deflection time history in Figure 2.31. Finally, the longitudinal cyclic behaves similarly to the results from literature; however, the sign and magnitude change slightly depending on the center of gravity positioning.

A few more figures are discussed for completeness in order to show that the simulation environment is producing valid trends. An important constraint during this pop-up maneuver is that the vehicle heading does not change. Figure 2.32 displays the

vehicle attitude time histories for the pop-up simulation. The heading of the vehicle is shown in the bottom of the figure and is maintained at zero throughout the maneuver. The other two attitude angles are pitch and roll. The pitch attitude corresponds directly to the longitudinal cyclic control with time. The negative longitudinal cyclic angle indicates a tipping forward of the tip-path plane, which creates a forward velocity component in the body reference frame. Since the maneuver is specified as acceleration in the z-axis of the navigation frame, the pitch of the vehicle has to adjust to move the forward acceleration into a vertical component; hence, the vehicle pitches backward. Finally, the roll angle is a function of the tail collective and the lateral cyclic setting combination.

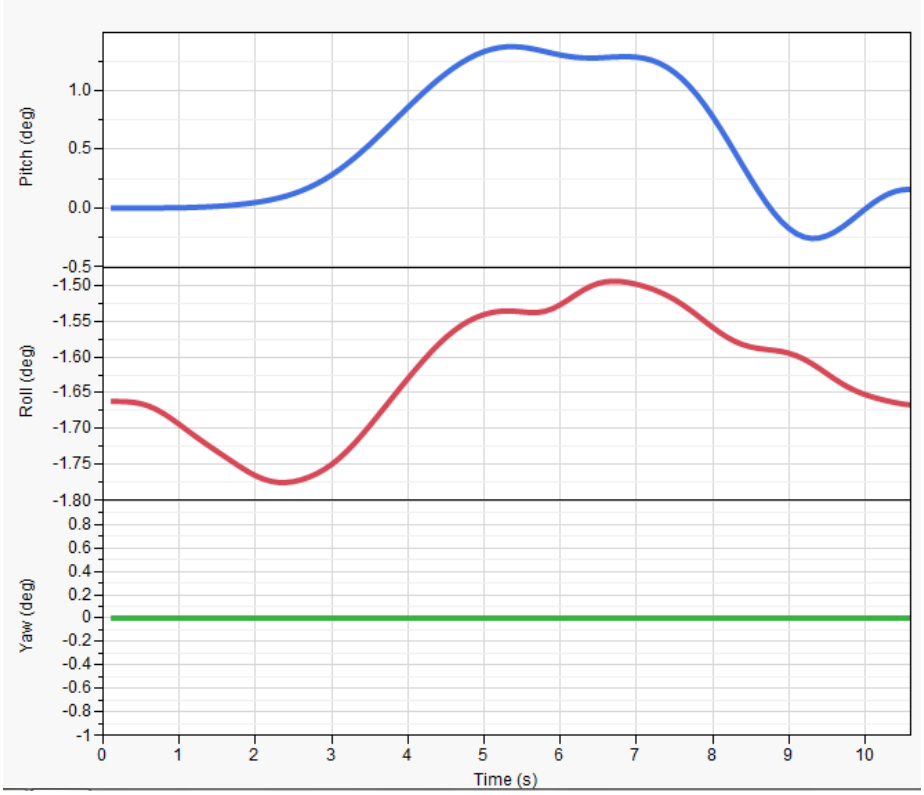

Figure 2.32: Vehicle Attitude Time Histories

The next series of examinations involves the relationship of forces and moments to the maneuver definition. The longitudinal forces and moments are displayed in body coordinates in Figure 2.33. The main idea of the pop-up maneuver is a vertical acceleration in the z-axis of the navigation frame. This requires a vertical force component, which may be viewed in the middle section of Figure 2.33. An important observation is that this force is in the body coordinate system, which is almost aligned with the navigation frame during hover. This is viewed by seeing that the pitch angle during hover is close to zero degrees.

However, the helicopter equations of motion have large coupling terms, which results in accelerations in other axes of the vehicle. A major effect of this coupling may be viewed in the pitch moment, which is displayed in the bottom portion of Figure 2.33. The main rotor is offset from the center of gravity of the vehicle. As a result, as the collective is increased, the moment changes drastically, which results in a pitch rate. This pitch then forces the body coordinate system out of line with the navigational system. This pitch means that a component of the force required to accelerate must be incorporated into the x-axis of the body frame. The forces and moments are highly dependent upon one another. Additionally, it may be observed that the moment is increasing throughout the maneuver. After the motion is completed, this oscillation damps back to steady-state. The speed at which this damping occurs is dependent on the design parameters of the system.

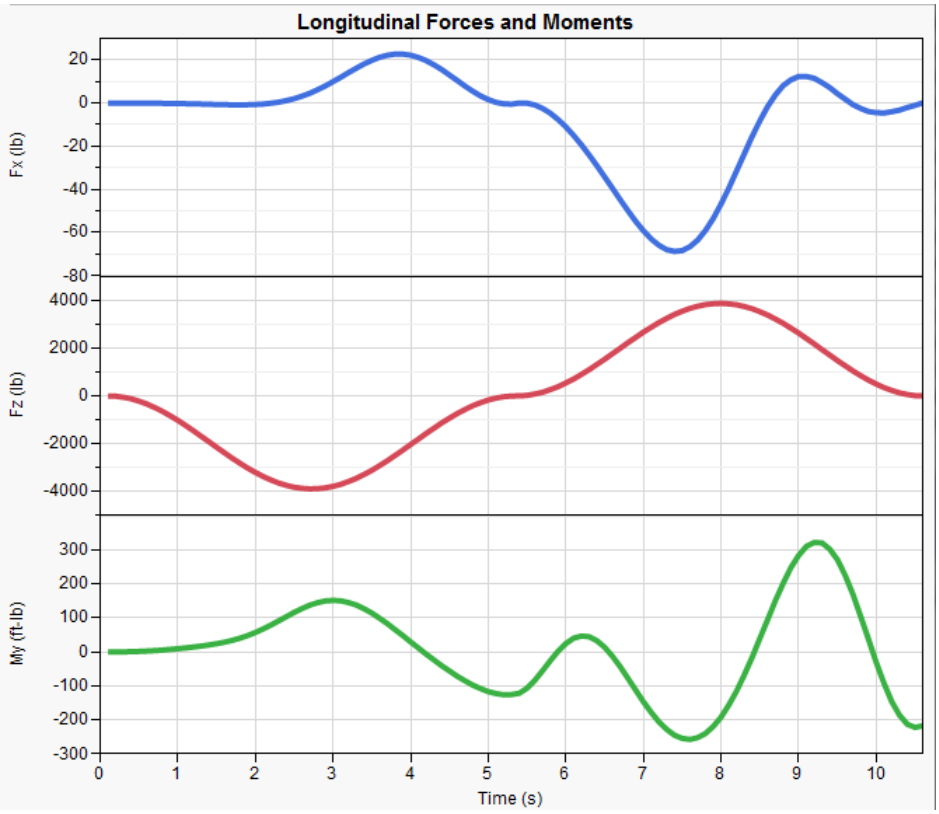

Figure 2.33: Longitudinal Forces and Moments

Another important set of outputs from the simulation that are essential in showing that the energy-based formulation is not capable of capturing the necessary outputs is the power decomposition. As presented previously, power required is decomposed into induced, profile, and parasitic in this analysis. Additionally, the power available is not set as a design variable but is allowed to vary as a requirement during post processing. When viewing Equations 4, 5, and 6 it can be seen which variables are impacting each power directly. For example, the induced power is a function of lift of the main rotor; hence, during the initial portion of the pop-up maneuver, the induced power spikes to provide the lift necessary to accelerate. While in the second portion of the maneuver the induced power drops. This may be viewed in the top portion of Figure 2.34.

Profile power is a linear function of velocity and density, which means that there is initially a slight increase as velocity during the maneuver. A drop in the profile power at the end of the simulation results because of the altitude increase impacting the density of air. Profile power remains close to constant throughout the maneuver because the overall changes in velocity and altitude are small. Parasitic power is a cubic function of velocity such that it peaks in the middle of the pop-up when velocity is highest and tapers back to zero during hover.

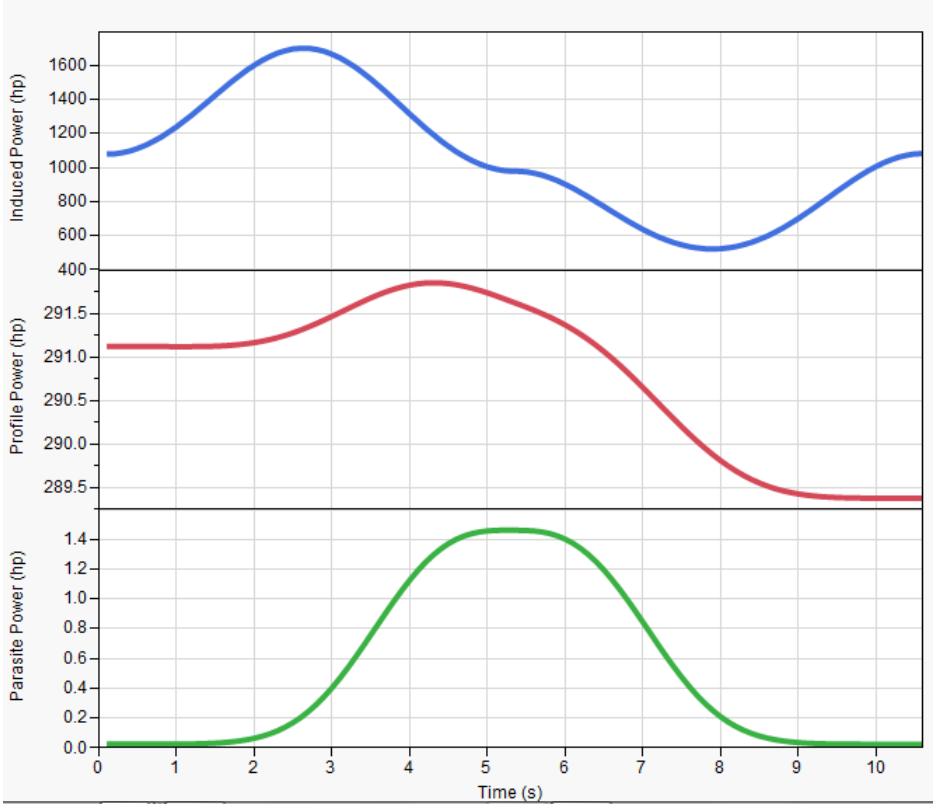

Figure 2.34: Power Required

2.4.4 Post Processing/Data Filtering

The post processing component of the process consists of the Filtered Monte Carlo approach, which stores all of the pop-up simulations in data tables such that all of the trades can be conducted real-time. The capabilities are best shown through example. First, the static power requirements are analyzed by looking at the power required in trim. An example is presented that shows the filtering of the power required design space. Second, similar filters are applied to rigid body characteristics to show that the data may be viewed instantly for various states and controls.

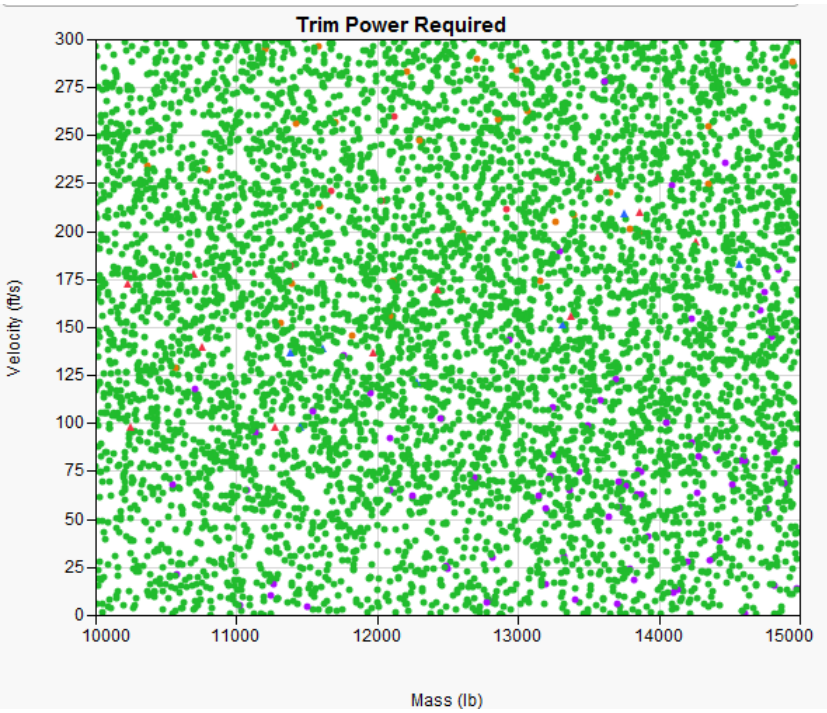

Figure 2.35: Design Space of Velocity versus Mass

Two variables that contribute largely to the variation of power required in trimmed flight are flight velocity and vehicle mass. All successful maneuvers are

displayed in Figure 2.35, which indicates that maneuvering flight is possible for the entire range of mass and velocities examined. Each point within the figure represents a different design and maneuver combination. Additionally, the data analysis environment is dynamic in nature such that at any time during the analysis the designer may select a single or a few points to compare the attributes as indicated in Figure 2.36. This can be used within any figure using FMC because all of the data is stored in the background.

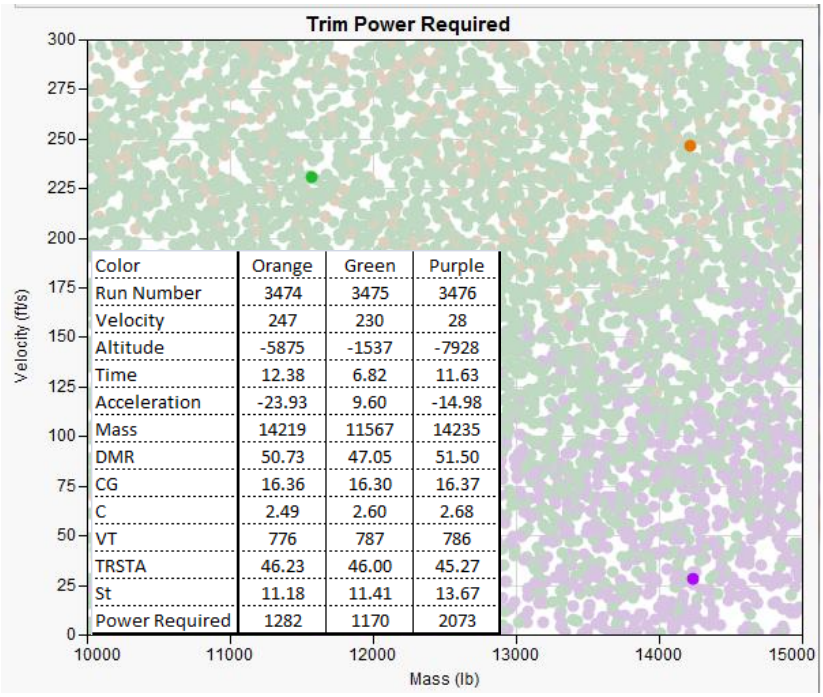

Figure 2.36: Real-Time Data Point Comparison

Through additional filtering of the data, valid insight into relationships between these variables and trim power required is uncovered, which may be observed in Figure 2.37. Using the data filter on the discrete set of designs, the points may be color coded according to the trim power requirements. The color coding legend is displayed to the right of the figure. This type of diagram becomes helpful when selecting the engine of the

helicopter because the power required dictates the amount of power that must be supplied to achieve the trim condition. For example, if power available is selected to be 1150 hp, then no design and maneuver combinations that are colored purple or orange will be able to trim, let alone perform a pop-up maneuver. Additionally, power available must be at least 1300 hp in order for some of the designs near 10k lb to hover (zero velocity) as indicated by the purple points. This is just one example of how the data filtering can provide valuable design information real-time, which leads to greater tradeoff capabilities and more thorough understanding of the problem.

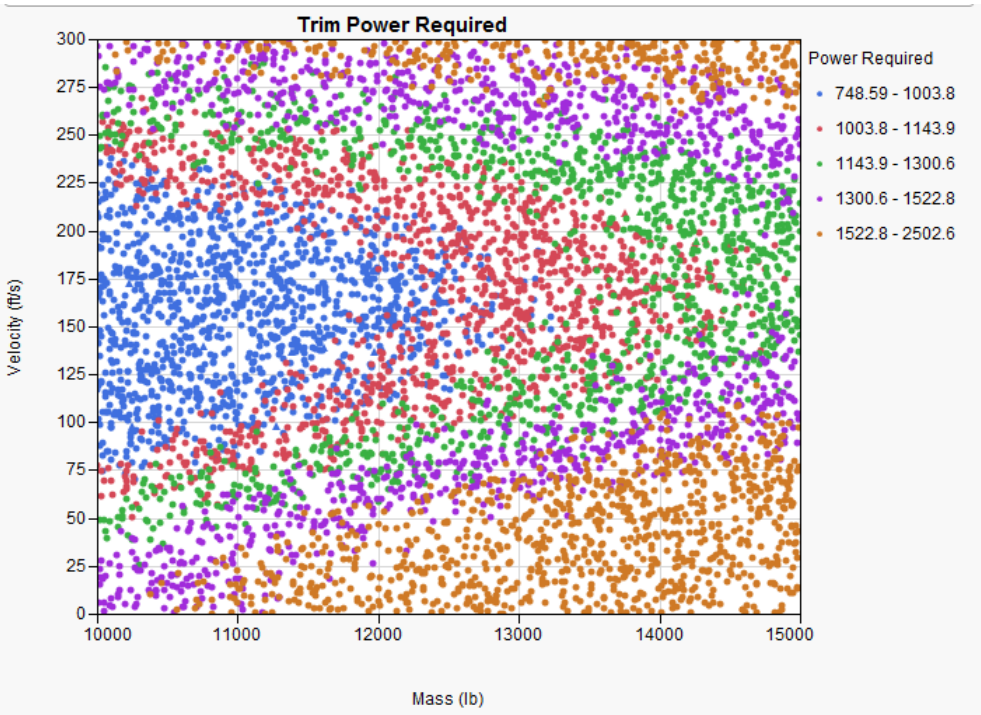

Figure 2.37: Power Required Relation to Design Parameters

Kinematic control limits resulting from the inclusion of the rigid body EoM can be used in the filtering process to aid in feasible design selection. Data filters are used to color code particular ranges of controller deflection within the design space. It is

understood that the minimum longitudinal cyclic during a maneuver is greatly impacted by the CG location. For example, in aircraft dynamics design, the CG location of aircraft is moved aft to provide greater maneuverability, while at the same time sacrificing stability characteristics. Additionally, forward flight velocity is also known to be a major contributor. Figure 2.38 depicts the trim longitudinal cyclic as a function of velocity and CG location for the successful maneuvers. The data filter is used to cluster the results according to longitudinal cyclic deflection, which is viewed to the right of the figure. For all of the successful maneuvers, the minimum longitudinal cyclic has a range of -11 degrees to almost 4.5 degrees. Using this information the designer may apply control deflection constraints to narrow the design parameter space, which are enabled through the rigid body formulation.

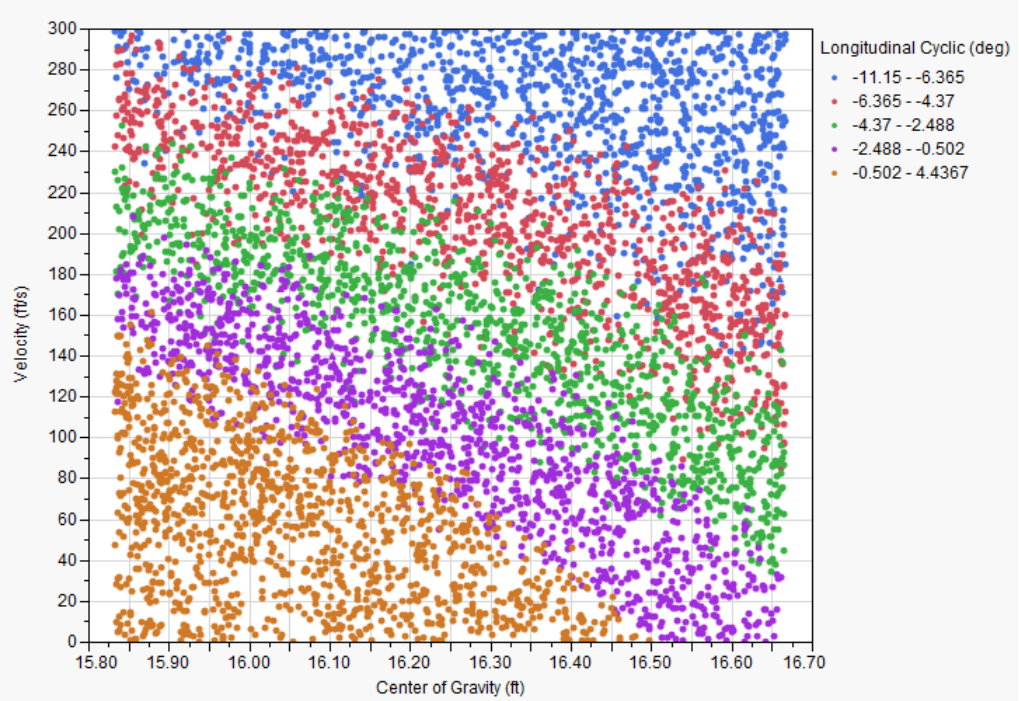

Figure 2.38: Trim Longitudinal Cyclic Design Space Clustering

2.5 Experimentation and Results

Although much insight about the problem is gained through analysis of individual simulations within the environment, it is not efficient to view each maneuver in order to make design decisions or to view the impact from changes in design parameters. Well structured data analysis is required to enable the designer to view all the designs simultaneously in multiple dimensions. As stated previously, 9000 runs were completed using the environment for the design variable ranges in Table 2.2. In addition to the design variables, sweeps of the pop-up maneuver definition were completed, which included variations in velocity, altitude, time, and maximum vertical acceleration. The data analysis section is divided into subsections in order to present the large quantity of information in a clear and traceable manner. This section is divided into maneuver success determination, energy-based filtering, and rigid body filtering, and minimum time maneuver selection. It is shown through data analysis that the rigid body formulation constraints are required in order to provide more conservative maneuverability estimates, while the parametric properties of the formulation allow for defining the entire configuration design space. Through conducting quantitative performance design trades, it is demonstrated that the energy-based method fails to exclude some kinematically infeasible designs.

2.5.1 Maneuver Success Determination

The main point of the maneuver success determination section is to analyze the data and determine which runs out of the 9000 were unable to complete the defined

maneuver. During simulation, the optimization algorithm calculates the control deflections necessary to follow the prescribed path. The ability to follow the path is returned in the form of a function value during each time step. The path is feasible if the function value is near zero. Conversely, the function value grows as the actual path diverges from the defined path.

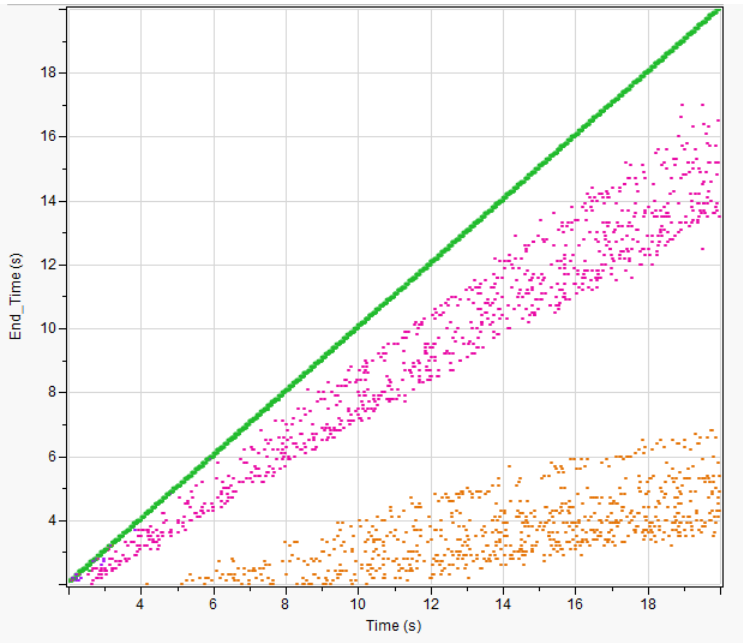

Figure 2.39: Maneuver Defined Time versus Simulation End Time

One manner in which to check for maneuver completion is to observe the final time in the maneuver definition versus the actual time at the end of the simulation. Figure 2.39 depicts this relation with the defined final time on the x-axis and the simulation end time displayed on the y-axis. The points that fall on the 45 degree line are the design and maneuver combinations that were successful in completing the entire maneuver, while the other points indicate failure to follow the defined path due to rigid body limits. Of the 9000 total runs, 6200 simulations completed the entire maneuver

successfully and are colored green in the figure. The failed points follow two different but very distinct trends and have been colored differently in order to see the relationship in other dimensions within the design space. It turns out that one failure mode occurs during increases in altitude resulting from a negative acceleration parameter, while the other corresponds to decrease in altitude.

Another way to view maneuver success is to plot the maximum function value that occurs within the time frame of the simulation. The function value corresponds directly to the difference in defined path versus current path. Hence, a large function value indicates divergence from the path. If the function value stays below 1e-8 throughout the simulation, then the maneuver is defined as successful. Otherwise, the maneuver is categorized as failed. The failure criterion is parametric and can be adjusted real-time according to the preferences of the designer. The failed cases are largely a function of the maneuver acceleration, which is shown as the x-axis in Figure 2.40. Observation of the figure shows that maneuvers with accelerations between +/-20 ft/s are achieved for all of the designs that are tested; however, above these accelerations only a few designs achieve the maneuver. Through comparison of Figure 2.39 and Figure 2.40, it is observed that both methods produce similar results. The coloring scheme applied through filtering is used in both figures such that the clustering of the failed cases may be seen. The negative accelerations indicate increases in altitude, while the positive accelerations result in a decrease in altitude. This results due to the manner in which the reference frames are defined.

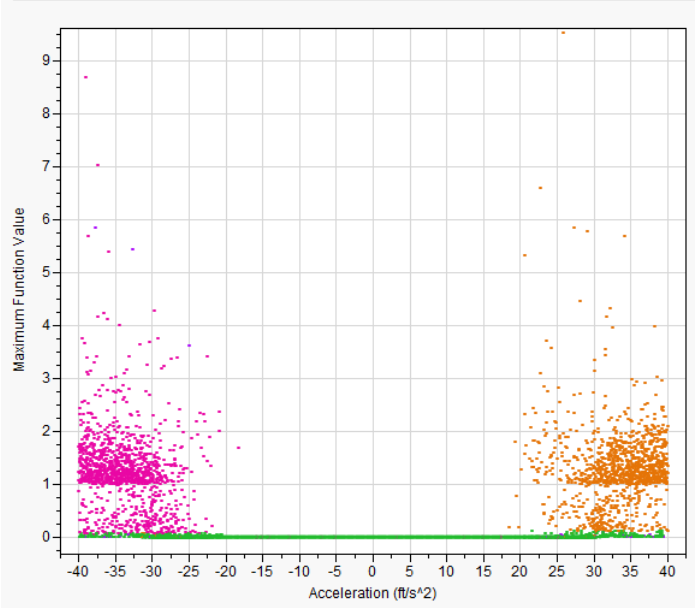

Figure 2.40: Maximum Function Value for Each Simulation

In the previous figure, it was observed that the failed cases have direct correlation to the defined maneuver acceleration. At this point it may be interesting to see if any of the other maneuver parameters have a major impact on the failure of the maneuver. A multivariate plot of the four maneuver parameters is displayed in Figure 2.41, with the green points indicating successful simulation runs.

The multivariate plot displays all four maneuver parameters simultaneously in one figure. Each block displays all 9000 simulations, which represents the interrelations of the various input parameters. As expected, acceleration appears to drive the success of the maneuver, where the orange points are descent operations and the pink are climbing maneuvers that failed. Additionally, more failed runs occur at very low and very high velocities, which is also an expected trend because the forces and moments become greater in these regions of flight. The last trend to discuss is the coupling of the velocity

and acceleration, which may be viewed in the upper right subplot of the figure. There is an interesting trend that causes failure in path execution at low velocities and high accelerations. As the velocity increases, the maneuvers again become feasible, while at the highest velocities the failures again gradually appear. The trend appears because of the velocity and power required relationship.

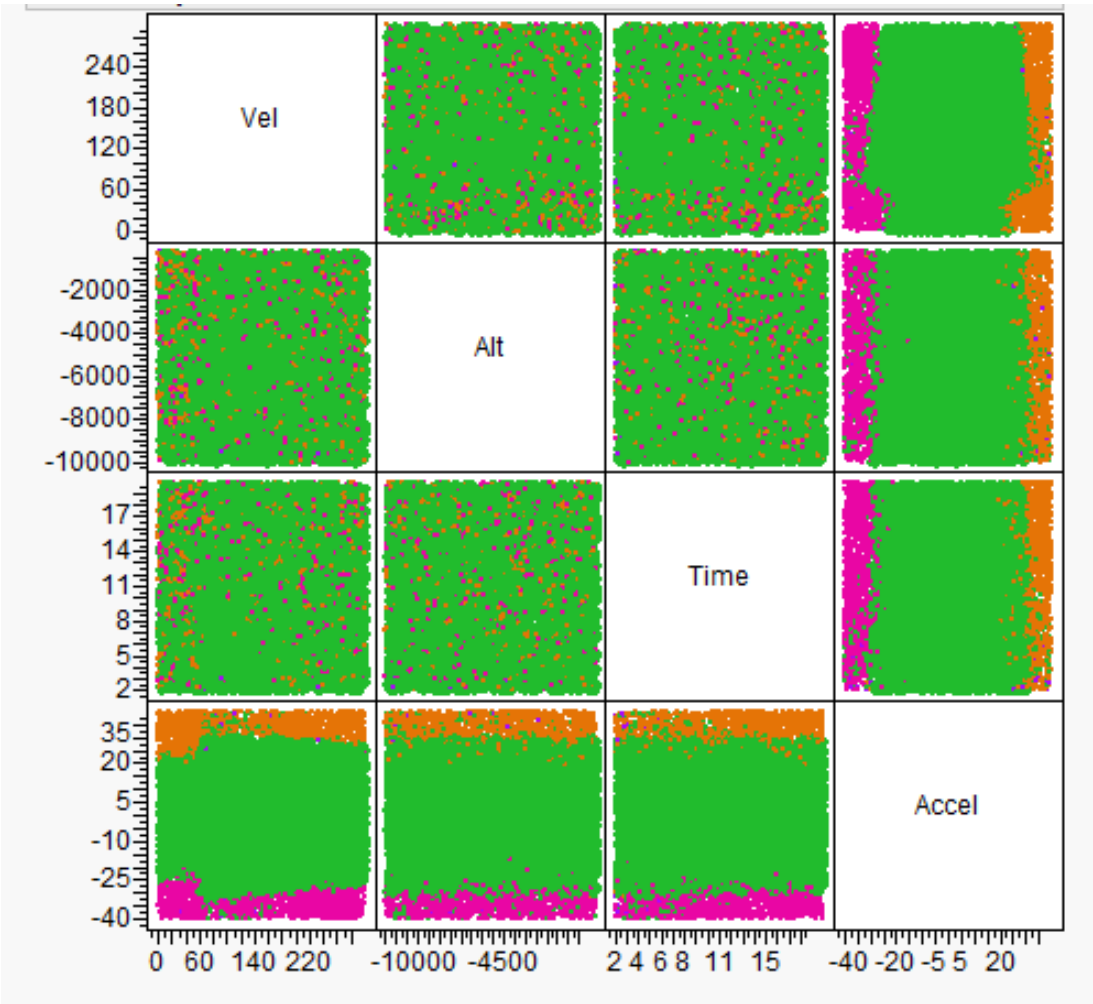

Figure 2.41: Multivariate Plot of Maneuver Parameters

2.5.2 Energy-Based Filtering

The energy-based method makes all design decisions based on the power results and by using the power decomposition alone, it is hypothesized that the necessary information for design selection is not captured. The trim power required design space is displayed in Figure 2.42 where the inputs are shown on the x-axis and the y-axis displays the trim power required value. The first four inputs on from the left are the maneuver inputs and the remaining inputs are design parameters of the vehicle. All successful runs are displayed as individual points in each block of the figure. Applying the power available is an extension in this work through the integration of FMC into the maneuverability and design process. By viewing the data in this manner one may observe the relationship between power required and every input at the same time. The following examples demonstrate the benefits and flexibility of the process. First, the trim power required is analyzed subject to the power available constraint. Next, the maximum maneuver power is analyzed through applying the same power available constraint. This example shows that dynamic maneuver analysis provides more conservative estimates and greater traceability than using steady-state analysis alone.

As discussed previously, the power available to the helicopter is supplied by the engine. Previous research efforts would fix this number during simulation to view the capabilities of a single rotorcraft design; this variable is left as a constraint during post processing of the data in this approach. Hence, the impact of the engine selection may be observed real-time. When viewing Figure 2.42 it is observed that the trim power required ranges from 748.5 to 2502.5 hp for the ranges of maneuver and vehicle parameters tested.

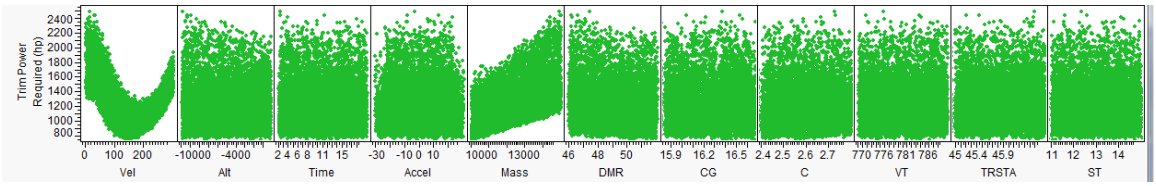

Figure 2.42: Trim Power Required versus Model Inputs

Using the data filtering approach the designer can dynamically change the power available and view the impact on all the dimensions of the space. Assume that an engine with 2200 hp maximum output is being considered for this design. This constraint means that any simulation point that has a power required value greater than 2200 hp is no longer feasible due to this design decision. This data filter is shown in Figure 2.43 were the left portion of the figure shows the power required range for all 9000 runs. The right portion of the figure shows the number of designs when the 2200 hp requirement is applied. It is observed that 83 out of the 9000 runs violate this constraint.

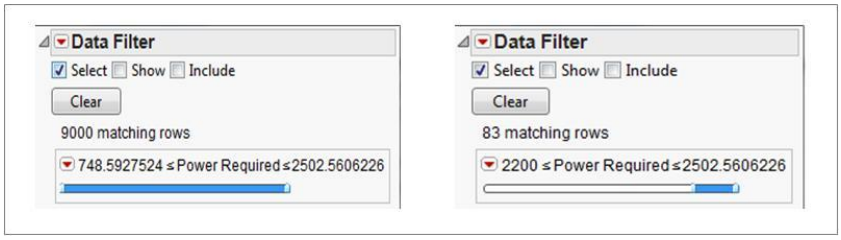

Figure 2.43: Power Available Constraint – 2200 hp

Knowing that 83 points violate the power available requirement is information that is relayed to the designer real-time. Using the power requirement figure presented earlier, the location of the infeasible points can be viewed with respect to all of the input parameters. This is shown in Figure 2.44, where the top portion of the figure shows the design space before the constraint and the bottom portion of the figure shows the points

that violate the 2200 hp constraint highlighted in purple. The figure indicates that most of the failures occur when the mass is large and the vehicle is attempting to hover. Additionally, more failed points occur for small diameter rotors and at high altitude. At this point, the designer may wish to relax this constraint because these results are only showing static power. It is expected that dynamic power will be more constraining. Additionally, the designer can select any point and instantly view the maneuver time history data.

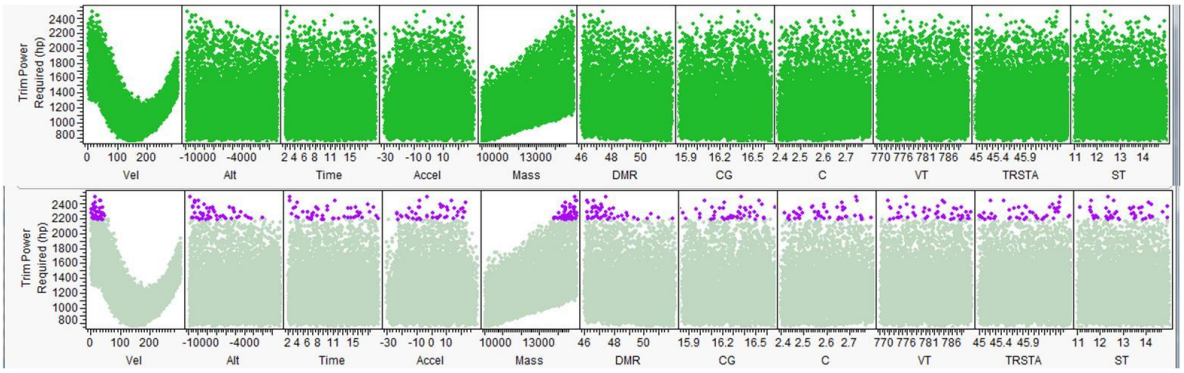

Figure 2.44: Trim Power Required Constraint – 2200 hp

For this reason, the designer may wish to view the impact of a few power required constraints. Figure 2.45 shows a constraint of 2500 hp applied to the design space, which is represented by a single purple point in the bottom subplot. Hence, with the 2500 hp constraint only one design is infeasible. By viewing the various subplots of the figure it is observed that this run is at the highest altitude and mass range settings, while the steady-state condition is defined close to hover. As the constraint is changed, the impact on all of the design inputs may be observed real-time rather than requiring a new set of simulations to be run, which provides the designer with greater tradeoff capabilities.

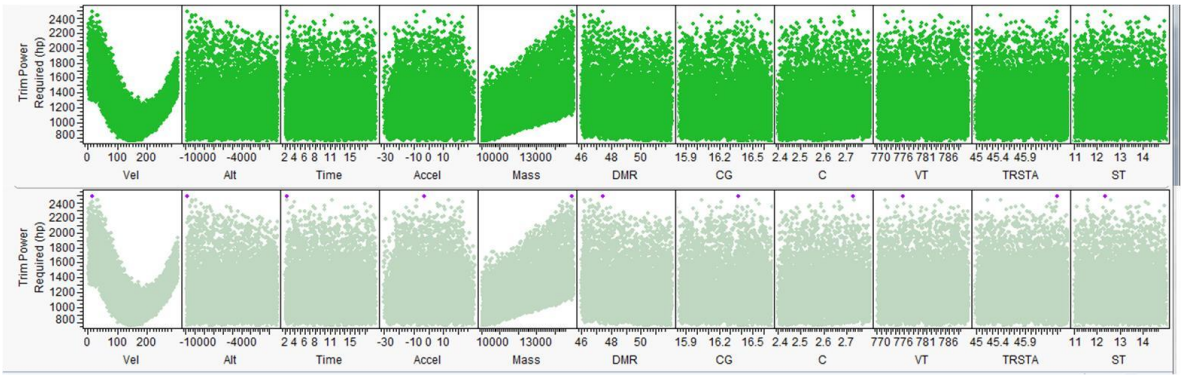

Figure 2.45: Power Available Constraint Applied

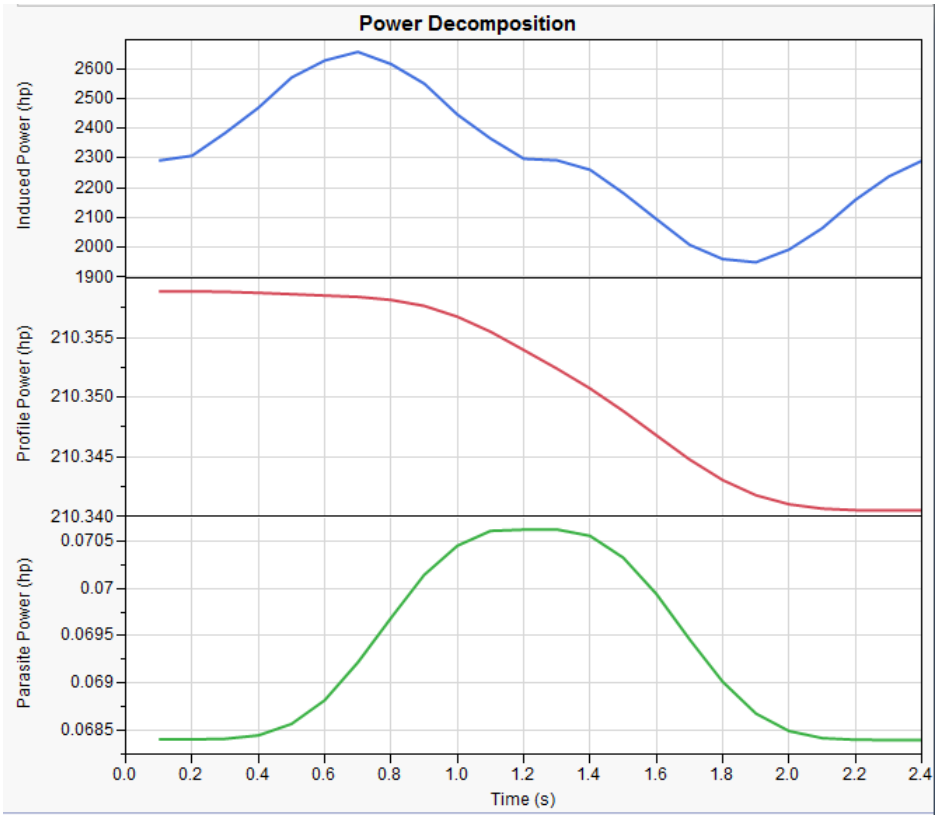

Figure 2.46: Time History of Failed Maneuver

Further emphasizing the traceability of the process, the failed design and maneuver combination time histories may be viewed instantly. The previous power available filter of 2500 hp resulted in a single failed run. The failure to complete the maneuver results because the power required is greater than the power available, which can be observed in the power breakdown in Figure 2.46. Using the time history information, the designer can instantly and systematically determine why particular design and maneuver combinations are infeasible. Only the power required information is presented here; however, the FMC approach provides the capability to view any of the state, control, or auxiliary maneuver information instantly.

A similar process can be applied to other design requirements and constraints as desired. The other form of constraint placement is on input parameters. As information about the system becomes available, the variability in each of the design inputs may decrease. Assume that through a detailed weight breakdown a better idea of the overall mass is determined. An example of decreasing the ranges on mass is shown in the bottom subplot of Figure 2.47. The mass of the vehicle is further constrained to be between 13000 and 15000 lbs. The infeasible points are colored gray in the figure, while the feasible points remain green. In this example, the strength of adding dynamic constraints to input variables is shown. The top portion of the figure shows the design space with no constraints; while the bottom portion shows the feasible points once the low mass designs are removed from the analysis. At any point in the analysis, this mass constraint can be removed or adjusted real-time. Additionally, constraints can be applied to any number of

the inputs and outputs simultaneously. This enables the designer to instantly view if a feasible region of the design space exists as requirements change.

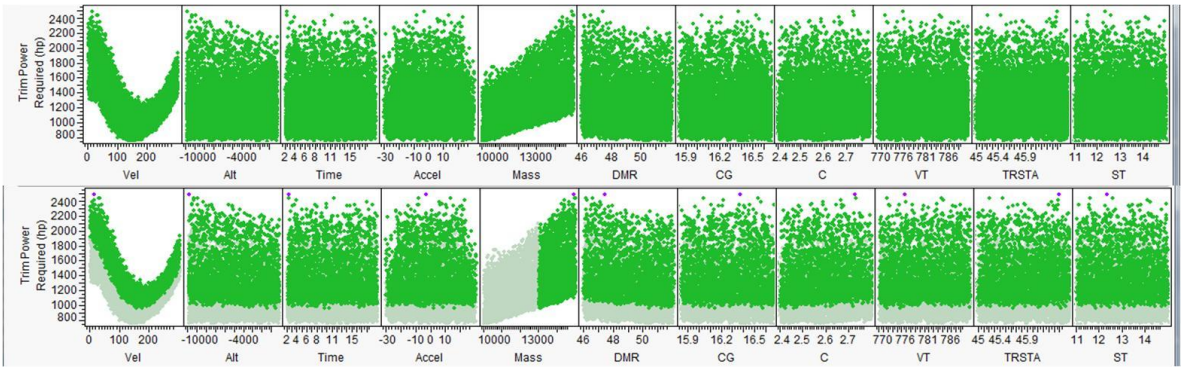

Figure 2.47: Power Required Input Range Filtering

The strength of the energy-based formulation over static power analysis is the ability to look at power requirements during the maneuver rather than at only steady-state conditions. The top portion of Figure 2.48 displays the maximum maneuver power required for all 9000 maneuver simulations. The y-axis now corresponds to maximum power required during each simulation rather than trim power required. The first observation is that the maximum maneuver power is much higher than the trim power required. The trim power required maximum value is just over 2500 hp, while the maximum maneuver power is just over 5000 hp. Another interesting investigation is to view where in the maximum power range that the failed trim power occurs. This is best shown by highlighting the failed run as shown in the middle portion of Figure 2.48.

In order to show that dynamic simulation is needed over static analysis. The engine power constraint of 2500 hp is applied to the maximum maneuver power, which may be viewed in the bottom portion of Figure 2.48. The purple points in the figure

represent the infeasible design and maneuver combinations. Hence, it is observed that this constraint is much more limiting than the static power requirement. This observation shows the importance of including dynamic maneuvers in the design space rather than only steady-state analysis procedures. If only the static power is used many of the unsuccessful designs and maneuvers would not be captured leading to increase in design cycle time and cost due to rework in the later stages of design. The benefits of real-time energy-based constraint analysis are demonstrated through this set of experiments, which analyzed the entire pop-up maneuver space. Additionally, the process was shown to enable systematic and traceable design and constraint trades, which provides improved tradeoff capabilities over traditional analyses.

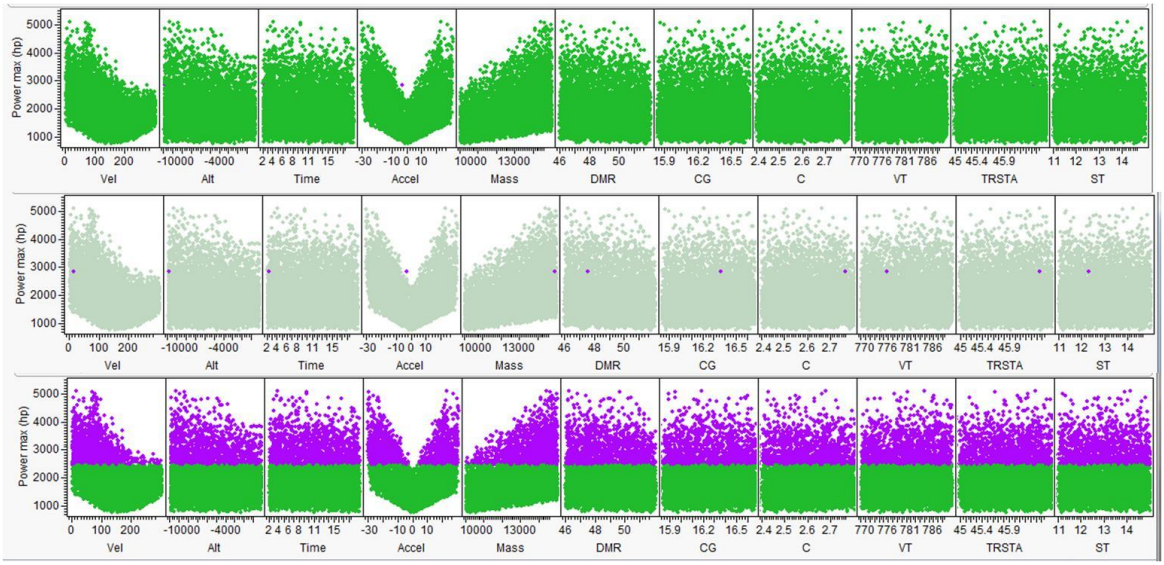

Figure 2.48: Maneuver versus Trim Power Required

2.5.3 Rigid Body Filtering

The rigid body formulation includes all of the capabilities to filter the power results as the energy-based method in addition to the rigid body constraints. In this section, the impact of rigid body constraints associated with kinematic control limits are analyzed. The control deflection constraint is applied and several designs that were deemed feasible by the energy-based method are determined infeasible through the rigid body analysis, thus, showing the importance of this analysis. The experiment will show the importance of integrating the rigid body model into the design process for maneuverability analysis.

The previous section viewed the maximum maneuver power on the y-axis with all of the inputs on the x-axis. In addition to the maximum maneuver performance constraint of 2500 hp, the kinematic control limit constraints are also applied. The feasible (green) and infeasible (purple) designs found through the energy-based filtering are shown in the top portion of Figure 2.49. The bottom portion of Figure 2.49 displays the advantages of using the rigid body formulation over the energy-based approach. The orange points indicate all of the designs that exceed the control deflection kinematic limit of +/- 13.5 degrees. The kinematic limit constraints eliminate most of the points that are filtered due to maximum maneuver power; however, only the points that the energy-based method missed are displayed (orange). The energy-based approach is not capable of removing these solutions from the design space and the designer may select a design that is later in the process deemed infeasible. This example shows that the rigid body formulation is required over the energy-based method to provide more conservative design estimates,

which prevent rework. Additionally, through filtering of the data, it is determined that both the energy-based information and the rigid body information are necessary to fully constrain the space to obtain the most conservative results. The control deflection limit is just one of the many rigid body constraints that can be applied and adjusted real-time. More conservative estimates of maneuverability characteristics result as additional rigid body constraints are applied.

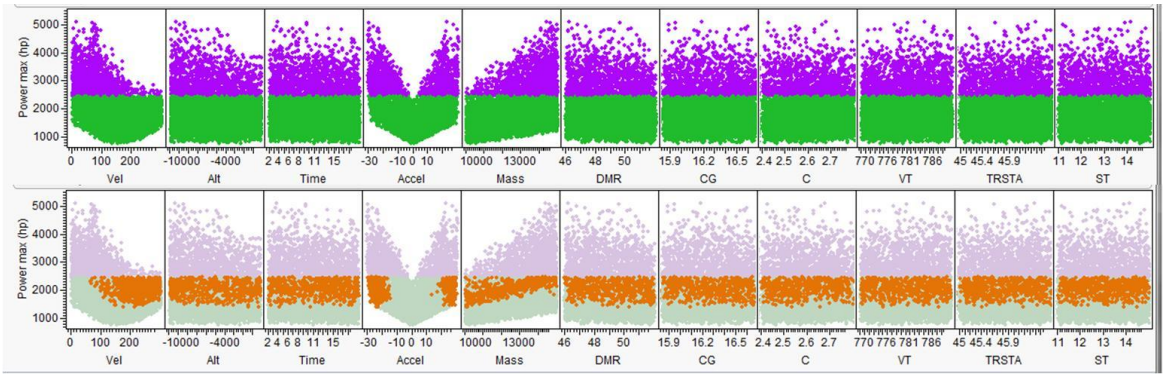

Figure 2.49: Filtering Control Deflection Limits

2.5.4 Minimum Time Maneuver Selection

In addition to allowing for constraint placement through real-time data filtering, the method enables traceable minimum time maneuver and design down selection. A broad range of pop-up maneuvers were simulated and in order to select the minimum time maneuver, the results must first be filtered according to final vertical displacement. This allows the designer to only compare maneuvers that offer similar vertical displacements, which can vary drastically depending on acceleration and time. The final vertical displacement for all 9000 simulations is shown in Figure 2.50 as a function of time and acceleration. The vertical displacement can range between +/- 1500 ft, with a

negative displacement resulting in an altitude increase since z-axis is defined downward. This figure provides the designer with a visual tool for selecting a pop-up maneuver to analyze by showing what combinations of time and acceleration provide the desired end state. Although, useful in a general case for understanding the motion space, data filtering is required to truly down select to the desired maneuver.

A pop-up maneuver resulting in an altitude increase of between 150 and 250 ft is selected for this exercise, which includes much of the red colored region in Figure 2.50. All the other points were removed for this exercise, which leaves approximately 400 points out of the original 9000. The resulting points may be observed in Figure 2.51. This maneuver is selected because it fits well into the AHS 2012 design competition mission scenario, which specifies a pop-up maneuver of approximately 200 ft.

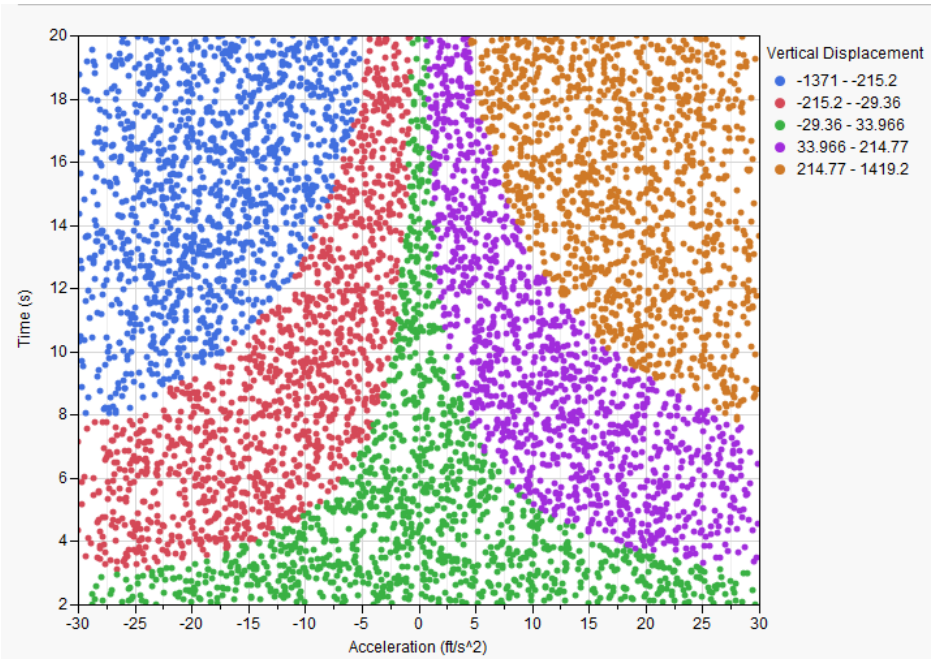

Figure 2.50: Final Vertical Displacement

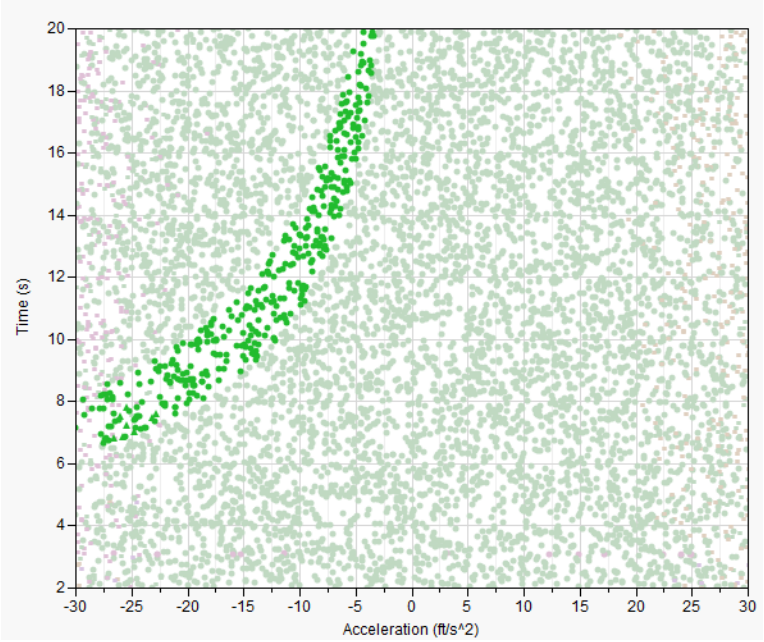

Figure 2.51: Feasible Design Space for Defined Pop-Up

Now that the data set has been filtered to a few maneuvers that result in a similar vertical displacement, further analysis must be conducted to constrain the design space to a feasible set. The two constraints from the energy-based and rigid body examples applied in earlier experiments are used in this experiment. The constraints are maximum maneuver power and maximum control displacements. This filtering approach to the design problem allows particular designs and mission scenarios to be filtered real-time, which provides a systematic framework for viewing the impact of requirements on the design space. It is also shown through this filtering exercise that using the power information alone is not adequate and the rigid body constraints provide improved tradeoff capabilities through more conservative maneuverability estimates.

The 400 points that meet the vertical displacement requirement are shown in Figure 2.52 with the color indicating the power required for the design and maneuver

combination. The maximum power required ranges from 930 to 4850 hp. It was noted earlier that the engine is selected to only provide 2500 hp. As a result, many of the points within this space are in violation of the power available constraint. The points that are in violation are displayed in orange and many of these scenarios correspond to minimum time maneuvers. Through analysis of the maximum power the highest seven acceleration defined maneuvers are shown to be infeasible cases.

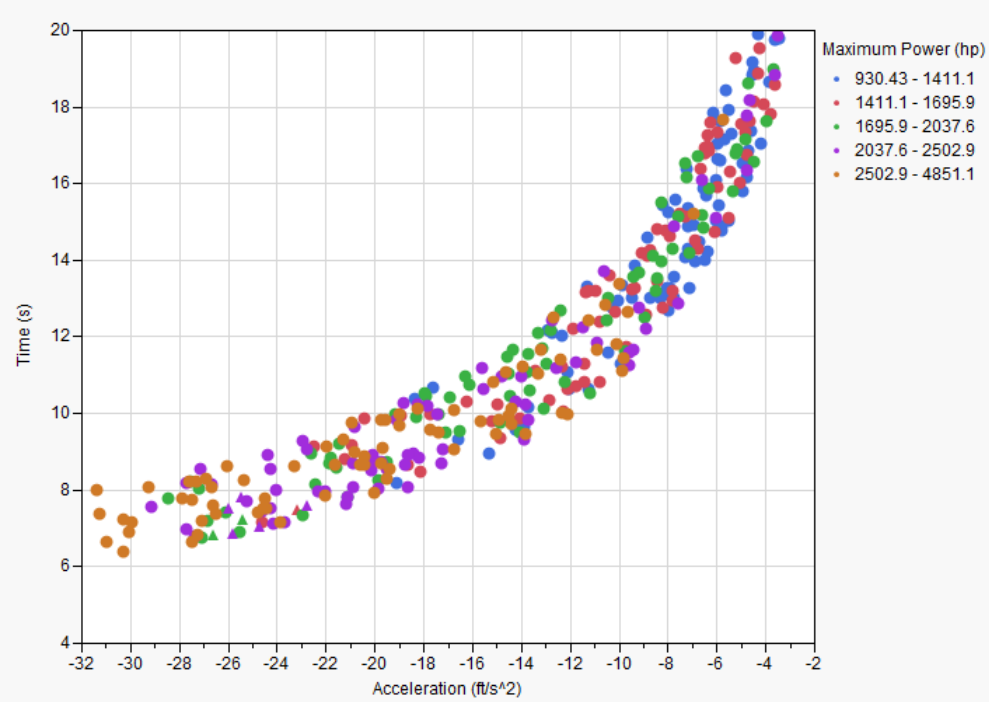

Figure 2.52: Maximum Power Constraint

Figure 2.52 shows many maneuvers within the design space fail to execute the maneuver due to power available requirements through the energy-based equations. Moreover, the impact of considering the rigid body equations into the formulation must also be shown. The requirements imposed are in the form of control deflection limits, where any of the four controls can reach a minimum or maximum limit. However, other

rigid body constraints may also be applied. To make this example simpler, all of the control deflections are compared at each time step and only the maximum magnitude control deflection is recorded. This step allows for the data to be filtered with one requirement rather than eight separate deflection requirements. The results from this filtering is observed in Figure 2.53, where the maximum deflection ranges from 3 to 30 degrees.

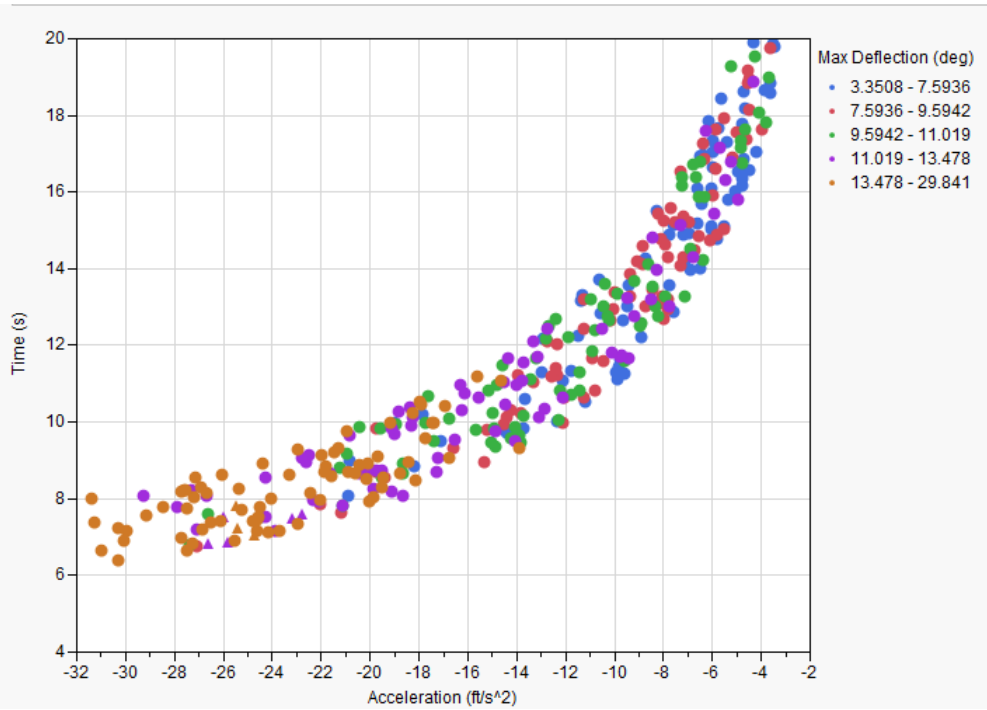

Figure 2.53: Maximum Magnitude Deflection Constraint

At this point the designer may select the maximum deflection limit real-time, which is selected as 13.5 degrees in this example. With this selection, the orange points in the figure correspond to design and maneuver combinations that violate the maximum deflection constraint, which produces many more failed cases than the maximum power available constraint. However, some designs that do not violate the maximum deflection

constraint are shown to violate the maximum power constraint. As a result, these two constraints must be applied together in order to determine the most conservative set of feasible designs.

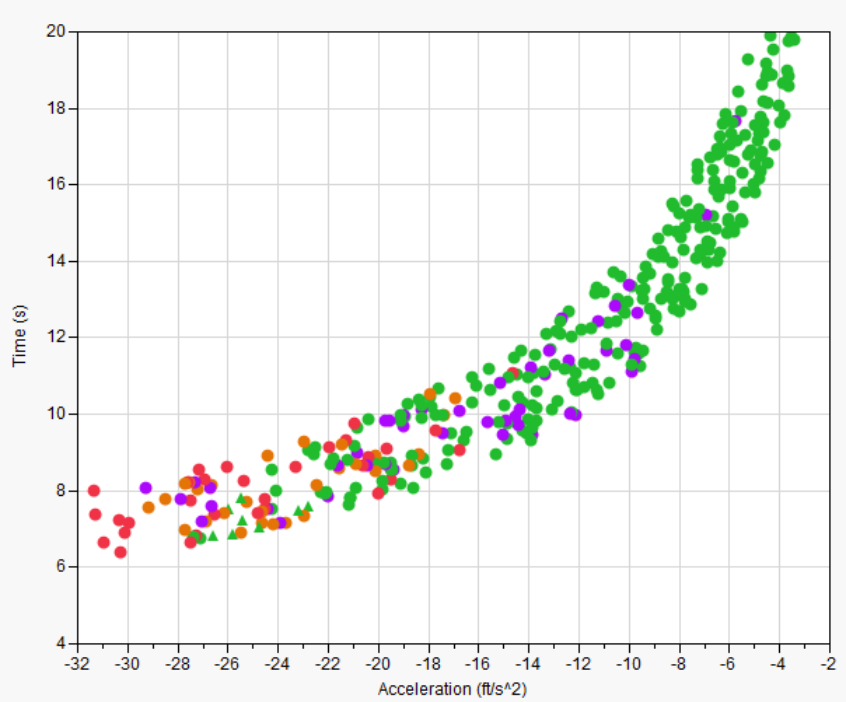

Figure 2.54: Both Power and Deflection Constraints

Both constraints are applied in unison and the resulting data set is displayed in Figure 2.54. The results are presented together to show the importance of including both types of constraints in the analysis. The green points represent feasible maneuver and design combinations, while the orange and purple points represent infeasible design scenarios due to the max deflection and the max power constraints, respectively. The maximum power constraint is first applied, which is indicated by the purple points. Second, the maximum deflection constraint is applied. The red points are representative

of the design and mission combinations that violate both the power and deflection constraints.

The data filtering process provides additional benefit by offering the ability to view the data in any number of dimensions and as the requirements change, the filter can be adjusted real-time and the resulting process provides traceability. An additional filter can be placed on the data set to only maintain the designs that complete the maneuver in less than a particular threshold, which in this example is set to be 8 seconds. The results are viewed in Figure 2.55 and the feasible design and maneuver combinations are displayed as blue triangles. The top performing design achieves a time of 6.75 seconds.

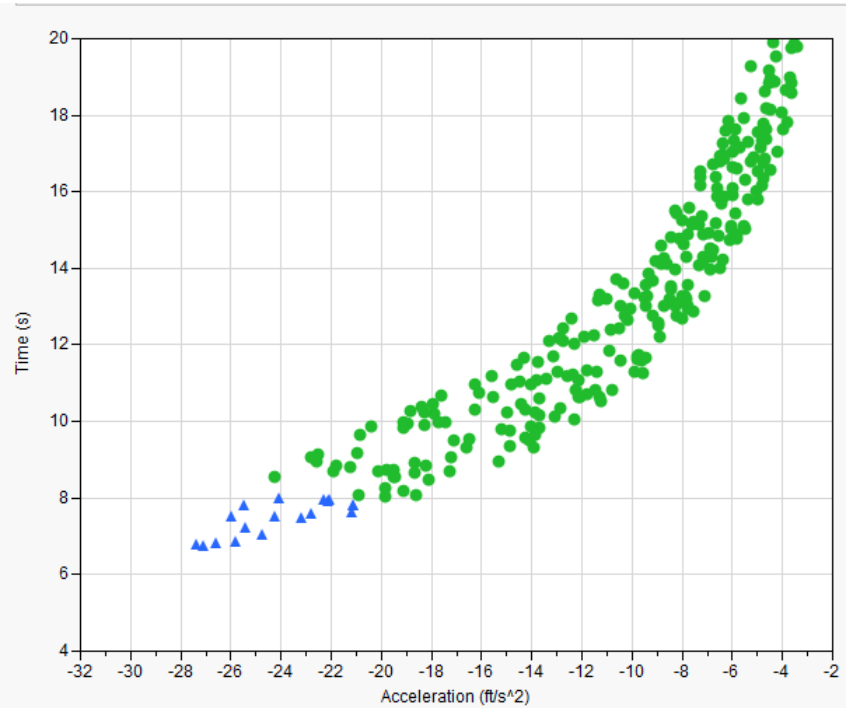

Figure 2.55: Top Designs for Minimum Time Maneuver

The attributes of the top performing scenario can be instantly viewed because each point is stored in a database when using the data filtering method. Additionally, it is common among the design community to have interest in multiple designs that provide the solution rather than a single point. Any number of the top performing designs can be analyzed simultaneously; however, only the top three designs are shown. The design parameter settings of the top performing designs can be shown through numerous methods. First the data is shown in tabular form, which may be observed in Table 2.3. The description is separated into three major categories. The first of which specifies an individual color to each of the three designs. The second and third categories present the input parameters for the maneuver model and the helicopter model, respectively. Prior to fully explaining these observations, the second type of viewing method is also shown. A parallel plot is shown in Figure 2.56, which enables a more visual and holistic approach when comparing the information.

Table 2.3: Top Performing Designs

		Design		
Variable Name	**Unit**	**1**	**2**	**3**
Color	-	Orange	Purple	Green
Velocity	ft/s	98	140	98
Altitude	ft	-2320	-4780	-489
Time	s	6.75	6.8	6.77
Acceleration	ft/s^2	-27.1	-26.6	-27.3
Vehicle Mass	lb	10250	10750	11272
Diameter Main Rotor	ft	51.1	51.7	50.46
Center of Gravity	ft	15.96	16.1	15.93
Main Rotor Chord	ft	2.68	2.77	2.54
Main Rotor Tip Velocity	ft/s	786	780	773
Tail Rotor Moment Arm	ft	46.2	46.1	46.2
Horizontal Tail Area	ft^2	12	11.3	12.8

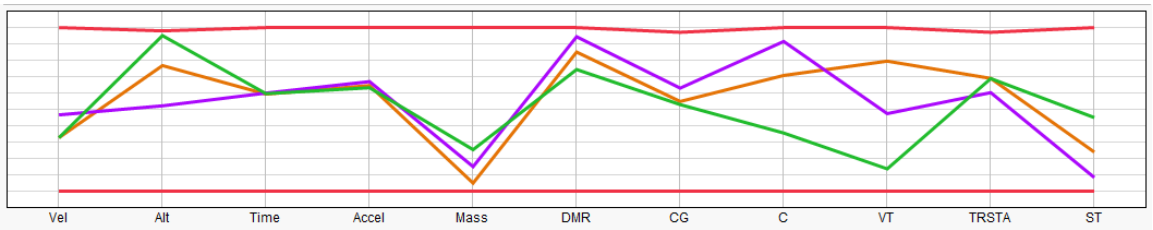

Figure 2.56: Parameter Breakdown of Top Performing Designs

The parallel plot enables all of the design parameters to be viewed simultaneously for all three top performing designs. The red lines provide the upper and lower bounds of the figure, which represent the range limits on the input parameters. Each of the three designs is shown as a separate color and corresponds to the colors column in Table 2.3. The designer can now investigate the various inputs and find commonalities between the various designs. For example, both the orange (1) and the green (3) perform the mission in a similar amount of time with the same velocity and vertical acceleration; however, the altitudes are different at 2320 and 489, respectively. This means that within this range, altitude is not a major factor in completion of the maneuver. Additionally, it may be observed by comparing the orange and the green lines in Figure 2.56 that the designs only vary substantially in rotor chord and rotor tip velocity.

These same trends in vehicle design parameter values are true for the purple (2) maneuver as well, which requires a different velocity for completion. The important fact about this observation is that specific design parameter selections allow for completion of the maneuver in minimum time in multiple paths. As long as the mass, CG, main rotor diameter, tail rotor moment arm, and tail area are within the ranges of the first three design points, the vehicle can perform the defined pop-up via two different maneuver

definitions. The maneuver can be either completed at around 98 ft/s or around 140 ft/s. Additionally, the green design is close to reaching the maximum power limit and the purple design is approaching the longitudinal cyclic limit, which may be viewed in Figure 2.57. Hence, the design parameters associated with the orange path provide the less risky design selection option and the most robust to the applied constraints. This observation can be further explored using the data filtering process.

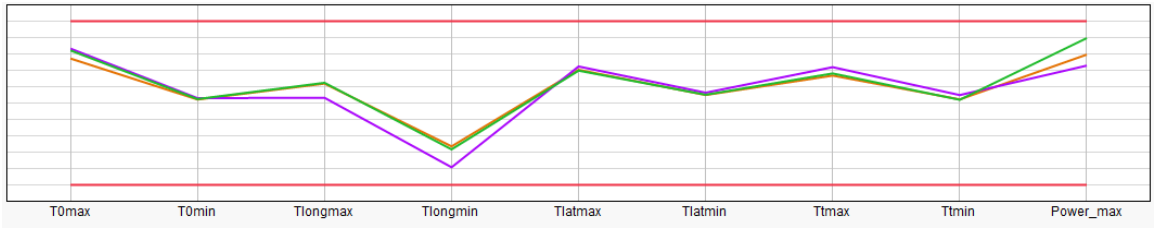

Figure 2.57: Kinematic Control and Maximum Power Constraints

Running a few more simulations in the area of interest for each of the three designs is conducted. The mission is fixed to the parameters defined by the top performing maneuver definition, while the design parameters are allowed to vary by +/- 5% of each of the designs in Table 2.3. This analysis provides the designer with an idea of the relationship of design parameters to the applied constraints subject to design variability. Additionally, this step displays the flexibility of the method and that the appropriate hooks are in place for future uncertainty analysis strategies. The results are most easily observed by viewing the design parameter ranges for each of the three designs similar to the process employed earlier using the parallel plot. The results are shown in Figure 2.58, where the colors correspond to the same designs described earlier with +/- 5% variation. As before, the first three designs display similar mass, rotor

diameter, cg, tail rotor moment arm, and tail area values; however, the tip velocity and main rotor chord vary substantially.

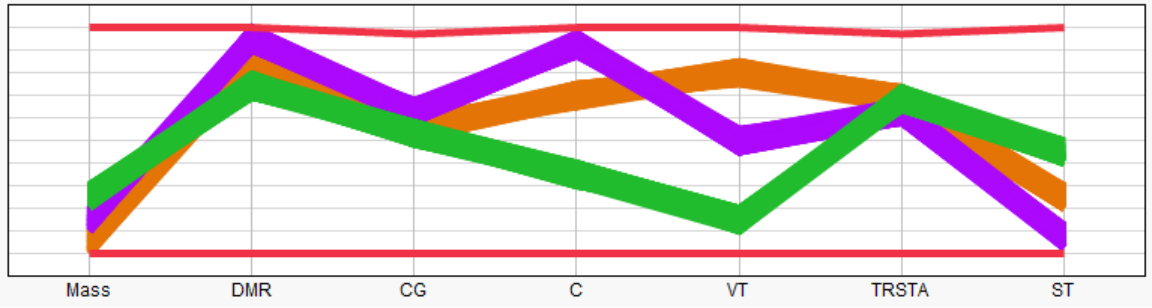

Figure 2.58: Design Variability for Minimum Time Maneuver

The constraints of the corresponding designs are shown in Figure 2.59, where the distributions for each of the power and deflection limits are shown for the range of design parameters. These results show that the control deflection limits are almost always maintained for the design variability ranges. At this point, other maneuvers with mission definition may aid in further down selection of the rotor tip velocity and main rotor chord, which are the only differences between the top three designs.

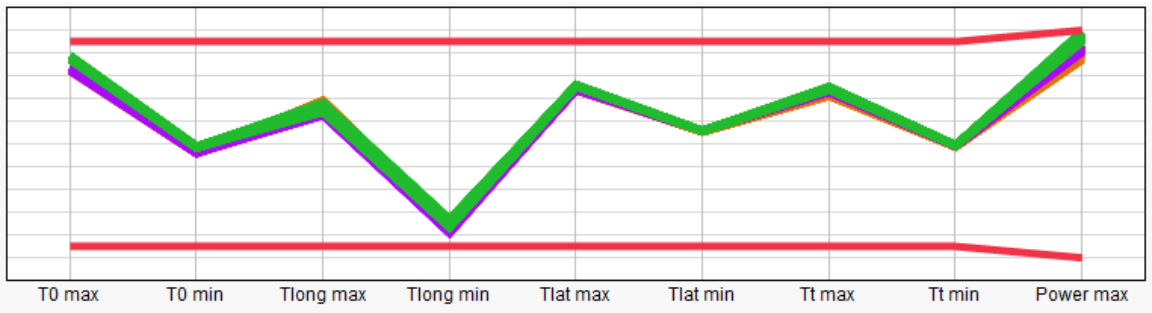

Figure 2.59: Constraint – Design Relationship for Variability

2.6 Summary of Contribution

The key components of the hypothesized method allow for the established need to be fully addressed. First, the combination of a parametric rotorcraft model and inverse simulation technique were shown to provide the essential framework to conduct quantitative maneuverability analyses of helicopters independent of control design. The results using the framework were compared to previous research efforts that employed inverse simulation, as well as, actual flight test data. The rigid body formulation was shown to offer significant advantages over the energy-based approach and was deemed essential in capturing more conservative maneuverability estimates. Additionally, by expanding on the work from previous research efforts by integrating a parametric rotorcraft model, the design variables can be specified as ranges rather than point solutions. This allows the designer to view the design space in a holistic manner and view multiple dimensions simultaneously. Secondly, the important design parameters were chosen from a source in literature that used an established screening method. The ranges on these inputs can change as knowledge about the design is gained; hence, a data filtering technique was integrated that allowed the design ranges to be restricted dynamically as knowledge about the design increases. Finally, in addition to filtering the input parameters, the data filtering technique permitted constraints and requirements to be added and removed from the trade studies in a dynamic manner. Through combination of these components and a helicopter example using a pop-up maneuver, the first contribution of this thesis work was presented and the relationship of design parameters to maneuverability was assessed. The design parameter variability impacts on maneuver

performance of the minimum time maneuver designs were investigated and important relationships were discussed.

Contribution 1: A six degree-of-freedom rigid body parametric rotorcraft inverse simulation model in combination with Filtered Monte Carlo that provides improved quantitative maneuverability tradeoff capabilities over traditional design methods.

CHAPTER 3

CAPTURING CONTROLLABILITY CONCERNS

3.1 Introduction

Although the maneuverability must be assessed independent of the control maneuverability degradations in order to capture the true limits of the vehicle, some measure of controller characteristics must be included. The inverse simulation approach assumes perfect control knowledge and does not include any measures associated with control system design characteristics. The problem is that the control system design decisions have a major impact on the feasibility of a maneuver, which may substantially degrade from the performance of the ideally controlled system. These degradations decrease the maneuver capabilities of a design, while at the same time cause errors that result in divergence from the desired path. In order to better understand the direction of this chapter, the overall research objective is re-presented.

Overall Research Objective: Develop a methodology that enables real-time and traceable assessment of:

- **Design parameter impacts on maneuverability characteristics**
- **Maneuverability degradations due to control system characteristics**
- **Entire helicopter operational envelope maneuverability**

The focus of Chapter 3 is addressing the second aspect of the overall research objective, which is capturing maneuverability degradations due to control system integration characteristics. The degradation of maneuverability is summarized by Figure

3.1, where the blue curve indicates the time required to perform the mission with an ideal controller. The horizontal axis displays the individual maneuvers and the combination of the maneuver times form the entire mission time. The other two curves in the figure represent two different types of control architectures applied to the vehicle and the resulting maneuverability limits. The decrease in maneuverability from the ideal case is measured by an increase in time for each maneuver. It is observed that the control decisions have an impact on the maneuverability limits with varying amounts of degradation occurring for different maneuver definitions. Each maneuver is affected differently by the control design decisions, but no matter the case, the controller integrated design can never outperform the ideally controlled design.

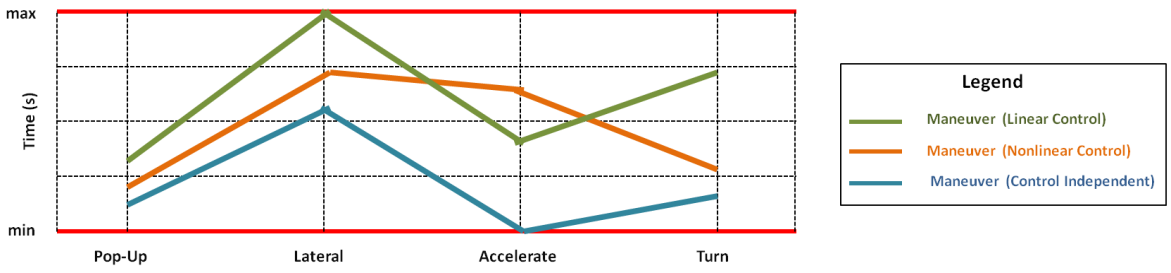

Figure 3.1: Performance Degradation Due to Control Decisions

Thus far the control system design has been only separated by a simple delineation of linear controller versus nonlinear controller. However, this is just a simple notional case. The performance degradations between the various curves in Figure 3.1 can also be calculated and shown for the same linear controller with two different types of actuators or different sensor placement schemes, which represent just two decisions among others. At this stage in the design process, gaining a general understanding of the

control system design requirements is important because detailed controller development is limited by the combinatorial nature and the lack of detailed knowledge required, thus, cannot be completed. If no control integration measures are included in the process, the design may progress to the next stages only to find out that the design is not feasible due to controllability limitations. For example, assume that the "optimum" design requires control actuator rates of 300 degrees/sec in order to perform the maneuver. The control designer may see this requirement on actuator rates and realize early in the process that this is not feasible, thus, mitigating design time, risk, and cost. Moreover, control design is a human-driven iterative process that requires detailed knowledge of the system that is not available at the conceptual design stage. For this reason the focus of this chapter is in addressing control integration characteristics rather than fully designing the controller. In order to address this problem, the control integration process must be investigated.

3.2 Literature Review

In order to fully understand the control design and maneuverability analysis problem, literature is reviewed with the focus of understanding the relationship of key control integration characteristics to maneuverability characteristics. A general set of control related characteristics that can be integrated into maneuverability analysis for conceptual design are investigated. The selection of these measures requires careful balance between gaining enough information about the control system quantitative requirements, while at the same time remaining in the conceptual design level. Additionally, due to the curse of dimensionality during design this number must be kept to a minimum set.

3.2.1 Controller Integration Characteristics

The control characteristics can be captured in a number of ways; however, through literature review of motion planning problems and control design, a few facets of information are determined important. Chipperfield [22] states, "these include, but are not limited to, the type and location of sensor and actuator devices, the sensed parameters used to close control loops, the form of control to be employed and the size of design margins for stability, robustness, and degradation." Measures must be integrated into the early design process in order to develop requirements related to these control integration considerations; however, there are major hurdles that must be overcome.

The first problem is that control design is very human-driven process and requires more detailed information not available in early design stages. Some approaches have been made to remove the human from the control design loop; these include the weighted sum and goal attainment methods [191]. However, such expressions require precise expression of a usually not well understood set of weights and goals, which result in less than optimal solutions. Additionally, Perez [8] notes that flight dynamics and control "does not have an obvious figure of merit that can be used for design optimization", hence, the process requires human interactions. Through these observations, it is demonstrated that the decision maker must aid in determining the localization of the search performed rather than obtaining the entire solution from an optimization algorithm [103].

It is important to capture performance impacts due to controller integration, both hardware and software, during early design; however, additional difficulties arise because of the quantity and quality of data required for these types of trades. For example, in order to differentiate the impacts from the sensors and the actuators, the modeling environment must contain detailed information for both of these subsystems. Another example is the impact of control architecture choice. As soon as the control architecture is chosen for the system, a large number of controller specific tuning parameters are introduced. The curse of dimensionality prevents the addition of all the parameters required for comparing multiple architectures with detailed actuator and sensor information. Chipperfield [22] states that "the task of selecting a suitable control configuration is thus further complicated by the number of possible, but perhaps undesirable, configurations." Hence, there must be a tradeoff in the amount of control information in the design process and the capability to make quantitative trades that aid in controller development.

The remaining hurdles are addressed by reviewing the control integration and design process, which is displayed in Figure 3.2. Commonly, the control system design problem consists of the specification of a plant and a few operating points of interest, and the control designer is required to meet some performance criteria [23]. This process involves a compromise in order to meet the performance requirements at the various points within the envelope. As determined through literature review, the link between the control design and the maneuverability appears through the control system characteristics.

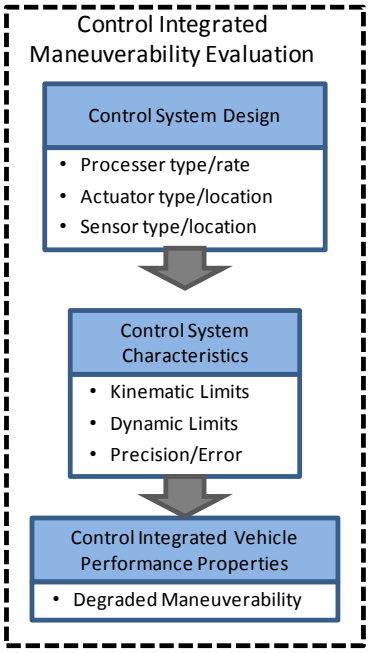

Figure 3.2: Control Integrated Maneuverability Evaluation

The objective is to address the degradations due to controller choices; however, the controller cannot be developed during conceptual design because the detailed information is unknown. The second step of the control integrated maneuverability assessment process is to gather general characteristics and requirements stemming from the control system design decisions. These control system characteristics are then employed to conduct the maneuverability degradations. The focus is to relate the impact on quantitative maneuverability limits to control system requirements, which can be used as control system requirements during control development. This information enables the control designer to develop an overall system, hardware and software combination, to a set of requirements such that the integrated system produces the desired performance thresholds.

Three control characteristics, which include kinematic limits [22, 23], dynamic limits [192], and error propagation [193-195], are provided for the conceptual design phase. The kinematic control limit is already included through the rigid body constraints in the form of control deflection constraints; however, the remaining two control characteristics require further elaboration.

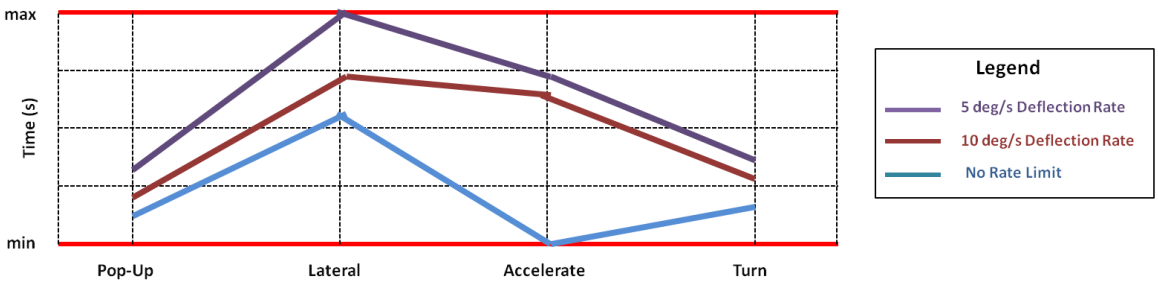

Figure 3.3: Control Deflection Rate Real-Time Constraint Placement

The dynamic limits include both state and control variables within the rigid body formulation. One example of a dynamic limit is control deflection rate constraint, which when provided at the conceptual design phase can be used to capture the dynamic rates of multiple control system components. For example, the control deflection limit can capture the impact from actuator, sensor, and processer properties. Figure 3.3 displays a notional representation of applying control characteristics to the maneuverability analysis through the control deflection rate constraint. The implications of choosing an actuator that provides control deflection rate of 5 degrees/sec versus an actuator that provides 10 degrees/sec are shown in the figure via the purple and red curves, respectively. The x-axis displays four different mission maneuvers. The performance for the mission is indicated by the summation of the maneuver times. As constraints become more limiting, the

performance limits degrade which leads to a greater mission time. This analysis shows what the corresponding controller constraints must be to achieve a desired performance, which leads to development of control system design requirements.

The second control characteristic provided through literature review is control error propagation information, which includes errors associated with multiple components such as sensors, actuators, and feedback loop properties. For example, Celi [21] showed divergence from the desired path due to errors introduced through the pilot. Furthering the research in this area, Serr [196] established a method for parametrically modeling the pilot error and displayed the cumulative divergence from the intended path. The effect of pilot error such as reaction times, overreaction or the repeatability of actions is investigated in order to assess safety margins in flight trajectory [196]. This knowledge requires sensing rates of the system to be defined in addition to how the controller will account for the error. Since this information is not known at this stage in the design, some alterations are necessary to integrate these error measures into conceptual design.

The error in trajectory that results due to error in commanded deflection is a valuable measure that, if specified correctly, provides general control system requirement information. Figure 3.4 demonstrates the divergence from the intended path due to commanded control errors. In this example, the divergence in performance capabilities due to commanded error is being used to generate requirements on the control properties. The defined pop-up maneuver is shown as the orange curve in the figure, which was discussed in detail in Chapter 2 analysis. The blue and green error bars represent divergence in path due to commanded control error of 1 and 5 percent, respectively. The

bars indicate the divergence bounds from the desired trajectory resulting over each individual time step. Using this information the designer can specify a maximum divergence from the path over the specified time step that is acceptable, which leads to a control system design requirement associated with acceptable commanded control error.

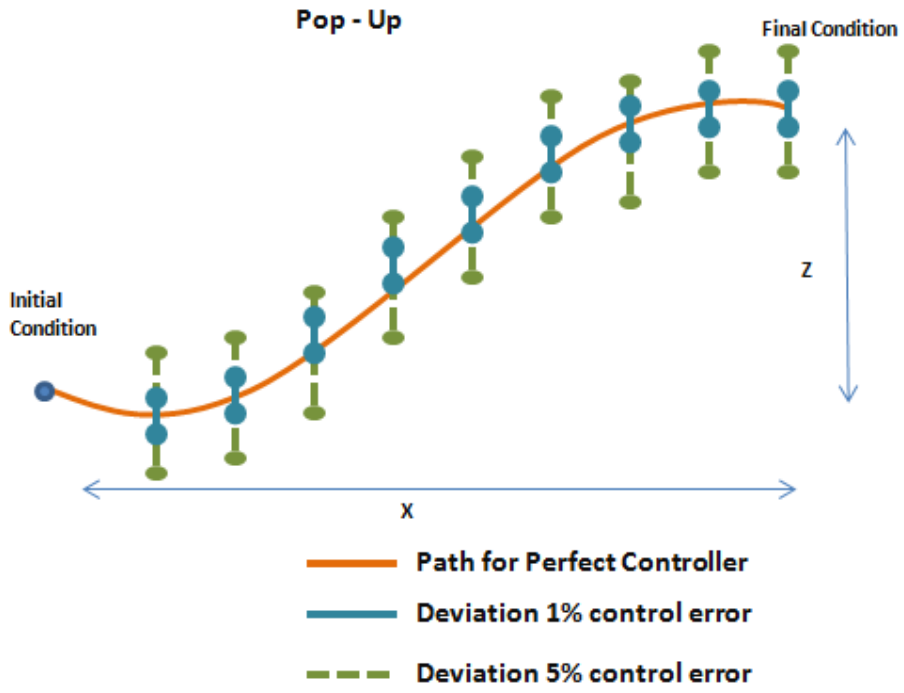

Figure 3.4: Trajectory Divergence due to Commanded Control Error

This type of information deals with error in a general sense, while at the same time does not require information on sensor and actuator placement and rates. The control designer can relate the control system design to these quantitative divergence requirements when making important control integration decisions. Additionally, incorrect control deflection setting can result from a multitude of sensor errors across the entire vehicle and an understanding of how this error propagates to maneuver completion is required. Murray-Smith [48] acknowledges that "the inverse approach can show very

clearly when a particular task is likely to be beyond the capabilities of a human due to dynamic limitations such as reaction time and neuromuscular lags." This type of analysis can also be applied to determine limits of the actuation rates of the control system.

3.3 Approach

The approach to integrating control design characteristics into the maneuverability assessment framework is addressed in four parts. First, a research question is formulated based on the needs that are provided by assessing the control integration shortfalls of the process developed in Chapter 2. Secondly, it is shown that through modification of the process developed in Contribution 1 of this thesis, the controllability concerns of the problem may be addressed. A hypothesis is then presented based on literature review in an attempt to address the needs defined in the objective. Finally, a test plan is presented that details the experiments that are to be simulated and how the data is to be analyzed.

3.3.1 Research Question

The need to capture control integration characteristics in a design-focused inverse simulation framework in order to provide valuable information to the designer regarding control system requirements is investigated. In order to accomplish this task, two key measures associated with controller integration degradation on maneuverability are integrated. The investigation results in two modifications of the systematic process developed in Chapter 2, which are applied to the rotorcraft pop-up problem. A large amount of information could be integrated into the process for design of the control

system; however, the idea here is to integrate as few measures as possible that provide the most information to the control designer during conceptual design. Both fidelity of the model required for maneuverability analysis and dimensionality concerns stemming from the control design process are forcing this requirement. As a result, control system design is not feasible at this stage; however, the controllability concerns must be included.

Research Question 2: How can the quantitative impact of control integration decisions on maneuver performance be used to develop control system requirements independent of control design?

The integration of control characteristics impact on maneuverability is applied in early design because detailed control design is not feasible. The main objective of this research question is to offer quantitative trades to drive overarching design decisions and provide key problem areas to track during the design process for the control system designer. The first need posed by the research question is that the control system integration measures must be determined and included into the quantitative dynamic performance design framework. More importantly, these measures must be independent of control design because little information is known about the control hardware or software at this point in the design. These characteristics must be assessed real-time in order for the designer to understand how the maneuverability of the vehicle is impacted, thus leading to development of control system design requirements.

3.3.2 The Modified Process

The process discussed in Chapter 2 of this thesis captures the impact in maneuverability limits due to design variability for a single mission maneuver. Prior data analysis techniques did not apply a real-time data filtering approach to the maneuverability problem and design approaches did not employ the rigid body formulation. The process uses an inverse simulation algorithm in order to determine the maximum performance for the system independent of the control system. However, in conducting the analysis in this manner, measures on control design and integration requirements leading to cost and risk decisions are not captured. The inverse simulation technique assumes perfect control and control knowledge. For this reason, the second contribution is included such that maneuverability degradations due to non-perfect control characteristics can be assessed. This is accomplished through modifying the control integrated maneuverability assessment process, which is shown in Figure 3.5. Rather than completing the control system design, which is not feasible in conceptual design, the process starts by determining control system characteristics. These characteristics are a function of the control system design and are based on the design stage and detailed level of the model.

The second contribution of this work extends the capabilities of this systematic and traceable process to include two measures, which are highlighted red in Figure 3.6. These improvements are essential in capturing the relationship of control integration degradations on maneuverability in a quantitative manner in the early stages of design. As the design progresses into the later design stages, these measures can be adjusted to

include more detail. The first control characteristic is the inclusion of the control deflection rate limits, which allows for the designer to analyze the maneuverability limits subject to dynamic control constraints. This characteristic is included in the post processing step of the overall methodology.

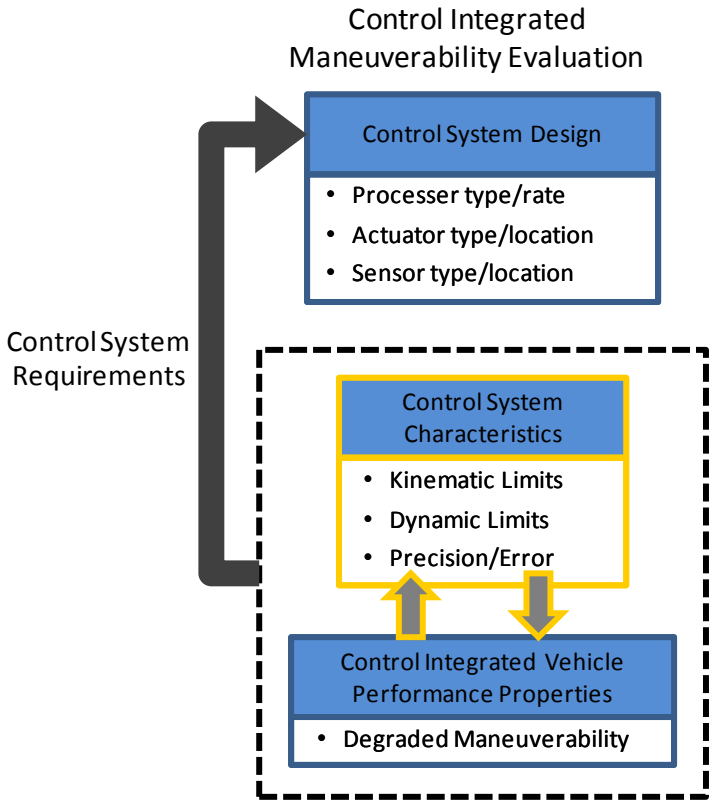

Figure 3.5: Control Requirements Definition Extension

The second control characteristic is the trajectory divergence measure, which provides quantitative trajectory divergence rate information that enables the designer to visualize how fast the given design and maneuver combination will diverge from the desired path as error is introduced into the control loop. Both of these extensions are integrated in order to capture the control characteristic impact on maneuverability and are

discussed in more detail in the implementation section. The maneuverability impact from these characteristics is utilized to form control system design requirements. These requirements provide the control designer with a set of characteristics that the control design must achieve in order to achieve the desired maneuverability. This process of using the control characteristics in combination with a parametric inverse simulation framework to provide quantitative control design requirements is the extension in this work. The two control characteristics are just two measures used to show the benefits of the extension, which are demonstrated through a detailed rotorcraft example during Experimentation.

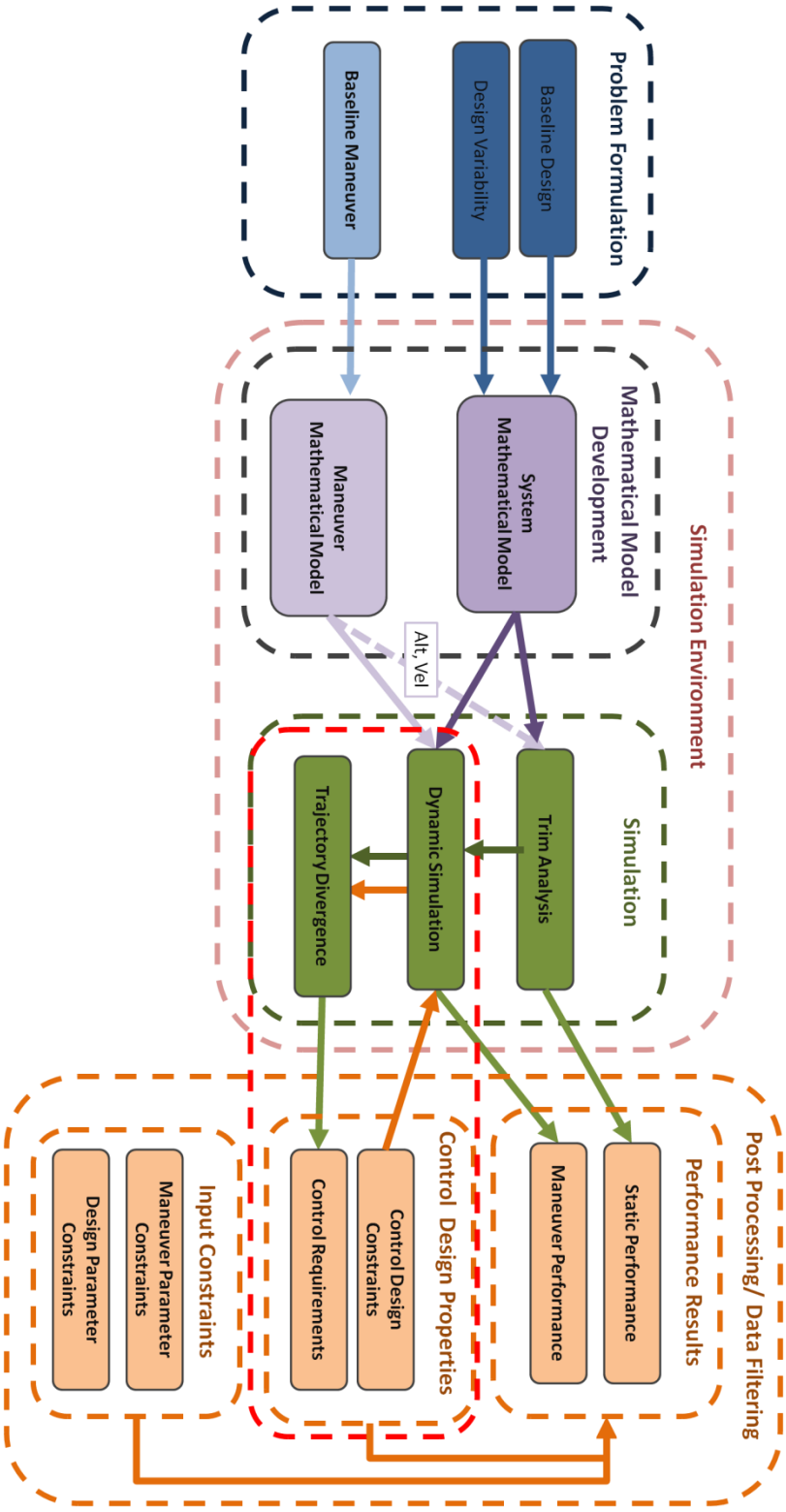

Figure 3.6: Modified Process

3.3.3 Hypothesis

By including the deflection rate limit, the ability to analyze more conservative performance estimates is realized. Additionally, the control rates for the four controls can be analyzed independently if desired using this process. The data filtering is conducted post processing, thus, the impact of changing control rate requirements on the design can be viewed in real-time, which enables important control design decisions. The control deflection information is stored during each time step of the simulation as a result of the approach presented in Chapter 2 for the range of design variables provided. The information related to control deflection rate is determined directly from the control deflection time history data set because the time step of the simulation is known. This process would be difficult with a variable step integration routine. Fortunately RK4 is employed in this work, which assumes a fixed time step. As a result, a data filtering technique can be used to determine the minimum time maneuver with the deflection, power, and deflection rate limits all imposed simultaneously.

The second component is a technique for bounding the maneuver divergence due to commanded control error. Through specifying maximum error deflections from the ideal solution, the bounds on the divergence can be assessed. Moreover, these maximum error deflections are specified in a parametric manner enabling the designer to relate error in control deflection directly to divergence in system states. As a result, the amount of error that can be tolerated within the various control system components can be determined and various options can be compared and contrasted. For this analysis, the control deflection error is included. This error can be directly correlated to error from

various components of the system including control deflection tolerances and inertial/position sensor errors. The optimization algorithm used for trim analysis in the simulation environment in Chapter 2 was shown to be accurate and robust. The routine can be easily adjusted to provide the maximum of the function rather than the minimum. This relates directly to the maximum divergence problem when provided a range of possible commanded control error. It is shown in the following sections through example that the attributes of the hypothesized method solve the stated research question, which in turn accomplishes the research objective.

Hypothesis 2: The real-time analysis of control system characteristics impact on the maneuverability limits provide improved estimates and traceability for development of control system design requirements.

3.3.4 Test Plan

The modifications to the process are previously discussed; however, the new information that is to be gathered from the simulation requires addressing. The inputs still consist of both the system and the maneuver model parameters, while the outputs are maneuver performance and time-based system properties. The system modeling parameters remain the same as determined through the process in Chapter 2, except for the addition of a max deflection error variable. The max deflection error variable indicates the maximum plus and minus change in deflection from the converged solution at each time step within the simulation. The maneuver definition is unchanged in this portion of the analysis.

The process modifications greatly impact the number of input and output variables that are parsed for post processing. The control deflection rate for each of the four controls is now extracted during each time step. In addition to introducing the maximum error deflection variable, all of the maximum state and auxiliary variable errors are extracted as a measure of divergence from the desired states. This information allows the designer to see the maximum divergence in desired state resulting from commanded control error, as well as, which controls are driving the error bounds. As stipulated in the original process, all the states, controls, and auxiliary variables are outputs from each simulation. The feasibility of a maneuver, which is determined by whether a set design completes the entirety of the maneuver, is also captured as before. With this information, the performance limit degradations due to control deflection rate limits and the divergence in the desired trajectory due to commanded control error are captured.

The post processing of these pieces of information is conducted on two levels. The control deflection rate analysis is analyzed in a holistic sense and applied when viewing the entire design space. The divergence in desired state is conducted on a single maneuver basis, which occurs after down selection using the entire data set and the constraints imposed in Chapter 2 analysis. Through this series of experiments, quantitative control system requirements are formed in a systematic and traceable manner. It is also shown that the improved conservative nature of the added constraints provides improvements in maneuverability estimates.

3.4 Implementation

The modifications to the proposed process are presented in Figure 3.8, where the newly integrated controllability elements are highlighted in yellow. The control integration characteristics and corresponding process extensions are discussed in detail. The extension in this work is the manner by which control characteristics impact on maneuverability is used to develop real-time and traceable quantitative control system requirements. The first control characteristic includes a dynamic limit measure, in the form of control deflection rates, in addition the control kinematic measures introduced earlier. The second characteristic requires integration of an additional module that enables trajectory error to be determined based on commanded control errors. An example is presented to show how the error information may be systematically traced from the entire design space analysis down to a single maneuver. Additionally, how this information can be used for real-time development of quantitative control design requirements is addressed.

As shown through literature review, inverse simulation approaches historically have not included capabilities for simultaneous design and maneuver analysis, let alone quantify control design characteristics impact on maneuverability. The control characteristics include two measures in this work; however, these measures can be expanded in future analyses. The first characteristic is included to allow for selection of feasible design alternatives through application of control deflection rate requirements. This maximum limit in control deflection rate is then passed on to the control designer as a requirement for control system design. The second characteristic includes system

attributes associated with trajectory divergence from error propagation. This means that the designer must select appropriate hardware and software combinations that provide particular control characteristics. If these characteristics are achieved then the maneuverability goals are obtained.

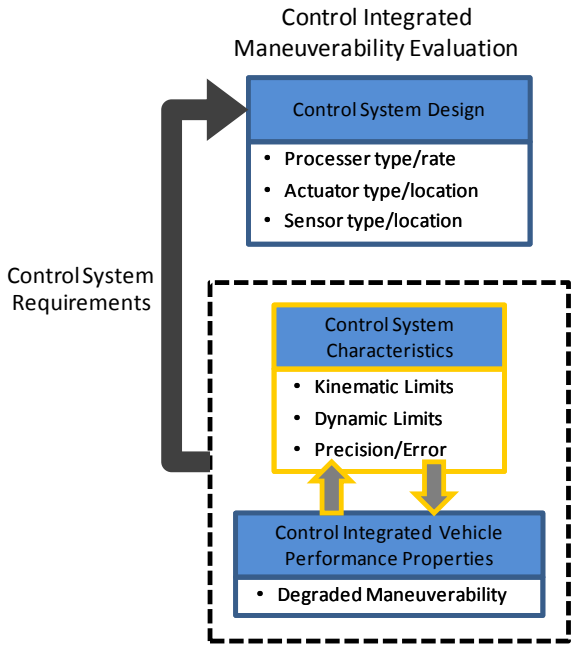

Figure 3.7: Control System Requirements Extension

This extension is displayed in Figure 3.7, where the output of this process are control system design requirements. Additionally, the method is made parametric such that the control characteristics can be adjusted real-time during post processing. If during control design it is determined that due to cost reasons the actuator performance must be lowered, then the designer can instantly view the impact on helicopter maneuver capabilities due to the actuator changes. Thus, the iterative nature of design can be conducted real-time and provides repeatability and traceability in the decision making.

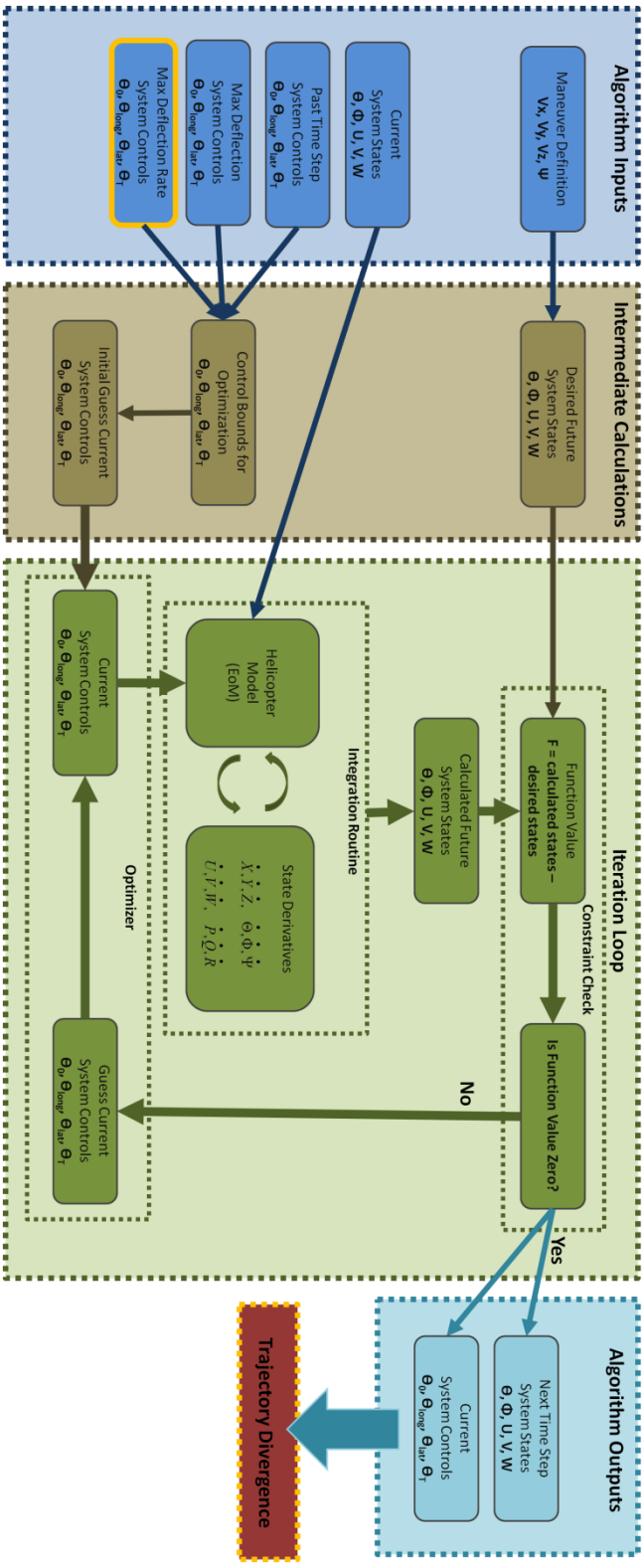

Figure 3.8: Modified Dynamic Simulation

3.4.1 Control Dynamic Limits

In order to include the ability to capture control deflection rate limits for the entirety of the maneuver, the process developed in Chapter 2 must be altered. The control deflections are recorded at each time step during the simulation as shown in Chapter 2 analyses. The resulting time history for the main rotor collective deflection is shown in the top portion of Figure 3.9. Initially the main rotor collective deflection is set at 2.2 degrees, which is the setting calculated in the trim analysis portion of simulation. Once trim is determined, the dynamic portion of the simulation begins. Through the first 3 seconds of simulation the setting changes from 2.2 degrees to approximately 4.2 degrees. This increase results from the need to increase thrust when performing the pop-up maneuver. During the second half of the simulation, the opposite occurs in order to decelerate the vehicle back to steady-level flight.

The control deflection rates can be determined by using the control deflection angles for each time step. By calculating the difference in the change in deflection over the time step, the control rate is calculated. The time step of the simulation is set to 0.1 seconds and from 0 to 0.1 seconds the controller changes from 2.27 degrees to 2.27001 degrees. Hence the rate near zero occurs over the first time step. This process is repeated until the end time is reached. This rate is shown as a function of time within the simulation as displayed in the bottom portion of Figure 3.9. The control deflection and corresponding deflection rates show that the rate is clearly the derivative of the deflection angle.

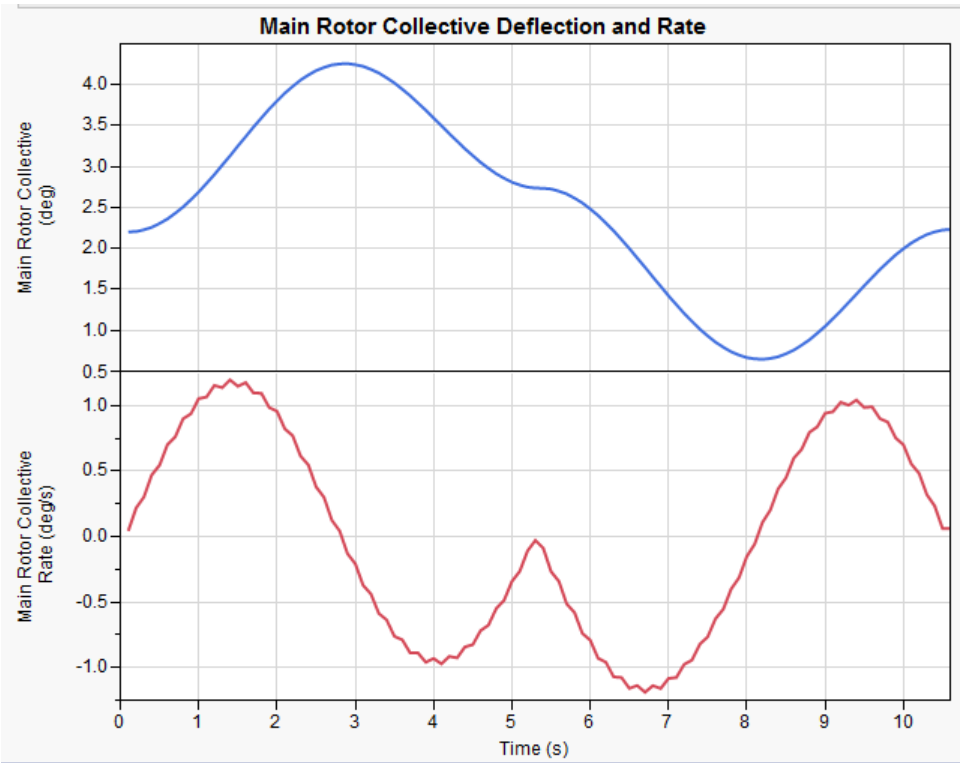

Figure 3.9: Main Rotor Collective Deflection and Deflection Rate

The important observation from this figure is that the maximum rate of approximately 1.2 deg/sec occurs at 1.5 seconds. If the control system does not offer this level of performance when integrated with the system, then this maneuver becomes infeasible. Although, the deflection rate is not large in this example, it is expected that the new rate constraint will provide more conservative maneuverability estimates. This process is applied to all four control surfaces such that they can be analyzed individually if desired and the deflection rates are shown in Figure 3.10.

Similar to other constraints, such as maximum power and control deflection angle, the maximum and minimum control deflection rate can be extracted for each simulation. This information can be used during data filtering to view the impact of

control rate limit on maneuver success or to remove points that exceed a maximum rate limit threshold, which enables real-time quantitative control requirements development.

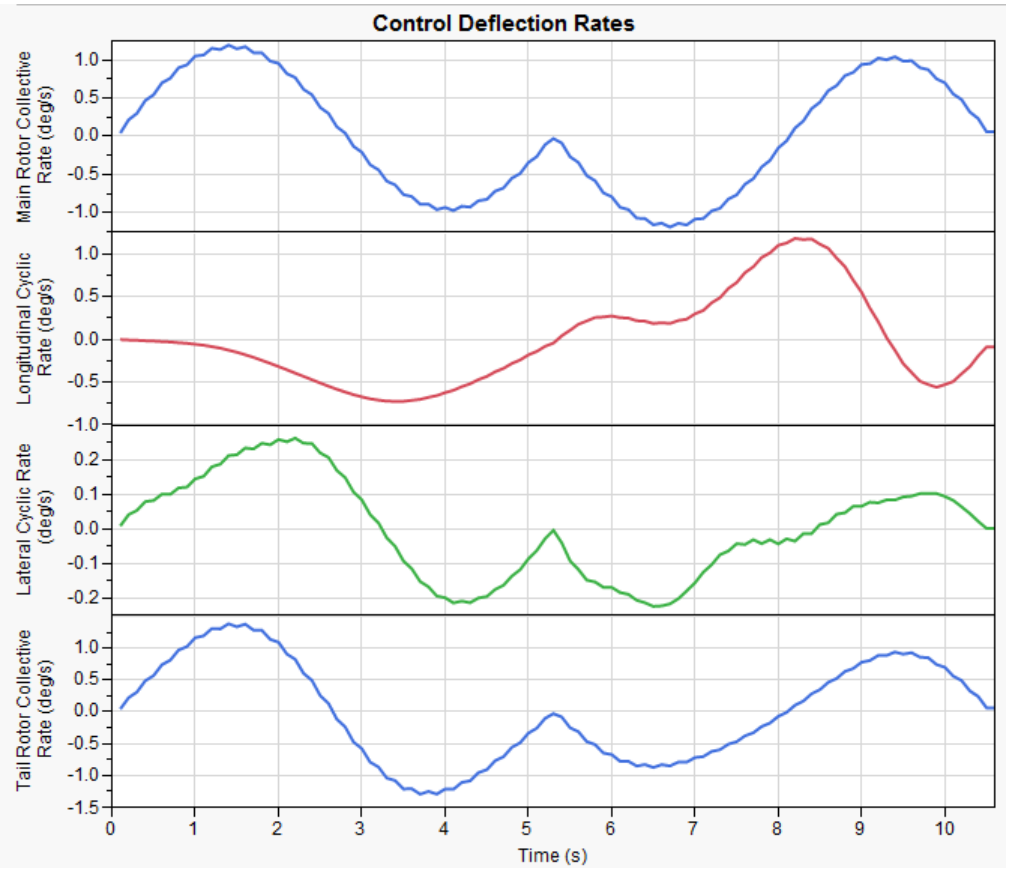

Figure 3.10: Control Deflection Rate Time Histories

3.4.2 Commanded Control Error

The inverse simulation method assumes perfect control and sensor knowledge, which in theory provides the best performance possible for a provided maneuver definition. The maximum performance knowledge is an important measure for design trades; however, the inability to follow a maneuver due to control degradations should also be included in the analysis. The second characteristic of control degradation requires

inclusion of an additional loop within each time step of the simulation in order to measure effects of control error on the maneuver divergence. The measure associated with control degradation is selected such to capture all of the errors within the sensor and control system, rather than focus on a single source of the error. Through consideration of this constraint, one new variable is added to the input set. This variable represents the maximum control deflection error resulting from incorrect information. The error in information can result due to sensor placement and fidelity characteristics, which may result in the wrong control deflection sent to the control algorithm. On the other hand, the poor information can result due to actuator errors and calibration errors. Hence, this variable is a catch all that can later be related to individual design characteristics in control system design.

With the integration of the new input variable, the calculation of the trajectory error resulting from the control deflection errors can be evaluated through modification of the process. Figure 3.11 summarizes this additional step where the dynamic simulation environment is provided control design constraints and the outputs from this step are feed into the trajectory divergence block. Hence, the divergence calculation must be done during each time step of the simulation after the dynamic simulation component is run. Outputs from the dynamic simulation environment are used in the divergence calculation, which leads to trajectory error bounds that can be used to generate control design requirements.

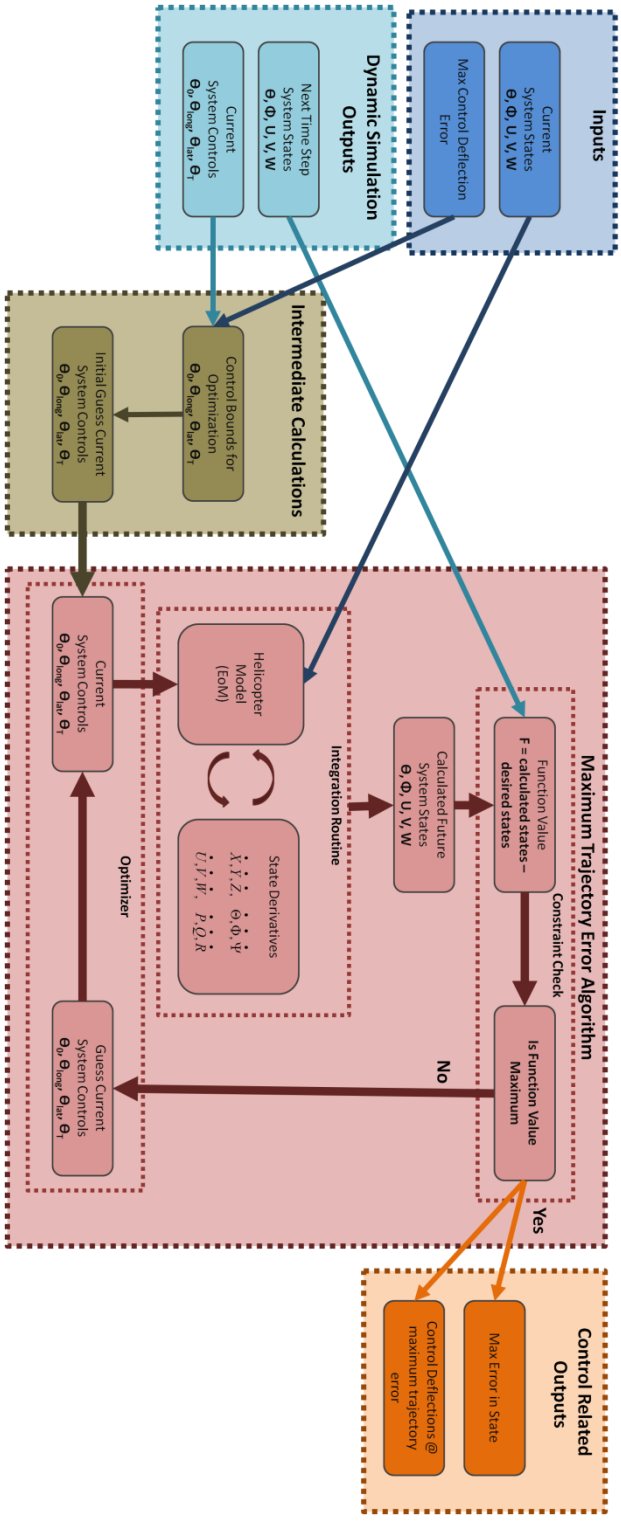

Figure 3.11: Trajectory Divergence

The outputs from the dynamic simulation portion of the analysis that are feed into the motion error calculation algorithm consist of the current system controls along with the resulting system state from the current settings. Two inputs are also included in the passing of information: the current system state, which is needed for motion simulation and the maximum control deflection error, which provides the bounds on error of the control in maximum divergence calculation. The inputs are shown in Figure 3.11 along with the entire trajectory error calculation process. The control deflection error feeds directly into an intermediate calculation block that uses the current control settings in addition to control deflection error to calculate bounds for the optimizer. These bounds also permit an initial guess for the controls that provide the maximum trajectory error.

Once the initial guess for the controls is established and the current state is supplied to the EoM, time integration is used to determine the end state for the current time step with the provided control settings. The output of this integration routine is then compared to the desired states, which is an output from the dynamic simulation step. The objective of this algorithm is to determine the maximum error in state. The maximum error in the current state when compared to the desired state provides the bounds on the maneuver divergence. The controls are adjusted throughout each loop through the maximum trajectory error algorithm using an optimizer until the maximum error control settings are determined. The algorithm outputs include the states that contain the most error due to the control deflection error ranges and the control deflection settings that cause this maximum error.

This concept is best explained through an example, which is chosen to be the pop-up maneuver used throughout this work. The first step of the process is to determine the trim conditions through adjustment of the state and controls of the system. The control settings necessary for trim are displayed in Figure 3.12, which correspond to the deflections at time zero. For this example, the main rotor collective is approximately 2.2 degrees. The longitudinal cyclic, lateral cyclic, and tail rotor collective are approximately -0.2, 2.9, and 0 degrees, respectively.

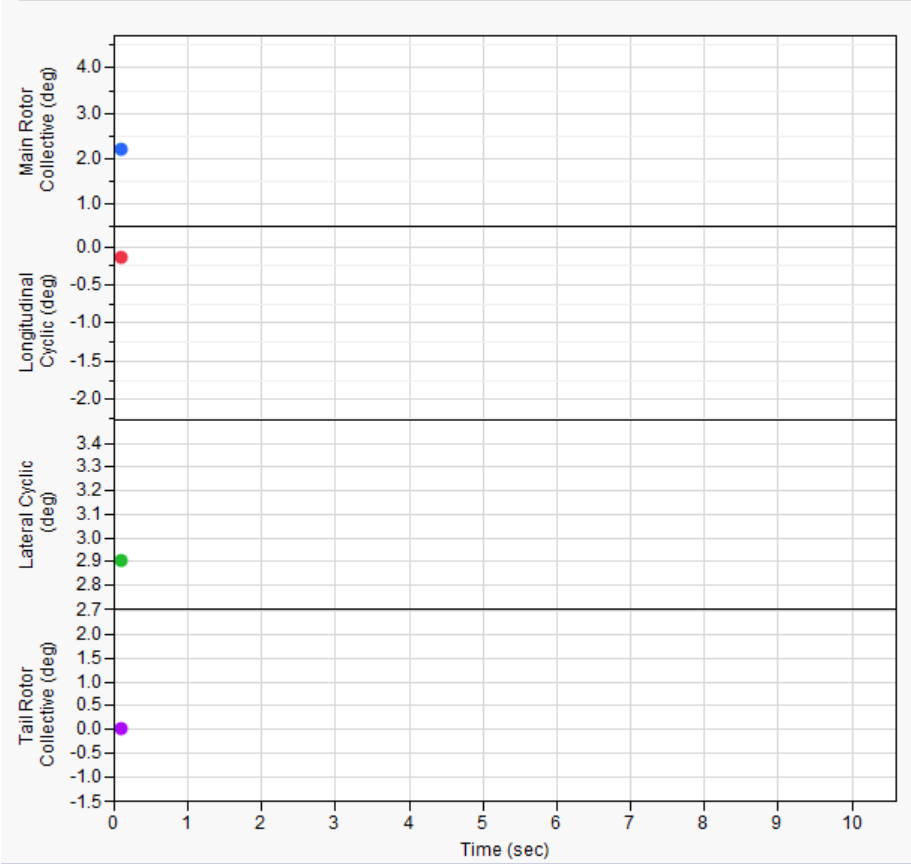

Figure 3.12: Control Settings at Trim

The process employed in Chapter 2 would continue onto calculating the necessary controls for the maneuver at the following time; however, with the inclusion of the trajectory divergence loop, the maximum divergence control settings for the current time must be determined before moving onto the next step. The maximum divergence control settings correspond to the set of controls that leads to the maximum divergence from the desired maneuver for each time step. The commanded control settings that create this divergence are limited by the maximum deflection error input. For this experimental run, the maximum deflection error is set to be 1 degree. This means that the commanded control can deviate from the desired control by +/- 1 degree in order to create the maximum maneuver divergence. The upper and lower bounds on the commanded control error are shown in Figure 3.13. The desired control is shown as the solid line, while the upper and lower bounds on the control settings are shown by the dashed lines.

The trajectory divergence loop uses these bounds directly in calculating the commanded control settings necessary to create the maximum divergence from the desired path. This process is employed in order to capture the most constraining case. The trajectory divergence algorithm is run and the resulting commanded control settings are calculated for this time step. The commanded control setting for the first time step is displayed in Figure 3.14 as the orange point.

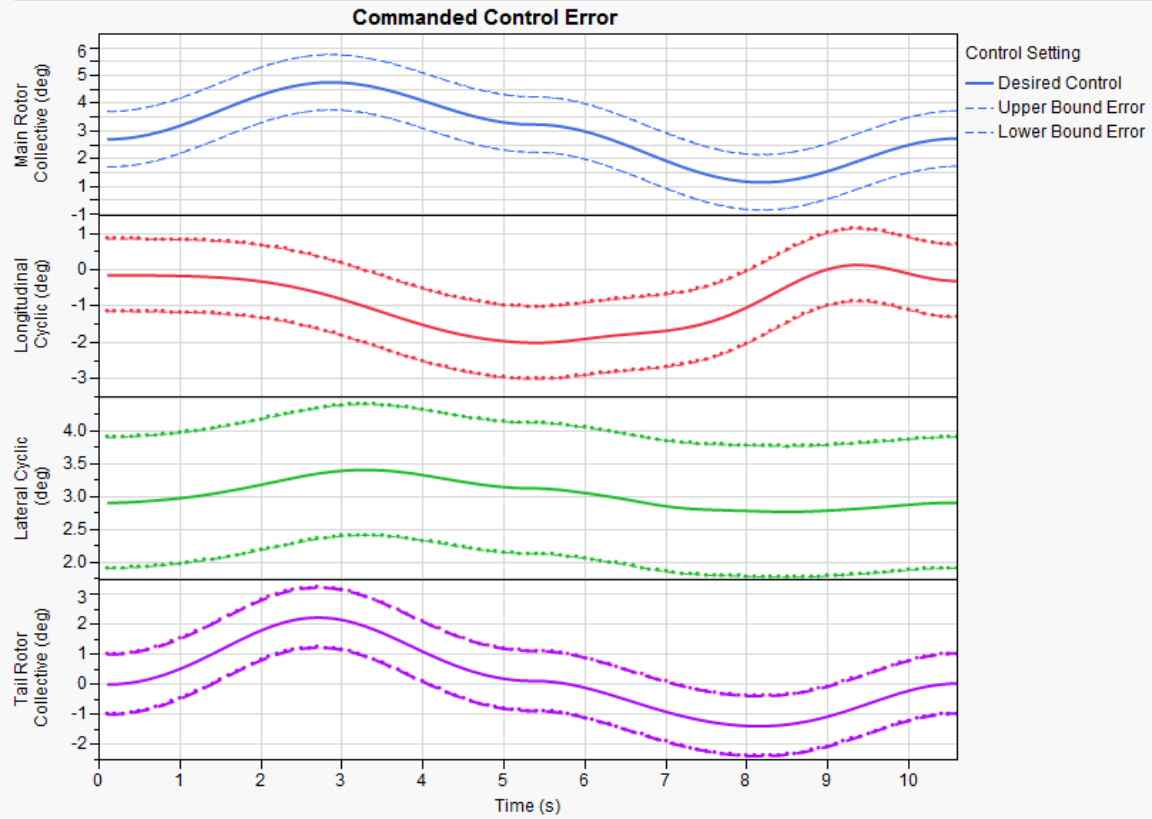

Figure 3.13: Commanded Control Error Bounds

The trim condition for the main rotor control deflection angle is around 2.2 degrees, which may be viewed in Figure 3.14. The deflection error variable is specified as +/1 degree in this example, which means that the optimization routine can select the main rotor collective between 3.2 and 4.2 degrees that provides the greatest error in trajectory. The only control setting that occurs somewhere between the bounds is the main rotor collective setting, which occurs slightly below the desired main rotor collective setting. Both the longitudinal and lateral cyclic control settings leading to maximum divergence occur at the lowest bound setting, while the tail rotor collective setting occurs at the upper bound.

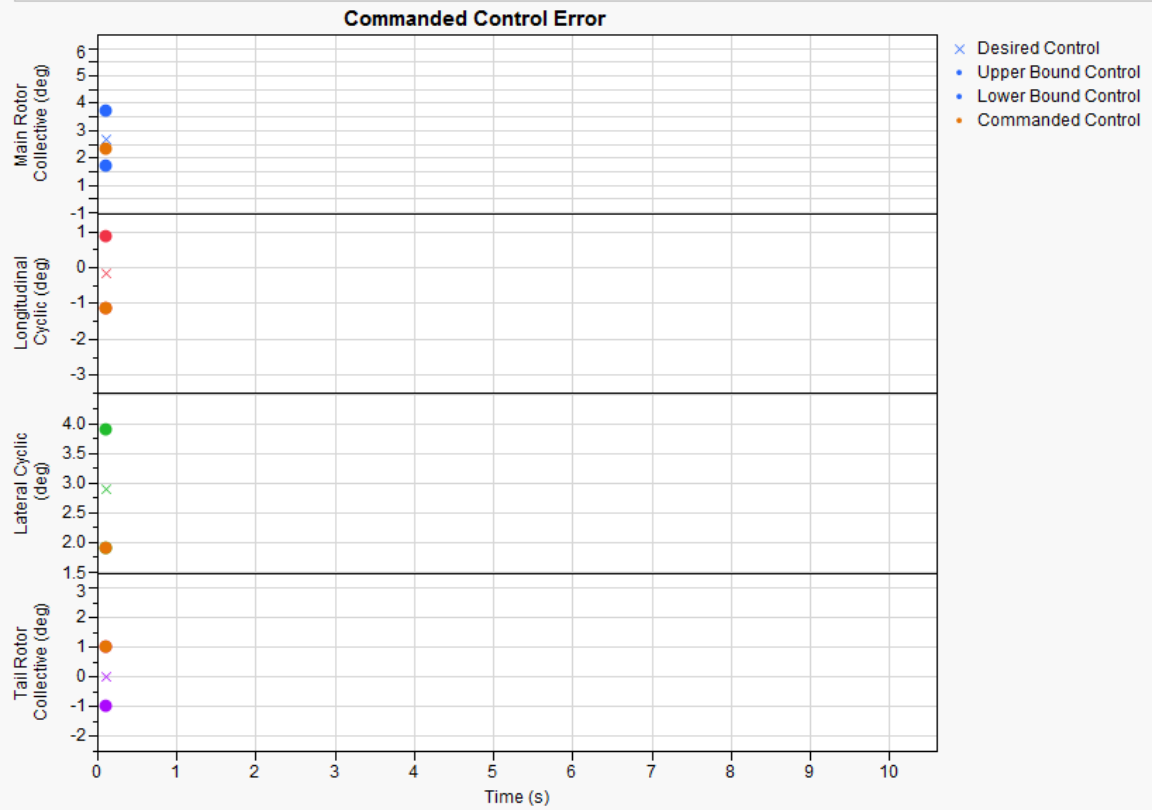

Figure 3.14: Trim Conditions with Control Error Bounds

The commanded control is always selected for the current time step independent of previous commanded control results. As a result, the divergence is a maximum divergence during each time step rather than the maximum divergence over the entire maneuver. The calculations are conducted in this manner because the feedback and the rate at which these errors are corrected are a function of control system design characteristics within hardware and software, which are not know at this time.

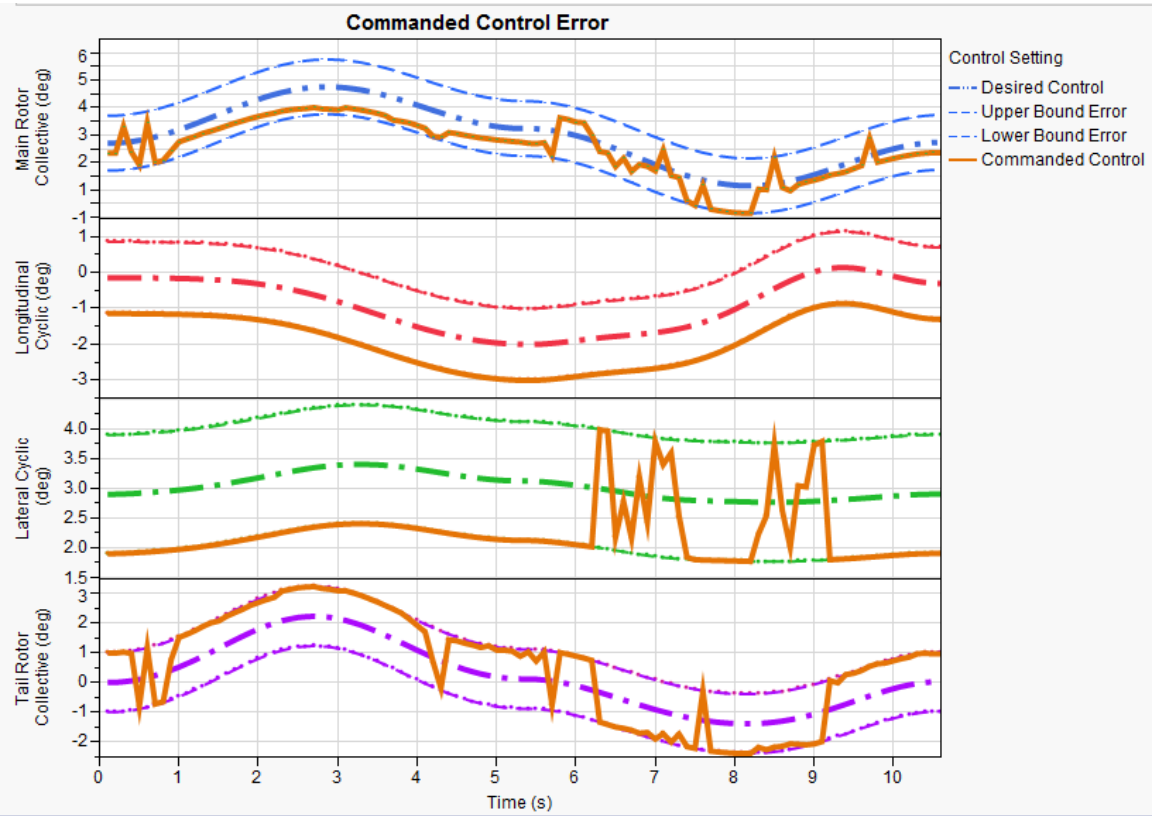

Figure 3.15: Commanded Control Setting for Maximum Divergence

Analyzing the commanded control for the entire maneuver in Figure 3.15, it is observed that the longitudinal cyclic remains at the lowest bound throughout the simulation. This should directly impact errors associated with x-axis and z-axis velocity divergence. The lateral cyclic remains at the lowest bound for most of the simulation; however, sometimes the upper bound of error enables a larger magnitude of divergence. The tail rotor collective commanded control follows mainly the upper bound limit for the first half of the simulation and the lower bound for the second half of the simulation. This results because of the acceleration changing signs at the half point. The main rotor collective almost always remains below the desired collective setting, but it usually is somewhere between both the lower and upper bounds. It is important that an optimizer is

needed to determine the maximum deflection control settings rather than just using the bounds of error to specify the limits. If the bounds were used, the most constraining case would not be captured, hence, the trajectory divergence loop is necessary.

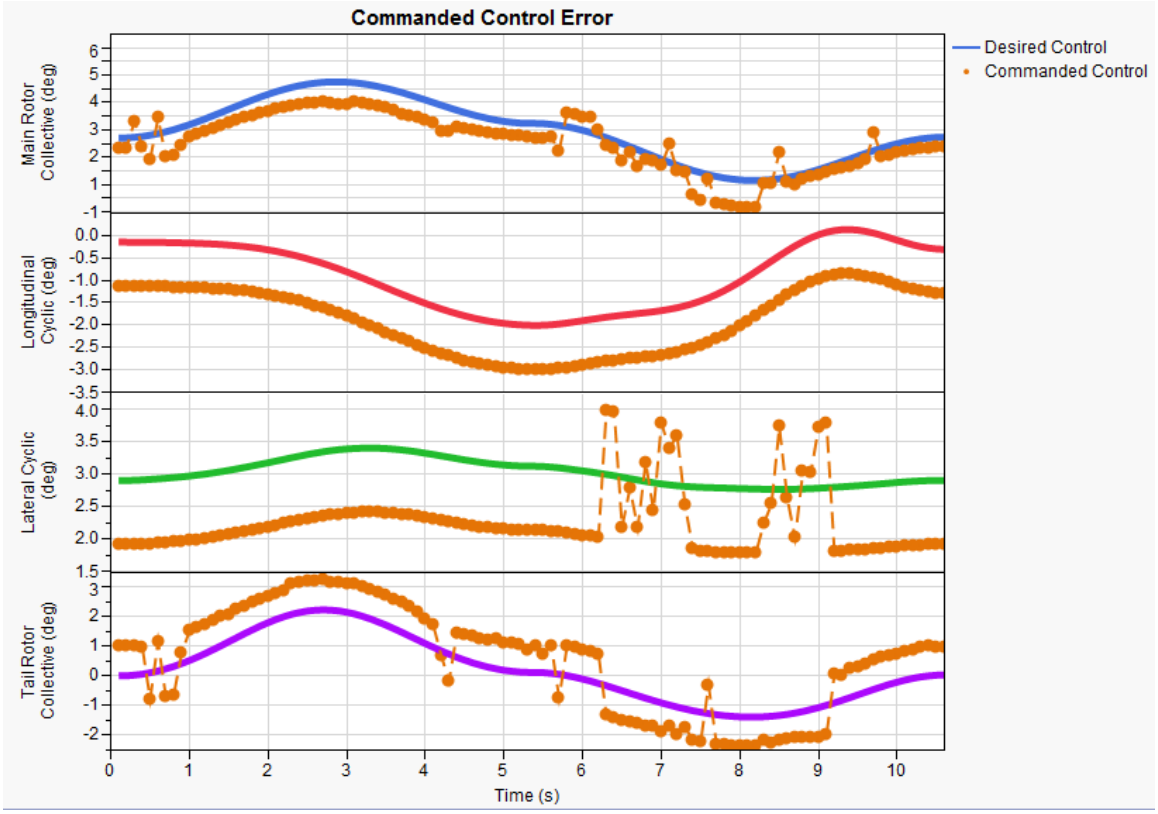

Figure 3.16: Control Time Histories with Commanded Control Error

In Figure 3.15, orange solid lines are shown along with the desired path and the deflection bounds. The commanded control settings, as stated previously, are a function of the current time step and do not take into account previous control settings. The desired control settings are shown as the solid line in Figure 3.16, while the commanded control resulting in the maximum divergence is shown as the points. The control bounds are removed from the figure to provide greater clarity of the trends. Since the

commanded control is calculating the maximum error of the current time independent of previous times, the commanded control time history is not going to be smooth or continuous.

The commanded control settings drive the maximum divergence from the defined maneuver. It is necessary to view this divergence in the various state dimensions. As in previous validation exercises, the divergence from the defined maneuver path is displayed through a series of figures representing the various states of the system. The first states to discuss are the differences in the desired velocity against the actual velocity when the control deflection error is introduced. The results are not shown in a cumulative nature but are displayed for each time step calculation. The three linear body velocities and the corresponding divergence due to incorrect controls are presented in top portion of Figure 3.17. The velocities are shown rather than position because the maneuver is defined by the three linear velocities and a yaw rate constraint. The solid line indicates the desired maneuver and the points show the divergence from the path. The diverged points are close to the desired maneuver path since the divergence is occurring over a 0.1 second interval and the maximum control error is set to be +/- 1 degree. For this range of time and error, the velocity does not diverge substantially from the desired velocity, which provides the designer with knowledge regarding sensing rate and deflection error propagation. Similarly, the attitude can be analyzed with regards to divergence during each time step due to commanded control error. These time histories are shown in the bottom portion of Figure 3.17 where the desired attitude is indicated by the solid line and

the divergence is shown as points. Again, for the 0.1 second correction rate and the small deflection error, the divergence is minimal.

In addition to the divergence in velocity and attitude, the vehicle trajectory may also be investigated, which is shown in the top portion of Figure 3.18. The velocities and attitudes are impacted much more in magnitude than the position because of the direct relationship to accelerations in the body frame. For this reason, viewing the trajectory error in a time step fashion shows that the desired trajectory and the divergence trajectory are almost identical. In order to overcome this challenge in analysis, previous research efforts have displayed the data as the cumulative impact of the error if no corrections are made. This is shown in the bottom portion of Figure 3.18, where both the x and z components of the position vary drastically from the desired trajectory. This divergence path offers a bound of the worst case scenario and assumes that no corrections are made to the path throughout the entire simulation. This analysis is overly conservative and not realistic since the controller would update and attempt to fix the error at some point during the divergence.

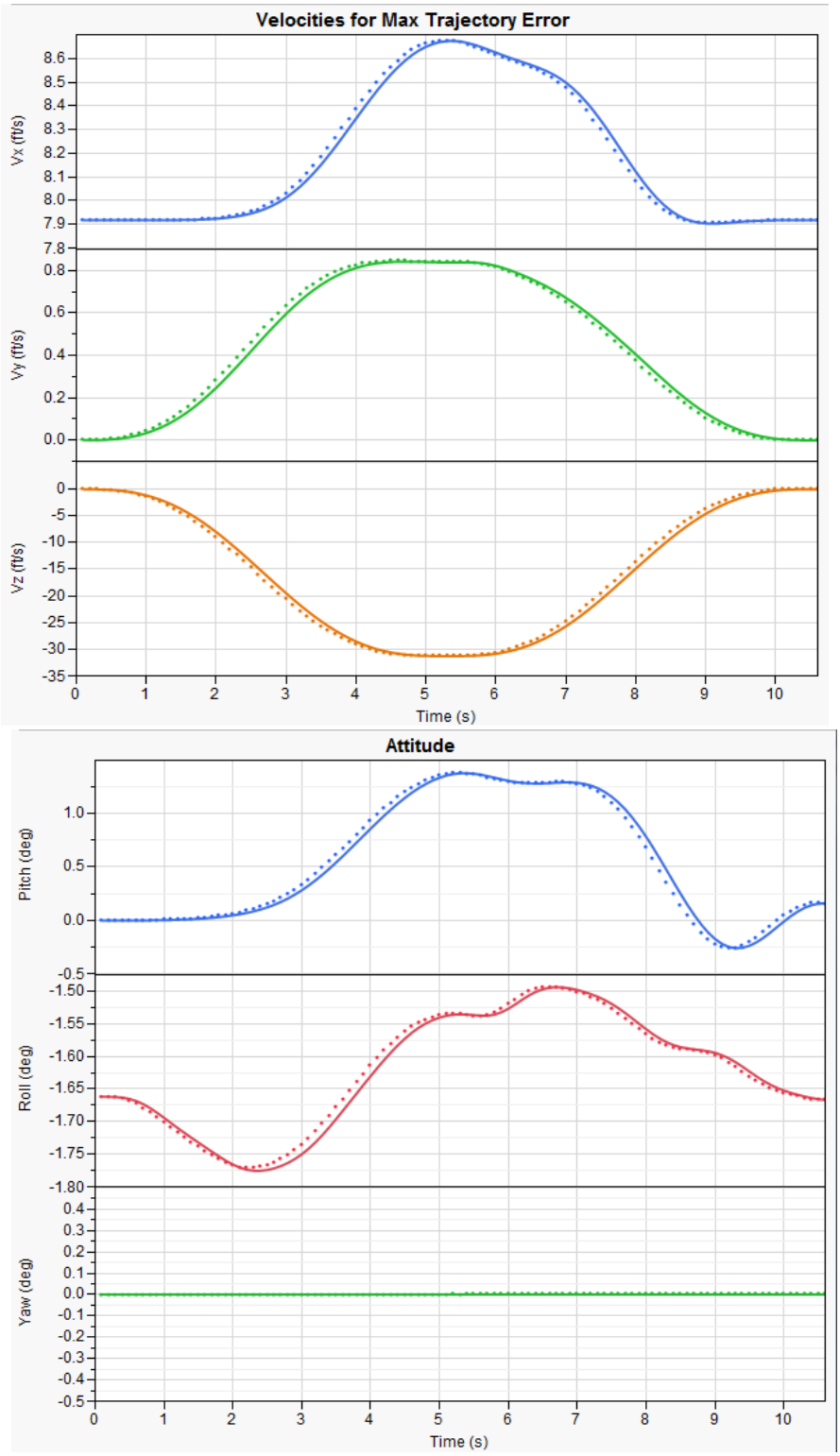

Figure 3.17: Linear Velocity and Attitude Divergence

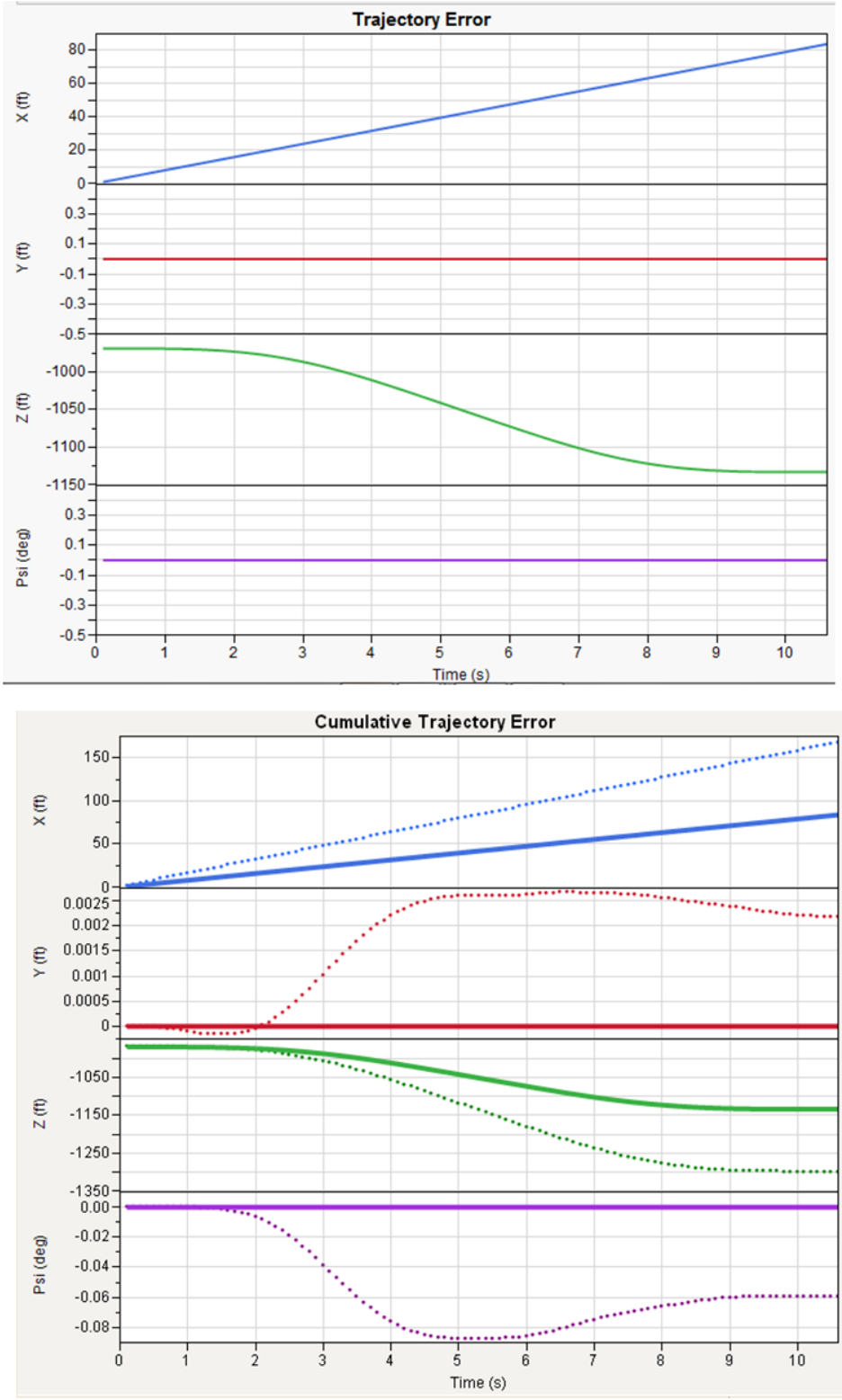

Figure 3.18: Trajectory Divergence

3.5 Experimentation and Results

The simulations are run and the data is analyzed using the dynamic constraint environment, which enables the designer to apply various constraints on the maneuver inputs, which in effect, provides the ability to quickly view maneuverability results for any state, control, or auxiliary variable constraint. The control system characteristics and maneuverability relationships are captured through conducting real-time trades. A single pop-up maneuver is used to demonstrate the effectiveness of the adjustments to the process regarding Contribution 2. As stated previously, 9000 runs are completed using the environment for the design variable ranges in Table 2.2, which also included variations in velocity, altitude, time, and maximum acceleration. The data analysis section is divided into subsections in order to present the two control characteristics integrated into the process. First, the control deflection rate constraint filtering is presented, which demonstrates that improved maneuverability estimates are obtained real-time to enable quantitative control requirements development. Second, the commanded control error filtering exercise is investigated. This involves analyzing the entire pop-up maneuver space and selecting the minimum time maneuver for time-series analysis. The systematic and traceable nature of the process is demonstrated through this example.

3.5.1 Control Deflection Rate Filtering

The pop-up example presented in Chapter 2 consisted of an altitude increase between 150 and 250 ft. During previous experiments, this space was constrained by

maximum maneuver power and the maximum deflection angle constraints. The first stemming from the energy formulation, while the later arising because of the inclusion of the rigid body kinematics into the design environment. The resulting feasible design space from Chapter 2 analysis is summarized in Figure 3.19, where the blue triangles represent the top performing designs below the 8 second threshold.

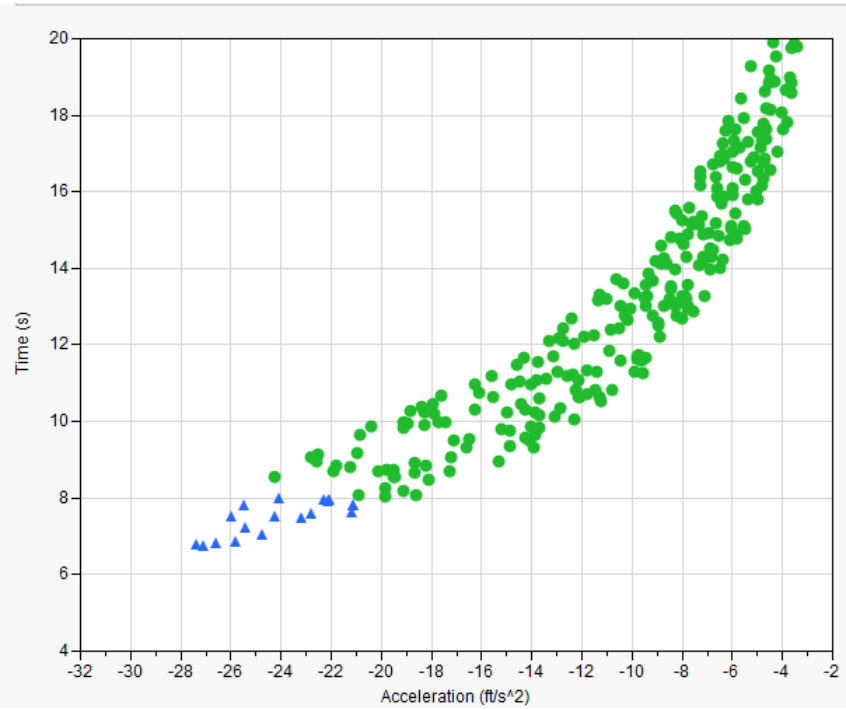

Figure 3.19: Top Performing Designs from Original Process

The first control characteristic is the maximum control deflection rate constraint, which is similar to the rigid body constraints applied earlier. The real-time data filtering approach is applied to the feasible design space determined earlier to understand the range of deflection rates required to perform the various maneuvers. The design and maneuver space impacts from control deflection rate filter can be viewed in Figure 3.20, which ranges from almost 0 degree/sec to 20.5 degree/sec. The control dynamic rates are

directly proportional to the maximum acceleration during the maneuver. The top performing design and maneuver combinations correspond to faster control rates as expected; however, this analysis provides quantitative relationship that could not be captured without the extensions to the process.

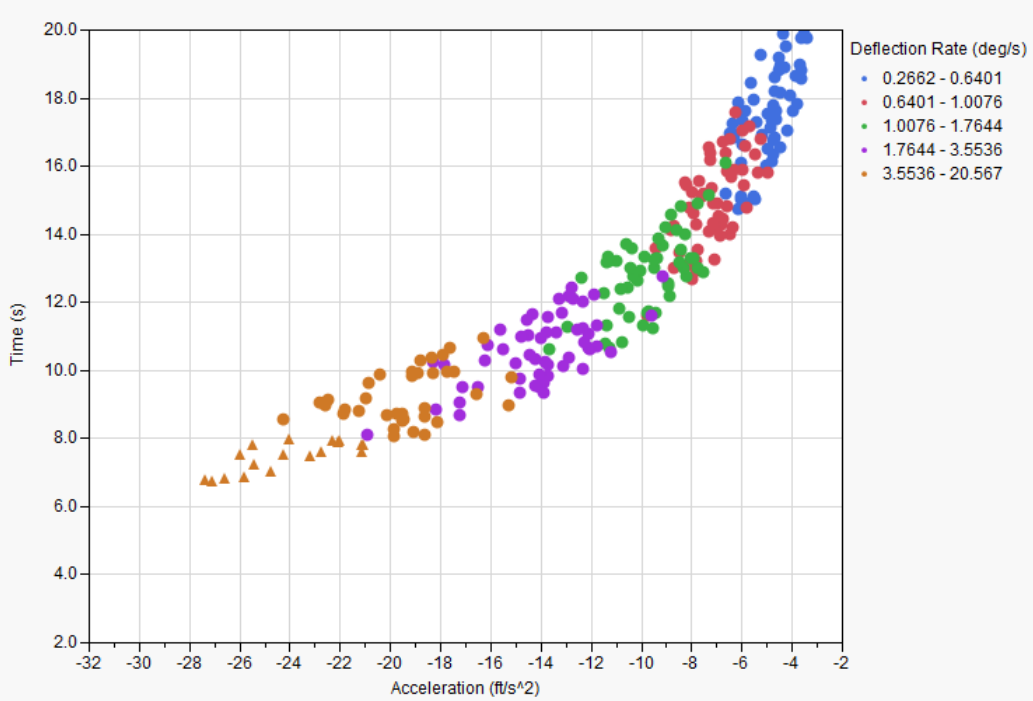

Figure 3.20: Data Filtering According to Maximum Control Deflection Rate

Similar to the steps applied in previous research steps, the designer may adjust the control deflection rate constraint real-time and view the impact on the feasible space. In this example a deflection rate limit of 10 degree/sec is chosen; however, this is only representative of one of the many trades that can be conducted. The deflection rate constraint is applied and the design and maneuver combinations that are feasible with the original process but fail to meet the new rate limit are colored red. This limit only removes 16 data points from the feasible space, which seems minor when we have over

255 points that are feasible. The major point here is that 11 points out of the 16 are among the top performing designs, which is shown in Figure 3.21.

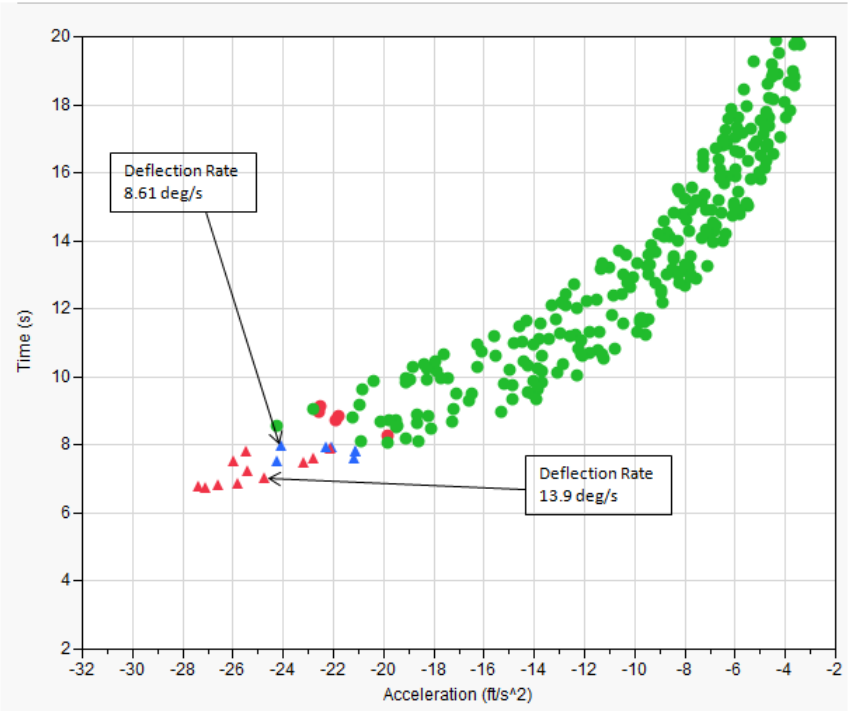

Figure 3.21: Infeasibility of Top Designs – 10 deg/s

It is observed that all three of the top performing designs are removed from the feasible solution set with a constraint of 10 degree/sec on the control rate. The minimum time maneuver increased from 6.75 to 7.75 seconds. At this point, the designer can adjust this limit real-time and view the impact of these design decisions that are in effect driving control requirements. The control deflection limit of 12 degree/sec is shown in Figure 3.22, which shows that small changes in this constraint provide a significant maneuverability increase. Two of the top three performing designs are again feasible and the minimum time is 6.75 seconds. Although, this constraint imposes more constraining requirements on the control designer through enforcing faster control rates, much

improved maneuverability characteristics are achieved. This constraint will impact control design risk and cost, while at the same time offering a jump in performance for this maneuver. Hence, a cost benefit trade exists and using the systematic process outlined in this work, important decisions become iterative and traceable. Using the parametric nature of the analysis technique, the deflection rate necessary for inclusion of all top three designs into the feasible set is 18 deg/s, which is almost double of the originally imposed 10 deg/s requirement.

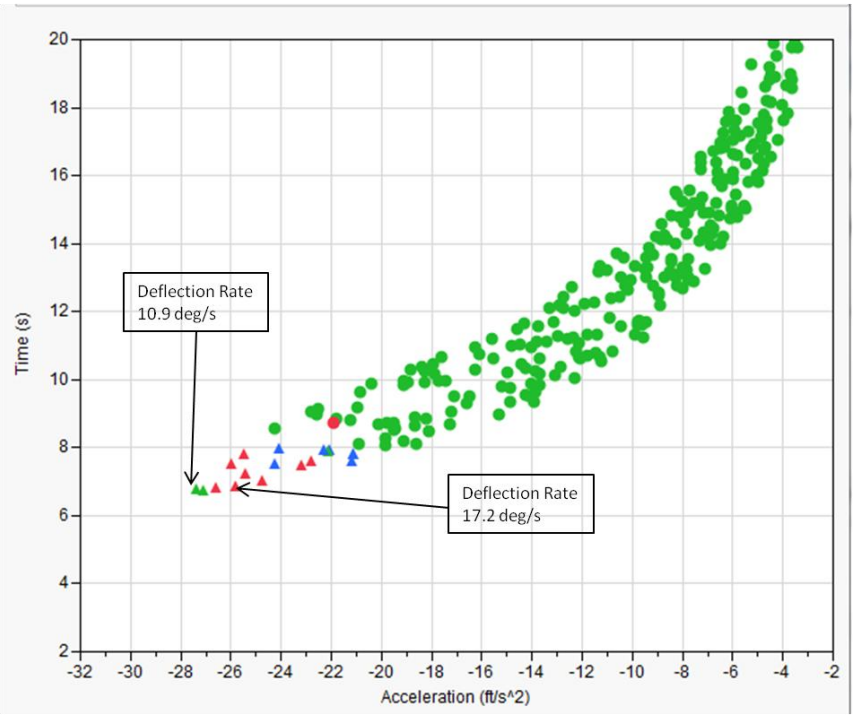

Figure 3.22: Infeasibility of Top Designs – 12 deg/s

The top two designs with +/- 5% variability in the design definition are shown for the control deflection constraint with the kinematic deflection and dynamic performance limits in Figure 3.23. These results are summarized from the Chapter 2 data analysis in order to further build on the analysis using the deflection rate constraints in a similar

manner. The variability of the top designs with regards to the newly added control deflection constraint of 12 degrees/sec is necessary. In order to fully understand the design variability impacts on the maneuverability, the relationship of each design to deflection rate constraints must be investigated.

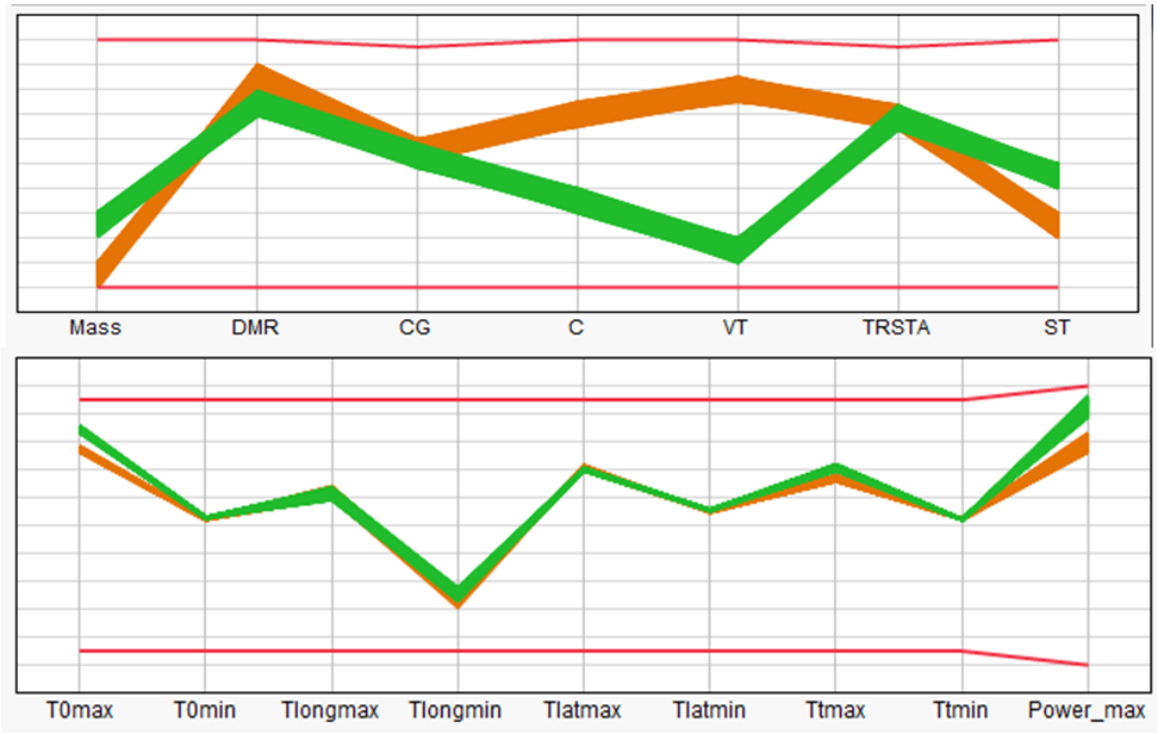

Figure 3.23: Variability in Design Definition Impact on Deflection and Power

The deflection rate constraints of 12 deg/sec are shown as the red lines bounding the responses from both designs with 5% variability in Figure 3.24. It is shown that the green design closely approaches the maximum power limit, while the orange closely approaches the lateral cyclic rate limit when comparing the results from Figure 3.23 and Figure 3.24. This observation results in a design trade between the various design parameters and is driven by whether the rate limit or the power constraint is more of a

concern. Together all three types of constraints restrict the design space to a much smaller feasible set than any one constraint alone, which shows the need to include all constraints. Additionally, the tradeoff between the various designs is shown to require an iterative process because each design has different constraints driving the success. The nature of these requirements changing enforces the benefits of the capabilities of the data filtering method. The best performance maneuver would be approximately 7.75 seconds if the optimization was originally fixed to a deflection rate limit of 10 deg/sec.

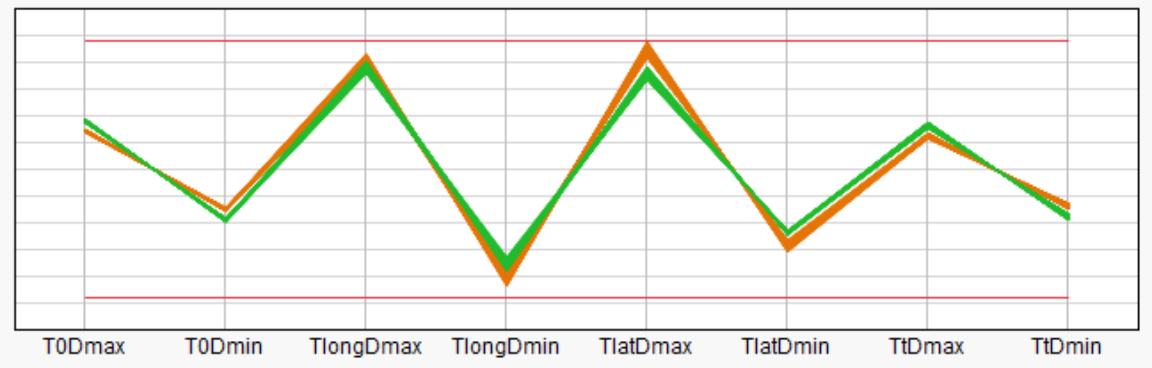

Figure 3.24: Variability in Design Definition Impact on Deflection Rate

However, the real-time data filtering method that is enabled by the parametric nature of the process allows the designer to see that by increasing this limit to 11 deg/sec, one of the original top three performing designs can perform the maneuver in 6.75 seconds. Furthermore, if the constraint is moved to 12 deg/sec, two designs are able to complete the maneuver in 6.75 seconds, which is substantially faster than the 7.75 seconds originally found, especially when the entire mission is considered later in this work. These trades demonstrate that the control characteristics impact on maneuverability

can be systematically analyzed, which enables traceable and improved quantitative control design requirements development.

3.5.2 Commanded Control Error Filtering

The results from the second control characteristic are discussed in this section through further analyzing trends in the entire maneuver space and then revisiting the pop-up maneuver example. The importance of including trajectory divergence into the analysis for control design considerations is first emphasized by viewing the entire pop-up maneuver space. The velocity errors are captured through an iterative calculation loop requiring time integration that determines the maximum divergence from the desired path due to errors introduced through the control system integration. The errors are calculated at each time step, which is set to 0.1 seconds for all 9000 simulation runs. The short time scale makes comparisons of velocities rather than position a better choice since the error in position resulting from 0.1 seconds in runtime is minimal. Additionally, the maneuvers are defined by three linear velocities and a yaw rate constraint, which makes velocity a better divergence measure.

The entire pop-up maneuver space is shown in Figure 3.25, where the points are colored to indicate various ranges in velocity divergence rate. Velocity divergence rate is the maximum change in velocity that occurs over each of the 0.1 second time steps. The divergence cannot be viewed in a cumulative sense because this would require knowledge of the sensing rate, update rates, and controller software algorithm for correcting the path error. Therefore, the velocity divergence over each time step is

calculated independent of the previous time step. The maximum velocity divergence over the entire maneuver is parsed from the time series results and is converted into an acceleration value by dividing by the time step.

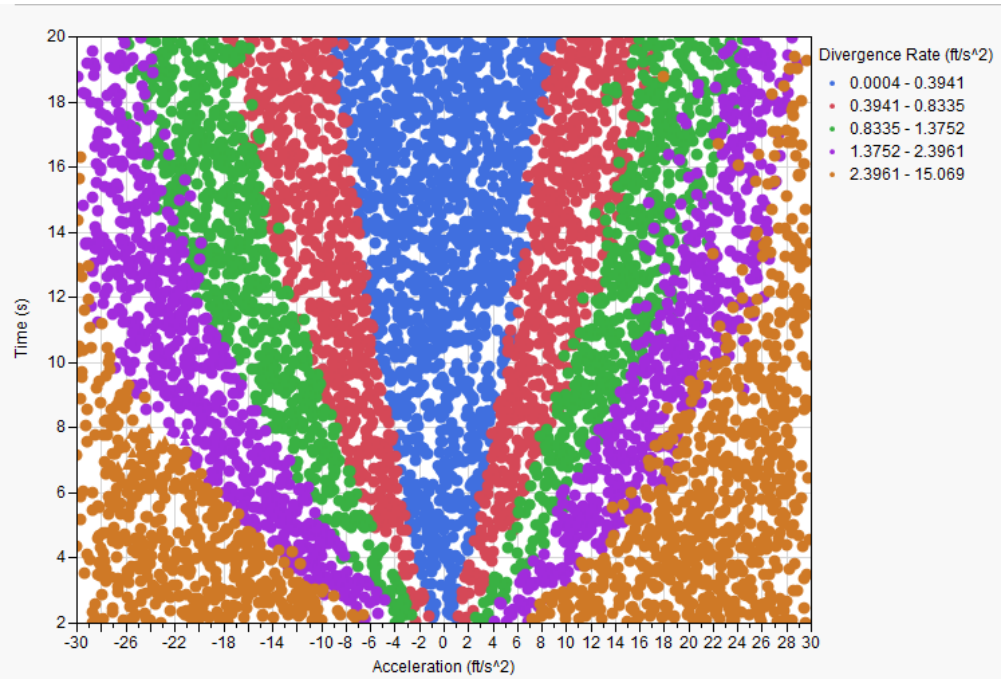

Figure 3.25: Velocity Divergence Rate

It is observed in Figure 3.25 that velocity divergence rate is largely a function of acceleration and time, with the minimum divergence rates corresponding to maneuvers with low accelerations. Additionally, maneuvers that occur over a shorter period of time result in higher divergence rates. Using this information the designer may decide the limit on divergence rate. This limit depends heavily on delays and errors in control and sensing for the given design. For, example, the orange points in the figure that correspond to divergence rates between 2.4 and 15 ft/s^2 may require more sophisticated sensors and

control algorithms to guarantee safety. This analysis provides the control designer with valuable information when determining key control system attributes.

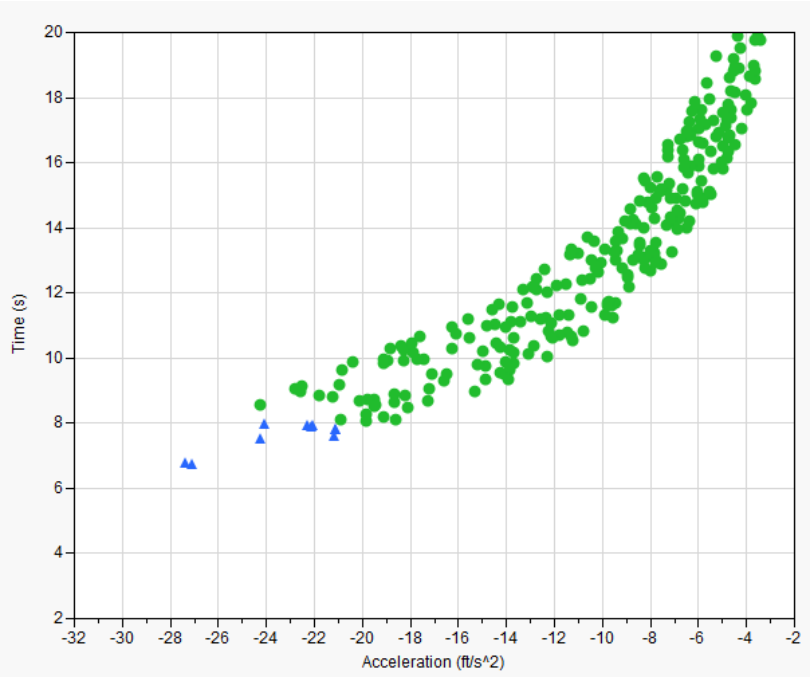

Figure 3.26: Designs for Power, Control Kinematic and Dynamic Limits

Now that the concept of divergence rate is introduced, the measure can now be applied to the pop-up maneuver example. Figure 3.26 displays the feasible design and maneuver combinations for a 150 to 250 ft pop-up maneuver. The maximum maneuver power required, kinematic control limits, and dynamic control constraints are all applied. Only two designs out of the approximately 250 points produce a pop-up maneuver in under 7 seconds, with the next closest performers around 8 seconds in time. These designs are very similar except for some variation in main rotor chord and rotor tip velocity. The next filtering exercise provides an understanding of the velocity divergence of these designs when compared with the other combinations in the design space.

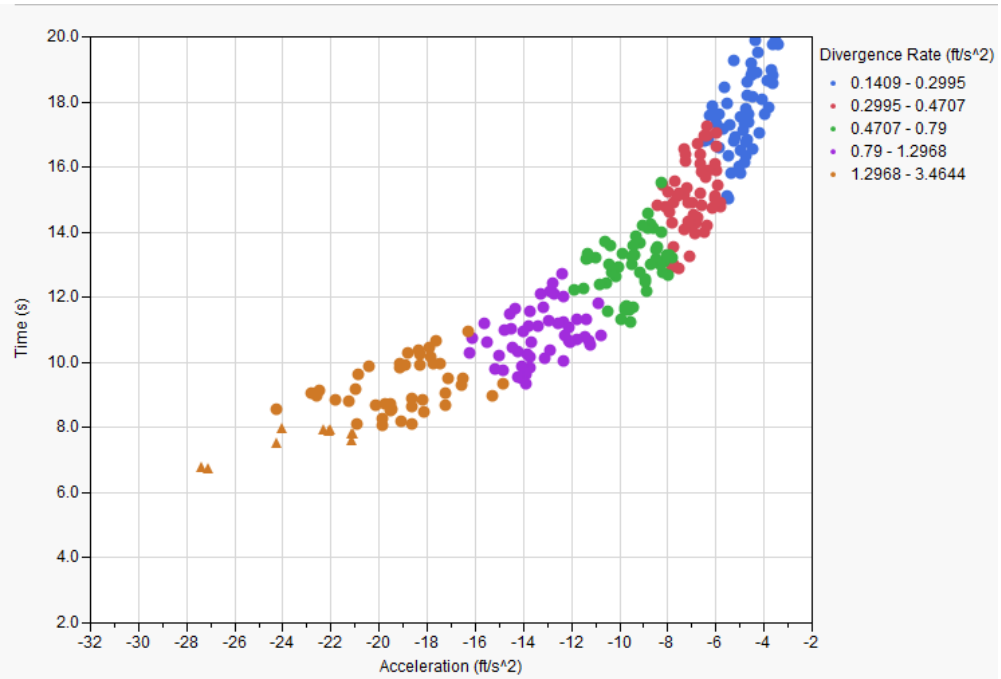

Figure 3.27: Maximum Velocity Divergence Rate

The data filtering process is applied to the remaining feasible designs to categorize the individual points in relation to the maximum velocity divergence during the maneuver. The results are shown in Figure 3.27, where the orange points include a maximum divergence rate ranging from 1.2 to 3.5 ft/s^2. These values represent the rate at which the design will diverge from the desired velocity. The divergence accelerations for the top two designs are approximately the same with a value of 3.5 ft/s^2. In order to move forward with the top designs, the control designer must be able to develop a control system that is able to stabilize the vehicle, while at the same time correct for velocity divergence of this magnitude. The maximum deflection error variable is set at around 1.5 degrees for both of these designs.

A divergence rate of 3.5 ft/s^2 is difficult to visualize. Fortunately, the data filtering method applied in this work contains the time history data from each individual run. Now that the design space has been filtered down to a few designs, each of the maneuver and design combinations can be analyzed in the time domain. Since the top two designs in this example have the same maneuver definition and almost identical design parameter settings. It is sufficient to just view one of the designs in a time history manner. The top performing design is chosen for this analysis, although, the 0.01 time second difference is negligible between the top two designs. An additional concern that needs to be investigated is the impact of the maximum control deflection error variable on the divergence characteristics for this design combination. For this reason, three additional runs were completed with design and mission definition held constant and only the max deflection error variable changing. The variable is shown for three different levels tested, 0.2 , 1, and 2 degrees deflection error with the perfect control setting in Figure 3.28. The solid line indicates the desired main rotor collective setting throughout the 6.75 second pop-up maneuver. The three different commanded control error settings are displayed as point series data of different colors. The orange points indicate the main rotor collective settings with error deflection bounds of 0.2 degrees. The purple and green show similar information for the 1 and 2 degree bounds, respectively.

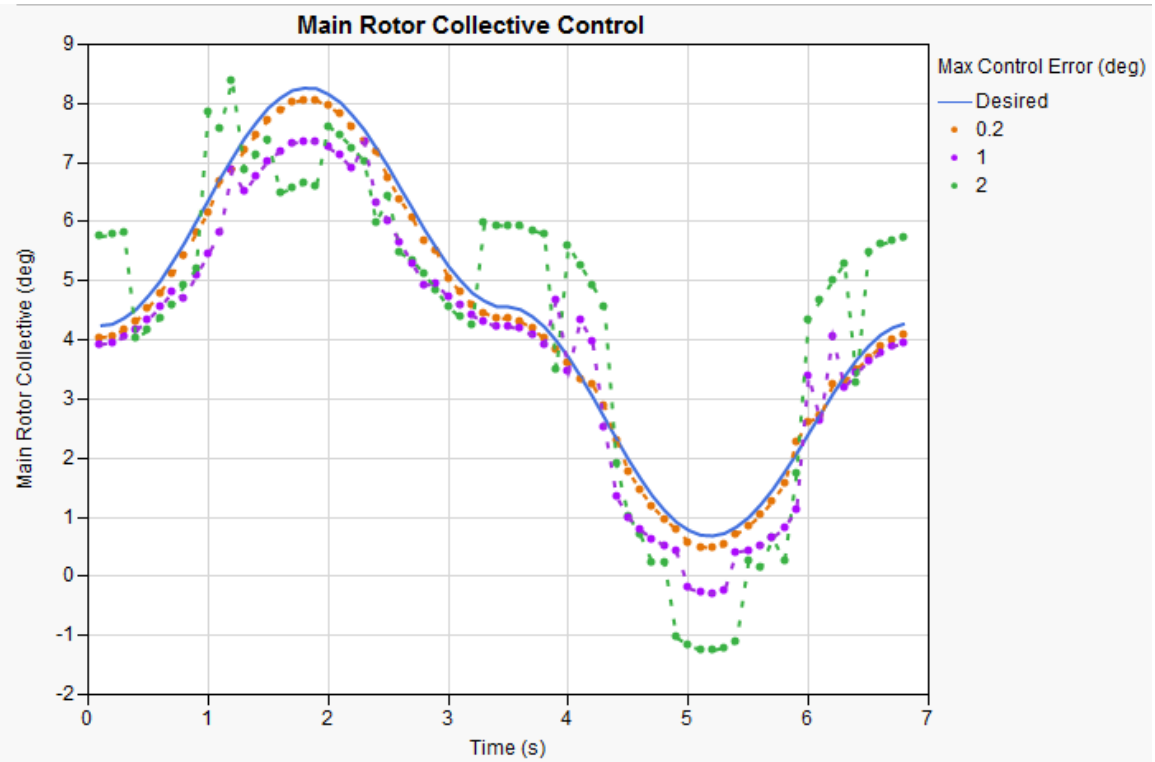

Figure 3.28: Varying Levels of Commanded Control Error

It is observed in the figure that the maximum error in trajectory does not always occur at the maximum deflection bounds. In reality, sometimes the green points (2 degree max) lie inside the purple points (1 degree max). The reason for this is that all of the controls are allowed to vary over the max deflection range so one or more of the other control settings are driving the error higher during those time steps. This assumption is verified by viewing all four of the controls simultaneously and comparing the commanded control errors resulting in max divergence.

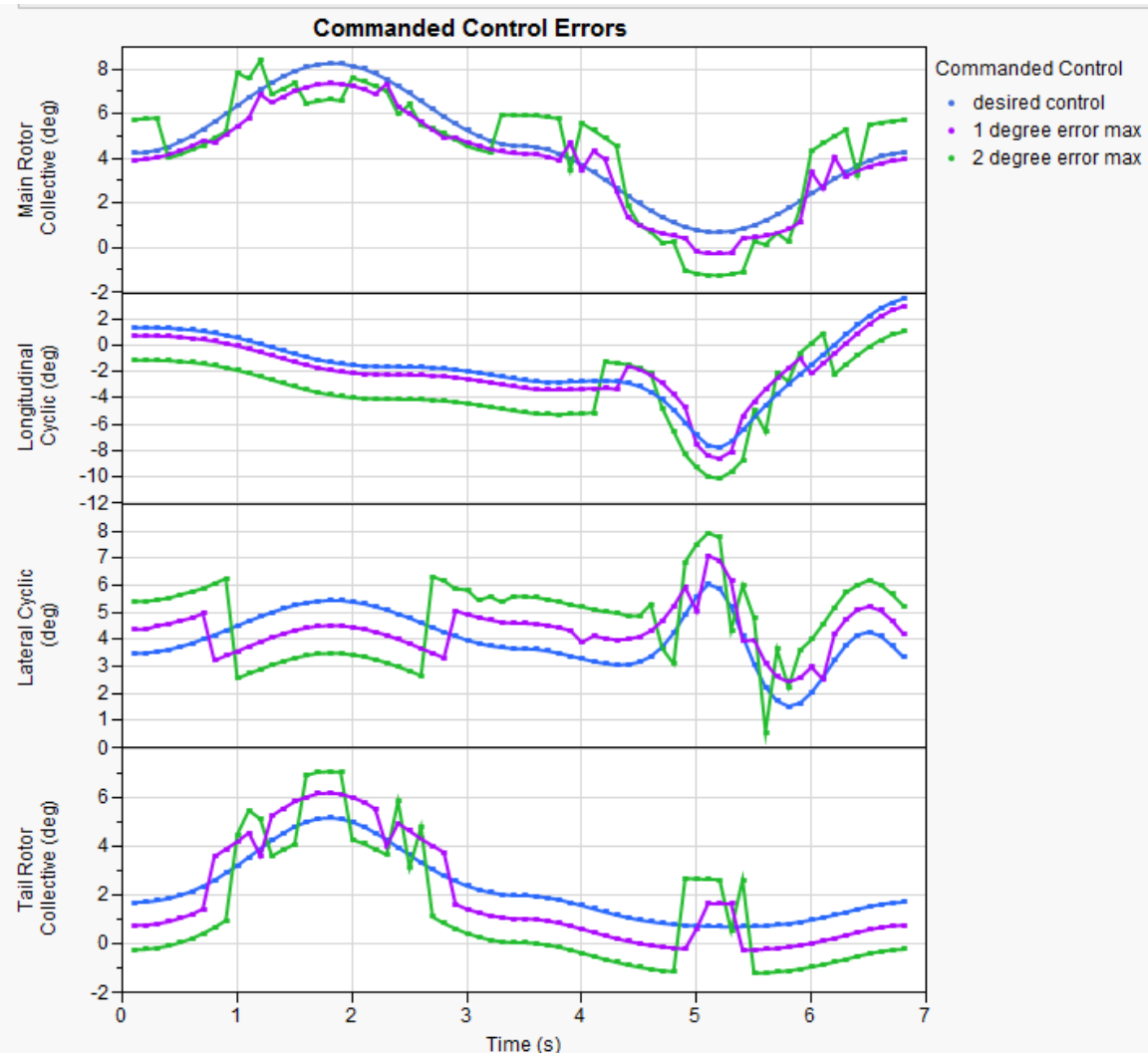

Figure 3.29: All Controls Commanded Control Error

All four controls are shown in Figure 3.29 with the same coloring scheme presented for Figure 3.28. At multiple times throughout the simulation the main rotor collective commanded control is not at the maximum error bounds. Further analysis shows that during these times, both the lateral cyclic and the longitudinal cyclic are at the maximum settings for the error bounds specified. This demonstrates that the different control settings are driving the maximum divergence at different points during the

simulation. Additionally, the type of divergence changes as the control that is contributing most to the error response varies. This is most easily viewed in the velocity and attitude space in Figure 3.30. The top portion of the figure displays the velocity error bounds due to the commanded control errors, while the bottom portion of the figure shows the vehicle attitude time histories. The green line represents the velocity divergence due to the 2 degree max control error constraint. This error constraint mostly impacts the x-axis velocity and the vehicle pitch, both of which are in the top of their corresponding sections. The 1 degree error (purple) and the 2 degree error (green) diverge in different directions from the desired trajectory (blue). The green x-axis velocity divergence is almost always a positive direction divergence from the desired, while the purple x-axis velocity is in the negative direction. This results because the main rotor collective error is driving the divergence in the 1 degree error case, while the longitudinal cyclic is driving the error on the 2 degree error case.

The divergence in the attitude of the vehicle is similar because of the relationship of the body velocities to the navigational frame velocities. The z-axis velocity is also impacted by the error in control; however, the magnitude is much larger so this variation becomes more difficult to observe. All of the other velocities and attitude angles are not greatly impacted by the magnitude of the commanded control error. This example provides a visual representation of the divergence rate constraint in the time domain, which in turn aids the designer and the control engineer with additional quantitative data to make key constraint and requirement decisions that drive the design selection and enable more conservative maneuverability estimates.

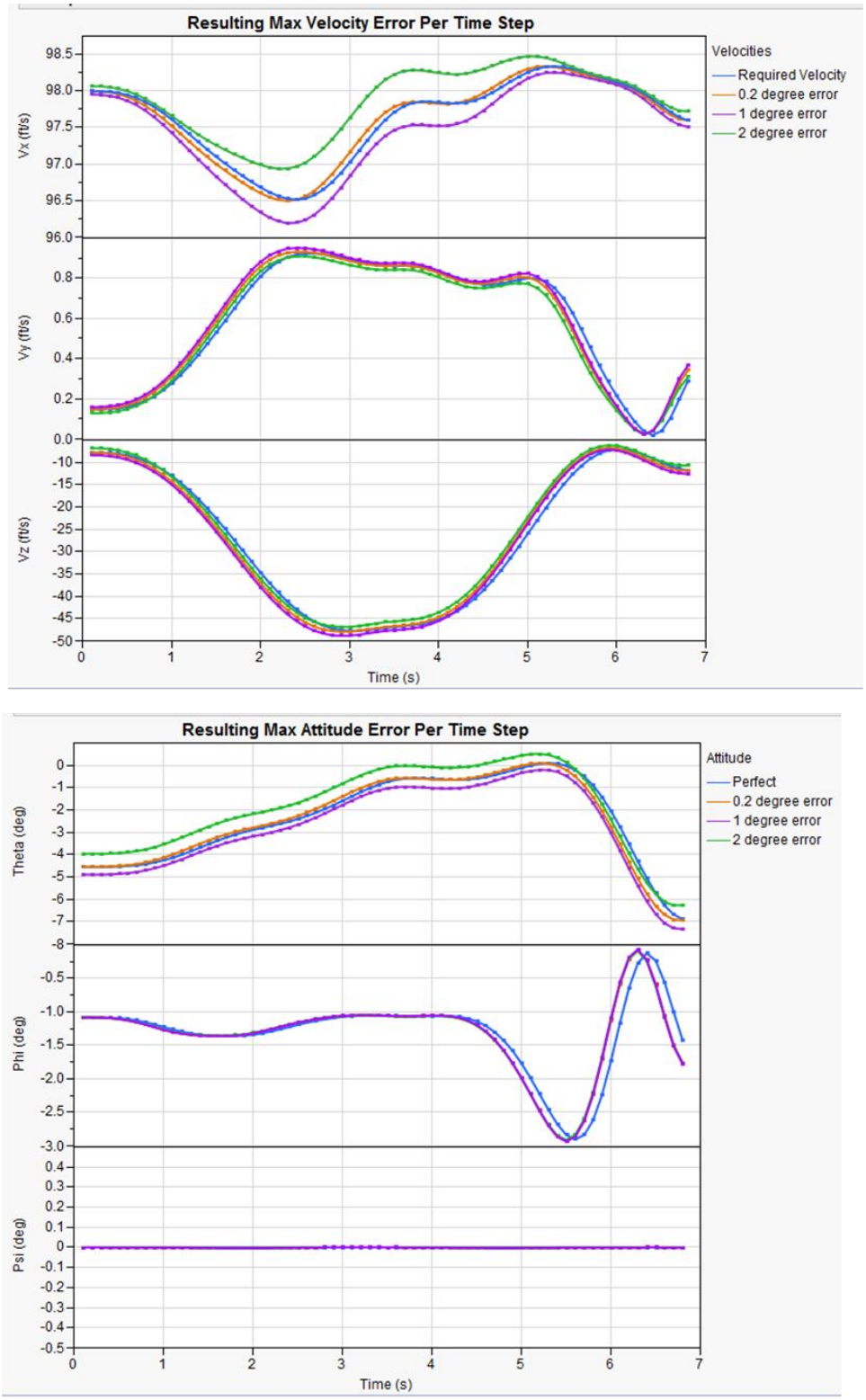

Figure 3.30: Velocity and Attitude Divergence for Commanded Control Error

3.6 Summary of Contribution

The maneuver performance is obtained through a combination of a mathematical rotorcraft model, a maneuver model, and inverse simulation techniques. Additionally, by using parametric models, the input variables can be easily adjusted such that the impact on maneuverability due to changing design or mission can be captured. As stated previously, inverse simulation allows the maneuver performance to be quantitatively calculated independent of control design. The control system is removed from the analysis loop when determining the maximum performance of the system, which results in the motivation for the second research objective. The key components of the second contribution of this work are summarized to show that the need of including control system measures into the design for maneuverability is being addressed. Literature shows that including the control development into the early design process is a difficult task. Additionally, it is established that control design requires detailed system knowledge, which is not feasible in early design. Hence, the control characteristics are forced to be at a general level rather than including specific control parameter settings and architecture choices.

This problem is addressed by the integration of two control characteristics, which allow the designer to perform design trades on the feasible space, while at the same time determine control requirements to be passed downstream to the control designer. The first measure, a control deflection rate constraint, addresses the need presented in the path planning communities, which deals with capturing the dynamic constraints of the control system in the assessment of maneuvering performance. This variable is quantitative

measure of control system performance, while at the same time is not linked directly to one control component but is a measure of performance of the hardware and software combination. The second measure required the integration of a trajectory divergence loop such that the maximum trajectory divergence rate could be calculated for each run. This measure indicates the maximum rate that a given design can deviate from the desired velocity. Velocity is used because it defines the maneuver path. The trajectory divergence rate is calculated independent of other time steps such that particular control system attributes are not included in the analysis, such as sensor sampling rate. These quantitative control performance measures were used along with the process developed to perform design trades that were not possible with traditional formulations. The data analysis portion demonstrated that with the inclusion of these measures, the design risk is mitigated because a more conservative design is determined. The second contribution of this thesis work is established through solving this need in rotorcraft literature.

Contribution 2: Real-time maneuver analysis capabilities that include control characteristic constraints, which provide improved estimates and traceability for development of control system requirements.

CHAPTER 4

DEFINING THE MISSION MANEUVERS

4.1 Introduction

In capturing the dynamic performance capabilities of rotorcraft designs, the AHS 2012 design competition [6] specified multiple maneuvers that cover a wide range of the helicopter operational envelope. The importance of mission definition in design is shown in the 2011 AHS design competition that focused on analyzing a rotorcraft design under mission maneuver uncertainties by specifying three mission definitions, which are shown in Figure 4.1.

The missions represent fundamental helicopter missions that span the military helicopter capability needs. Although expressed separately, the combination of the two requests represents a need within the rotorcraft design and analysis community [197]. Assume that an optimum design is determined using the mission maneuvers as stated in the 2012 RFP. What is the impact of changes in the mission maneuvers on the performance of the chosen design? For example, assume that the competition is moved from sea level to somewhere in the mountains such that the impacts of altitude are drastic or that the maneuvers are combined in a different order to define the mission. Consequently, the detailed level requirements of each of the maneuvers can change as well. These examples demonstrate the need to capture the impacts from the overall mission, while at the same time allowing for detailed maneuver level adjustments.

	Mission 1	Mission 2	Mission 3
Title	Search and Rescue	Insertion	Resupply
Start up/Warm Up	5 minutes	5 minutes	5 minutes
6K95 HOGE	1 minute	1 minute	1 minute
Climb	Best Altitude	Best Altitude	Best Altitude
Outbound Leg	225 nm @ V br	250 nm @ V br	250 nm @ V br
Descent	To Search Altitude	To 6K95 HOGE	To 6K95 HOGE
Loiter	30 minutes @ V be	N/A	N/A
Descent	To 6K95 HOGE	N/A	N/A
6K95 HOGE	5 minutes	N/A	N/A
6K95 Landing	N/A	1 minute	1 minute
Unload (Hot) /Load (Hot)	N/A	10 minutes	20 minutes
6K95 HOGE	N/A	1 minute	1 minute
Climb	To Best altitude	To Best Altitude	To Best Altitude
Inbound Leg	225 nm @ V mcp for 50 to 70 minutes	250 nm @ V br	250 nm @ V br
Descent	To 6K95 HOGE	To 6K95 HOGE	To 6K95 HOGE
6K95 HOGE	1 minute	1 minute	1 minute
Landing / Cool Down / Shutdown	5 minutes	5 minutes	5 minutes

Figure 4.1: 2011 AHS Design Competition Mission Definition

An important contribution to rotorcraft literature, as visualized through these competitions, is the ability to capture the maneuverability characteristics for the entire operational envelope. Additionally, the required mission maneuvers are constantly being adjusted and redefined throughout the design process, as a result, the benefits of capturing these changes in a traceable real-time manner is evident. The number and types of maneuvers within the mission definition can change drastically. Thus, a technique is needed that is capable of formulating any maneuver within the helicopter operational envelope, while at the same time the method must mitigate the combinatorial concerns plaguing the design for maneuverability problem.

Traditionally, mission requirements and constraints are stipulated using fixed maneuver definitions within the mission. Recently the importance of including maneuver variation within the design process has been presented in literature. One reason for this

need is that fixed maneuver definitions alone do not capture the necessary performance thresholds associated with most rotorcraft missions. Additional difficulties arise because of the need to analyze dynamic maneuvers, such as pop-ups and slaloms, which are more computationally demanding than steady-state operation. The historical problem formulations require the mission maneuvers to be defined precisely in order to determine the maneuverability characteristics. Variability in the maneuver definition is not traditionally included in the design process because of the maneuver formulation requirement and computational concerns.

The helicopter mission performance, which is time in this analysis, depends on the contributions from the various individual maneuvers. This concept is summarized by Figure 4.2 where the mission is decomposed into 7 maneuvers. The maneuvers may or may not be dependent upon one another and each maneuver has a different magnitude contribution to the performance. The y-axis is the maneuverability measure, which is time for this example. The axis is normalized from 0 to the maximum maneuver time.

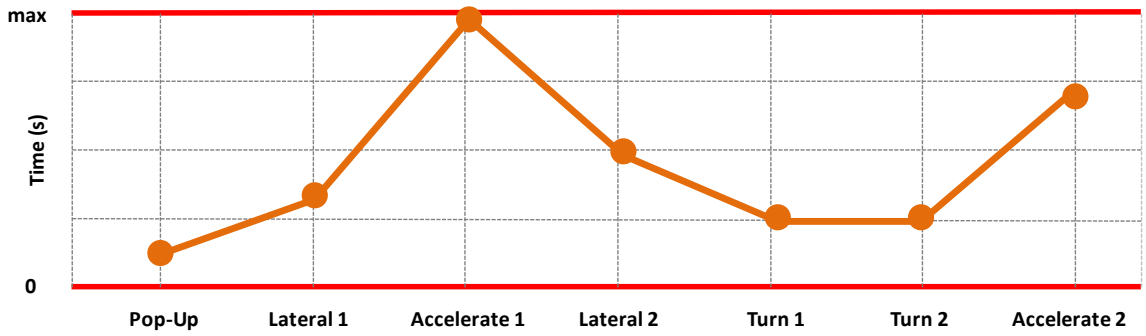

Figure 4.2: Mission Minimum Time

Various maneuvers are shown on the x-axis. The orange maneuverability curve shifts upwards in that maneuver dimension as the time to complete the maneuver increases. During the early stages of design, the contribution of the individual maneuvers in relation to the overall mission is often overlooked because only the entire mission time is analyzed. The maneuverability characteristics may drastically change with slight changes in the maneuver definition, and as a result, the selected design may no longer be the optimum. On the other hand, small changes may impact a single maneuver, while leaving the other maneuvers unaffected by the change. In this situation it is best to select the design that is most robust to changes in maneuver definition, while still meeting the dynamic maneuver requirements. Moreover, each maneuver may be dependent upon the maneuver that comes previous or post the current maneuver, which creates additional difficulties during mission maneuverability analysis. As a result, the trade space grows exponentially and selecting the 'optimum' becomes more difficult as multiple maneuvers are combined to form the overall mission. This is demonstrated in Figure 4.3 where two different optimization schemes are used to select the optimum design and maneuver combination. The orange curve represents the minimum time maneuver for the maximum mass design, while the green curve represents the minimum time maneuver for the minimum rotor diameter design. The ability to adjust the optimization scheme real-time is essential to provide traceability and improved quantitative maneuverability tradeoffs to the design process.

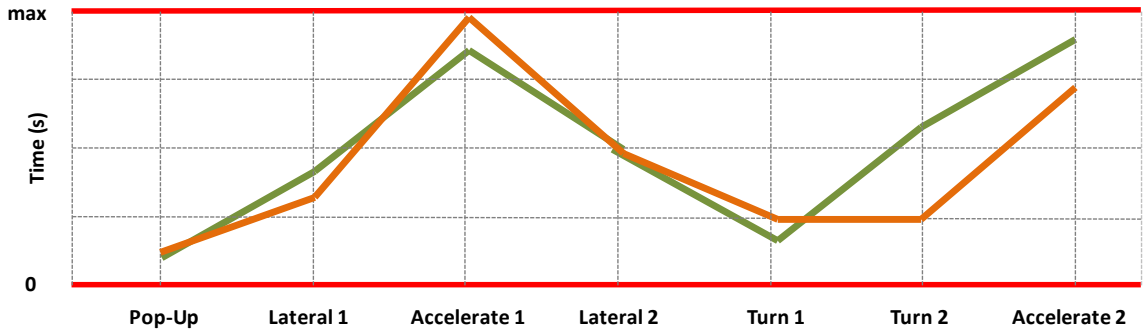

Figure 4.3: Various Optimization Strategies

The numerous maneuvers within the helicopter operational envelope create for a difficult problem. In order to capture the entire mission space, the formulation must capture all of these maneuvers, while at the same time the number of parameters must be minimized due the combinatorial nature of the problem. Through literature review, a set of the necessary helicopter dynamic maneuvers that encompass the entire operational envelope must first be determined. The difficulty in expressing the entire flight envelope in a finite set of maneuvers that span the entire operational envelope remains an open research problem for conceptual design. As a result, the focus of the final area is to develop a method that allows quantitative assessment of all the dynamic maneuvers that form the operational envelope.

Overall Research Objective: Develop a methodology that enables real-time and traceable assessment of:

- **Design parameter impacts on maneuverability characteristics**
- **Maneuverability degradations due to control system characteristics**
- **Entire helicopter operational envelope maneuverability**

4.2 Literature Review

The literature review required to fully address the third area of the overall research objective is separated into two major tasks. First, a set of helicopter maneuvers must be determined that encompass the entire helicopter operational space. This requires analyzing previous research efforts and maneuver path modeling techniques. Once a set of maneuvers is defined, the second portion of the literature review determines a method to mitigate the combinatorial issues such that the envelope of maneuvers may be analyzed in conceptual design. The following section is divided into helicopter maneuver envelope determination and maneuver taxonomy development.

4.2.1 Helicopter Maneuver Envelope

The determination of the set of maneuvers that enclose the entire envelope for helicopter maneuvering flight must be determined in order to analyze design implications on maneuverability characteristics for the overall mission. Historical evidence shows that critical flight regimes are often missed during conceptual design efforts [106]. As a result, several methods have been developed in order to systematically capture this space. For example, Thomson [134] defined a set of standard maneuvers as part of demonstrating compliance with US handling qualities for military rotorcraft [198]. Thomson [199] further elaborates by saying that "helicopter performance and handling qualities are now routinely assessed in relation to specific maneuvers." The problem is that this analysis is occurring much later in the design process for a fixed design. The Aeronautical Design Standard 33 [198] specifies handling qualities for military rotorcraft

design where the maneuver is not defined precisely but is fulfilled by a list of constraints. This poses computational concerns when integrating with the design process; additionally, the handling qualities should be assessed in conjunction with controller design. Therefore, this type of maneuver definition is not appropriate for this work.

Another approach that has been applied to the fixed-wing problem is Design Constraining Flight Conditions (DCFC). DCFCs are the minimum set of flight conditions with an overall governing effect on aircraft hardware sizing. Chuboda [200] has applied the technique for stability and control purposes and presents a method for the identification and formulation of a generic set of DCFCs as applied to control effector sizing. Several papers have been presented that develop the expressions for various regions of flight [201-203]. One major problem with the process is that defining DCFCs requires an understanding of the design evolution of all types of aircraft configurations, knowledge of certification requirements, and familiarity with flight test processes [204]. Consequently, this method attempts to develop all constraining flight conditions in order to bound the operational flight envelope; however, these constraints are problem specific and subject to variability. The absolute bounds can only be determined if the entire maneuver envelope is examined.

Another analysis tool that has been proposed in recent years uses the concept of equilibrium sets. When analyzing nonlinear systems, equilibrium points may only be locally asymptotically stable. Because of this, it is important to analyze the points around the operational conditions of interest [205]. At dynamically unstable flight regimes, aircraft motion is often represented by linear time invariant system with unstable

eigenvalues [206]. However, as stated by Goman [206], "the unstable linear system with constrained control inputs has a bounded controllability region, which means that the stabilization problem under the restriction on control input can be solved only for a limited number of initial states of the system."

The method of attainable equilibrium sets computed on a grid of points for two selected parameters provides much insight into a broader flight envelope. In order to specify a particular steady maneuver, additional kinematic constraints are required. This involves augmenting the equations of motion with auxiliary equations that specify maneuver kinematics and parameters [207]. The stability characteristics of the equilibrium points determined in this 2-dimensional grid are then evaluated using eigenvalue analysis of the linearized system [208]. The analysis produces local stability maps that provide a qualitative understanding of equilibrium and stability for two of the state variables. The attainable equilibrium states belong to a wide class of aircraft steady helical trajectories that are bounded by control effector size and max deflection angles.

The end result is a 2-dimensional depiction of the equilibrium and stability space, which may be viewed in Figure 4.4 [207]. This diagram shows the equilibrium space for angle of attack and sideslip combinations with all other state variables held constant. The controls are adjusted to trim the vehicle and are limited by deflection rate and maximum deflection angle. The dark points indicate dynamically stable equilibrium points, while the lighter points show unstable regions. A similar diagram would be required to analyze each operational scenario and each subset of states of interest, which would culminate

into a large number of equilibrium set studies making this method infeasible for conceptual design.

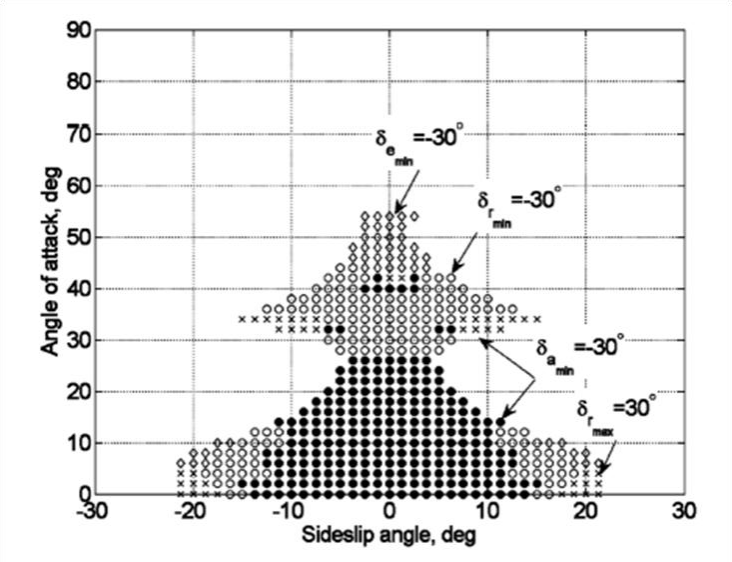

Figure 4.4: Attainable Equilibrium Sets

Flight Systems, Inc in partnership with the U.S. Army Aviation Research and Development Command conducted a thorough analysis on the topic and generated a set of missions that encompass the entire operational region for military helicopters [19]. The research focus is analyzing helicopter operations with intent of identifying key parameters and understanding the importance of various maneuvers through quantification of agility. The agility is defined as a requirement to rapidly maneuver from point-to-point, thus, time to execute is the defining measure of performance. The researchers note that in order to have greater performance than an opponent, the vehicle must perform the mission in less time. The missions are defined by a combination of various maneuvers with each maneuver weighted according to importance within the overall mission. In order to make analysis more systematic, the operational envelope is

separated into three flight senarios, each of which having particular maneuvers within. The mission segments are defined as: initial vectoring, pre-attack, and close-air combat. Each of the three segments is composed of a subset of maneuvers, which are stitched together to form the entire mission phase. The maneuver definitions are selected by subject matter experts in a rigourous study for conventional military helicopter configurations and only energy-based analysis is conducted. In total, the three phases of the mission include 29 different maneuver segments, which are stated to cover the entire operational envelope of the helicopter. This method has been systematically developed by experts in the field of helicopter maneuverability and is the most thorough of the operational envelope definition methods. Additionally, this formulation has been used in previous rotorcraft maneuverability design studies.

4.2.2 Maneuver Taxonomy

The 2011 AHS design competition states three separate missions, while the 2012 competition required multiple dynamic maneuvers within a single mission. Combining these observations shows that the helicopter maneuver space is immense and in order to capture the dynamic performance relationship to design parameters, a taxonomy of maneuvers is required. These maneuvers must be chosen such to encompass the entire helicopter operational space, while at the same time remaining low in dimension for computational reasons resulting from integrating maneuver performance into design. As stated by Frazzoli [209], “the state space of nontrivial systems is typically very large, and the curse of dimensionality makes the solution” in such large-dimension spaces computationally intractable.

There exists an immense space of possible motions that need to be included and analyzed in order for completion of a mission. Mission analysis through the use of decomposition methods have been employed since the 1970s in spacecraft trajectory optimization problems. The method developed by Petersen [210], splits the overall mission into segments and applies the analysis to the low-level maneuvers. An additional, routine is applied to ensure smoothness when transitioning from one maneuver to the next. Thomson [134] states that "given a generic math model it is possible to study the effect of varying key configuration parameters on the performance of the vehicle while performing a maneuver." Rahn [211] applies this concept to the simultaneous optimization of the trajectory and design for a space transportation system. Extending the literature, Braun [212-214] applies the Collaborative Optimization architecture to the design of a launch vehicle, which included design using multiple disciplines along with a trajectory optimizer.

The motion-planning literature approaches the problem in a similar manner, which involves generating motion primitives and using a discrete optimization algorithm to form the overall path [215]. These primitives are generated based on kinematic constraints imposed on the EoM of the system, which results in a subset of maneuvers that can be combined to fully define the maneuver space of the vehicle [38]. The motion primitive path-planning approach is best summarized by Frazzoli [45], "without sacrificing too much of the vehicle capabilities, we restrict the class of nominal trajectories to the family of trajectories that can be generated by the interconnection of appropriately defined primitives." One downfall is that most path-planning methods are

only at the kinematic level and do not account for dynamic characteristics of the vehicle or the controller [216]. As a result, the feasibility of the path is not guaranteed because it is possible that no control setting exists that allows the aircraft to follow the proposed motion primitive without violating the control or state constraints. Likhachev [217] analyzes the set of actions and calculates whether any single action can be approximately recomposed out of a combination of other, shorter actions. If so, these longer actions are removed from the fundamental maneuver set. Likhachev [217] further elaborates the problem by stating that "there exists a wide spectrum of smooth, dynamically-feasible paths between the vehicle and goal configurations and it is waste of time and memory to explore all of them."

Frazzoli [40] presents a Maneuver Automation (MA) strategy, which is a method of determining the minimal set of maneuvers that includes all the primitives that are defined by the start and end steady-states of the maneuver. The methodology essentially represents a transfer function that relates the state before a maneuver to the states after the maneuver. The results of this analysis are summarized in a diagraph, which is shown in Figure 4.5. The vertices of the digraph represent steady-state operation and are represented via Greek letters in the figure. The edges of the digraph represent the fundamental maneuvers necessary to transition from one steady-state to another. Any steady-state in the envelope can be modeled in this sense and the maneuvers required to enter and exit the trim primitive are required to enable path planning of trajectories. The major benefit of this approach is that the velocities can be discretized and combined through the maneuver definitions to enable smooth path generation in position, velocity,

and acceleration. The structured digraph approach is applied in this work because it offers a systematic and traceable process, unlike any of the other literature reviewed. In combination with a complete definition of the helicopter operational envelope, the MA method may provide benefit in the design domain if appropriate adjustments are implemented.

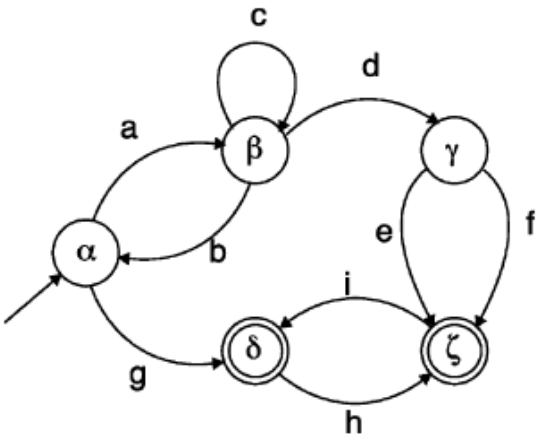

Figure 4.5: Motion Primitive Digraph

4.3 Approach

The approach to the immense envelope problem through a taxonomy development technique is presented in four parts. First, a research question is formulated based on the needs that are provided in the AHS design competitions and helicopter literature. It turns out that through modification of the process developed in Contribution 1 and 2 of this thesis, the final characteristic of the problem may be addressed. Third, a hypothesis is presented in an attempt to address the remaining mission and maneuver related needs. By fulfilling the needs introduced through the hypothesis; the final contribution of this work is realized. This contribution is the final component necessary to fully address the

motivating problem, which culminates into a traceable, systematic, and cohesive process that addresses all the needs of the problem simultaneously. Finally, a test plan that details the experiments that are to be simulated and what data is to be analyzed is presented.

4.3.1 Research Question

The third research question results in one final modification of the systematic process that has been developed and expanded upon in this work. The research question is formulated based on extensive review of the helicopter maneuver envelope and maneuver definition strategies. The remaining question regarding maneuver variability and envelope inclusion is first presented, which is followed by a discussion that details attributes of the problem and the corresponding needs.

Research Question 3: Given that the maneuver space is combinatorial, how can the maneuverability characteristics be captured for the entire helicopter operational envelope, thus, enabling analysis of complete missions?

The third research question has several key considerations, which are discussed more fully in the following section. The first need posed by the research question is that the solution must encompass the overall mission performance, while at the same time allowing for the effects of the individual maneuvers to be distinguished. Inclusion of all of the various types of rotorcraft mission maneuvers into the design framework presents computational considerations due to the large helicopter maneuver envelope. Moreover, the hypothesized process must be robust such that it can capture the variability in maneuverability limits resulting from changes in the mission definition. Additionally,

fully defining the maneuvers using performance results will aid in developing a clear mission definition if the mission requirements are not well defined initially. The fourth requirement of the hypothesized method is that the analysis methodology must provide quantitative results that are independent of vehicle controller. Finally, the decision making framework must allow for easy manipulation of design constraints because variability causes changes in mission maneuver definition throughout the design process. In combination, these attributes create a very difficult problem that requires a well structured, traceable, and systematic process that expands upon the method developed through the first two contributions of this work.

4.3.2 The Final Process

The process discussed in Chapter 2 of this thesis captured the variability in maneuver performance limits due to design variability for a single mission maneuver. The maneuver was selected because of the amount of literature available for validation purposes. The second contribution extended the capabilities of this systematic and traceable process to include control characteristics, which enabled control system requirements development. The final adjustment is made to the process in this chapter such that multiple maneuvers can be simulated in order to assess the maneuverability characteristics over the entire helicopter operational envelope. The modified process is displayed in Figure 4.6 with the changes required for the third contribution highlighted in red.

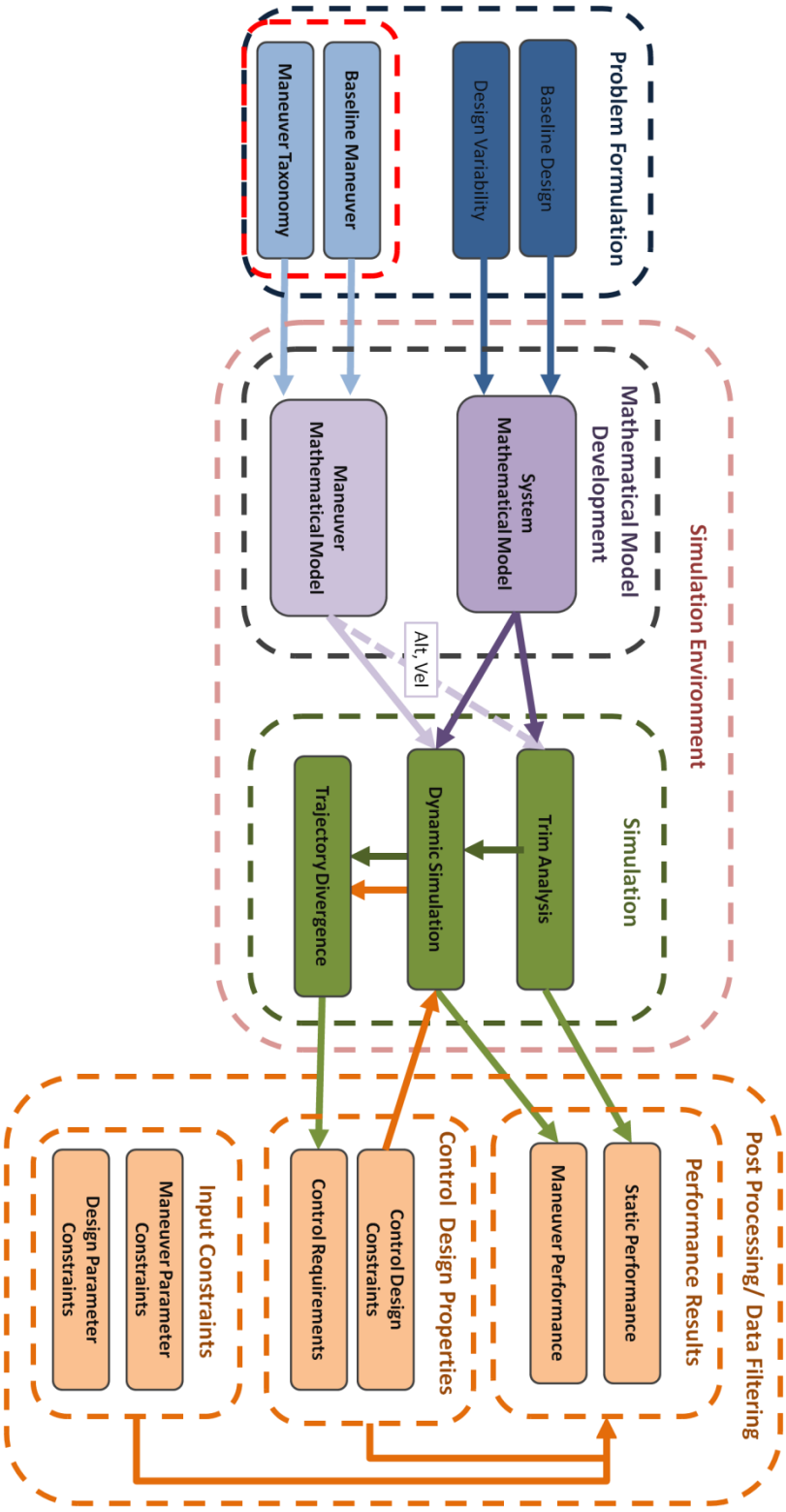

Figure 4.6: Modified Process for Maneuver Variability

Contribution 1 assumed fixed type of maneuver; however, this assumption is not valid and as a result it is necessary that the methodology be expanded to capture the entire operational envelope of the helicopter. This is accomplished by the final modification to the process, which requires the addition of the maneuver taxonomy block. As before, the process consists of four major elements: Problem Formulation, Mathematical Model Development, Simulation, and Post Processing/Data Filtering.

4.3.3 Hypothesis

In order to define the operational envelope, the maneuvers that are encompassed within this space must be defined. This requirement takes the form of a taxonomy development approach that is based on helicopter operational procedures and maneuvers. This taxonomy is added at this step in the process such that each design and maneuver combination may be evaluated for each fundamental maneuver within the taxonomy. Additionally, it must be shown that the taxonomy spans the entire operational space of interest and the individual maneuver types must be verified to show that the time histories are valid. The maneuver space is determined through a combination of literature review and a structured decomposition process that is based on techniques used in motion primitive development. The primitive development process decomposes missions into sub maneuvers until the most fundamental motions are found. This set of the most fundamental operations is termed primitive motions and can be combined to form any maneuver within the operational space.

The key components of the hypothesized method are discussed here briefly to show that the need is being addressed. The first characteristic is fulfilled by the development of a taxonomy approach to analyzing the helicopter maneuvers, which allows the designer to capture the performance measures for the individual maneuvers. These individual quantitative performance results can then be looked at together to form the performance for an entire mission. The dynamic performance is obtained through a combination of a mathematical rotorcraft model, a maneuver model, and inverse simulation techniques. Additionally, by using parametric models, the input variables can be easily adjusted such that the impact on maneuver performance due to variability in maneuver definition can be captured. As stated previously, inverse simulation allows the maneuverability to be quantitatively calculated independent of control design. Finally, the impact of changing mission definitions can be assessed real-time using a filtered data approach over the operational space for the range of inputs selected. The final contribution of this thesis work is established through analyzing and testing Hypothesis 3.

Hypothesis 3: Analyzing the maneuverability characteristics by decomposing into a set of fundamental parametric maneuvers enables quantitative design comparison for the entire mission.

4.3.4 Test Plan

The modifications to the process are previously discussed; however, the new information that is to be gathered from the simulation requires addressing. The inputs consist of both the system and the maneuver model parameters, while the outputs are

dynamic performance and time-based system properties. The system modeling parameters remain the same as determined through the process expanded upon in Chapter 3, except for the addition of a maneuver type variable. The maneuver definition now consists of the five maneuver parameters: altitude, velocity, time, and acceleration plus a variable to indicate which of the fundamental maneuvers from the taxonomy to simulate. All of the maneuvers are simulated independent of one another and can be combined in numerous ways to perform design trades.

The third contribution greatly impacts the number of simulations that are required because each type of maneuver introduced through the taxonomy. As stipulated in the original process, all the states, controls, and auxiliary variables are outputs from each simulation. The feasibility of a maneuver, which is determined by whether a set design completes the entirety of the maneuver, is also captured as before. With this information, the performance limits due to maneuver variability can be analyzed for the various maneuvers defined in the taxonomy. This is demonstrated through a series of three experiments. The first step of the analysis discusses the decomposition of the AHS competition mission into a series of maneuvers for analysis. Second, the first maneuver of the mission is analyzed to show the process required for constraining individual maneuvers within the mission. Third, the interdependencies of the maneuvers are discussed and the capability to analyze multiple maneuvers simultaneously is demonstrated. Finally, two different optimization schemes are applied and the maneuver capabilities are compared for the overall mission using the individual maneuvers.

4.4 Implementation

The modifications to the proposed process are presented with regards to the rotorcraft problem in this section. First, the extensions to the maneuver model development are presented, which includes the decomposition of the maneuver space using motion primitive generation techniques. A set of maneuvers developed based on helicopter experts is used as the base operational space for this exercise. The usefulness and validity of the parametric motion primitives are shown through example.

4.4.1 Taxonomy Development

The work on the helicopter operational envelope presented by Flight Systems, Inc [19] is the most thorough of all the literature reviewed, while at the same time offering complete maneuver definitions rather than a series of constraints. Additionally, these definitions have been used in previous rotorcraft studies for analyzing dynamic performance capabilities in design. The complete maneuver definitions are important because the design space dimensionality concerns arise whenever the maneuver is provided greater degrees of freedom. The mission and the corresponding maneuver definitions are separated into three subcomponents: high speed flight to combat area, aggressive concealed movement, and combat phase. Each of which is detailed in this section for clarity. No mission will follow all the maneuvers specified in the exact order. The intent is that the mission reflects the spectrum of maneuvers that would be conducted and encompass the entire helicopter operational envelope.

The initial vectoring phase may be viewed in Figure 4.7 and consists of eight defined maneuvers. The first maneuver is acceleration from hover to a maximum velocity. The concept of this maneuver is that hover performance, acceleration capabilities, and maximum speed level flight are all captured through this maneuver. The second series of maneuvers in this phase definition consist of climbs and descends at various angles. These maneuvers make up two through seven in the intial vectoring flight stage. The final maneuver in this mission phase is a terrain following maneuver that is very similar to a pop-up maneuver or a Nap-of-the-Earth operational procedure. In combination, the intial vectoring stage represents the performance of a design in traveling to a combat area. This segment only consists on longitudinal operation with a fixed altitude change for every maneuver within the phase. Hence, it is noted that the change in atltitude for every maneuver should not be constrained to a fixed number in this research effort.

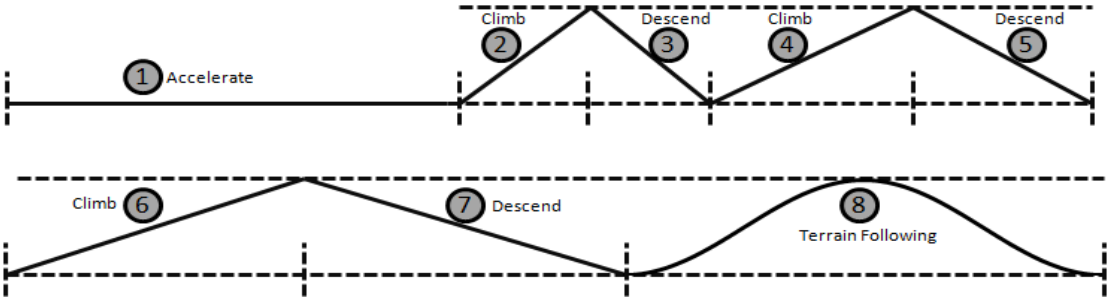

Figure 4.7: Initial Vectoring Phase

The second phase defined by the authors is the pre-attack phase. The first segment of this phase is a set of pop-up maneuvers from hovering at sea level to hovering at 50 ft altitude. The document specifies a certain number of pop-ups to perform in this segment.

These maneuvers are very similar to the terrain following maneuver in the initial vectoring phase. The second segment is a set of vertical axis turns both clockwise and counter-clockwise. The performance differences between the two turns may not be captured if only power required information is utilized. However, if the individual forces and moments from the various components are included in the analysis then the performance will be different between the two directions [218, 219]. Similar to the initial vectoring phase, the pre-attack phase also includes an acceleration segment; however, this time the linear acceleration is coupled with a deceleration to stop. This occurs in the third and fourth segments of the mission and provides an indication of the horizontal acceleration properties of the helicopter. The remaining segments all incorporate a set of turns to assess the turning performance of the helicopter. Segments 5, 6, and 7 analyze constant radius turns of different radii, while 8, 9, and 10 include a transient acceleration and deceleration in the turns.

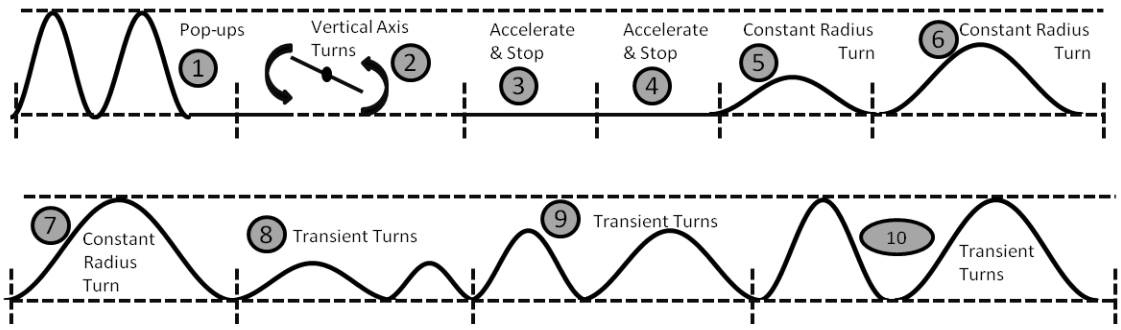

Figure 4.8: Pre-Attack Phase

The third and final phase is the combat phase, which attempts to include all of the necessary maneuvers required during air combat with enemy aircraft. Eleven maneuvers are included in this scenario, which encompasses accelerations in all the helicopter axes.

The first maneuver involves an acceleration to a specified velocity, which is followed by a maximum velocity that can be completed at the velocity defined in the first maneuver. The following six maneuvers are paired into an acceleration segment followed by a turn segment. Each turn is specified to various degree, thus, a different max velocity exists for each grouping. Finally, the phase ends with a climb and a descend segment. In total, the three phases of the mission include 29 different maneuver segments, which are stated to cover the entire operational envelope of the helicopter.

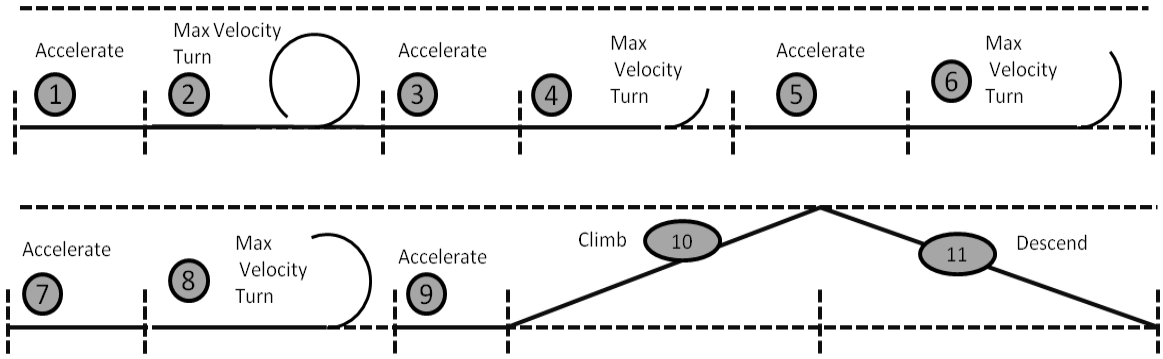

Figure 4.9: Combat Phase

All three mission phases together have a total of 29 maneuvers, which are presented together in Table 4.1. Beside each maneuver in the table is a column titled "Acceleration." This column is included in order to show which axis of the navigational frame is experiencing acceleration during the maneuver. For example, the first maneuver is an acceleration from hover to a final velocity with constant altitude. This involves an acceleration in the x-axis of the navigational frame; hence, an "X" is placed in the "Acceleration" column. The same process is completed for all of the defined maneuvers. This process is key in determining the fundamental maneuvers required to form the maneuver taxonomy. It is observed by viewing the "Acceleration" column in Table 4.1

that all of the maneuvers can be described by four different accelerations. The first three correspond to linear acceleration in all three axes of the navigational frame. The X acceleration allows the vehicle to speed or slowdown in x direction of the horizontal plane. The Y acceleration allows the vehicle to side step, creating the ability to perform lane change and slalom maneuvers that are required of the 2012 AHS problem description. The Z acceleration permits altitude increases independent of the forward velocity X. This allows for all types of climbs and pop-up maneuvers. This type of acceleration was discussed in detail in Chapter 2. The fourth acceleration is about the yaw (heading) axis, which allows for turning performance to be evaluated. The four accelerations are defined independent of each other allowing for a multitude of helicopter maneuvers. The only maneuvers that are not possible with this formulation are maneuvers involving purely pitch and roll; however, these are not included in requirements definition independent of other actions. The pitch and roll are usually included through post processing as maximum limits for human safety, aerodynamic, or structural reasons.

The control community requires that the maneuvers start and end at steady-state conditions for controller development purposes; however, selecting which steady-state conditions must still be determined. For example, it is possible to model a z-axis acceleration maneuver that starts at steady-level flight and ends with a steady-state climb. Conversely, the maneuver can start at steady-level flight and end at steady-level flight at a different altitude. Both specification techniques adhere to the steady-state requirement. The impact of this decision affects the number of basic maneuvers that form the

taxonomy. Additionally, the ability of these maneuvers to be combined to form the entire design space must still be verified.

Table 4.1: All 29 Mission Maneuvers

#	Maneuver Name	Acceleration	#	Maneuver Name	Acceleration
1	Accelerate to max velocity	X	16	Transient turn of 80 ft	Ψ,X,Y
2	Climb 30 degree hill	Z	17	Transient turn of 150 ft	Ψ,X,Y
3	Descend 30 degree hill	Z	18	Transient turn of 400 ft	Ψ,X,Y
4	Climb 20 degree hill	Z	19	Accelerate to 40 kts	X
5	Descend 20 degree hill	Z	20	Minimum radius turn at 40 kts	Ψ
6	Climb 10 degree hill	Z	21	Accelerate to 180 kts	X
7	Descend 10 degree hill	Z	22	Max velocity turn 80 degrees	Ψ
8	Terrain following of 600 ft	Z	23	Accelerate to 100 kts	X
9	Pop-ups of 50 ft	Z	24	Max velocity turn 120 degrees	Ψ
10	Vertical axis turns	Ψ	25	Accelerate to 160 kts	X
11	Accelerate and stop	X	26	Max velocity turn 180 degrees	Ψ
12	Accelerate and level stop	X	27	Accelerate to 100 kts	X
13	Constant radius turn of 100 ft	Ψ	28	Climb 1000 ft	Z
14	Constant radius turn of 400 ft	Ψ	29	Descend 1000 ft	Z
15	Constant radius turn of 2000 ft	Ψ			

The taxonomy development process continues with the modified Maneuver Automation technique presented by Frazzoli [40], which uses what is referred to as a digraph. The digraph is a method for displaying the various steady-states of the system and the manner in which each state transitions to the other steady-states. In order to progress from a current state to a desired end state, the operation may require traveling through multiple steady-states since not all steady-states have direct connection. An example digraph is presented in Figure 4.10 that represents the horizontal acceleration from hover to a forward flight of 40 ft/s. The vertices represent steady-states of the system, which in this context are steady-level flight. The edges represent maneuvers required to progress from one steady-state to the next, which is an x-axis acceleration.

The number of steady-states dictates the number of maneuvers since it is necessary to be able to transition both into and out of each steady-state. The forward velocity is decomposed into 20 ft/s increments in this exercise; however, this number is only chosen for the purposes of this example.

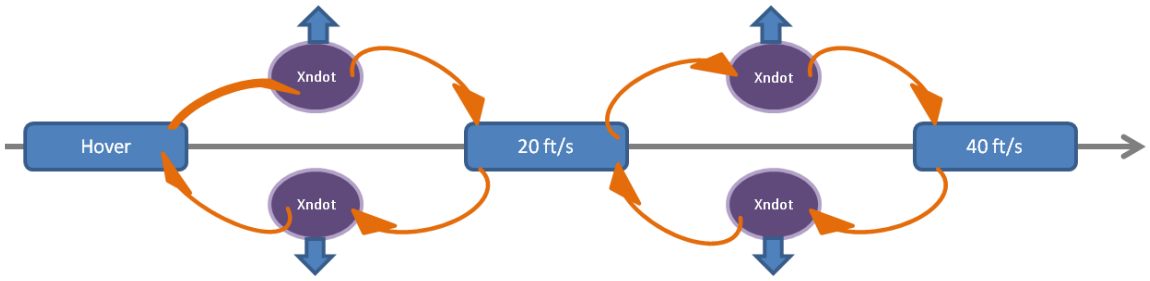

Figure 4.10: X-Acceleration Digraph

Figure 4.10 demonstrates that in order to accelerate from hover to a flight velocity of 40 ft/s requires two separate maneuvers. The first maneuver accelerates the vehicle from hover to 20 ft/s, while the second accelerates from 20 ft/s to the desired 40 ft/s. This is an example to show how the digraph representation applies to one of the accelerations within the maneuver taxonomy. For path planning purposes, the maneuvers must be decomposed into a smaller set like that shown in Figure 4.10, which uses a 20 ft/s discretization. However, since the maneuver model developed in this work defines each type of maneuver in a parametric sense, this discretization is not needed. The resulting digraph for horizontal velocity change takes the form shown in Figure 4.11. This representation covers all types of horizontal forward velocity changes.

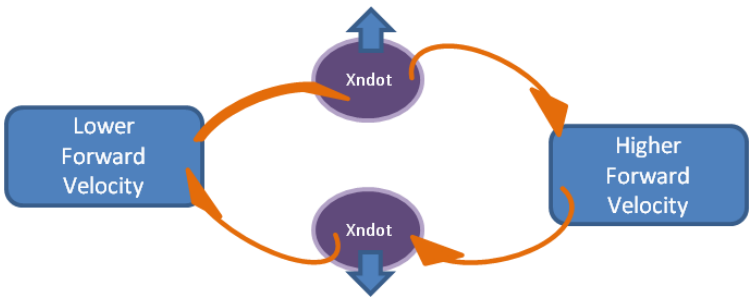

Figure 4.11: Horizontal Velocity Change Digraph

An example showing the resulting trajectory of the velocity based digraph from lower forward velocity block to the higher forward velocity block is displayed in Figure 4.12. The vehicle starts at a lower forward velocity steady-state, progresses through acceleration in the x-axis, which is shown as the top path in Figure 4.11 and ends at a higher forward velocity. At time zero the helicopter is traveling at 20 ft/s which can be viewed by the small amount of pitch forward required. This steady-state is maintained for 10 seconds. At 10.1 seconds the vehicle accelerates in the x-axis to the end velocity. By the end time of the maneuver the vehicle has reached a new higher steady-level velocity that requires more forward pitch of the vehicle.

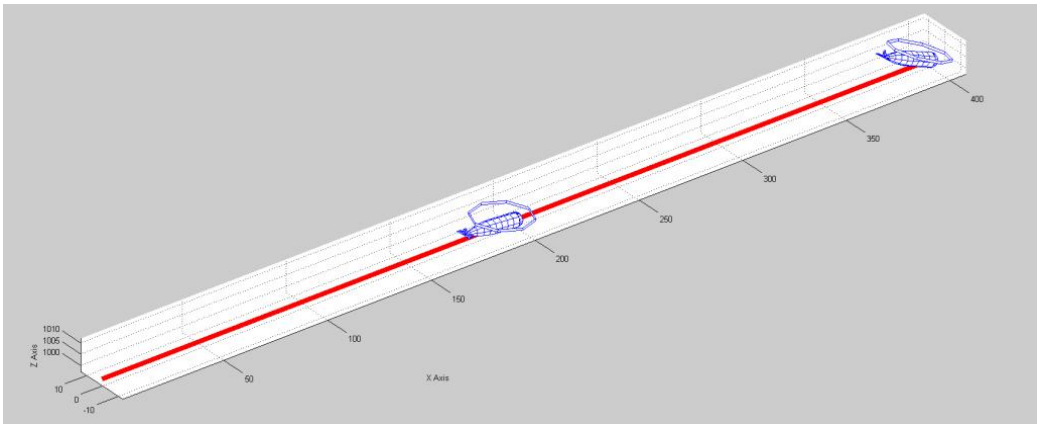

Figure 4.12: Increase in Forward Velocity

In order to formulate a digraph representation of the entire design maneuver space, all four of the acceleration maneuvers must be described and included. Figure 4.13 demonstrates all of the eight basic motions that can occur from a steady-level flight scenario of the helicopter platform. The x-axis acceleration maneuver that was just discussed is composed of the accelerate block. The deceleration of the x-axis maneuver is described by the decelerate block. The z-axis accelerations, which are used for pop-up maneuvers, are formed by the increase and decrease in altitude blocks. The y-axis accelerations include a sidestep left and right blocks, while the yaw axis acceleration is defined by the positive and negative rotations.

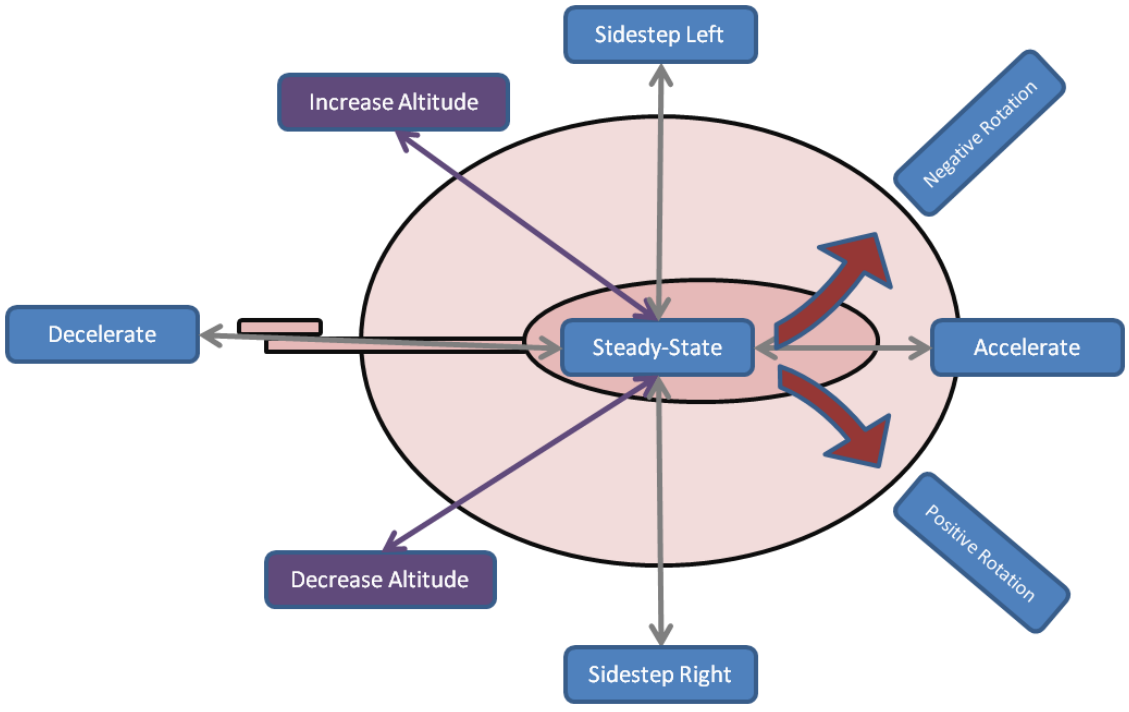

Figure 4.13: Possible Motions from Steady-Level Flight

The resulting digraph from decomposing the four needed accelerations is presented in Figure 4.14. It should be noted that only the positive change in all four

accelerations is presented for clarity reasons. If a negative acceleration is desired then the arrows of the figure are reversed. Hence, there are eight possible steady-states that can be reached from the current steady-state with the four accelerations determined through the literature review.

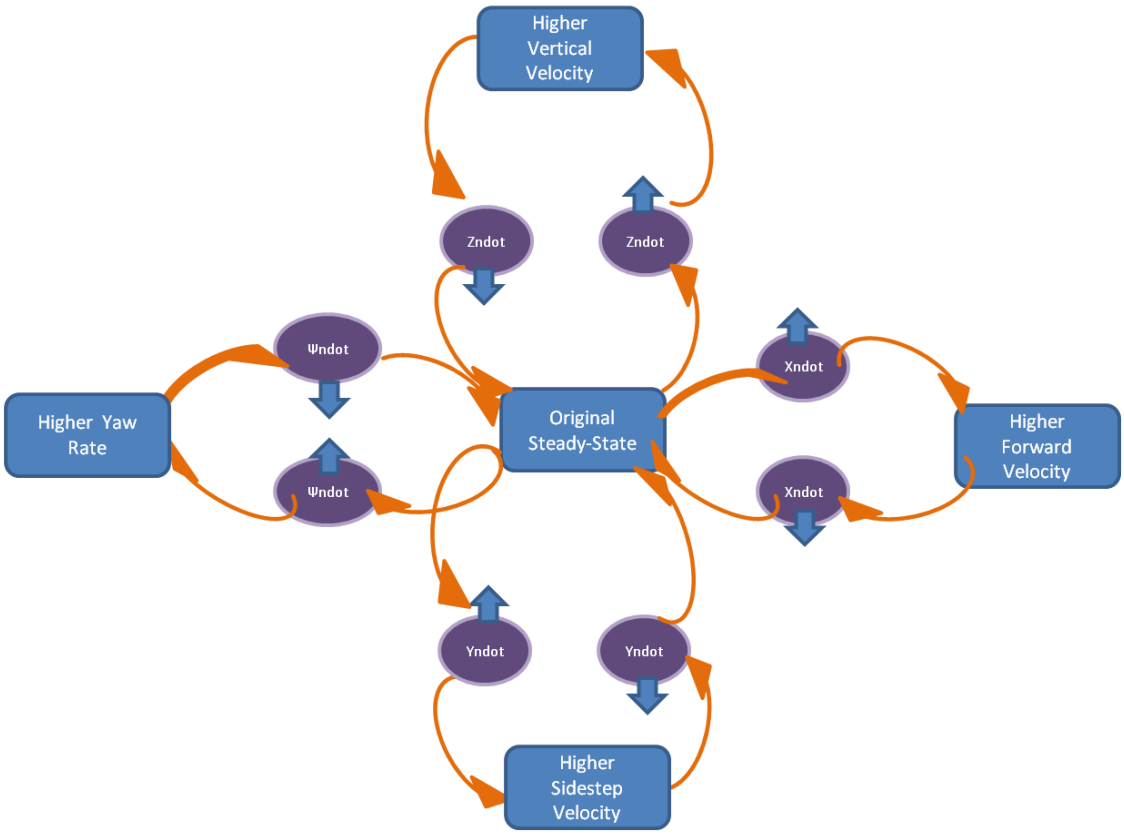

Figure 4.14: Digraph Representation of the Maneuver Space

For path planning purposes, each of the maneuvers in Figure 4.14, which are represented by the arrows, must be defined separately. In reality there are an infinite number of steady-states in the design space because the maneuvers from steady-state to steady-state are described in a parametric manner for design purposes. Hence, the steady-states in Figure 4.14 represent a class of steady-states rather than a particular point when

applied to the design problem. This extension in this work enables a parametric maneuver model to define the entire operational envelope. For example, the higher vertical velocity block represents all steady-state operations were a constant rate of climb is specified. Additionally, each positive acceleration maneuver has a corresponding negative acceleration maneuver. Using this observation in combination with the manner in which the maneuvers are defined in this work, the subset of eight maneuvers can be decomposed into four maneuvers. This is beneficial for two reasons. The first reason is that by simulating each maneuver as the combination of the acceleration and the deceleration, the opposite maneuvers are obtained with a single simulation. Secondly, it reduces the combinatorial maneuver space from eight discrete maneuver types to four discrete maneuver types, which further mitigates the dimensionality concerns that are problematic during design.

The four maneuvers that form the maneuver taxonomy are shown in Figure 4.15. The Z acceleration is displayed as a pop-up maneuver within the figure where the final condition is specified as a change in altitude to maneuver over an obstacle. The X acceleration is displayed second in the figure and is representative of horizontal accelerations and decelerations. The Y acceleration is shown third, which allows for side step maneuvers to be simulated. Finally, the Yaw acceleration allows for turning flight simulations. By including all four maneuvers in the simulation simultaneously and independently, any maneuver within the helicopter maneuvering envelope can be simulated. For example, by combining z-axis deceleration and a yaw rate, various helical descent trajectories can be analyzed. One instance of these settings is demonstrated in

Figure 4.16. The 29 maneuvers that were selected to represent the helicopter operational envelope have been decomposed into four parametric maneuvers through modification of the Maneuver Automation technique. The capability to model all of the maneuvers that form the AHS design competition mission can be analyzed by appropriate filtering and constraint placement.

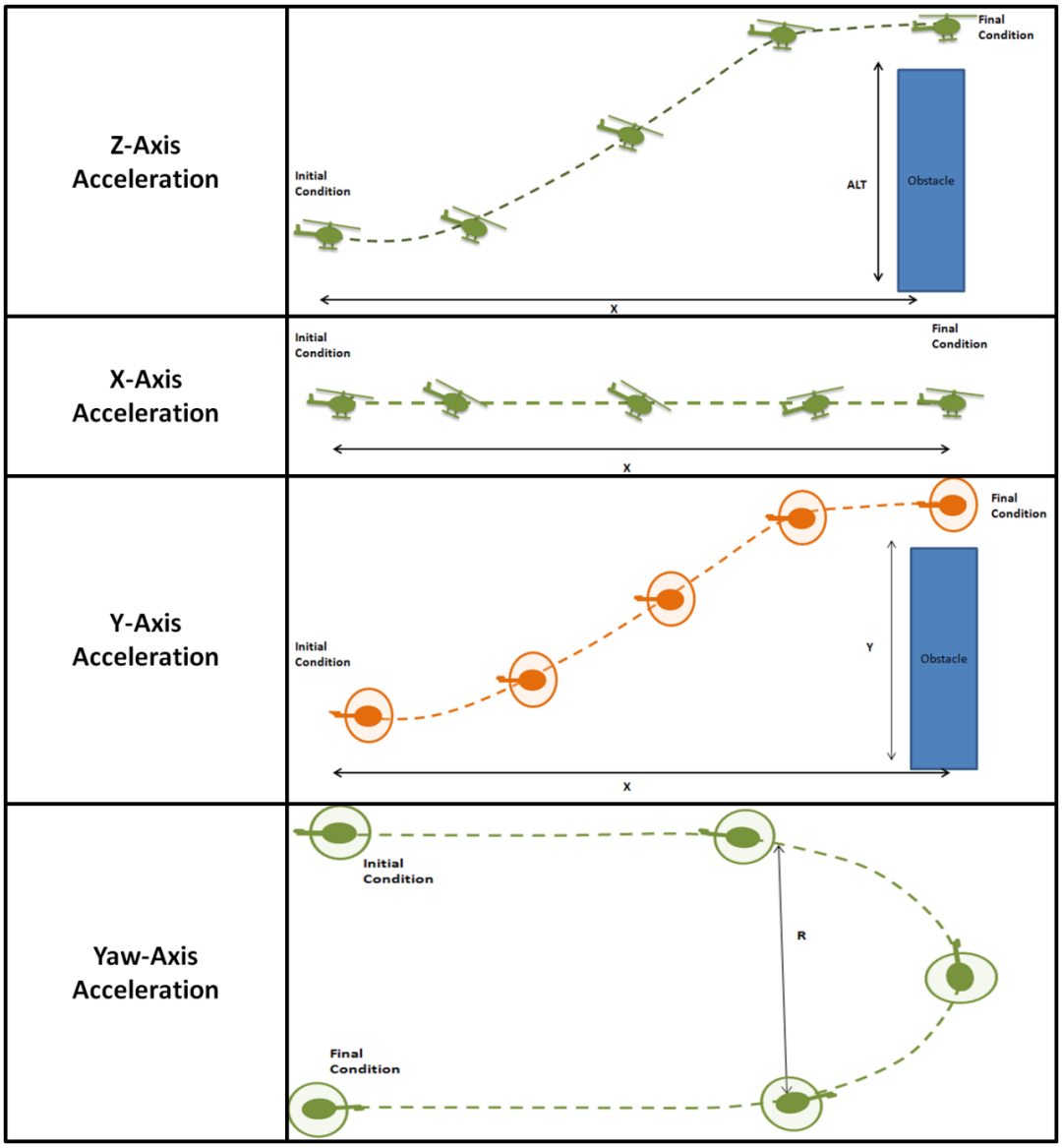

Figure 4.15: Maneuver Taxonomy

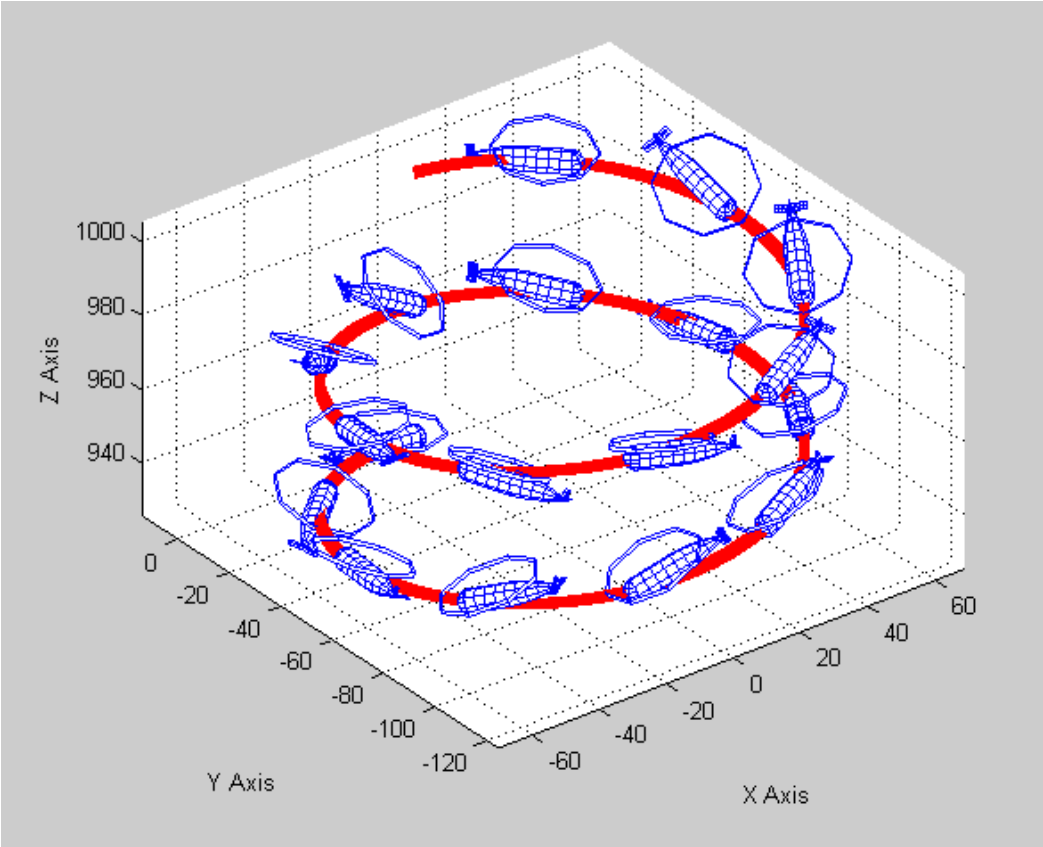

Figure 4.16: Helical Descent

4.5 Experimentation and Results

Finally, the simulations are run and the data is analyzed through application of various constraints on the maneuver inputs, which in effect, provides the ability to quickly analyze any maneuver within the envelope. Furthermore, this mission can be quickly adjusted to perform analysis for multiple missions. Through combining the three major contributions developed in this work, the motivating problem can now be analyzed. The previous chapters only applied analysis to a single pop-up maneuver to show the value in the proposed method over traditional approaches for maneuverability assessment during design. The development of the third contribution now allows for the analysis to

be completed for the entire range of mission maneuvers within NOE flight operations. The benefits are twofold: first, as the maneuver definition is changed during the design process, the data filtering method allows the mission to be adjusted and a new solution is determined real-time. Secondly, the various categories of helicopter maneuvers can now be simulated.

The series of experiments presented in this chapter demonstrate the taxonomy's capabilities for systematically analyzing the entire mission through investigation of the individual maneuvers. Three sections are required to fully present the benefits of the final process through application to the AHS design problem. The first section discusses the necessary decomposition of the overall mission into a series of maneuvers that can be assessed using the developed taxonomy. Second, the maneuverability analysis is shown for a single horizontal acceleration maneuver and the various constraints developed through Contributions 1 and 2 of this dissertation are applied. Third, the interdependencies of the maneuvers along with the most important and constraining maneuvers within the mission are discussed. Finally, the feasible design and maneuver space is summarized for the first four maneuvers of the mission and two different optimization schemes are displayed.

4.5.1 Mission Decomposition

A taxonomy of fundamental maneuvers is established in the previous section through a systematic and traceable process that is derived in this work from strategies employed in discrete path planning and space vehicle design literature. The maneuvers

can be combined to form any motion within the helicopter flight envelope. To show application of this strategy, the 2012 AHS design competition is addressed. In order to address the entire mission, it is necessary to decompose the mission into a series of fundamental maneuvers. This breakdown can be accomplished in as much detail as desired; however, for example purposes some simplifying assumptions are used.

First, although not required due to the formulation of the taxonomy, it is assumed that each decomposed maneuver within the AHS mission is only composed of one fundamental maneuver. For example, for a straight section of the path in which forward acceleration is required, it is assumed that x-axis acceleration is the only acceleration of the system, hence, altitude is maintained. The only exception being the pirouette, which requires accelerations in X, Y, and Psi simultaneously in order to form this complicated motion. An additional assumption that is applied is that the halfway time of the forward acceleration maneuver can be analyzed separately from the deceleration half of the maneuver. By separating this information in this manner, the maneuver can start at a 170 ft/s velocity and end at 100 ft/s velocity if desired.

Using these assumptions and constraints, the AHS design competition is decomposed into 31 maneuvers that when combined in series result in the complete mission definition. These 31 maneuvers are displayed in Figure 4.17 by marking the beginning and end of each maneuver with a pink point. Although, this is the easiest method for breaking down the maneuver, it is not the best for keeping track of the maneuver constraints for conducting the analysis. Hence, in combination to Figure 4.17, the corresponding maneuver breakdown is also presented in Table 4.2.

Figure 4.17: Mission Definition Decomposition

The first column of the table is a maneuver indicator, which corresponds to the pink points in the corresponding figure. The next five columns of the table display the position and heading of the vehicle at the end of each of the 31 maneuvers along with the acceleration that is required. As more information about the individual maneuvers is determined through analysis, further decomposition may be required. For example, maneuver 12 involves a 270 degree turn, which may need to be decomposed into a series of smaller turn maneuvers when analyzed. Another example of this further decomposition is demonstrated by the first two maneuvers of the mission. Originally, it is thought that the mission path prior to the first slalom maneuver only consists of an acceleration maneuver; however, once the slalom maneuver is investigated, it is determined that an acceleration followed by a deceleration is required in order to obtain the minimum time. This results because the slalom maneuver must be completed at a slower velocity than

that achieved by the end of the first acceleration portion. Each subsequent maneuver is dependent upon the maneuver that is performed prior; hence, each maneuver can be analyzed individually but the constraints must reflect the overall mission.

Table 4.2: AHS Design Competition Maneuver Breakdown

Maneuver	Xf	Yf	Zf	Psi	Acceleration
1	500 ft	-	-	-	X
2	500 ft	-	-	-	X
3	1000 ft	300ft	-	-	Y
4	1000 ft	-300 ft	-	-	Y
5	800 ft	-	-	-	X
6	800 ft	-	-	-	X
7	250 ft	250 ft	-	90 deg	Psi
8	250 ft	250 ft		90 deg	Psi
9	1650 ft	-	-	-	X
10	1650 ft	-	-	-	X
11	1650 ft	-	-	-	X
12	-	-	-	270 deg	X,Psi
13	900 ft	900 ft	-	90 deg	Psi
14	500 ft	-	-	-	X
15	500 ft	-	-	-	X
16	800 ft	200 ft	-	-	Y
17	800 ft	-200 ft	-	-	Y
18	625 ft	-	-	-	X
19	625 ft	-	-	-	X
20	400 ft	550 ft		90 deg	Psi
21	400 ft	550 ft	-	90 deg	Psi
22	625 ft	-	-	-	X
23	625 ft	-	-	-	X
24	-	-	-	-	Z
25	-	-	-	360 deg	X, Y, Psi
26	-	-	200 ft	-	Z
27	-	-	200 ft	-	Z
28	625 ft	-	-	-	X
29	625 ft	-	-	-	X
30	1500 ft	-	-	-	X
31	1000 ft	-	-	-	X

In order to show application of the process to the AHS design competition, it is decided to only show the analysis involved of the first four maneuvers. The reasoning is that if all 31 maneuvers are included in the analysis, the problem would become overwhelming as an example for application and understanding to the reader. Additionally, documenting the entire process would become immense, without providing further understanding of the process or the problem. The first four maneuvers consist of an acceleration phase, a deceleration phase, a left sidestep, and a right sidestep maneuver. The desired end states for each of the maneuvers is displayed in Table 4.3, while a graphical depiction of the first four maneuvers is shown in Figure 4.18.

Table 4.3: First Four Mission Maneuvers

Maneuver	Xf	Yf	Acceleration
1	500 ft	-	X
2	500 ft	-	X
3	1000 ft	300ft	Y
4	1000 ft	-300 ft	Y

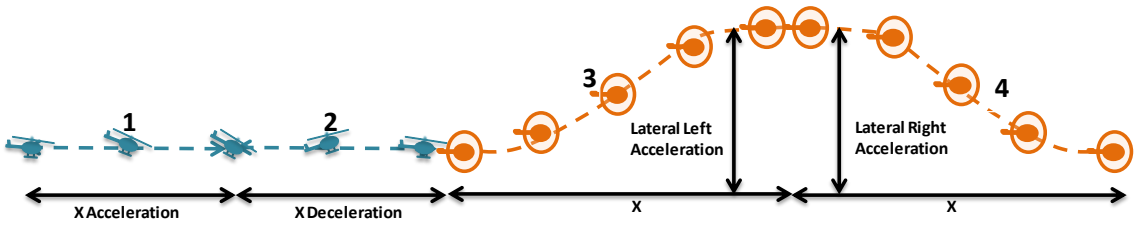

Figure 4.18: First Four Mission Maneuvers

4.5.2 Individual Maneuver Filtering

The data analysis starts with the 9000 runs conducted for each of the four fundamental maneuvers. The base set of data is exactly the same for both x-axis

maneuvers, while the similarly the y-axis maneuver data sets are identical. This is because only four maneuvers are in the taxonomy. The first maneuver of the mission consists of a horizontal acceleration, which is notionally represented in Figure 4.18.

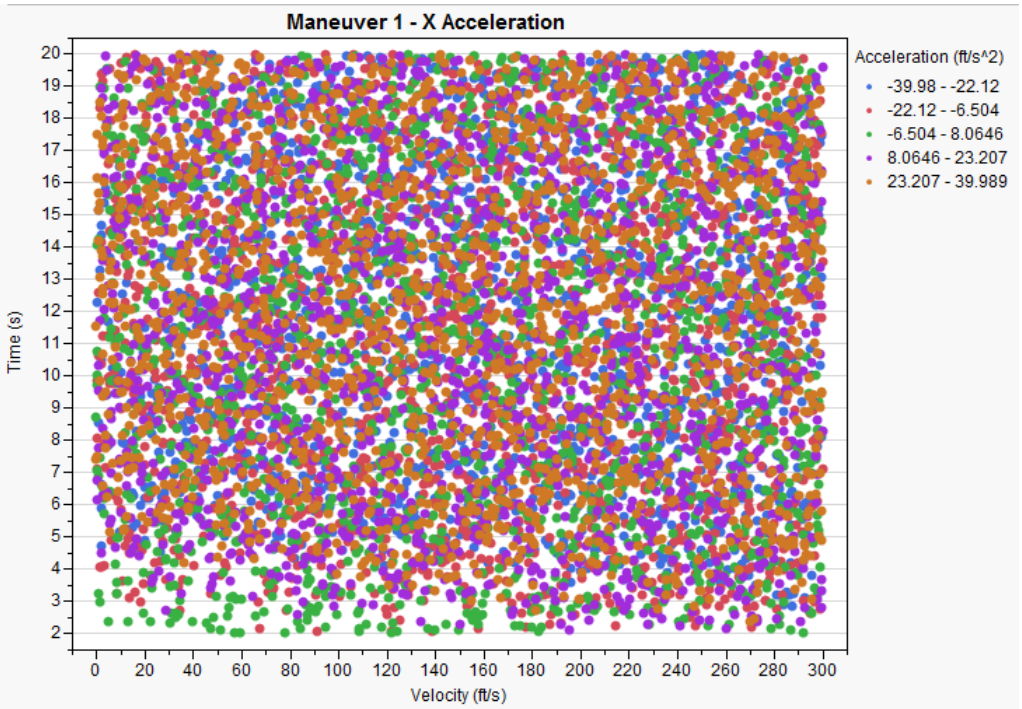

Figure 4.19: Horizontal Acceleration Maneuver Space

The entire horizontal acceleration and deceleration maneuver space is shown in Figure 4.19. Similar to previous maneuver analyses, the y-axis of the figure represents the time required to perform the maneuver. The horizontal axis now depicts horizontal velocity rather than acceleration, which was shown in previous filtering exercises. The reason for this change is that the forward velocity has a larger influence on the maneuver final distance than the acceleration variable. However, acceleration still has an influence; thus, the points are color coded according to horizontal acceleration. The color coding

legend may be observed to the right of the figure, where the horizontal acceleration ranges from -40 to 40 ft/s^2.

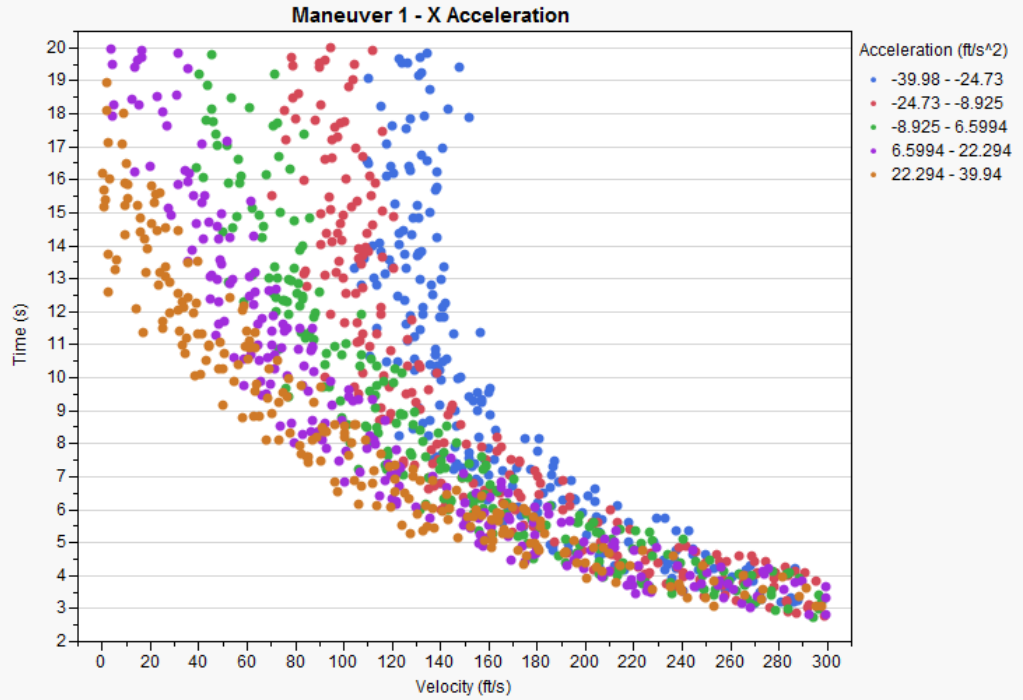

Figure 4.20: Feasible X-Acceleration Maneuver

All 9000 design and maneuver combinations are shown in Figure 4.19 and the next series of filters gradually prune the space to only successful maneuvers of interest. The filtering process starts with the addition of the maneuver success constraint, which is an indicator of maneuver feasibility. The value of 1e-08 was chosen as the function error cut-off, although, this number can be adjusted real-time. The second step of the filtering process involves applying the mission maneuver constraints as specified in the AHS design competition. The mission dictates a horizontal acceleration maneuver of between 400 and 600 ft. The resulting feasible design and maneuver combinations are shown in

Figure 4.20. With some of the points removed from the space, the trends with acceleration are now observed.

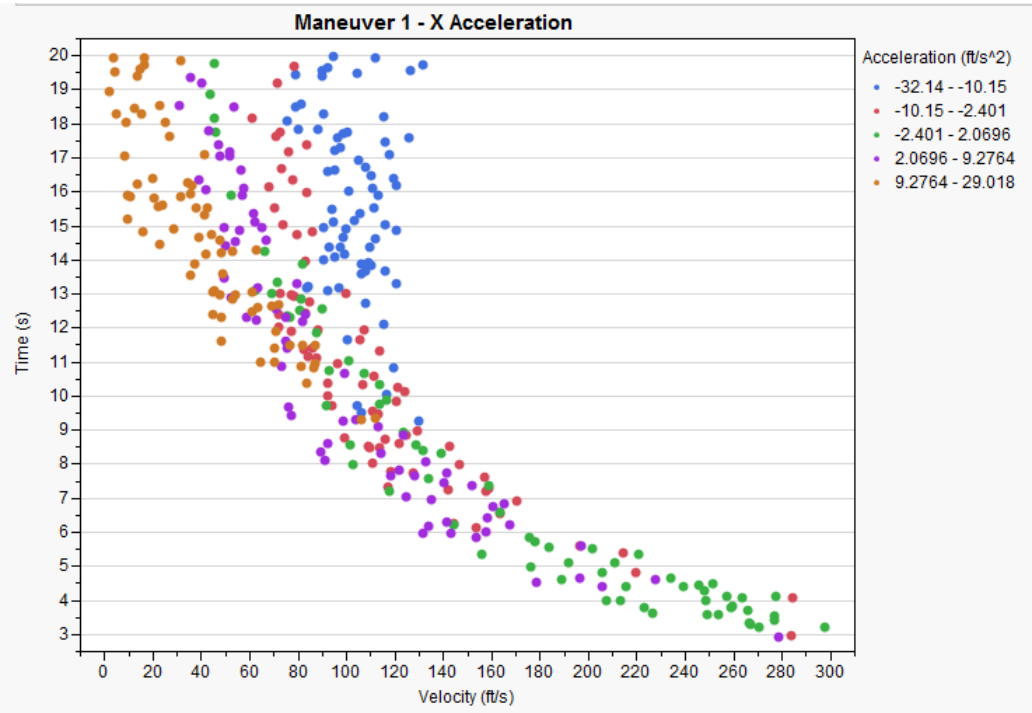

Figure 4.21: Feasible X-Acceleration Maneuver – Constraints Applied

Next, the maximum maneuver power, control deflection angle, and control deflection rate limits are applied. These steps remove any infeasible designs from the design space of alternatives. The constraints can be adjusted real-time; however, these capabilities were presented in previous experiments so only fixed constraint values are applied in this example. All of the constraint values used in Chapters 2 and 3 are reapplied, which correspond to a maximum power of 2500 hp, a maximum deflection angle of 13.5 deg, and a maximum deflection rate of 12 deg/s. The resulting feasible design and maneuver combinations are shown in Figure 4.21. The first maneuver within the mission involves a horizontal acceleration; however, it is observed that the feasible

space still contains deceleration maneuvers when viewing the legend to the right of the figure.

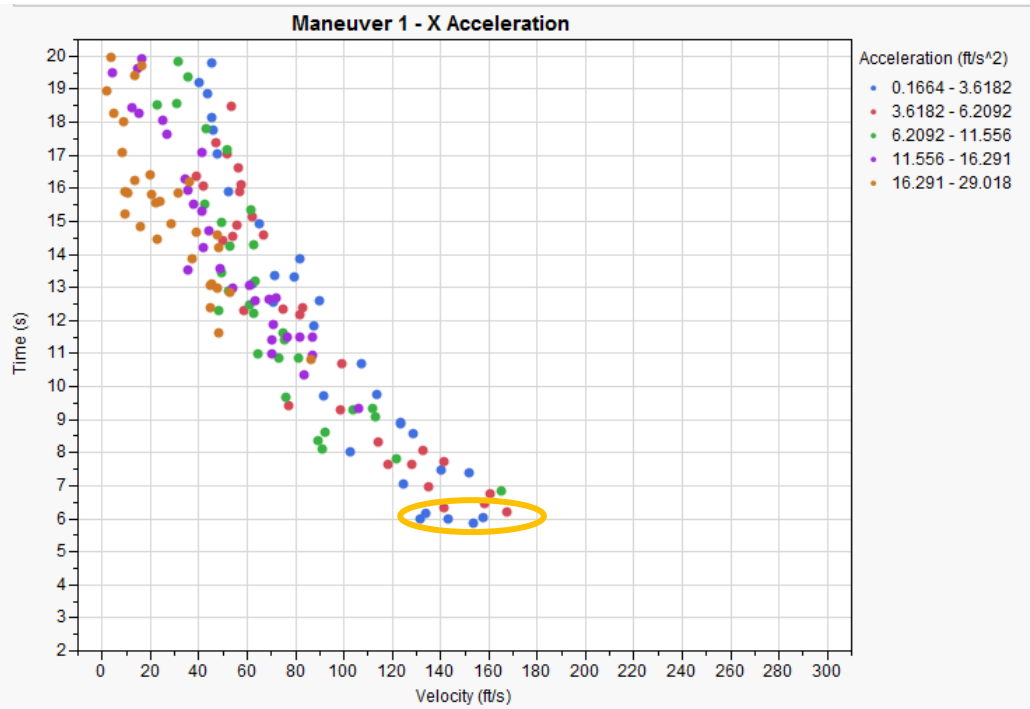

Figure 4.22: Acceleration and Initial Velocity Constraints Applied

Hence, another filter is applied that removes any maneuvers that involve a deceleration. Finally, the helicopter must enter the course no faster than 170 ft/s as stated in the 2012 AHS design competition requirements. Figure 4.22 displays the resulting implications on the feasible design and maneuver space. Through observing the figure, the acceleration for all of the remaining points is positive and the initial velocities do not exceed the 170 ft/s limit. The objective of the analysis is to determine the minimum time maneuver and design combination. This consists of the circled region in Figure 4.22 around the 6 second time. The solution space consists of approximately eight different design and maneuver combinations that result in the minimum time.

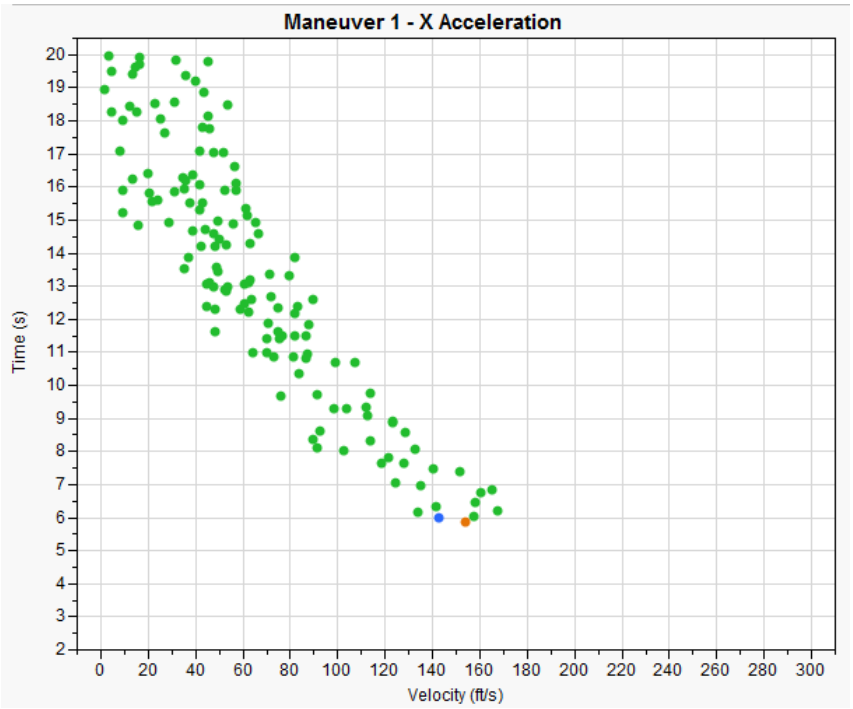

Figure 4.23: Two Optimization Schemes Applied

The top performing design and maneuver combination would be selected if an optimization algorithm was implemented to determine the minimum time design and the designer would not be aware of the other seven feasible solutions that are very similar in maneuverability performance. This example demonstrates the importance of real-time human-driven trades. Since this information is now known, the designer may analyze each of the eight points in detail using the time-series information. Additionally, the constraints and design space can be used to select the most robust solution to the applied constraints. The constraints may be adjusted real-time to view the sensitivities of the solution space to the various constraints.

Figure 4.23 displays the feasible design space for the first maneuver of the mission with the top solutions for two different optimization schemes applied. The

orange point represents the maximum mass design, while the blue point represents the solution for the minimum rotor diameter. The human-driven real-time capabilities enable improved understanding of the solution space and greater traceability in design and maneuver down selection. Numerous optimization schemes may be applied at this stage; however, the two methods discussed earlier are used throughout the remaining example. Figure 4.24 displays the maneuverability comparison for the two different design optimizations for the first maneuver of the mission. The maneuver times are half of the value shown in Figure 4.23 because only the acceleration phase of the fundamental maneuver is used in this portion of the analysis due to assumptions. The same analysis steps must now be conducted for the rest of the maneuvers in order to compare mission maneuver performance, which are discussed in more detail in the next section.

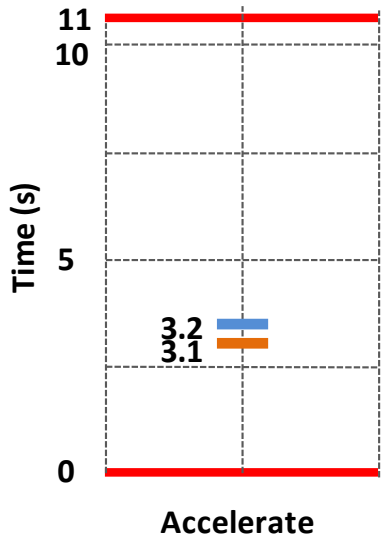

Figure 4.24: Accelerate Maneuver – Maneuverability Comparison

4.5.3 Maneuver Importance and Interdependencies

At this point, the designer is now ready to start taking into consideration the dependency due to the sequential mission definition. The maneuver position change constraints that are listed in Table 4.3 are applied to each of the four maneuvers in Figure 4.18. The maneuvers within the data set are defined as both the acceleration and the deceleration portion for each maneuver; hence, for the first two maneuvers of the AHS mission only the first half of each maneuver is desired. The third and fourth maneuvers are specified by a lateral distance change at constant velocity so the entire maneuver is used in these analyses. Because only half the x-axis maneuver is used in the first two mission segments, the final distance of the maneuvers are set to double of the requirement. Additionally, the filtering process allows for the designer to specify the end point as a range rather than an exact point which accounts for variability in the maneuver definition, thus, providing greater flexibility. Once the maneuver definitions are applied to the filtering process, only a small subset of the original 9000 runs are applicable for each maneuver. Moreover, maneuvers 3 and 4 are more constraining than maneuvers 1 and 2, with only 8 and 10 points remaining out of the 9000, respectively. The remaining feasible design space for maneuvers 3 and 4 is depicted in Figure 4.25.

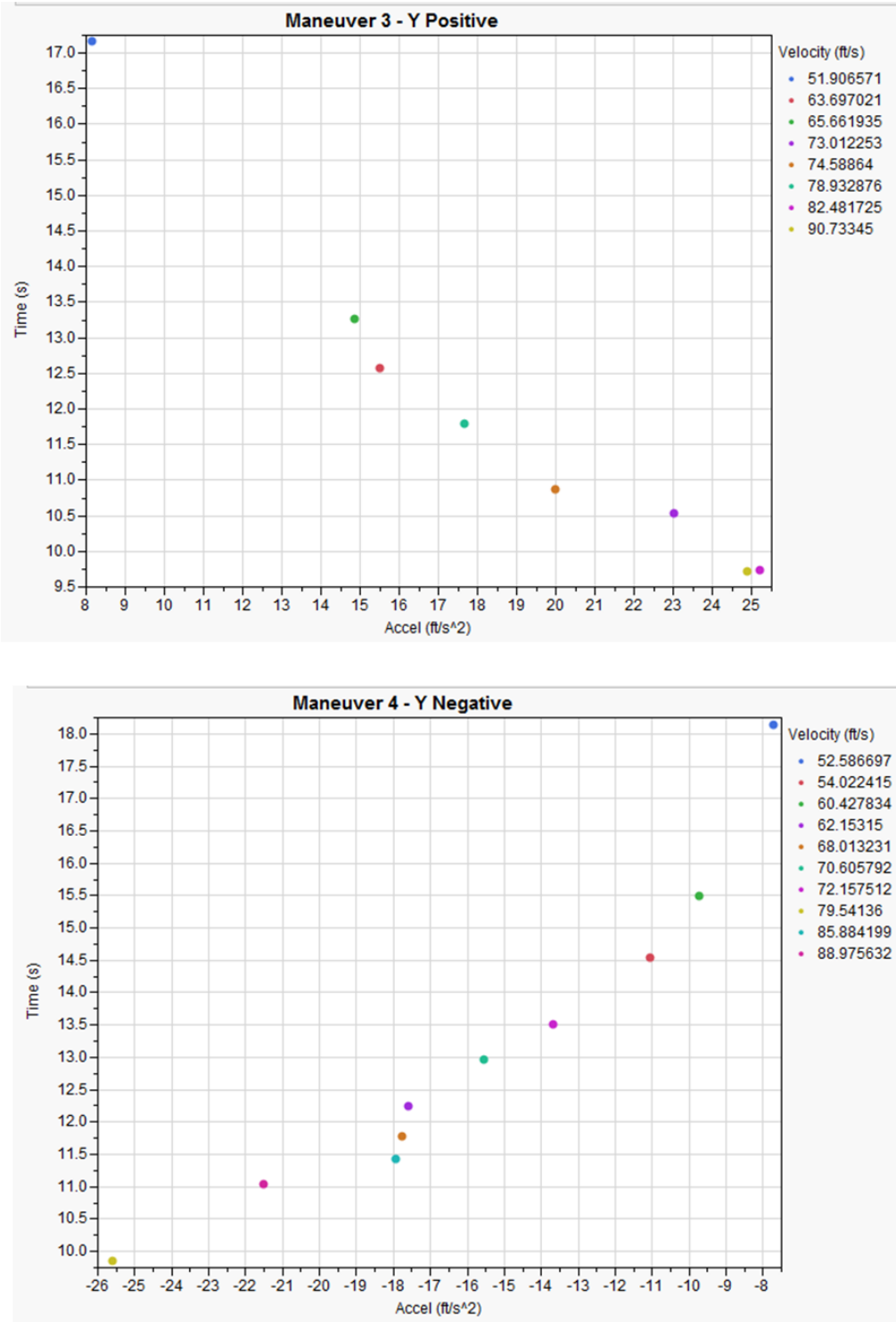

Figure 4.25: Maneuver 3 and 4 Feasible Design Space

The information within these small number of feasible points may aid in further filtering of maneuvers 1 and 2 because of dependencies. For, example, if the maximum velocity of maneuver 3 is around 100 ft/s then designs exceeding this velocity from maneuver 2 can be removed. As a result, some designs in maneuver 1 may no longer be compatible with maneuver 2. This demonstration of how small constraints propagate throughout the entire mission shows the difficult nature of applying an optimizer to this information. With an optimizer, the source of removal of solutions is not understood. In addition to providing more information about the process, the method also allows for these trades to be conducted real-time, which permits rationale for changing system constraints.

The data filter also keeps track of the remaining points in the feasible design space through each constraint that is applied. One final constraint is applied before analyzing the design parameters of the feasible solution set. The performance measure in this analysis is time to complete maneuver; hence, some upper limit can be placed on the time for each maneuver. Using knowledge of the design space and the mission, the designer can constrain the feasible set according to maneuver execution time. For this example, the constraint of 12 seconds is placed as an upper limit of execution time. Additionally, if more than 10 feasible points remain in the feasible space, this time is reduced until only 10 feasible points remain. It turns out that the 12 second limit is constraining enough to eliminate maneuvers 2, 3, and 4 down to 10, 5, and 4, feasible design points, respectively. Maneuver 1 design space still contains 30 feasible points after

the 12 second limit is applied so this limit is reduced to 7 seconds until only 11 designs remain.

The resulting feasible maneuver space for inclusion of mission dependencies is shown in Figure 4.26 and Figure 4.27 with each maneuver displayed as a separate subplot. The top portion of the Figure 4.26 displays the feasible maneuver space for the first maneuver in the mission with the top performing time around 5.85 seconds, while the second maneuver has a minimum maneuver time of 8.4 seconds. Recall that for both of the first 2 maneuvers, only the first half of the simulation is used; therefore, the times are actually around 3 and 4.2 seconds, respectively. Maneuvers 3 and 4 share similar performance limits around 9.75 seconds, which is viewed in Figure 4.27. The top portion of the figure displays the five remaining feasible points for the third maneuver within the mission, while the bottom portion of the figure shows the four remaining design combinations for the fourth maneuver. The points are colored according to velocity over the maneuver. The range of velocities are displayed to the right of each subplot. The velocities vary between 70 ft/s and 90 ft/s for each maneuver; hence, providing an additional constraint for maneuver 2 since the vehicle cannot enter maneuver 3 above the limit.

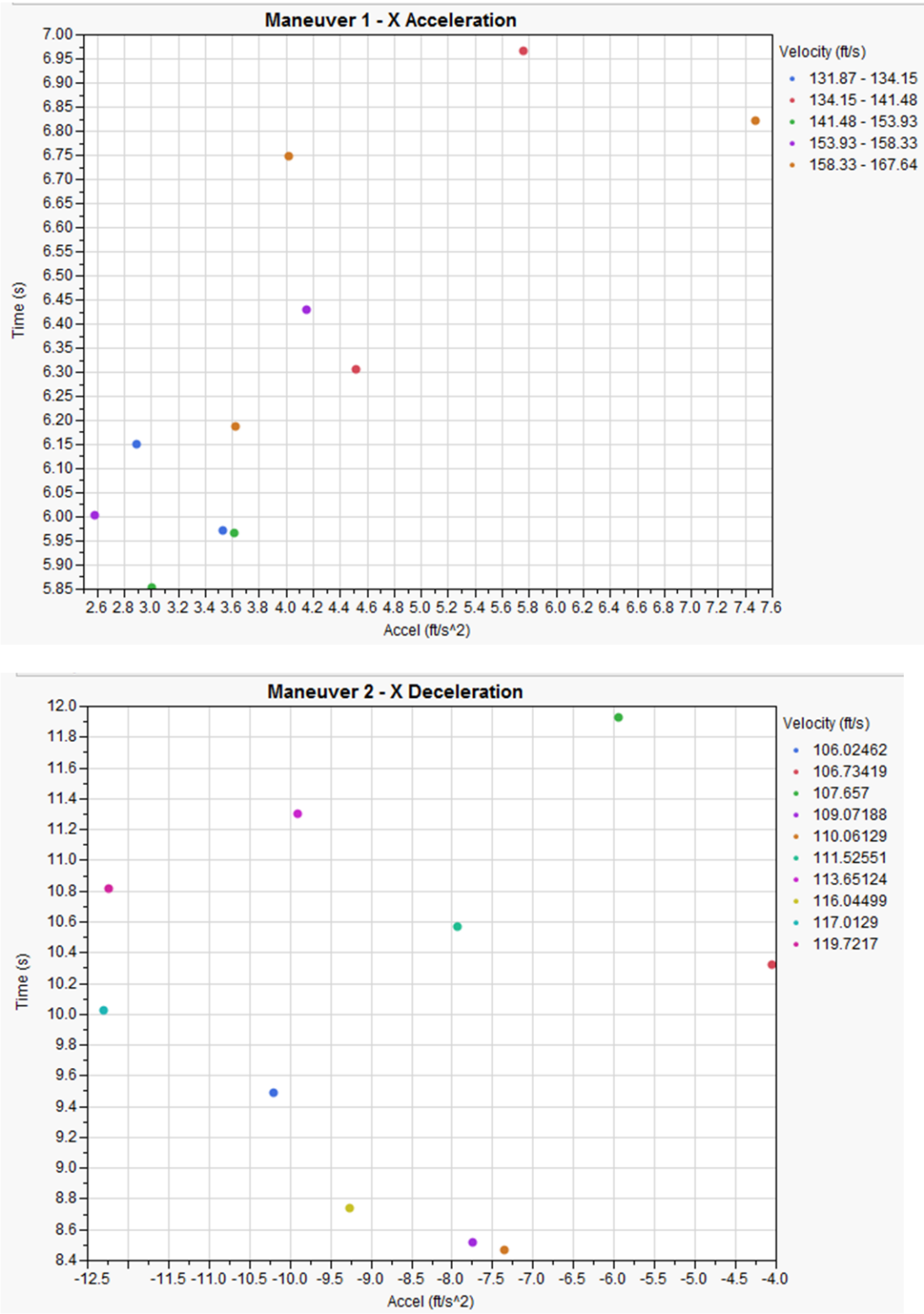

Figure 4.26: Feasible Design Space Maneuvers 1 and 2

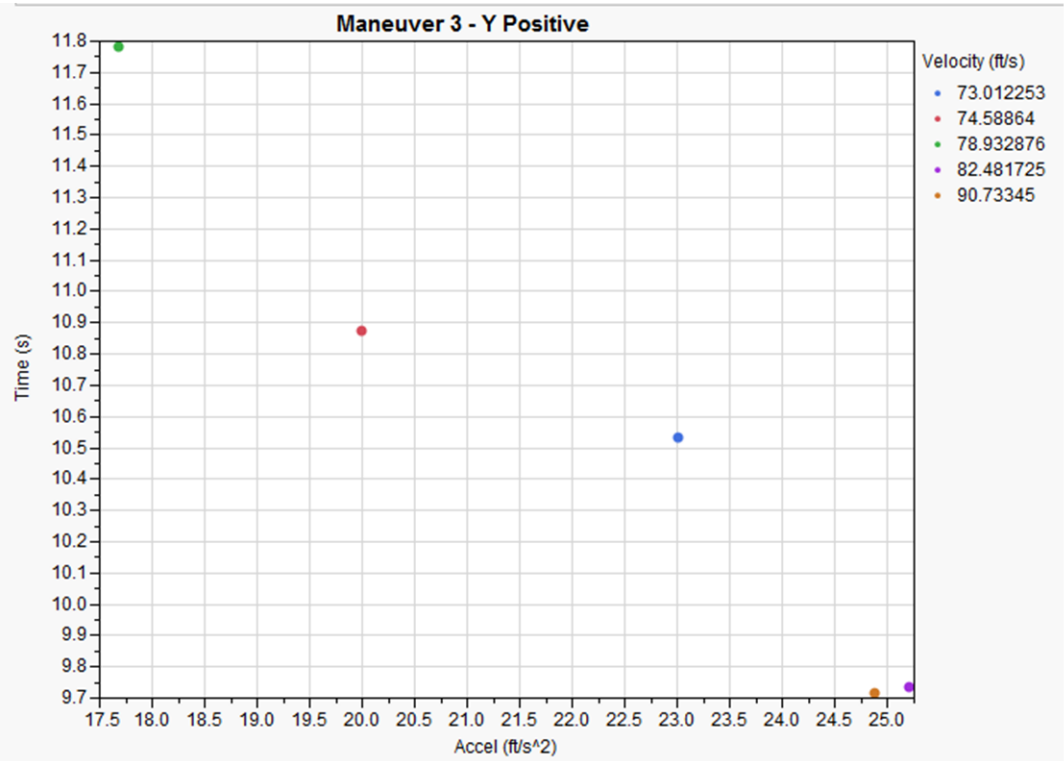

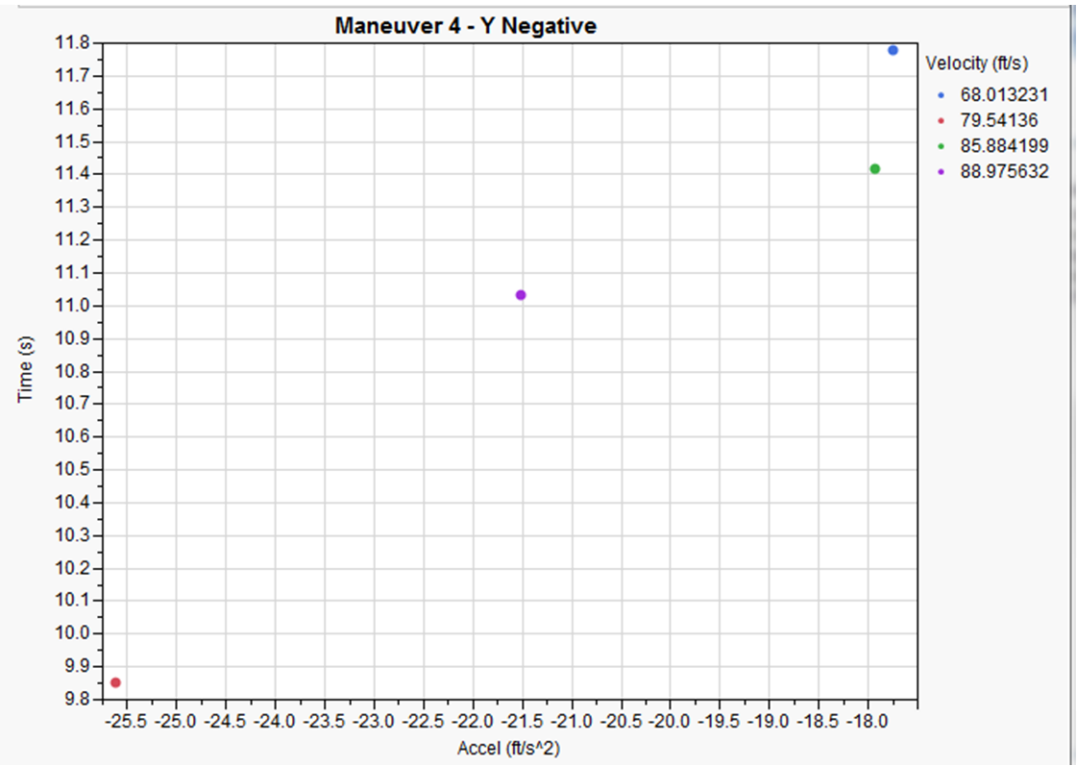

Figure 4.27: Feasible Design Space Maneuvers 3 and 4

The limit of 100 ft/s maximum velocity in the exit of maneuver 2 is applied. The propagation of this constraint also impacts the first maneuver within the envelope because maneuver 2 must decelerate to 100 ft/s from whatever velocity is provided by the end time of maneuver 1. The capability to decelerate limits the maximum velocity that is reached in maneuver 1. Additionally, the competition states that the mission may not be started at a velocity above 170 ft/s. Hence, the objective of the first maneuver is to accelerate above this velocity in order to provide a faster time over the first straight segment of the course, while at the same time not exceeding the maximum deceleration velocity needed by maneuver 2.

Viewing the data in this manner is great for filtering the feasible design space and viewing the corresponding effect on maneuverability limits; however, it does not provide any knowledge of the design parameter combinations that are required to obtain this performance. Similar to early analyses, the parallel plots are used in addition to the feasible design space plots to provide a greater amount of knowledge about the individual design combinations that result in the maximum performance. Prior chapters only viewed the mission and design parameters for a single type of maneuver. In order to account for multiple maneuvers, an additional maneuver number variable is added to the x-axis of the figure, which is shown in Figure 4.28.

Each of the four different maneuvers corresponds to a different color. The blue curves represent the mission and design parameters of the first maneuver. Orange lines show the mission and design parameters for the horizontal deceleration maneuver and purple and green demonstrate the inputs for the left and right sidestep maneuvers,

respectively. Observation of the figure shows that the CG location must fall towards the aft of the vehicle for all four of the maneuvers. Additionally, different design parameters and constraints impact different maneuvers by various magnitudes. For example, the left sidestep maneuver (purple) requires the highest settings for tail rotor moment arm and tail area, while right sidestep (green) requires smaller values for the ranges provided. This relationship deals with the direction of rotation of the main rotor and how the tail rotor must supply counter-torque.

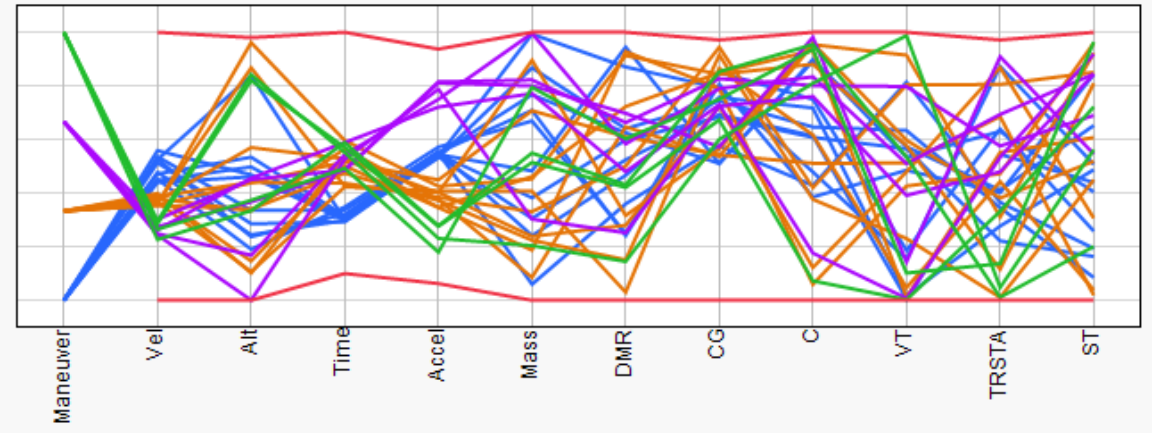

Figure 4.28: Design Parameter Space of Top Designs

The end goal of the analysis is to determine the total mission maneuverability. Similar to previous steps, two different optimization schemes are selected from all four maneuvers. The minimum time maneuver for the two different optimization schemes is summarized in Figure 4.29. The blue design corresponds to minimum rotor diameter optimization strategy, while the orange point represents the maximum mass design. Both designs complete the first four maneuvers in similar time, with the maximum mass design slightly outperforming the minimum rotor diameter design. The systematic and

traceability of the process provides further benefit in this situation because in addition to mission analysis, the taxonomy decomposition enables analysis of the individual maneuver contributions.

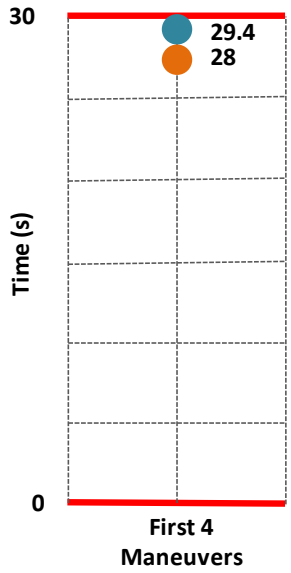

Figure 4.29: Mission Maneuver Time

This capability enables the designer to view the most constraining maneuvers within the mission, which provides the designer with traceability in selecting the appropriate design. This information allows for the designer to focus on designing for maximum maneuverability of the most important or constraining maneuvers, while at the same time viewing the impact on the other maneuvers within the mission. The mission maneuver breakdown is shown in Figure 4.30 for the two different optimization schemes.

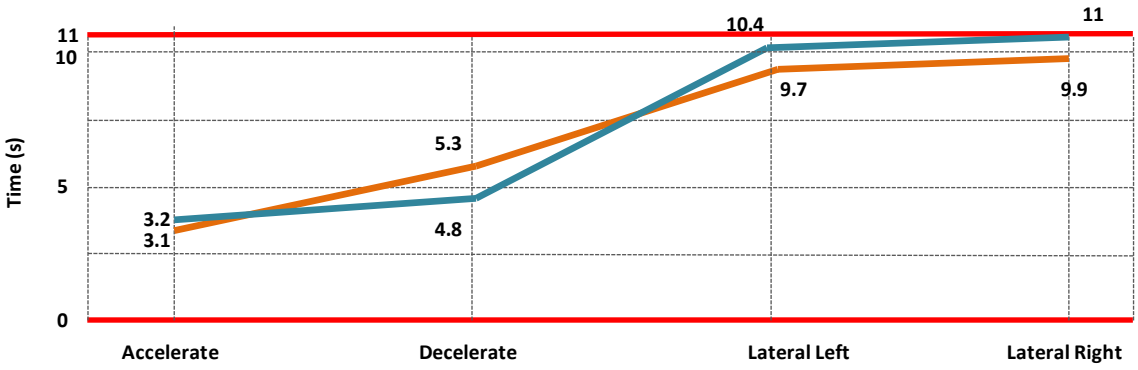

Figure 4.30: Mission Maneuver Decomposition

4.6 Summary of Contribution

The key components of the hypothesized method are discussed here briefly to show that the need is addressed. The first characteristic is fulfilled by the development of a taxonomy approach to analyzing the helicopter maneuvers, which allows the designer to capture the performance measures for the individual maneuvers. These individual quantitative performance measures can then be looked at together to form the performance for an entire mission. Additionally, the maneuvers can be analyzed independent of other maneuvers, if desired. The maneuver performance is obtained through a combination of a mathematical rotorcraft model, a maneuver model, and inverse simulation techniques. Additionally, by using parametric models, the input variables can be easily adjusted such that the impact on dynamic performance due to variability in maneuver definition can be captured. As stated previously, inverse simulation allows the maneuverability to be quantitatively calculated independent of control design. Finally, the impact of changing mission definitions can be assessed real-time using a filtered data approach over the operational space for the range of inputs

selected. The final contribution of this thesis work is established through solving this need in rotorcraft literature and addressing the motivating problem.

Contribution 3: Technique for developing the fundamental parametric maneuvers for quantitative assessment of maneuverability characteristics over the entire operational envelope.

CHAPTER 5

CONCLUSION AND FUTURE WORK

Expansion of design analysis capabilities is essential in meeting the requirements for successful design of complex systems such as helicopters. Furthermore, conceptual design is perhaps the most crucial task in engineering product design and development; hence, the focus of this dissertation is in the early stages of design. Traditionally, the early stages of design have not included analyses related to smooth dynamic maneuvers corresponding to Nap-of-the-Earth (NOE) flight. Military helicopter operations require precise maneuverability characteristics for successful NOE flight. NOE flight consists of precise maneuvering in and around obstacles, which make helicopter missions unique from other air vehicles. Many military helicopter NOE flight scenarios and problems are classified; therefore, literature was examined to find an unclassified canonical example that could be used as a surrogate for formulating the problem. The military helicopter problems are indirectly assessed through solving the 2012 AHS design competition, which is summarized in Figure 5.1. The AHS design problem is an unclassified example of NOE flight operations that must be addressed by the helicopter design community. Several contributions to literature are presented in this work as a result of addressing the needs of the motivating problem, which is followed by a discussion of potential areas for future work.

5.1 Conclusion

This dissertation addresses specific issues associated with integrating maneuverability assessment into the early stages of design. Although, the focus is in the early stages, much of this work can be utilized in the later stages of design with the inclusion of higher fidelity models. In order to provide the most traceability and understanding, the problem is decomposed into three major areas: designing for maximum maneuverability, capturing controllability concerns, and defining the mission maneuvers. This decomposition is represented in Figure 5.2.

Figure 5.1: 2012 AHS Design Competition

These three research areas relate directly to NOE flight requirements. The first area, which is designing for maximum maneuverability, is important for both military NOE operations and the AHS design competition because the design that can outperform the other helicopter designs will win in NOE combat scenarios. The ‘maximum

maneuverability' is defined by the minimum mission time although other measures, such as blade loading, could be considered simultaneously. The second research area specifies the need to capture the controllability concerns. This requirement is stated because during NOE flight operations a precise maneuver path must be followed. Any divergence from the path can be catastrophic because the helicopter is flying in and around obstacles. Similarly, the AHS design competition requires the helicopter to follow a specific mission path, while considering the implications of traveling into a pylon or the spectators. The third research area deals with the mission maneuver specifications since there are an immense number of NOE flight operations that must be analyzed. Additionally, the maneuver specifications are dynamic in nature and cannot be analyzed with only steady-state analysis techniques. These problem areas require a shift in design and maneuver analysis capabilities [13-15] to enable successful design for helicopter NOE flight.

Overall Research Objective: Develop a methodology that enables real-time and traceable assessment of:

- **Design parameter impacts on maneuverability characteristics**
- **Maneuverability degradations due to control system characteristics**
- **Entire helicopter operational envelope maneuverability**

Through addressing the three major areas, a methodology is developed that enables the impact of design choices on maneuverability to be assessed for the entire helicopter flight envelope, while enabling constraints from control system design to be assessed real-time. Each of the three areas was addressed separately in this work.

However, careful consideration was made during development of each contribution such that when integrated to form the final process, the overall method addresses all of the issues simultaneously. The validity of each of the components was addressed through quantitative rotorcraft examples related to subsets of the needs posed in the 2012 AHS design competition. These examples showed numerous benefits over the traditional approaches presented in literature and possessed all of the necessary attributes uncovered during literature review. The final methodology that is presented in Figure 5.3 is discussed, which is followed by a summary of the contributions of this work.

5.1.1 The Final Process

The combination of these techniques offers unique attributes and capabilities not possible using previously developed approaches. Five major elements are integrated in order to fulfill the needs when provided with the initial design information from the problem description. The first element is the parametric rigid body rotorcraft model along with a novel parametric maneuver model that enable design integrated maneuver analysis. Secondly, inverse simulation techniques are included in the process to enable trajectory analysis for NOE flight maneuvers independent of control design. Third, control integration considerations are integrated through a modified control characteristic tradeoff and evaluation framework. Fourth, a novel maneuver mathematical model and a parametric taxonomy combination allow for simulation of any maneuver within the helicopter NOE flight envelope. Finally, a filtered data technique is included in the post processing to provide systematic, traceable, and real-time design trade analysis capabilities. These elements are combined to form a four step process which consists of

the problem formulation, mathematical model development, simulation, and post processing/data filtering.

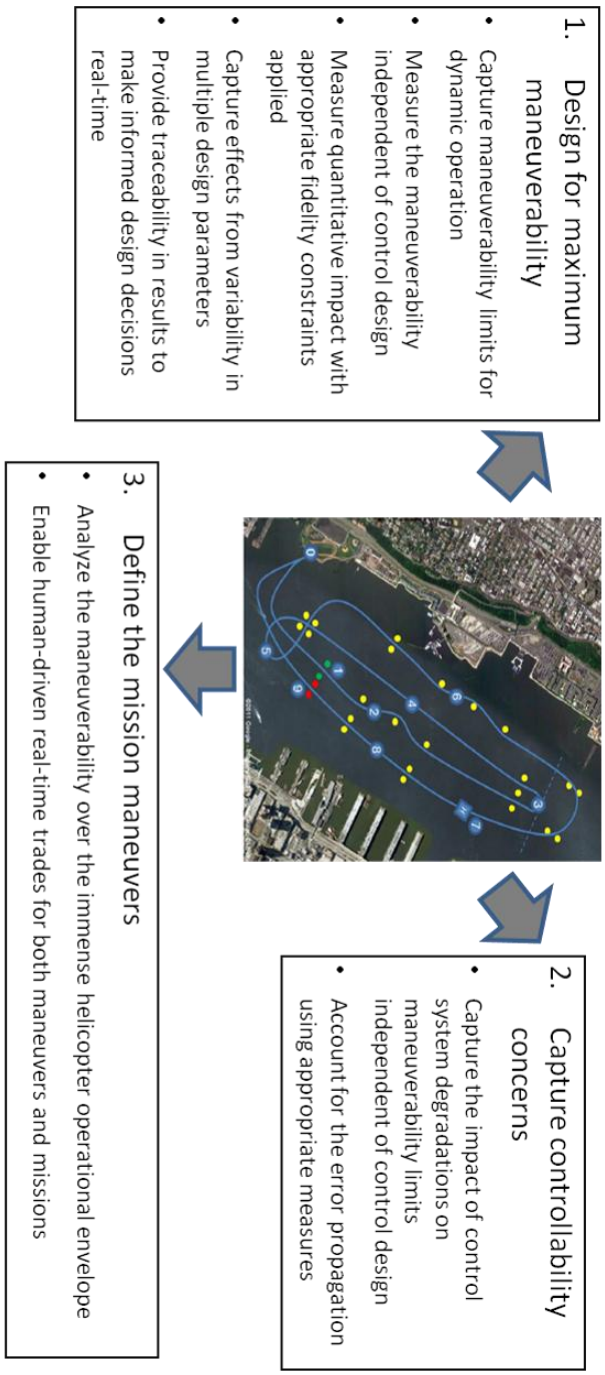

Figure 5.2: Research Contribution Decomposition

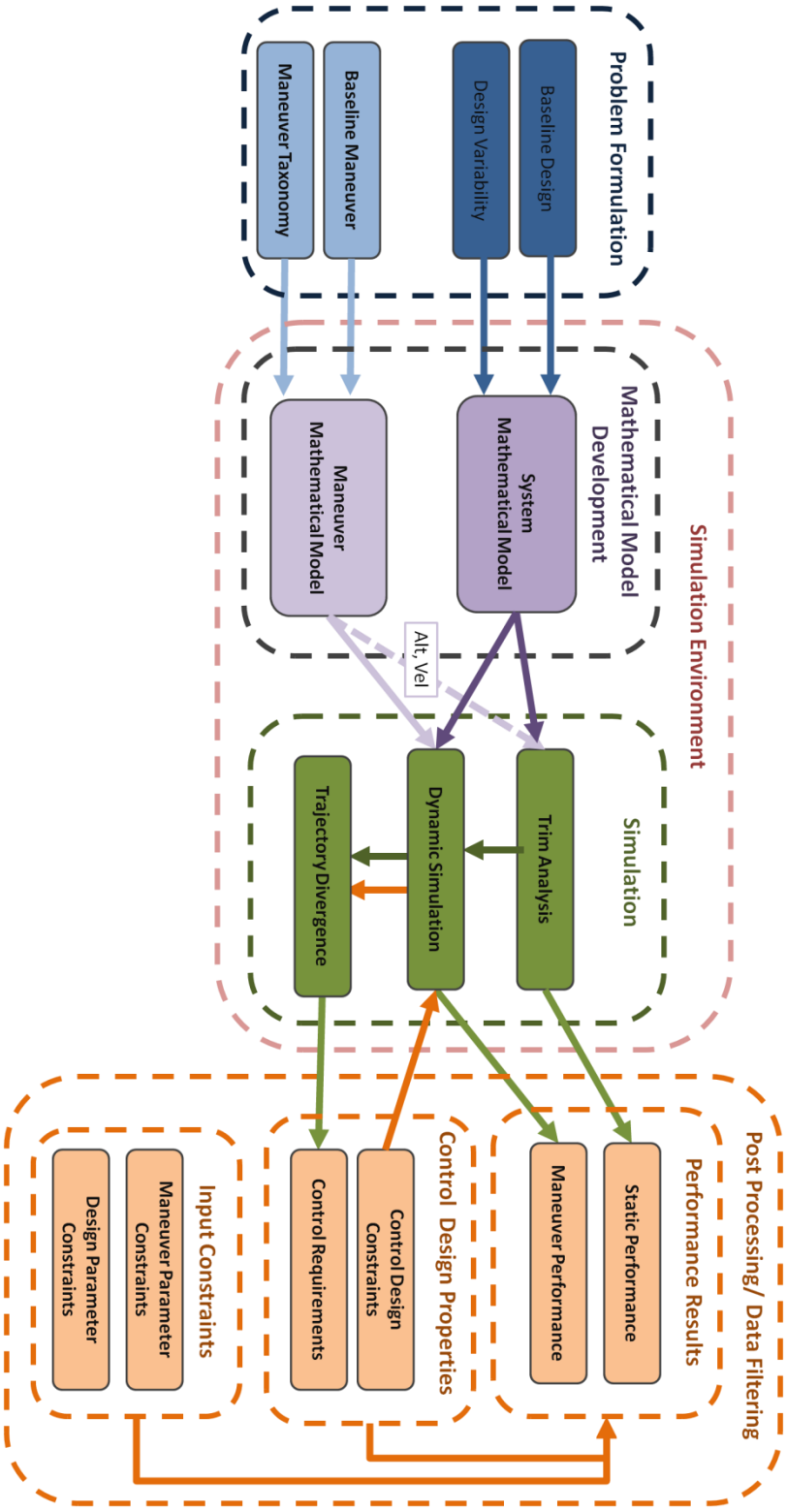

Figure 5.3: Final Methodology

The design information consists of the baseline design specification, upper and lower bounds on the variability of the design definition, and a baseline maneuver. All of which are assumed to be provided in order to begin the process. The mission definition is usually provided in the initial problem definition, while the baseline design may consist of a set of various designs that are being considered as potential solutions to the problem. Each design and maneuver combination needs to be executed through the process separately.

The second step of the process is to take the information provided and develop mathematical models of the system and the maneuver to be performed. The mathematical model of the system must be parametric such that design variations can be analyzed. Additionally, the system parameters must be maintained to a reasonable number to mitigate combinatorial issues, while at the same time offering the appropriate fidelity to include necessary constraints. The mathematical models must be structured for inclusion into the simulation environment, which requires careful selection of states and controls for the system definition. The system model development requires the second order ordinary differential equations of the system, which are the EoM of a helicopter in this analysis, to be described in a manner in which integration provides the next state when given the current state and control settings. The maneuver must also be modeled mathematically. Multiple maneuvers must be simulated in order to assess the maneuverability characteristics over the entire helicopter operational envelope, which is accomplished by the addition of the maneuver taxonomy technique.

Once the models are generated and the inputs defined, the simulation environment is used to determine the trim solution. This portion of the analysis does not require the entire maneuver definition, only the initial steady-state conditions. The second step of the simulation environment performs dynamic analysis of the system attempting to perform the defined maneuver. The important technique enabling NOE maneuver analysis independent of control design is inverse simulation. The simulation captures the change in maneuverability characteristics resulting from the variation in design parameters. Inverse simulation requires constraints for satisfactory optimization of the solution. Depending on the application, the designer may wish to constrain any combination of position, velocity, acceleration, or orientation. These constraints can be placed on any state or control variables.

The measures on control design and integration requirements leading to cost and risk decisions are not captured when using inverse simulation because the technique assumes perfect control and control knowledge. For this reason, the maneuverability degradations due to non-perfect control characteristics must be assessed. This is accomplished through developing and analyzing control system characteristics impact on maneuver performance. These characteristics are a function of the control system design and are based on the design stage and detailed level of the model. These improvements are essential in capturing the relationship of control integration degradations on maneuverability in a quantitative manner in the early stages of design. As the design progresses into the later design stages, these measures can be adjusted to include more

detail. These requirements provide the control designer with a set of characteristics that the control design must achieve in order to achieve the desired maneuverability.

The final element of the process is based on a Monte Carlo data filtering technique that permits real-time and traceable design space exploration with changing constraints and requirements. The Filtered Monte Carlo (FMC) method uses a database of previously computed maneuverability information. All prior rotorcraft dynamic analysis techniques applied constraints into the mathematical definition of the vehicle; however, this formulation allows constraints to be dynamically placed on design variables and performance measures. As a result, the designer can view the impact of these constraints real-time rather than being required to run an entirely new set of optimizations. Filtered data techniques allow for visual verification of trends in the data that can be helpful with validation purposes and provides traceability for developing understanding of the problem. Furthermore, FMC is robust and enables integration of the complex helicopter EoMs. The final process that corresponds to the integration of the necessary elements for NOE design and analysis is coined GT-RISE, which stands for Georgia Tech Rotorcraft Inverse Simulation Environment.

5.1.2 Summary of Contributions

The first research objective focused mainly on the mathematical model development and the simulation steps of the process. These steps of the process are relatively generic until the appropriate components are chosen to address all of the needs

posed by the motivating problem. The objective of the first section of research is summarized along with the corresponding contribution.

Research Question 1: How can the impact of design parameter variability on rotorcraft maneuverability limits be quantitatively captured independent of control design for changing requirements?

Contribution 1: A six degree-of-freedom rigid body parametric rotorcraft inverse simulation model in combination with Filtered Monte Carlo that provides improved quantitative maneuverability tradeoff capabilities over traditional design methods.

One characteristic of this work over previous research conducted in the area is the integration of rigid body helicopter model into the design environment. Previous efforts during early design commonly use only the energy-based formulation, which is shown to miss important constraints in Chapter 2 of this dissertation. The second alteration to previous research efforts is the integration of inverse simulation approaches into a design framework, which enables analysis of Nap-of-the-Earth maneuvers. Previous efforts only analyzed fixed helicopter designs using this simulation technique. The final advancement presented through the first contribution is integration of the filtered data analysis approach to design space exploration for maneuver performance related design trades. This tool is used throughout all three of the contributions and the benefits are shown in Chapters 2, 3, and 4. In combination, the integration of these advancements allows for

design impacts on maneuverability limits to be assessed quantitatively and design space trades to be conducted real-time.

The second research question required analysis of techniques for including controllability measures into a control independent simulation and design. The motivation for this research is that maneuvers that are deemed feasible with energy-based formulations are often found to be infeasible when rigid body constraints are later analyzed. This required a literature search in multiple areas including: helicopter design, spacecraft design and optimization, and path-planning strategies. Difficulties arose because these measures must account for a multitude of control design decisions, while remaining at the appropriate level of detail for conceptual design.

Research Question 2: How can the quantitative impact of control integration decisions on maneuver performance be used to develop control system requirements independent of control design?

Contribution 2: Real-time maneuver analysis capabilities that include control characteristic constraints, which provide improved estimates and traceability for development of control system requirements.

The second contribution, which is presented in Chapter 3, introduced control integration measures into the process. Although the control system design is not directly integrated into the conceptual design process, it is important to capture control constraint and requirement information as early as possible. Two measures were integrated in this work, which included control deflection rate and trajectory divergence rate. This

integration allowed for the maneuver feasibility to be constrained by dynamic control limits, which was noted to be of high importance by the discrete path planning communities, since often times infeasible paths are deemed feasible unless dynamic measures are included. This new constraint offers a more conservative and robust solution. The second control characteristic provided quantitative measure of divergence from the ideal trajectory due to errors in the sensors and controllers. This measure is general enough to be applied to any control architecture at the early stages of design, while at the same time providing quantitative measure to be used as a requirement during control system design. Similarly, the process enables these trades to be conducted in real-time. These control characteristics are formulated for conceptual design; however, they can be easily decomposed into more detailed measures as more detailed models or information become available.

The final research question and corresponding contribution deals with mitigation of the dimensionality concerns stemming from the immense helicopter operational envelope. The previous contributions enabled the design parameter effects on maneuverability limits to be captured and assessed quantitatively; however, this analysis could only be performed on a small number of maneuvers. Hence, the third research objective determines a manner in which to handle the immense maneuver space, while simultaneously enabling specific missions to be analyzed quantitatively for design trades.

Research Question 3: Given that the maneuver space is combinatorial, how can the maneuverability characteristics be captured for the entire helicopter operational envelope, thus, enabling analysis of complete missions?

Contribution 3: Technique for developing the fundamental parametric maneuvers for quantitative assessment of maneuverability characteristics over the entire operational envelope.

The third contribution was presented in Chapter 4 of this dissertation and addressed the final research question associated with integrating the entire maneuverability envelope into early design. A systematic and traceable process was presented for developing a maneuver taxonomy. The taxonomy was developed using helicopter literature, which enables analysis of any maneuver within the operational envelope. However, the complexity of the maneuver mathematical formulation presented further difficulties when integrating into a design framework. Therefore, the maneuver mathematical formulation was modified to reduce the number of variables required, while still enabling the operational envelope to be described. The combination of the maneuver model and the taxonomy enabled for the performance of individual maneuvers to be analyzed such that the impact of design constraints or changes in the maneuver definition can be fully explored real-time.

The benefits of the contributions were shown by applying the final process to the 2012 AHS design competition, which was the motivation for this work. The entire mission in the competition consists of at least 31 maneuvers. For clarity purposes, analysis of only four maneuvers was shown. However, the analysis can be easily expanded to all of the maneuvers using the process developed. Consequently, this example showed that the combination of all three contributions presented in this dissertation enable the motivating problem to be addressed. Furthermore, this systematic

and traceable methodology can be easily adjusted to include many different types of systems and at all stages of the design process such that any NOE flight design can be completed.

5.2 Future Work

As with any complex problem, there are always additional contributions that can offer improvement. Four areas of further research are offered in this section to further expand the process developed: integration of a design module, higher fidelity helicopter modeling, inclusion of more controllability measures, and incorporation of a mission optimization routine.

5.2.1 Integration of Design Module

The process could benefit through integration of a design module that allows for mission sizing prior to the dynamic analysis loop. Additionally, this process should allow for iterations such that the maneuverability characteristics can aid in selection of an appropriate sizing mission and performance combination. All of the inputs to the helicopter model derived in this work correspond to the helicopter sizing code GTPDP developed at Georgia Institute of Technology. This sizing code would need to be integrated into the process and an iteration routine applied to enable the performance analysis to drive the sizing mission definition.

5.2.2 Higher Fidelity Helicopter Modeling

Simpler rotor models that are based on momentum theory or dynamic inflow are useful for predicting net rotor performance, especially for flight mechanics work where there is an emphasis on computational brevity. However, capturing the main rotor wake rotor flapping response during maneuvers is important for analyzing transient maneuvers and predicting cross-coupling effects [220-222]. As stated by Hennes [223], "a transient maneuver is a short-time event, typically initiated through pilot control, which significantly perturbs the rotor system from its steady-state operating condition". The blade motion and aerodynamic loading are aperiodic during a transient maneuver, which makes computation difficult. Additionally, Krothapalli [224] notes that "for many years, helicopter simulations have predicted off-axis response in hover and low speed forward flight that is opposite in sign to the corresponding flight test data." Several authors have investigated methodologies for integrating time-accurate free wake models into flight dynamics simulation. Ribera [225] found that "sophisticated aerodynamic models are needed for accurate predictions in a variety of practical problems of helicopter flight dynamics, such as the response to pilot inputs in moderate and large amplitude unsteady maneuvers, trim in turning flight, trim and response in descents, including near and through the vortex ring state, and the off-axis response to pilot inputs." Bottasso [226] and Ribera [227] recommend hierarchical approaches of increasing modeling complexity using a time accurate free wake model coupled with a comprehensive flight dynamics simulation model. One approach using hierarchical strategy in combination with inverse simulation techniques is presented by Cao [228], where the rotor control settings and

helicopter flight attitudes are first obtained using inverse solution technique, and then "the unsteady rotor forces are numerically simulated by synthetically applying the vortex theory, dynamic inflow theory and unsteady airfoil aerodynamic models." Higher fidelity rotor models should be included in order to analyze a greater number of NOE maneuvers.

5.2.3 Inclusion of Additional Controllability Measures

In Chapter 3 several controllability measures were introduced in order to quantitatively constrain the design space and aid in formulation of control system design requirements. These measures can be expanded to include more information to the control design engineer. At this point, the control engineer can provide the designer with additional measures that can provide more information to enable mitigation of control integration concerns. Additionally, some additional measures for stability and handling qualities can be incorporated.

5.2.4 Mission Optimization Integration

The fourth area for future work is the incorporation of an optimization algorithm for forming the optimum path mission. Currently, the process is setup such that the trades are conducted real-time by the designer. The reason is that much information is gained through conducting the optimization in this manner. However, added benefit can be gained through integration of an algorithm to conduct this analysis. In this manner, the designer can step through the results obtained by the optimizer and can adjust constraints accordingly. One manner to progress is integrating path planning strategies into the

analysis framework. Gillula [229] states that “the control of a complex system can be made easier by modeling the system as a collection of simplified hybrid modes, each representing a particular operating regime.” Another important aspect to consider is the switching of dynamics between maneuvers such that the aircraft completing one maneuver is able to begin the next maneuver without being an infeasible configuration [230]. A final adjustment is the performance measure. The performance measure used throughout this work was minimum time; however, a multitude of measures are possible such as minimum power or minimum fuel burn. These measures can be added to the process to enable a greater number of problems to be addressed.

APPENDIX A

Maneuver Model Time Histories

A taxonomy that consists of four fundamental maneuvers is laid out in the previous section and consists of motions in the X, Y, Z, and Heading axis of the navigation frame. The mathematical representation and validation is shown for each type of maneuver in this section for completeness. A maneuver is modeled using each of the remaining 3 fundamental maneuver types. The longitudinal maneuver involving Z-axis motion, aka pop-up, was discussed in detail in Chapter 2 so it is not readdressed. Once all of the maneuvers are validated, the ability to model complex maneuvers through combinations of the various fundamental maneuvers is discussed; however, incorporation into the design framework is left for future work. The remaining 3 maneuvers in the taxonomy are Lateral Maneuvers (Y axis), Longitudinal Maneuvers (X axis), and Heading changes (Psi).

Lateral Maneuvers – Y Axis Motion

The lateral maneuver grouping of the taxonomy contains helicopter motions that involve accelerations in the y axis of the navigation frame. This acceleration results in side step and lane change trajectories, which are commonly referred to in rotorcraft literature as lateral jinks. A simple example of three different lateral jinks are shown in Figure A.1, which were generated using the models and methods derived in this work. This example is simplified as compared to the DoE used for simulation in the data analysis section in that the time, altitude, and initial velocity are all fixed. These

constraints are applied here only for figure generation and understanding. Each of the three maneuvers within the figure represents a different y-axis acceleration as specified through the DoE. The pink trajectory in the middle of the paths represents the case of zero acceleration.

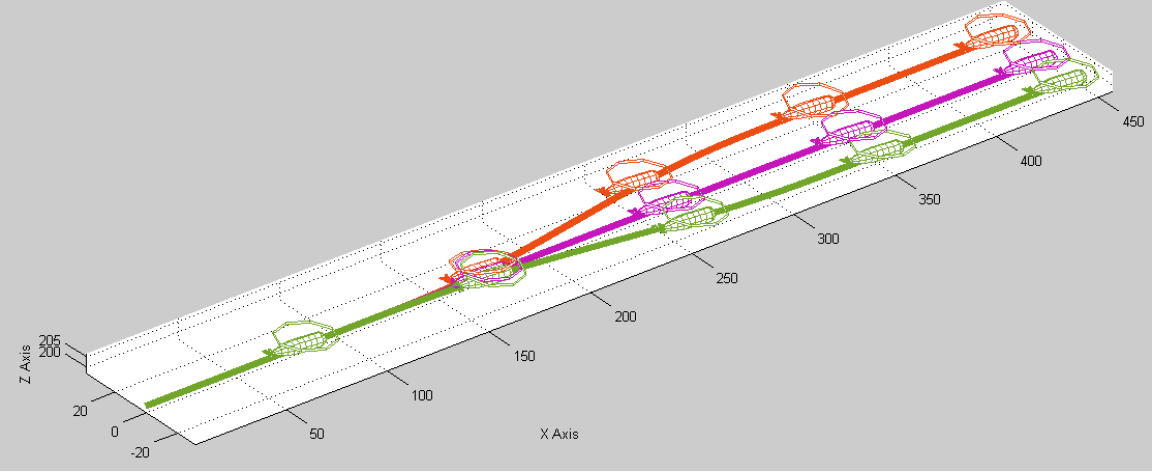

Figure A.1: Multiple Lateral Trajectories

A single maneuver within the maneuver design space must be selected for validation. Hence, a maneuver trajectory is shown in Figure A.2 where a constant forward velocity of 8.5 ft/s is maintained throughout the maneuver, which lasts for 10 seconds. The y component of the velocity starts at a value of zero because the helicopter is initially in trimmed level flight. Throughout the maneuver, the y velocity changes from zero to a negative maximum value at 5 seconds and finally returns to a value of zero at the end of the maneuver. This velocity profile results in the lane change maneuver shown in Figure A.2.

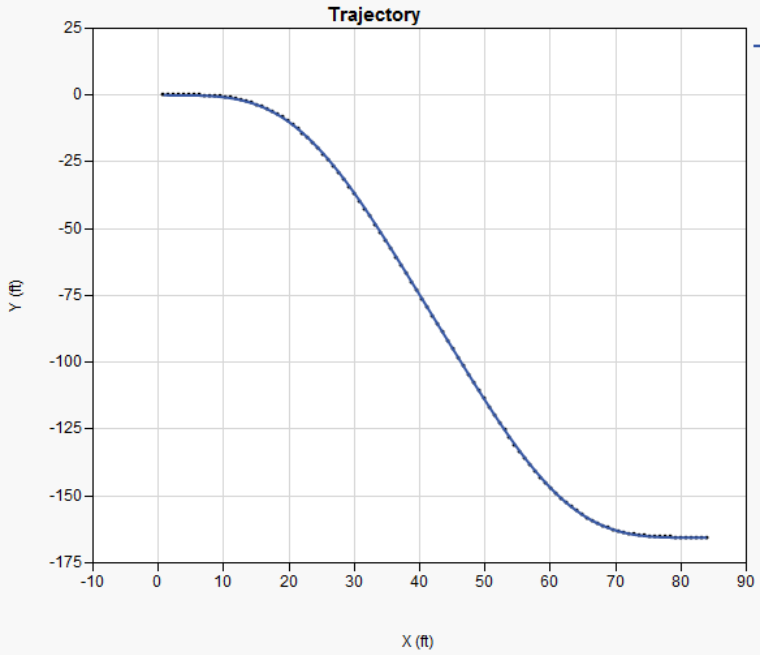

Figure A.2: Y-Axis Maneuver

The key trends to investigate for this maneuver are the y axis velocities and accelerations relationships to the lateral displacement, which are summarized in Figure A.3. The top portion displays the y axis displacement with time, which results from the velocity profile that is specified as the constraint. The velocity profile may be viewed in the middle of the figure. The profile is specified to start and end at a value of zero velocity with a smooth curve to a maximum velocity of approximately 32 ft/s occurring 5 seconds into the simulation. The acceleration profile is a byproduct of the manner in which the velocity is defined. It is observed that the lateral displacement and acceleration are indeed correct for the defined velocity profile.

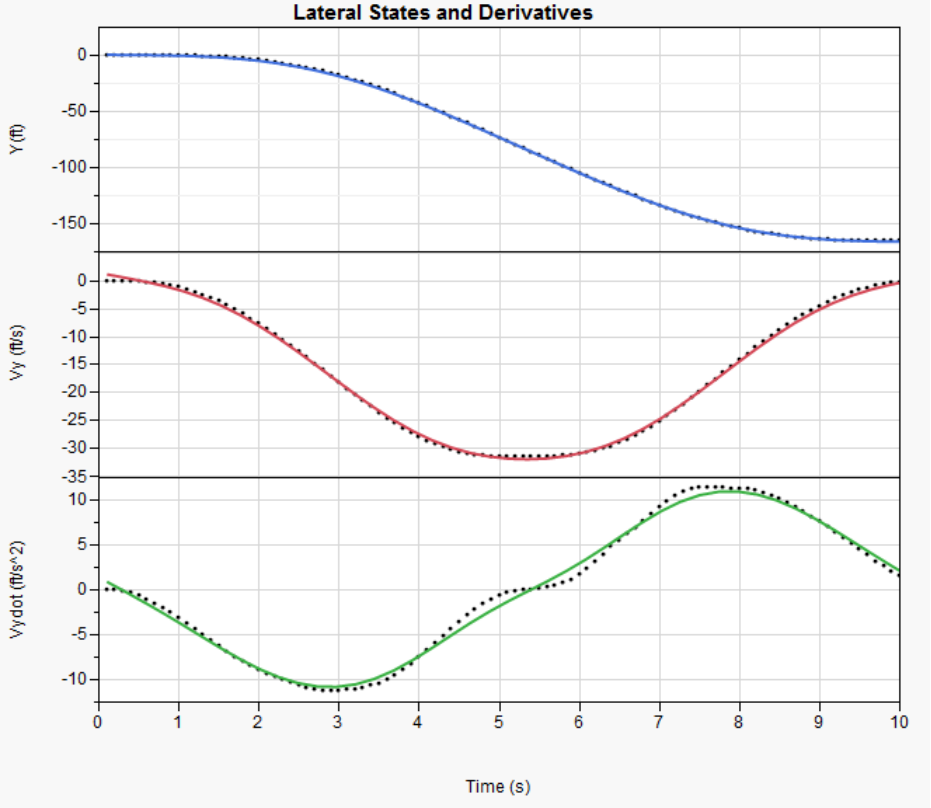

Figure A.3: Lateral States and Derivatives

The velocity profile and corresponding displacement and acceleration time histories are very similar to those presented in [25, 136, 144]. Additionally, the control time histories for the lateral side step maneuver must be examined to ensure that the results through dynamic simulation are representative of actual helicopter motion and control. Figure A.4 displays the time histories of the four helicopter controls for the simulated lateral maneuver. The main rotor collective appears at the top portion. As expected, the collective must increase during the maneuver in order to maintain the forward velocity and accelerate the vehicle laterally, while balancing out the weight component in the z axis. The collective reaches a maximum deflection when the acceleration is maximum and tapers off slightly; however, it does not decrease much

because the velocity is still increasing in the lateral direction which requires more collective to balance the drag components that are introduced. The collective again reaches maximum deflection when acceleration is a minimum value. At the end of the maneuver, the collective is again at the trim value that was observed at the beginning of the maneuver.

The longitudinal cyclic is the second subplot in Figure A.4. The key function of the longitudinal cyclic is to maintain the forward velocity throughout the maneuver; hence, as main rotor thrust is being diverted to produced lateral accelerations and the corresponding drag forces increase, the longitudinal cyclic must increase in magnitude to maintain the constant forward velocity. The lateral cyclic and tail collective are displayed in the final two portions of the figure. These controls are used to provide the lateral forces necessary to accelerate, while at the same time balancing the moments to prevent rotation of the vehicle about the yaw axis. The tail collective is maximum deflection when acceleration is maximum as expected, while the lateral cyclic follows a sinusoidal function of time as shown in Hess [25].

As in keeping with previous verification and validation efforts, the attitude of the vehicle throughout the simulation is also presented. The pitch angle of the vehicle changes because of coupling of forces and moments within the EoM of the helicopter model. Additionally, the pitch should follow a similar trend to that already discussed of the longitudinal cyclic. Through comparison of Figure A.4 and Figure A.5 it can be observed that this trend is correct. As the longitudinal cyclic decreases, the pitch of the vehicle increases to balance out the effects. Additionally, Figure A.5 indicates that the

constraint of zero heading change is enforced throughout the entire maneuver. The final angle to discuss is the roll angle, which appears in the middle portion. As expected the helicopter must roll in order to complete the lane change maneuver and the maximum roll angle occurs during maximum lateral acceleration. Finally, the roll angle returns to trim conditions at the end of the maneuver.

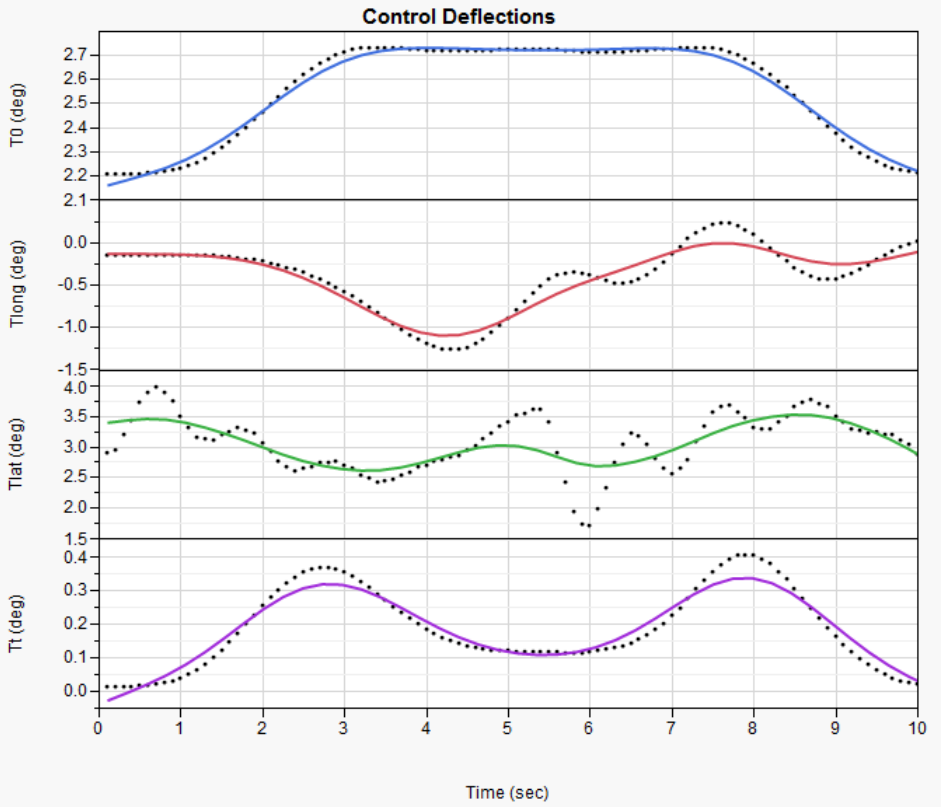

Figure A.4: Lateral Motion Control Histories

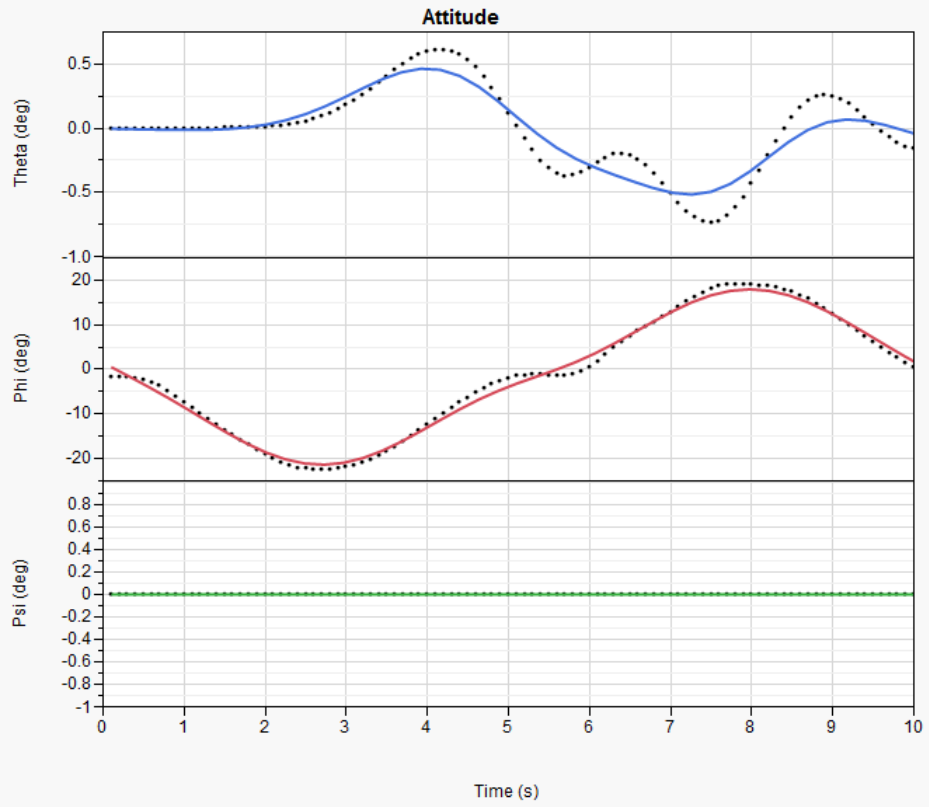

Figure A.5: Helicopter Attitude during Lateral Maneuver

As previously mentioned, the tail collective is used to counteract the torque generated by the main rotor. This torque is related to the power required and the rotor tip speed. This observation indicates that there must be a direct relationship of the tail rotor collective to the power decomposition. The power decomposition for the lateral maneuver is shown in Figure A.6 where the induced power time history corresponds directly to the time history of the tail rotor collective that was discussed in Figure A.4. Moreover, the profile power and parasitic power both are a function of induced velocity and freestream velocity, which increases during the maneuver. As a result, both powers increase as shown in the bottom two portions of Figure A.6.

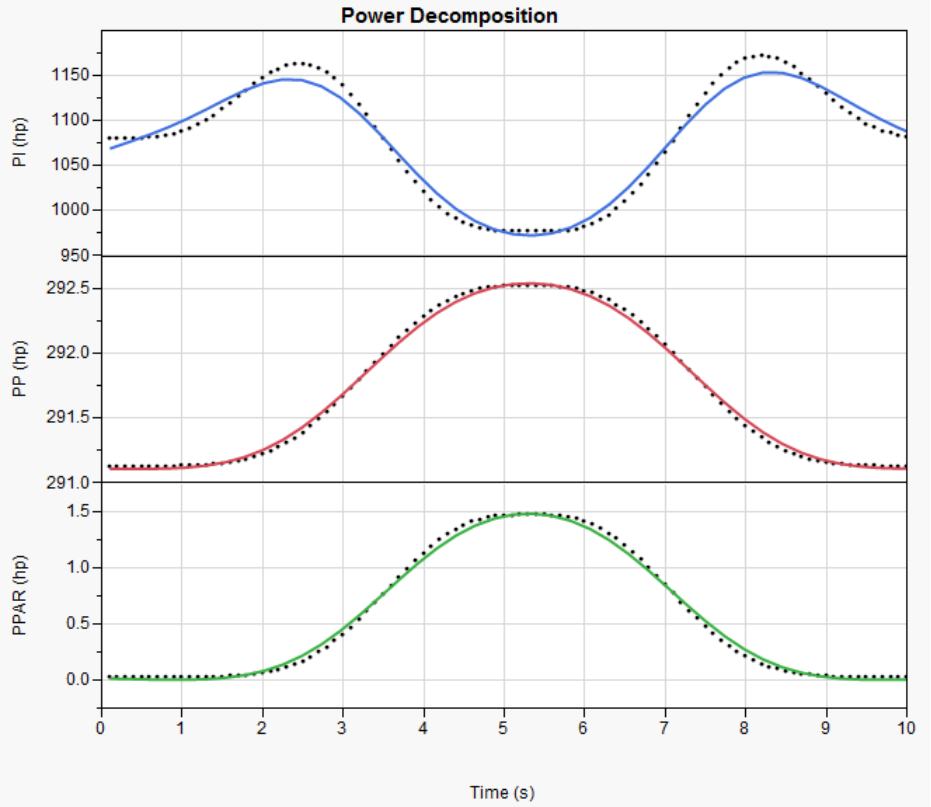

Figure A.6: Power Decomposition for Lateral Maneuver

Accelerate Maneuvers – X Axis Motion

The trajectory of the acceleration maneuvers is not as easily visualized as the other fundamental maneuvers within the taxonomy. In order to better view what is taking place during the maneuver, power required is added to the trajectory shown in Figure A.7. The acceleration maneuver consists of an increase in the forward velocity until a maximum is reached halfway through the maneuver. At which time the velocity then decreases back to the initial velocity by the end of the maneuver. The only position variable that changes is the x-axis location. Because of the trajectory profile and the relationship of velocity to power required, the maximum power required occurs at the

start and end of the maneuver. The velocity at the start of the maneuver is defined to be 52 ft/s and reach a maximum of 95 ft/s at the halfway point.

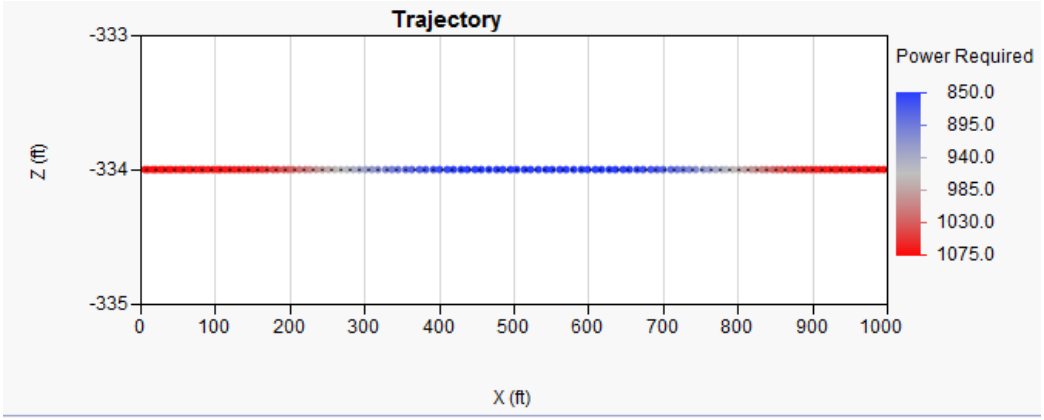

Figure A.7: X-Acceleration Maneuver Trajectory

The velocity decomposition may be observed in Figure A.8, where the x-axis body velocity closely approximates the maneuver defined velocity initially. During the maneuver, the helicopter must pitch forward to accelerate, which causes an increase in the z-component of the velocity as shown in the bottom of the figure. Moreover, during the second portion of the maneuver the helicopter must decelerate, which requires a positive pitch angle resulting in a positive z-component of velocity. The y-component velocity remains close to a zero value throughout the simulation but changes slightly due to coupling effects within the EoM. This is viewed in the middle subplot of Figure A.8.

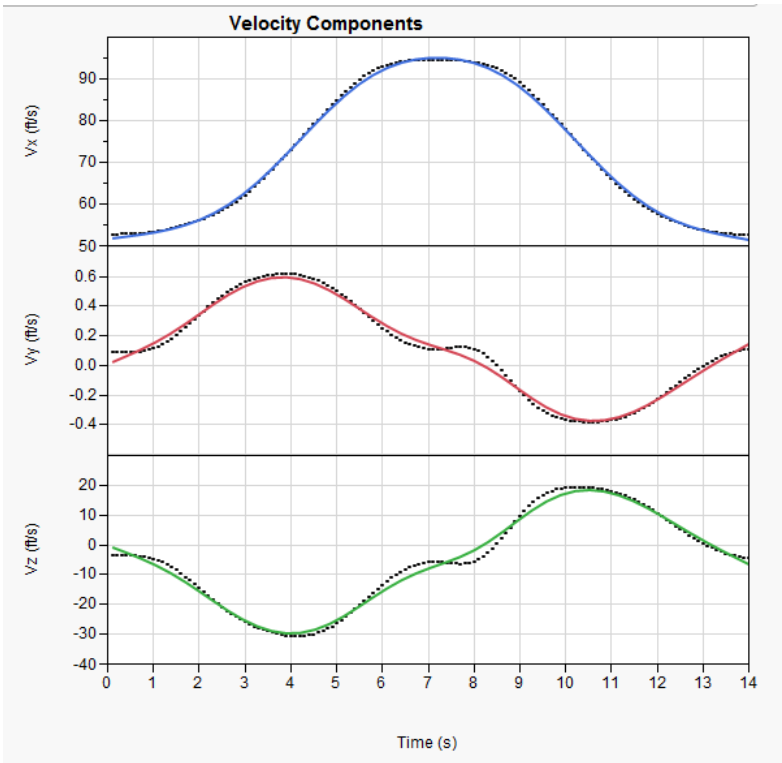

Figure A.8: X-Acceleration Velocity Decomposition

The pitch angle was previously mentioned with regards to the z-component velocity value. The attitude of the vehicle throughout the simulation, including the pitch angle, is shown in Figure A.9 to verify that the correct body rotations are present. The x-axis acceleration maneuver requires the helicopter to increase in horizontal velocity. This requires that the vehicle initially pitch forward to accelerate to a faster velocity and then decelerate back to the initial velocity. For the maneuver tested, this pitch corresponds to a maximum magnitude of 23 degrees, while at the initial velocity only a -5 degree pitch angle is required. Throughout the maneuver, the pitch angle follows the trends as expected and returns back to the equilibrium value at the end of the maneuver. Heading may be viewed in the bottom of Figure A.9 and maintains the constrained zero value

during the entire duration of the maneuver. As in past verification efforts, the roll angle directly correlates with the power required and since the power required is a minimum at the midpoint of the maneuver, the roll angle is smallest at this time. The roll angle is shown in the center segment of the figure. It should be noted that all the angles remain smooth throughout, which is essential to simulating actual flight scenarios.

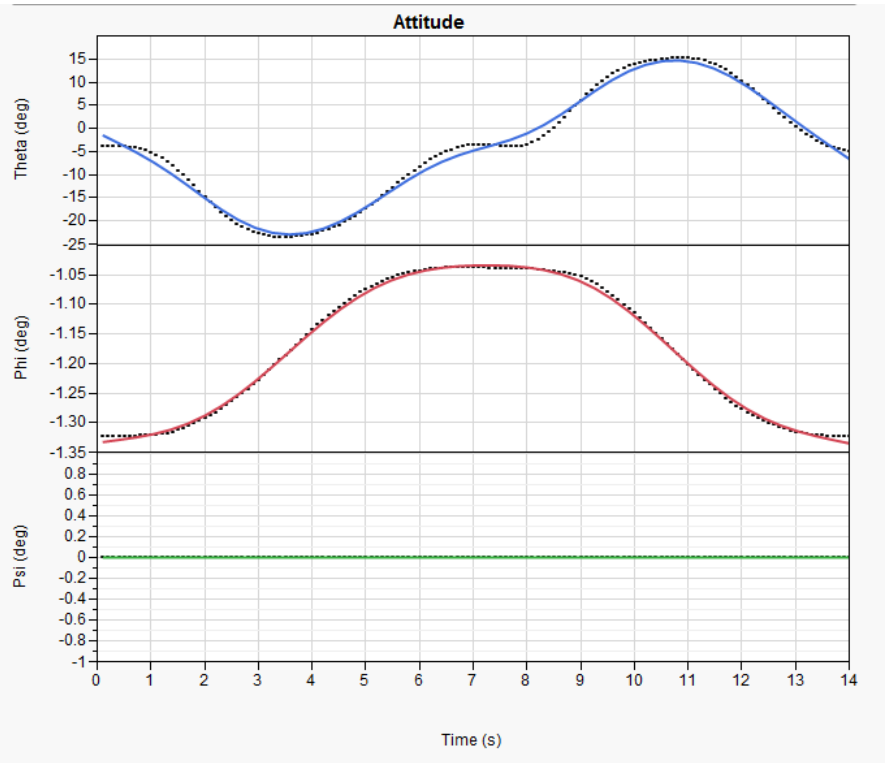

Figure A.9: X-Acceleration – Attitude

The states are shown to follow the correct trends and magnitudes throughout the maneuver. Next, the control deflections must also be presented and discussed. When the pitch of the vehicle changes in order to tilt a component of the thrust vector toward the required acceleration vector, the balance in weight and thrust in the z-axis of the navigational frame is lost. Without any adjustment in the main rotor collective, the

helicopter would loss altitude. Since the dynamic constraint is applied such to maintain altitude, the main rotor collective must increase for the duration of the maneuver because during both acceleration and deceleration in the x-axis the vehicle must pitch. This is viewed in the top portion of Figure A.10.

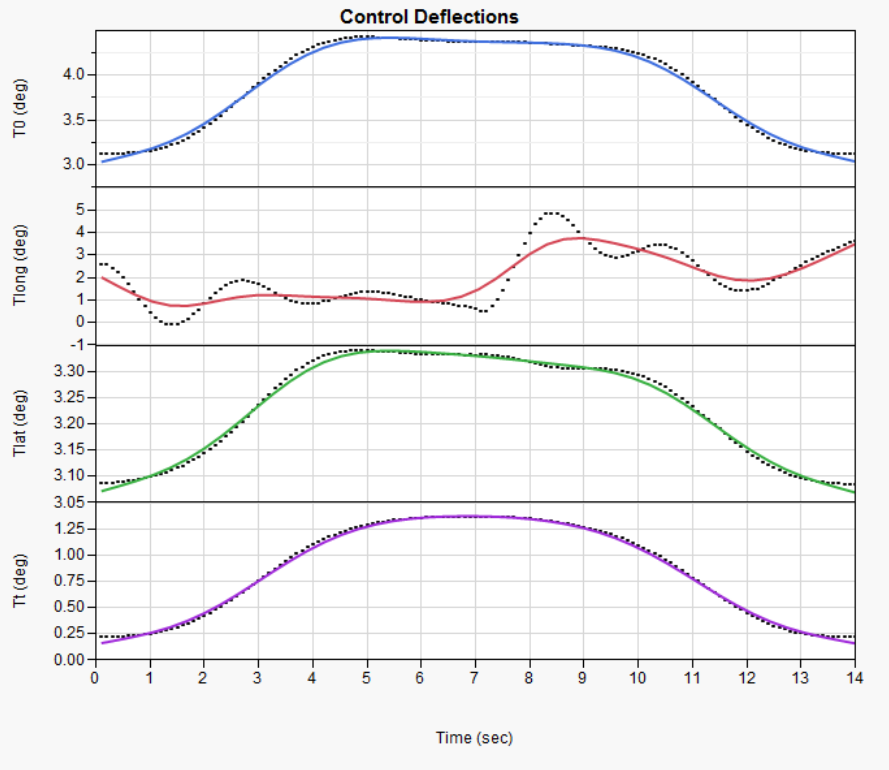

Figure A.10: X-Acceleration - Control Settings

As in previous verification studies, the tail collective, shown in the bottom subplot, must increase in order to counter the torque generated from the increase in main rotor collective. Similarly, the lateral cyclic is increased to cancel out the additional side force and corresponding rolling moment that is generated at the tail. The longitudinal cyclic response is the most complicated of all the controls. This is because it is required to tilt the tip-path plane, while at the same time balancing the longitudinal forces and the

pitching moment. Analyzing Figure A.10 it is observed that the longitudinal cyclic degreases in the acceleration phase of flight meaning the TPP is tilting forward. The oscillation is caused by the balancing of the pitching moment but a steady-state is reached by the midpoint of the simulation. At this point the vehicle is required to decelerate, which requires the TPP to tilt aft. This action again causes stable oscillations that subside at the end of the simulation.

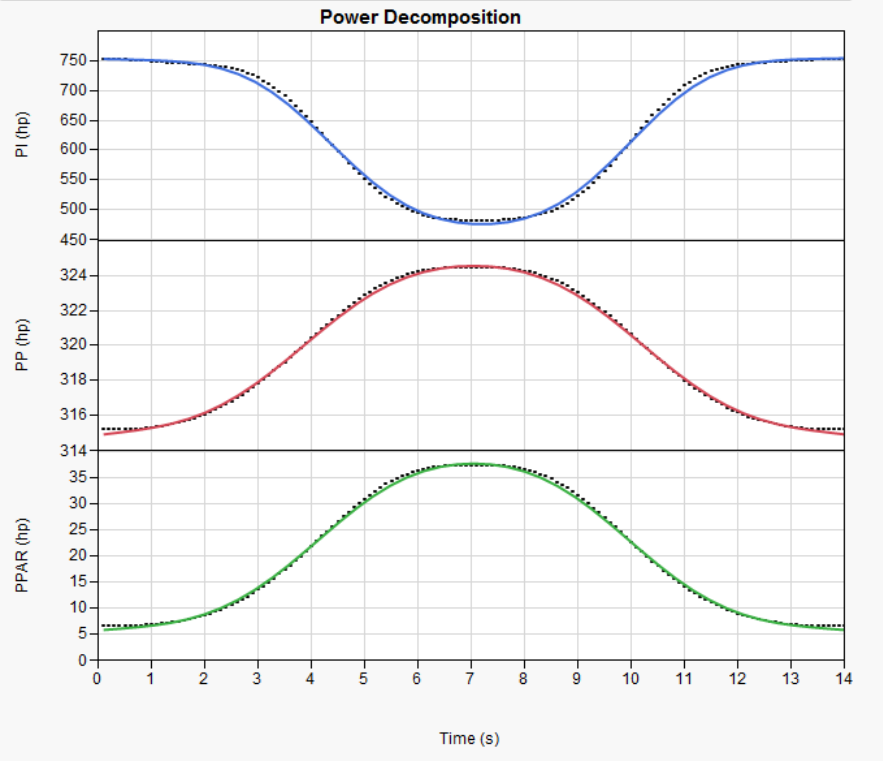

Figure A.11: X-Acceleration – Power Decomposition

The power decomposition corresponds directly to the freestream and induced velocity components. The vehicle velocity increases as the system accelerates, which results in a decrease in the induced power. The induced power time history is shown in the top portion of Figure A.11 and is inversely related to the velocity profile. On the other

hand, the profile and parasitic powers increase with velocity and the time histories are shown in the bottom two subplots of Figure A.11. Because the velocity increases and decreases with no change in heading or altitude, all three powers return to the initial power settings.

Heading Maneuvers – Psi Changes

The fourth and final maneuver within the taxonomy is the heading change maneuver. This maneuver is essential in changing the heading of the system within the flight envelope. All of the other maneuvers previously discussed enforced a constraint that required that heading maintain a zero value throughout simulation. The helicopter is not symmetric since the tail rotor is providing a force in the y-axis of the system and the main rotor is rotating the same direction for all maneuvers. As a result, a clockwise turn has different performance limits than a counter-clock wise turn. This concept is displayed in Figure A.12 where tighter clockwise turns are possible because of tail rotor force direction. Each maneuver within the figure represents a different maximum yaw acceleration with one of the maneuvers maintaining zero heading change. With this fundamental maneuver, turning performance can be assessed.

A single clockwise maneuver is discussed in the following paragraphs to verify that the final maneuver within the taxonomy contains the correct trends. The trajectory of the 165 degree turn that occurred over a 14 second interval is shown in Figure A.13. The forward velocity of the specified maneuver is 8 ft/s. The path starts in the upper left corner of the figure with a zero displacement in both the x and y axes. A maximum

displacement of 35 ft in the x-axis of the inertial frame is reached about halfway through the simulation, while the final y-axis displacement of 37 ft occurs at the end of the simulation. If the heading acceleration rate was increased slightly, the vehicle would complete an entire 180 degree turn rather than only 165 degree.

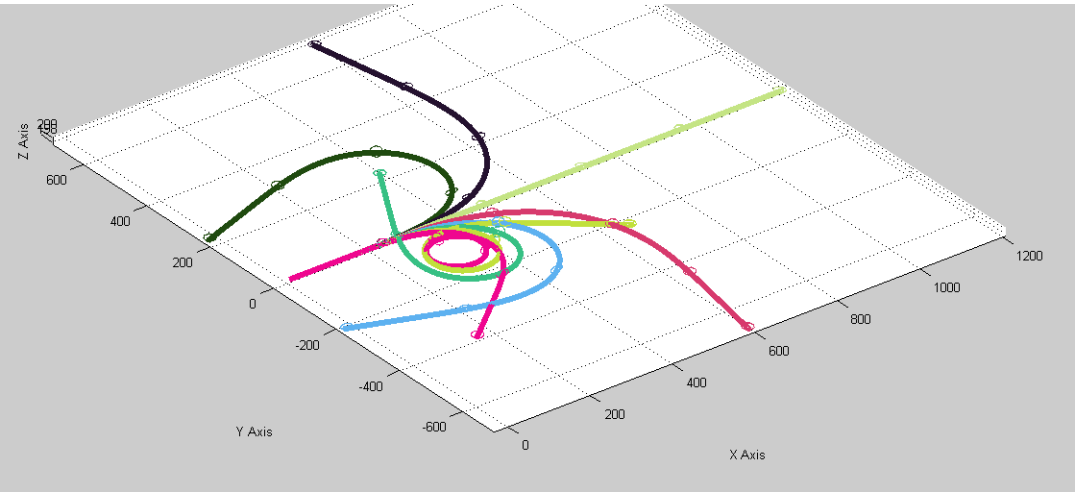

Figure A.12: Multiple Turning Maneuvers

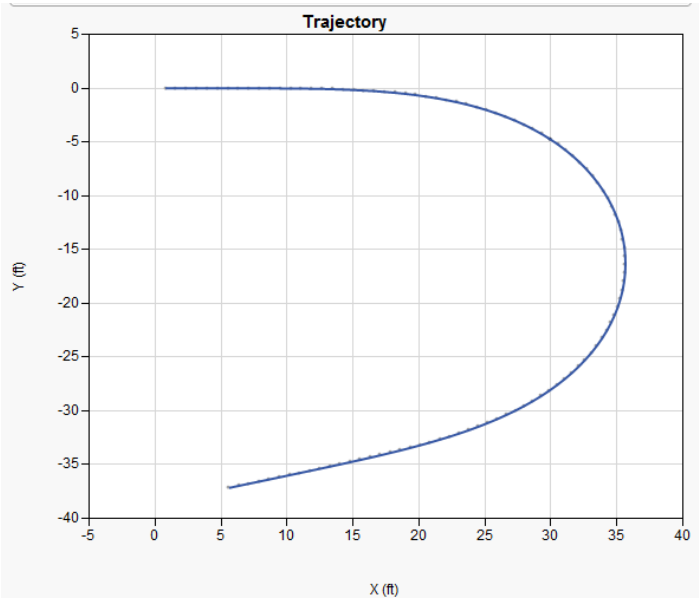

Figure A.13: Turning Maneuver Trajectory

A forward velocity of 8 ft/s is constrained throughout the simulation through the maneuver definition. Additionally, the lateral and vertical velocities are constrained to zero values. All of these constraints are met during simulation and are viewed in Figure A.14. The top portion of the figure displays the x-axis velocity of 8 ft/s throughout the simulation time, while the bottom two portions show that the other components of velocity remain near zero. There are minor deviations in the other two velocities because keep in mind that the navigational frame velocities are constrained while the body velocities are displayed.

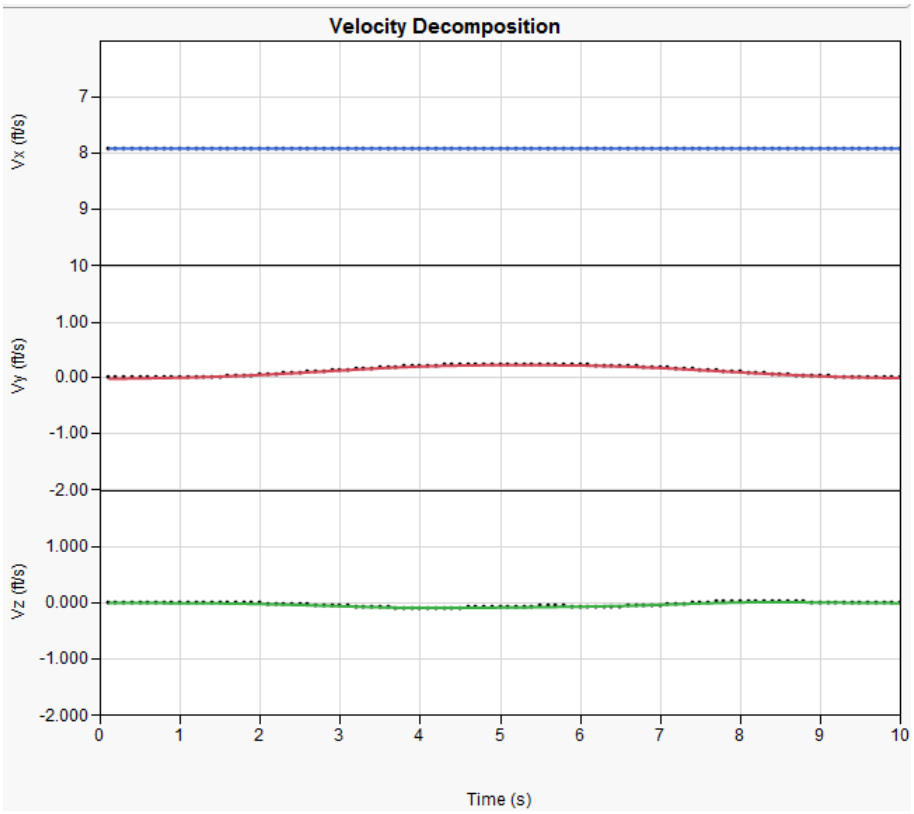

Figure A.14: Heading Acceleration - Velocity Decomposition

Unlike the other maneuvers within the taxonomy, the heading acceleration maneuver imposes a change in heading constraint. It must be viewed that this constraint is smooth and that the impact on other vehicle angles results in smooth time history profiles. The heading change as a function of time may be observed in the bottom section of Figure A.15. The heading starts at the initial value of zero and ends at a heading of 165 degrees as stipulated in the maneuver definition. The value is negative because the clockwise rotation is defined as negative when comparing the navigational frame to the inertial coordinate system. The pitch of the vehicle, which is shown in the top portion of the figure, remains around the initial angle but diverges slightly as expected from viewing the velocity components in Figure A.14. The roll angle of the helicopter is displayed in the middle subplot of Figure A.15. The sign of the roll angle is opposite because of the heading transformation from the navigational frame to the inertial frame. Hence, the roll angle is actually the opposite direction to that shown in the figure. As a result, the helicopter is now viewed as rolling into the turn as expected with a maximum roll value occurring at maximum roll rate.

The only controls that require discussion are the lateral cyclic and the tail rotor collective settings. The main rotor collective and the longitudinal cyclic remain almost constant throughout the simulation because the forward velocity and altitude are maintained. The control time histories for the turning maneuver may be viewed in Figure A.16, with the lateral cyclic and tail rotor collective displayed in the bottom two subplots, respectively.

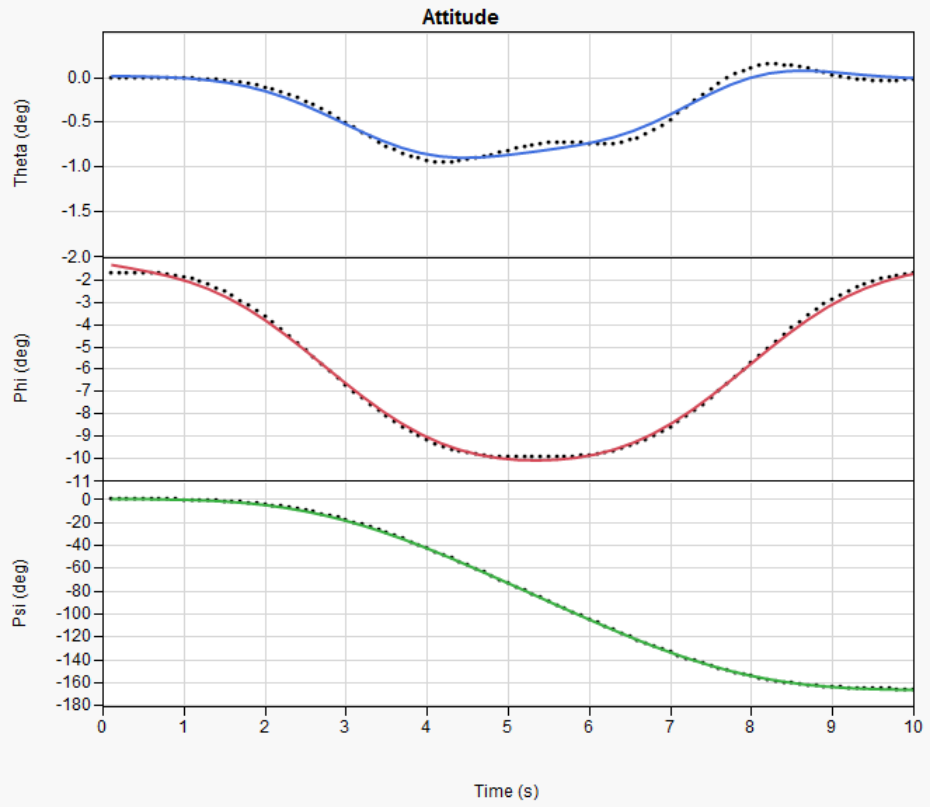

Figure A.15: Vehicle Attitude – Heading Acceleration

In order to perform the turn, the lateral cyclic must be increased in order to provide the necessary rolling moment and the side force to enter the turn. The lateral cyclic reaches the maximum value in mid-maneuver and returns to initial conditions at the end of the simulation. Additionally, the tail collective must increase to balance out the side force generated by the lateral cyclic such that the constant radius turn can be performed. Otherwise, there would be a change in the lateral velocity component leading to constraint violation. Both lateral controls correspond directly to the heading profile change with time as necessary.

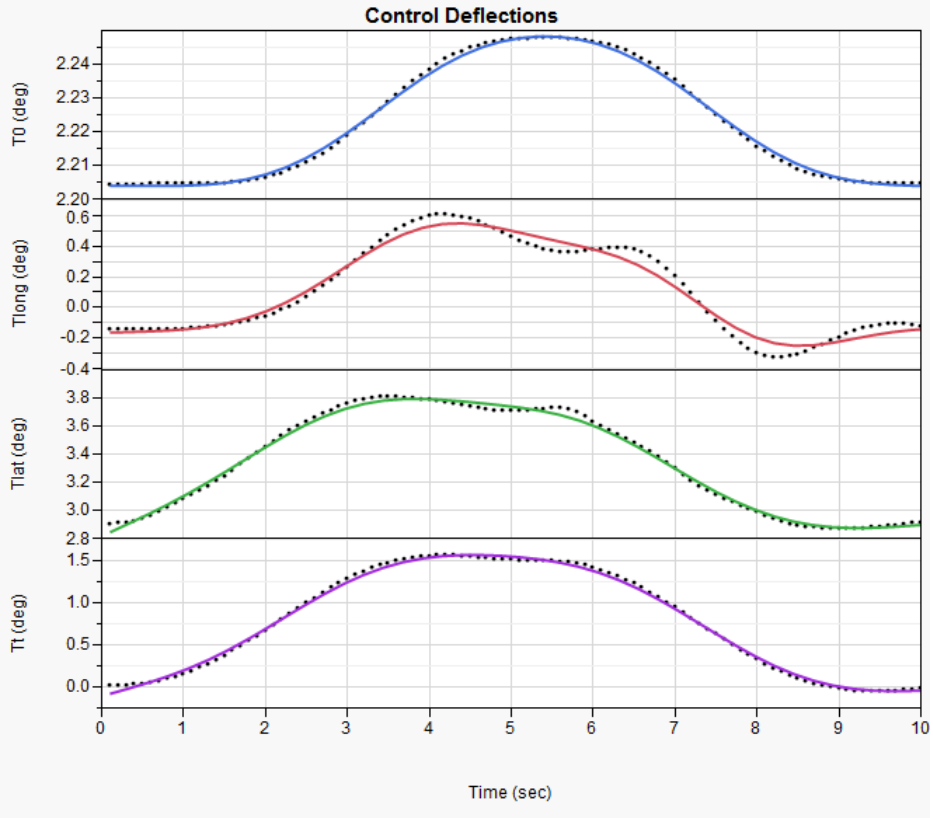

Figure A.16: Control Settings – Yaw Acceleration

Through analyzing the velocity decomposition, it was shown that the velocity is maintained constant throughout the maneuver. As a result, the profile and parasitic drags remain constant through the simulation as viewed in Figure A.17. The induced power increases slightly with an increase in main rotor collective and thrust setting. The induced power time history is shown in the top portion of the figure with a maximum power requirement of 1100 hp in the middle of the maneuver when the yaw rate is a maximum value.

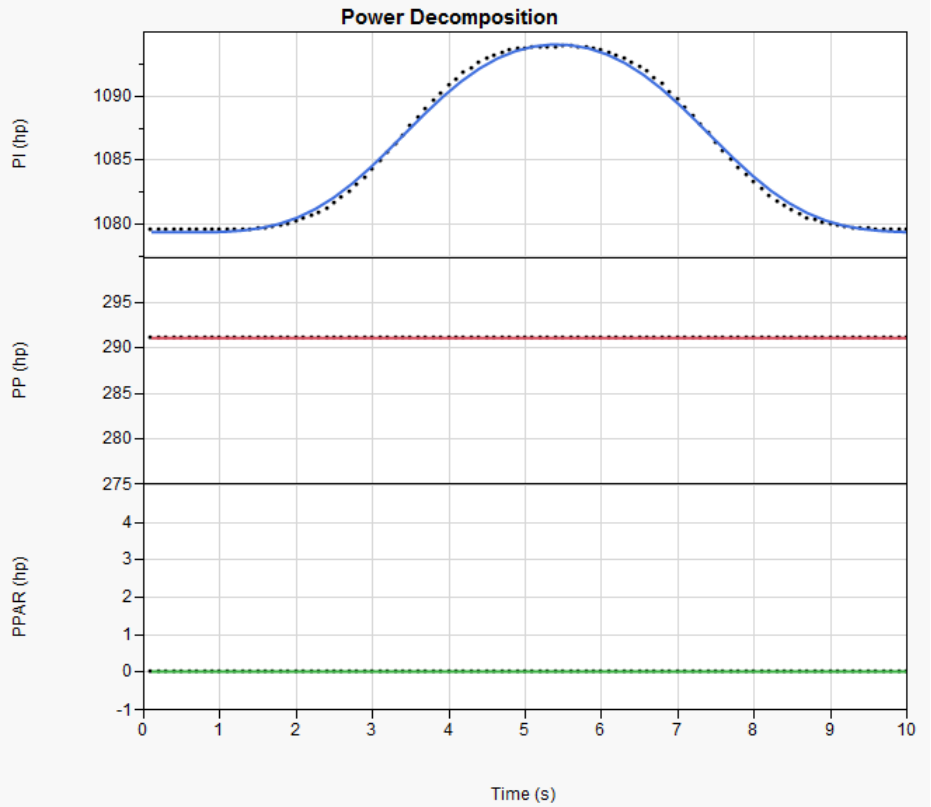

Figure A.17: Power Decomposition – Yaw Acceleration

APPENDIX B

Multivariate Analysis of Trim Algorithm

The trim condition corresponds to five states of interest and four controls. The states consist of three linear velocity components, pitch angle, and roll angle. The angular rates and yaw angle are forced to be zero through the trim constraints so they are not included in the trim analysis. The relationship between all of the states and controls may be observed in a multivariate manner in Figure B.1. This figure is an excellent resource for verifying that the trends in the data are accurate. The multivariate plot shows all nine variables of interest such that the relationship between any two variables can be easily observed. For example, as the velocity increases, the horizontal velocity (Vx) and the pitch angle (theta) must increase, which results in an increase in the magnitude of the vertical velocity (Vz) component. The other trends can be verified through similar structured reasoning.

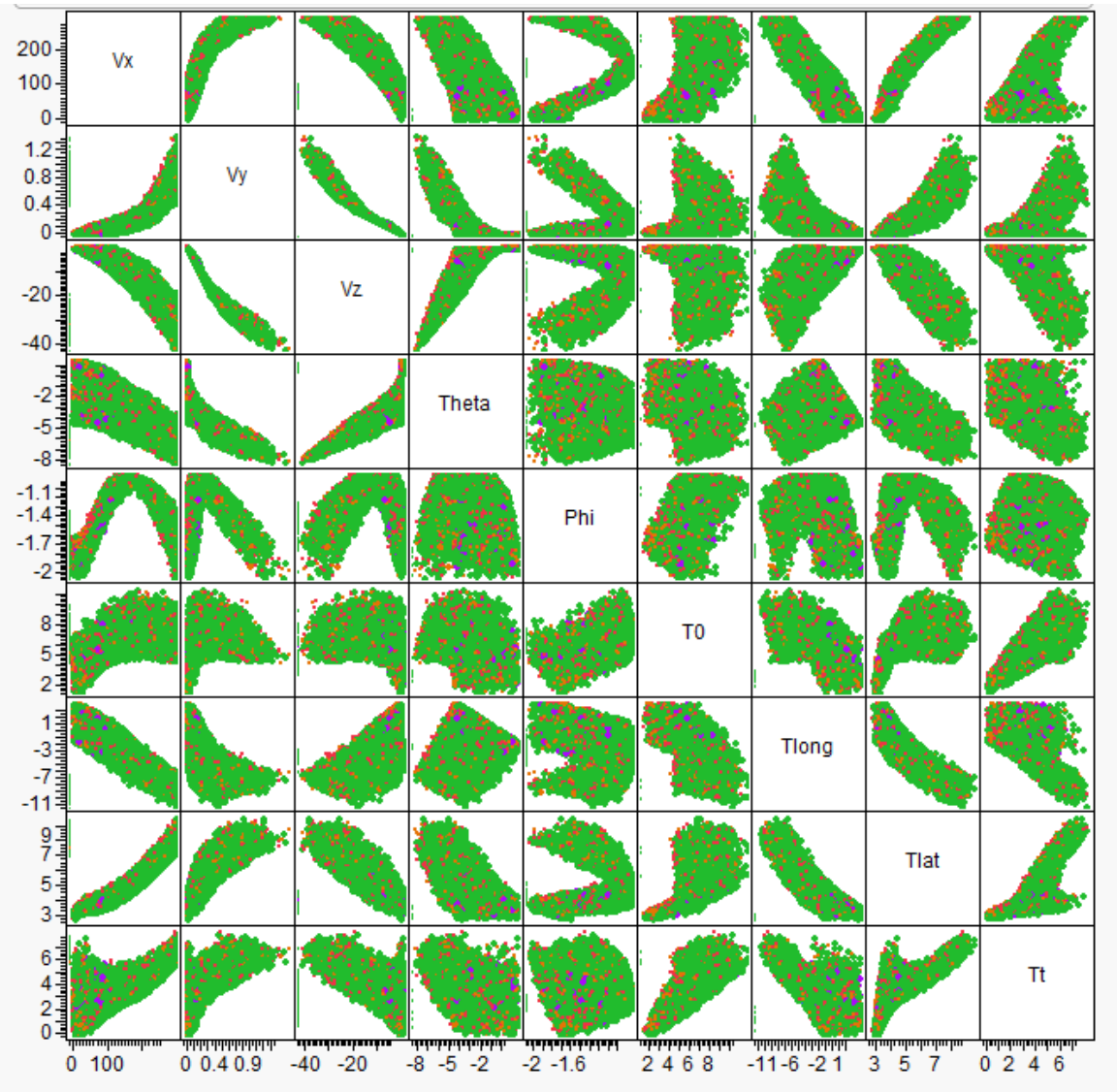

Figure B.1: Multivariate Plot of Trim States and Controls

APPENDIX C

Various Design Optimization Strategies

Since this ability was already demonstrated in Chapter 2, another trade within the multiple maneuver space is conducted to demonstrate the power of the filtered data method. It is common during design that the weight of a given design increases as it progresses through the design stages; as a result, the designer may wish to select the maximum weight vehicle earlier in the design stages that is capable of performing all of the missions within the performance threshold. In order to conduct this trade using the approach applied in this work, a data filter is placed on the vehicle mass. This filter is adjusted real-time until a design is achieved that can perform all four of the mission maneuvers. This filter is applied and a vehicle mass of 13700 lbs is determined and the resulting design parameter settings for this scenario are displayed in Figure . Observation of the figure shows that for a similar mass vehicle of approximately 13700 lbs, the diameter of the main rotor must be within the upper-middle region of the ranges set. Additionally, the maximum mass constraint also dictates design variable ranges for CG, Chord, Tail Rotor Moment Arm, and Tail Area.

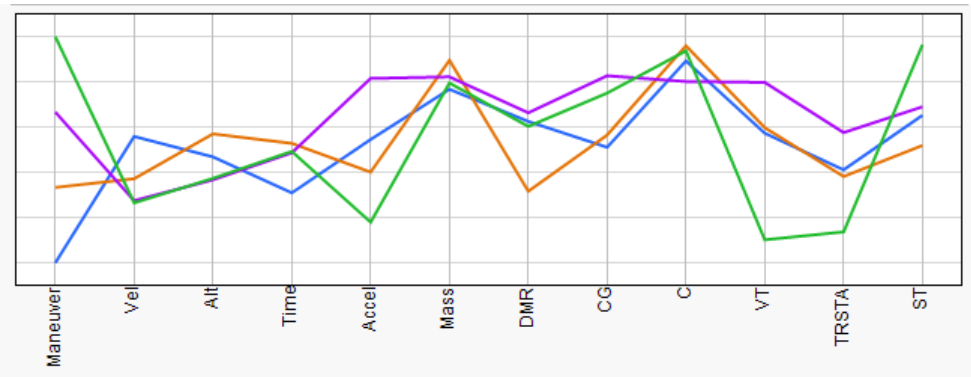

Figure C.1: Maximum Mass Vehicle for Mission Success

Assume that the designer finds out after this analysis that minimizing the main rotor diameter is actually the driving requirement due to the pylon width constraints. Fortunately, the filtered data approach allows for real-time adjustment of the constraints. The design parameter ranges for the minimum rotor design are shown in Figure . Using this method, the minimum rotor diameter for success is determined to be around 48 ft. This requirement substantially reduces the maximum weight of the vehicle as compared to the previous exercise. Additionally, the Chord, Tail Rotor Moment Arm, and Tail Area all decrease as expected; however, without the simulation environment, this value could not be quantified.

Although only the first 4 maneuvers of the mission are analyzed, the overall process is fully demonstrated with the above example. In order to include all of the maneuvers requires multiple trades similar to those conducted in this section; however, these trades are just an extension of the data analysis that is shown. Therefore, the approach proposed in this work for analyzing the entire AHS 2012 Design Competition is verified. Additionally, the ability to conduct real-time trades is shown through the two

different approaches of maximum mass solution and minimum rotor diameter footprint examples.

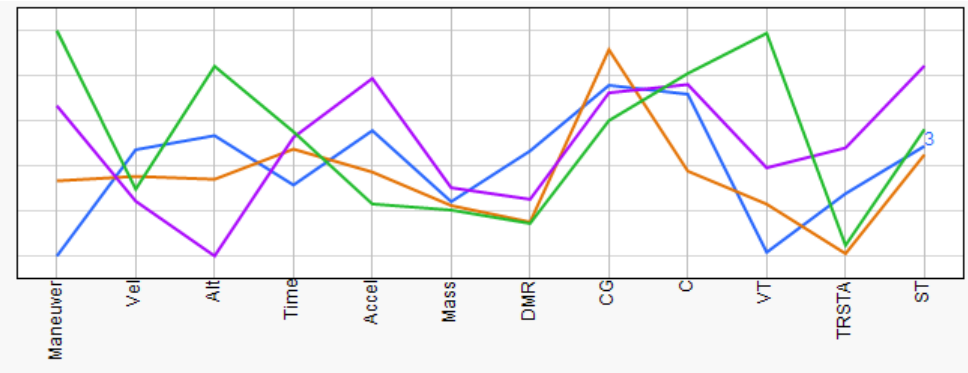

Figure C.2: Minimum Rotor Diameter for Mission Success

REFERENCES

1. Sieger, D., *Conceptual Design Tool for the Systematic Design Method.* Concurrent Product Design and Environmentally Conscious Manufacturing, 1997. **94**(5): p. 145-152.

2. Al-Salka, M., *A Framework for a Generalized Computer-Based Support Environment for Conceptual Engineering Design.* Journal of Engineering Design, 1998. **9**(1): p. 57-88.

3. Wang, L., *Collaborative Conceptual Design: State of the Art and Future Trends.* Computer-Aided Design, 2002. **34**: p. 981-996.

4. Takahashi, T.T., Fanciullo, T., and Ridgely, D.B. , *Incorporation of Flight Control Design Tools into the Multi-Disciplinary Conceptual Design Process*, in *45th AIAA Aerospace Sciences Meeting and Exhibit*2007, AIAA: Reno, Nevada. p. 43.

5. Kirby, M.R., *A Methodology for Identification, Evaluation, and Selection in Conceptual and Preliminary Aircraft Design*, in *Aerospace Engineering*2001, Georgia Institute of Technolgoy: Atlanta.

6. Sikorsky, *Request for Proposal for Rotary Winged Pylon Racer*. 29th Annual American Helicopter Society Student Design Competition, 2012: p. 21.

7. Kehrer, W., *Design Evolution of the Boeing 2707-300 Supersonic Transport*, in *43rd AGARD Flight Mechanics Panel Meeting*1973, Aircraft Design Integration and Optimization.

8. Perez, R., Liu, H., and Behdinan, K., *Multidisciplinary Optimization Framework for Control-Configuration Integration in Aircraft Conceptual Design.* Journal of Aircraft 2006, 2006. **vol.43**(no.6).

9. Sahasrabudhe, V., *Integrated Rotor-Flight Control System Optimization with Aeroelastic and Handling Qualities Constraints.* Journal of Guidance, Control, and Dynamics, 1997. **20**(2): p. 217-224.

10. Miller, G.D., Jacques, D.R., and Pachter, M., *Aircraft Trim Control*, in *Guidance, Navigation and Control Conference and Exhibit*2003, AIAA: Austin, Texas. p. 10.

11. Anderson, M.R., Mason, W. H., *An MDO Approach to Control-Configured-Vehicle Design*, in *NASA, and ISSMO, Symposium on Multidisciplinary Analysis and Optimization, 6th*1996: Bellevue, WA.

12. *Modernizing the Army's Rotary-Wing Aviation Fleet, Chapter 2 "Approaches to Modernizing the Fleet"*. . 2007 November 5]; Available from: http://www.cbo.gov/ftpdocs/88xx/doc8865/Chapter2.6.1.shtml.

13. Coleman, G.J., Jr., *A Generic Stability and Control Tool for Flight Vehicle Conceptual Design: Aeromech Software Development*, in *Aerospace Engineering*2007, University of Texas: Arlington. p. 283.

14. Von Kaenel, R., Rizzi, A., Oppelstrup, J., Goetzendorf-Graboski, T., Ghoreyshi, M., Cavagna, L., Berard, A., *CEASIOM: Simulating Stability and Control with CFD/CSM in Aricraft Conceptual Design*, in *26th International Congress of the Aeronautical Sciences*2008, ICAS. p. 14.

15. Morris, S., Kroo, I., *Aircraft Design Optimization with Dynamic Performance Constraints.* Journal of Aircraft, 1990. **27**(12): p. 1060 -1067.

16. Avanzini, G., *Model Predictive Control Scheme for Rotorcraft Inverse Simulation*, in *Guidance, Navigation, and Control Conference*2011, AIAA: Portland, Oregon. p. 11.

17. Avanzini, G., De Matteis, G., *Assessment of Helicopter Model Fidelity Through Inverse Simulation*, in *AIAA Atmospheric Flight Mechanics Conference*2011, AIAA: Portland, Oregon. p. 14.

18. AirforceWorld. *AH-1 SuperCobra*. [cited 2013 January 2013]; Available from: airforceworld.com.

19. Flight Systems Inc., *Helicopter Effectiveness in Air-to-air Combat*.

20. Kim, H.-S., *Conceptual Design Optimization for Military Helicopter Maneuverability and Agility*, in *Aerospace Engineering*1997, Georgia Institute of Technology.

21. Celi, R., *Optimization-Based Inverse Simulation of a Helicopter Slalom Maneuver.* Journal of Guidance, Control, and Dynamics, 2000. **23**(2): p. 289-297.

22. Chipperfield, A., *More Integrated Gas Turbine Engine Controller Design*, in *Genetic Algorithms in Engineering Systems: Innovations and Applications*1997, IEE. p. 357-363.

23. Chipperfield, A., *Systems Integration Using Evolutionary Algorithms*, in *International Conference on Control*1996, IEE. p. 705-710.

24. Gao, C., Hess, R., *Inverse Simulation of Large-Amplitude Aircraft Manoeuvres.* Journal of Guidance, Control, and Dynamics, 1993. **16**: p. 733-737.

25. Hess, R., Gao, C., *A Generalized Algorithm for Inverse Simulation Applied to Helicopter Maneuvering Flight.* American Helicopter Society, 1993: p. 13.

26. Hess, R., Gao, C., Wang, H., *A Generalized Technique for Inverse Simulation Applied to Aircraft Flight Control*, in *29th Aerospace Sciences Meeting*1991, AIAA: Reno, Nevada. p. 12.

27. Hess, R., Gao, C., Wang, H., *Generalized Technique for Inverse Simulation Applied to Aircraft Maneuvers.* Journal of Guidance, 1990. **14**(5): p. 920- 926.

28. Holloway, R., *Aircraft Performance Benefits from Modern Control Systems Technology*. Journal of Aircraft, 1970. **7**(6): p. 550-553.

29. Celi, R., *Recent Applications of Design Optimization to Rotorcraft - A Survey*. Journal of Aircraft, 1999. **36**(1): p. 176-189.

30. DeLaurentis, D., Mavris, D., *Uncertainty Modeling and Management in Multidisciplinary Analysis and Synthesis.* AIAA, 2000: p. 12.

31. Scharl, J., Mavris, D., Burdun, I., *Use of Flight Simulation in Early Design - Formulation and Application of the Virtual Testing and Evaluation Methodology*, in *2000 World Aviation Conference*Oct. 10-12, 2000 San Diego, CA.

32. Phillips, W., *Mechanics of Flight*. 2004, Hoboken, New Jersey: Wiley.

33. Cao, Y., *A New Inverse Solution Technique for Studying Helicopter Maneuvering Flight.* Journal of the American Helicopter Society, 2000: p. 43-53.

34. Wood, T., Ford, D., Brigman, G., *Maneuver Evaluation Program*, 1974.

35. Wood, T., Waak, T., *Improved Maneuver Criteria in Evaluation Program.* 1979. **AD-A080408**.

36. Cao, Y., Zhang, G., Su, Y., *Mathematical Modeling of Helicopter Aerobatic Maneuvers.* Aircraft Engineering and Aerospace Technology, 2004. **76**(2): p. 170-178.

37. Bottasso, C., *Rotorcraft Trajectory Optimization with Realizability Considerations.* Journal of Aerospace Engineering, 2004.

38. Frazzoli, E., Dahleh, M., Feron, E., *Robust Hybrid Control for Autonomous Vehicle Motion Planning*, 1999.

39. Tomlin, C., Lygeros, J., Sastry, S. *Aerodynamic Envelope Protection Using Hybrid Control*. in *Proc. American Control Conference*. 1998.

40. Frazzoli, E., Dahleh, M., Feron, E., *Maneuver-Based Motion Planning for Nonlinear Systems with Symmetries.* IEEE Transactions on Robotics, 2005. **21**(6): p. 15.

41. Celi, R., *Simulation and Analysis of ADS-33 Quickness Maneuvers for an Articulated Rotor Helicopter*, in *61st Annual Forum*2005, American Helicopter Society: Grapvine, TX. p. 12.

42. Johnson, W., *Helicopter Theory*. 1980, New York: Dover Publications, Inc. 1089.

43. Leishman. *Freewake Aero Image*. Available from: http://terpconnect.umd.edu/~leishman/Aero/Freewake/images/Isometrics.gif.

44. Leishman, G., *Principles of Helicopter Aerodynamics - 2nd Edition*. 2005: Cambridge University Press.

45. Frazzoli, E., Dahleh, M., Feron, E., *A Hybrid Control Architecture for Aggressive Maneuvering of Autonomous Helicopters*, in *38th Conference on Decision and Control*1999, IEEE: Phoenix, Arizona. p. 6.

46. Avanzini, G., De Matteis, G., *Analysis of Aircraft Agility on Maximum Performance Maneuvers.* Journal of Aircraft, 1998. **35**(4): p. 529-535.

47. Innocenti, M., Jauty, R., Beck, J., *Airframe Agility: Flight Mechanics.* AGARD, 1994. **AR-314**: p. 18-35.

48. Murray-Smith, D.J., *The Inverse Simulation Approach: A Focused Review of Methods and Applications.* Mathematics and Computers in Simulation, 2000. **53**: p. 239-247.

49. Prouty, r., *Helicopter Performance, Stability, and Control*. 1990, Malabar, Florida: Krieger Publishing Company, Inc.

50. Anderson, D., *Modification of a Generalized Inverse Simulation Technique for Rotorcraft Flight.* Journal of Aerospace Engineering, 2003. **217** (Part G): p. 61-73.

51. Tomlinson, B., Padfield, G. , *Piloted Simulation Studies of Helicopter Agility.* Vertica, 1980. **4**(2-4).

52. Padfield, G., *Helicopter Flight Dynamics*. 1996: Blackwell Science, Ltd.

53. Shi-Cun, W., Zhi, X., *A Simplified Method for Predicting Rotor Blade Airloads,* in *7th European Rotorcraft and Powered Lift Forum*1981: Garmishch-Partenkirchen, Federal Republic of Germany.

54. Bivens, C., *Directional Handling Qualities REquirements for Nap of the Earth (NOE) Tasks*, in *41st Annual Forum of the AHS*1985, American Helicopter Society: Fort Worth, TX.

55. Dooley, L., *Handling Qualities Considerations for NOE Flight*, in *32nd Annual Forum of the AHS*1976, American Helicopter Society.

56. Cao, Y., Su, Y., *Helicopter Manoeuvre Gaming Simulation and Mathematical Inverse Solution.* Journal of Aerospace Engineering, 2001. **216**(Part G): p. 41-49.

57. Celi, R., *Calculation of ADS-33 Quickness Parameters with Application to Design Optimization*, in *29th European Rotorcraft Forum*2003: Friedrichshafen, Germany.

58. Thunnissen, D., *Propagating and Mitigating Uncertainty in the Design of Complex Multidisciplinary Systems*, 2005, California Institute of Technology.

59. Oberkampf, W., Helton, J., Sentz, K., *Mathematic Representation of Uncertainty.* AIAA, 2001.

60. Otto, K., Antonsson, E., *Design Parameter Selection in the Presence of Noise.* Research in Engineering Design, 1994. **6**(4): p. 234-246.

61. Bedford, T., Cooke, R., *Different Types of Uncertainty*. Probabilistic Risk Analysis: Foundations and Methods. 2001, Cambridge, UK: Cambridge University Press. 17-38.

62. Hacking, I., *The Emergence of Probability: A Philosophical Study of Early Ideas About Probability, Induction and Statistical Inference*. 1984, Cambridge, UK: Cambridge University Press.

63. Lin, Y., Stadtherr, M.A., *Deterministic Global Optimization of Nonlinear Dynamic Systems.* ALChE, 2007. **53**(4): p. 866-875.

64. Adjiman, C.S., Androulakis, I.P., Floudas, C.A., Neumaier, A., *A Global Optimization Method, ABB, for General Twice-Differentiable NLPs-I. Theoretical Advances.* Computers and Chemical Engineering, 1998. **22**: p. 1137-1158.

65. Adjiman, C.S., Androulakis, I.P., Floudas, C.A., Neumaier, A., *A Global Optimization Method, ABB, for General Twice-Differentiable NLPs - II. Implementation and Computaitonal Results.* Computers and Chemical Engineering, 1998. **22**: p. 1159-1179.

66. Esposito, W.R., Floudas, C.A. , *Deterministic Global Optimization in Nonlinear Optimal Control Problems.* Journal of Global Optimization, 2000. **17**: p. 97-126.

67. Esposito, W.R., Floudas, C.A., *Global Optimization for the Parameter Estimation of Differential-Algebraic Systems.* Ind Eng Chem Res, 2000. **39**: p. 1291-1310.

68. Kelley, C.T., *Iterative Methods for Linear and Nonlinear Equations*. 1995, Philadelphia: SIAM.

69. Press, W., Flannery, B., Teukolsky, S., Vetterling, W., *Numerical Recipes in C: The Art of Scientific Computing*. 2nd Edition ed. October 30, 1992: Cambridge University Press.

70. Chachuat, B., Latifi, M.A., *A New Approach in Deterministic Global Optimisation of Problems with Ordinary Differential Equations.* Frontiers in Global Optimization, ed. C.A. In: Floudas, Pardalos, P.M. . 2004, Dordrecht, The Netherlands: Kluwer Academic Publishers.

71. Papamichail, I., Adjiman, C.S., *A Rigorous Global Optimization Algorithm for Problems with Ordinary Differential Equations.* Journal of Global Optimization, 2002. **24**: p. 1-33.

72. Papamichail, I., Adjiman, C.S., *Global Optimization of Dynamic Systems.* Computers and Chemical Engineering, 2004. **28**: p. 403-415.

73. Singer, A.B., *Global Dynamic Optimization*, 2004, Massachusetts Institute of Technology: Cambridge, MA.

74. Byrne, R.P., Bogle, I.D.L., *Global Optimisation of Constrained Non-Convex Programs using Reformulation and Interval Analysis.* Computers and Chemical Engineering, 1999. **23**: p. 1341-1350.

75. Floudas, C.A., Akrotirianakis, I.G., Caratzoulas, Meyer, C.A., Kallrath, J., *Global Optimization in the 21st Century: Advances and Challenges.* Computers and Chemical Engineering, 2005. **29**: p. 1185-1202.

76. Floudas, C.A., Gounaris, C.E., *A Review of Recent Advances in Global Optimization.* Journal of Global Optimization, 2008.

77. Grossmann, I.E., Biegler, L.T., *Part II. Future Perspective on Optimization.* Computers and Chemical Engineering, 2004. **28**: p. 1193-1218.

78. Smith, E.M.B., Pantelides, C.C., *Global Optimization of Nonconvex MINLPs.* Computers and Chemical Engineering, 1997. **21**: p. 791-796.

79. Moore, R.E., *Automatic Error Analysis in Digital Computation.* Technical Report LMSC4-22-66-1, 1959. **Lockheed Missiles and Space Co**.

80. Moore, R.E., *Interval Arithmetic and Automatic Error Analysis in Digitial Computing*, in *Department of Mathematics*1962, Stanford University: Stanford, CA.

81. Good, D., London, R., *Computer Interval Arithmetic: Definition and Proof of Correct Implementation.* Journal of Association for Computing Machinery, 1970. **17**(4): p. 603-612.

82. Van Kampen, E., Chu, Q.P., Mulder, J.A., *Nonlinear Aircraft Trim using Interval Analysis*, in *Guidance, Navigation, and Control Conference and Exhibit*2007, AIAA: Hilton Head, South Carolina. p. 15.

83. Ichida, K., Fujii, Y., *An Interval Arithmetic Method for Global Optimization.* Computing, 1979. **23**: p. 85-97.

84. Kolev, L., *An Interval Method for Global Nonlinear Analysis.* IEEE Transactions on Circuits and Systems I: Fundamental Theory and Applications, 2000. **47**(5): p. 675-683.

85. Manetsch, T.J., *Toward Efficient Global Optimization in Large Dynamic Systems-The Adaptive Complex Method.* IEEE Transactions on Systems, Man, and Cybernetics, 1990. **20**(1): p. 257-261.

86. Zhu, X., Wei, X., Zhou, J., Zhang, Y., *Algorithm of Finding All Real Roots Based on Solution Space Compression*, in *International Conference on Artificial Intelligence and Computational Intelligence*2009, IEEE Computer Society.

87. Hansen, E., Walster, G.W., *Global Optimization Using Interval Methods*. 2nd ed. 2003: CRC Press.

88. Pedrycz, W., *Why Triangular Membership Functions?* Fuzzy Sets and Systems, 1994. **64**: p. 21-30.

89. Lodwick, W., Jamison, K., *Special Issue: Interfaces Between Fuzzy Set Theory and Interval Analysis.* Fuzzy Sets and Systems, 2003. **135**: p. 1-3.

90. Giachetti, R., Young, R., *A Parametric Representation of Fuzzy Numbers and Their Arithmetic Operators.* Fuzzy Sets and Systems, 1997. **91**: p. 185-202.

91. Dubois, D., Prade, H., *Fuzzy Numbers: An Overview*. Readings in Fuzzy Sets for Intelligent Systems. 1993, San Mateo, CA: Kaufmann Publishers.

92. Giachetti, R., Young, R. , *Analysis of the Error in the Standard Approximation Used for Multiplication of Triangular and Trapezoidal Fuzzy Numbers and the Development of a New Approximation.* Fuzzy Sets and Systems, 1997(91): p. 1-13.

93. Kaufmann, A., Gupta, M., *Fuzzy Mathematical Models in Engineering and Management Science*. 1988, Amsterdam: North Holland.

94. Moore, R., Lodwick, W., *Interval Analysis and Fuzzy Set Theory*. Fuzzy Sets and Systems, 2003. **135**: p. 5-9.

95. Albrecht, R., *Topological Interpretation of Fuzzy Sets and Intervals.* Fuzzy Sets and Systems, 2003. **135**: p. 11-20.

96. Stuckman, B.E., Easom, E.E., *A Comparison of Bayesian/Sampling Global Optimization Techniques.* IEEE Transactions on Systems, Man, and Cybernetics, 1992. **22**(5): p. 1024-1032.

97. Kuhne, C., Wiggs, G., Beeson, D. *Using Monte Carlo Simulation for Probabilistic Design*. in *2005 Crystal Ball User Conference*. 2005.

98. Mockus, J.B., *Bayesian Approach to Global Optimization*. 1989, New York: Kluwer Academic.

99. Metropolis, N., Ulam, S., *The Monte Carlo Method.* Journal of the American Statistical Association, 1949. **44**(247): p. 335-341.

100. Oberkampf, W., *A New Methodology for the Estimation of Total Uncertainty in Computational Simulation.* AIAA, 1999.

101. Doucet, A., Tadic, V.B. *On-Line Optimization of Sequential Monte Carlo Methods using Stochastic Approximation*. in *American Control Conference*. 2002. Anchorage, AK: ACC.

102. Li, Z., Scheraga, H.A., *Monte Carlo-Minimization Approach to the Multiple-minima Problem in Protein Folding.* Proc. Natl. Acad. Sci. USA, 1987. **84**: p. 6611-6615.

103. Tischler, M., *Conduit: A New Multidisciplinary Integration Environment for Flight Control Development*, in *Guidance, Navigation, and Control Conference*1997, AIAA: New Orleans, Louisiana.

104. Chudoba, B., Smith, H., *A Generic Stability and Control Methodology or Novel Aircraft Conceptual Design*, in *Atmospheric Flight Mechanics Conference and Exhibit*2003, AIAA: Austin, TX. p. 11.

105. Cotting, M., Cox, T., *A Generic Guidance and Control Structure for Six-Degree-of-Freedom Conceptual Aircraft Design*, in *NASA Paper*2005. p. 26.

106. Coleman, G., Chudoba, B., *A Generic Stability and Control Tool for Conceptual Design: Prototype System Overview*, in *Aerospace Sciences Meeting and Exhibit*2007, AIAA: Reno, Nevada.

107. Rizzi, A., *Modeling & Simulating Aircraft Stability & Control – SimSAC Project*, August 2010, AIAA Atmospheric Flight Mechanics Conference: Toronto, Ontario,.

108. Beaverstock, C., Richardson, T., Lowenberg, M., Isikveren, A. , *Methods for Conceptual Flight Control System Design*, in *47th AIAA Aerospace Sciences Meeting including The New Horizons Forum and Aerospace Exposition*Jan. 5-8, 2009 Orlando, Florida.

109. Rugh, W.J., Shamma, J.S., *Research on Gain Scheduling.* Automatica, 2000. **36**: p. 1401-1425.

110. Shamma, J.S., Athans, M., *Analysis of Gain Scheduled Control for Nonlinear Plants.* IEEE Transactions on Automatic Control, 1990. **35**(8): p. 898-907.

111. Shamma, J.S., Athans, M., *Gain Scheduling: Potential Hazards and Possible Remedies.* IEEE Control Systems, 1992. **12**(3): p. 101-107.

112. Shamma, J.S., Cloutier, J.R., *Gain-Scheduled Missile Autopilot Design Using Linear Parameter Varying Transformations.* Journal of Guidance, Control, and Dynamics, 1993. **16**(2): p. 256-263.

113. Shamma, J.S., Athans, M., *Guaranteed Properties of Gain Scheduled Control for Linear Parameter-Varying Plants.* Automatica, 1991. **27**(3): p. 559-564.

114. Ananthkrishnan, N., Sinha, N.K., *Level Flight Trim and Stability Analysis Using Extended Bifurcation and Continuation Procedure.* Journal of Guidance, Control, and Dynamics, 2001. **24**(6): p. 1225-1228.

115. Paranjape, A., Sinha, N., Ananthkrishnan, N., *Use of Bifurcation and Continuation Methods for Aircraft Trim and Stability Analysis - A State-of-the-Art*, in *45th AIAA Aerospace Sciences Meeting and Exhibit* Jan. 8-11, 2007 Reno, Nevada.

116. Avanzini, G., De Matteis, G., *Analysis of Helicopter Rotor Nonlinear Dynamics by Numerical Continuation Method*, in *Atmospheric Flight Mechanics Conference and Exhibit*2007, AIAA: Hilton Head, South Carolina. p. 12.

117. Iqbal, S., *Bifurcation analysis methods used in a multi-disciplinary optimisation framework*, in *AIAA Atmospheric Flight Mechanics Conference and Exhibit*Aug. 6-9, 2001: Montreal, Canada.

118. Baghdadi, N., Lowenberg, M.H., *Use of Bifurcation Methods in the Identification and Control of Flexible Aircraft Dynamics*, in *52st Structures, Structural Dynamics, and Materials Conference*2010, AIAA: Orlando, Florida. p. 19.

119. Crawford, J.D., *Introduction to Bifurcation Theory.* Reviews of Modern Physics, 1991. **63**(4): p. 991-1037.

120. Strogatz, S.H., *Nonlinear Dynamics and Chaos*. With Applications to Physics, Biology, Chemistry, and Engineering. 1994, New York: Addison-Wesley Publishing Company.

121. Ananthkrishnan, N., Gupta, N.K., Sinha, N,K., *Computational Bifurcation Analysis of Multiparameter Dynamical Systems.* Journal of Guidance, Control, and Dynamics, 2009. **32(**5): p. 1651-1653.

122. Pashilkar, A.A., Pradeep, S., *Computation of Flight Mechanics Parameters Using Continuation Techniques.* Journal of Guidance, Control, and Dynamics, 2001. **24(**2): p. 324-329.

123. Bedford, R.G.a.L., M.H., *Bifurcation Analysis of Rotorcraft Dynamics with an Underslung Load*, in *AIAA Atmospheric Flight Mechanics Conference and Exhibit*2004, AIAA: Providence, Rhode Island. p. 25.

124. Bedford, R.G., Lowenberg, M.H., *Flight Dynamics Analysis of Periodically Forced Rotorcraft Model*, in *Atmospheric Flight Mechanics Conference and Exhibit*2006, AIAA: Keystone, Colorado. p. 19.

125. Paranjape, A., Sinha, N., Ananthkrishnan, N., *Airplane Level Turn Performance, Including Stability Constraints, using Extended Bifurcation and Continuation Method*, in *Atmospheric Flight Mechanics Conference and Exhibit*2005, AIAA: San Francisco, CA.

126. Poli, C., Cromack, D., *Dynamics of Slung Bodies Using a Single-Point Suspension System.* Journal of Aircraft, 1973: p. 80-86.

127. Avanzini, G., De Matteis, G., *Bifurcation Analysis of a Highly Augmented Aircraft Model.* Journal of Guidance, Control, and Dynamics, 1997. **20**(4): p. 754-759.

128. Lowenberg, M.H., Richardson, T.S., *The Continuation Design Framework for Nonlinear Aircraft Control*, in *Guidance, Navigation, and Control Conference and Exhibit*2001, AIAA: Montreal, Canada. p. 15.

129. Sibilski, K., *Prediction of Helicopter Critical Flight Regimen by Continuation and Bifurcation Methods*, in *Atmospheric Flight Mechanics Conference and Exhibit*2006, AIAA: Keystone, Colorado. p. 27.

130. Goman, M., Zagainov, G., Khramtsovsky, A., *Application of Bifurcation Methods to Nonlinear Flight Dynamics Problems.* Prog. Aerospace Sci., 1997. **33**: p. 539-586.

131. Guicheteau, P., *Bifurcation Theory: A Tool for Nonlinear Flight Dynamics.* Philosophical Transactions of the Royal Society, 1998. **356**: p. 2181-2201.

132. Milam, M., Mushambi, K., Murray, R. *A Computational Approach to Real-Time Trajectory Generation for Constrained Mechanical Systems*. in *34th IEEE Conference on Decision and Control*. 2000. New York: IEEE.

133. Faiz, N., Agrawal, S., Murray, R., *Trajectory Plannning of Differentially Flat Systems with Dynamics and Inequalities.* Journal of Guidance, Control, and Dynamics, 2001. **24**(2): p. 219-227.

134. Thomson, D., Bradley, R., *The Principles and Practical Application of Helicopter Inverse Simulation.* Simulation Practice and Theory, 1998. **6**: p. 47-70.

135. Nannoni, F., Stabellini, A. *Simplified Inverse Simulation for Preliminary Design Purposes*. in *15th European Rotorcraft Forum*. 1989. Amsterdam, The Netherlands.

136. Whalley, M., *Development and Evaluation of an Inverse Solution Technique for Studying Helicopter Maneuverabilty and Agility*, in *NASA Technical Memorandum 102889*, U.T.R. 90-A-006, Editor 1991, NASA: Moffett Field, CA.

137. De Matteis, G., De Socio, L.M., Lenonessa, A., *Solution of Aircraft Inverse Porblems by Local Optimization.* Journal of Guidance, Control, and Dynamics, 1995. **18**(3): p. 567-571.

138. Bottasso, C., Ragazzi, A., *Deferred-Correction Optimal Control with Applications to Inverse Problems in Flight Dynamics.* Journal of Guidance, Control, and Dynamics, 2001. **24**(1): p. 101-108.

139. Rutherford, S., *Simulation Techniques for the Study of the Manoeuvring of Advanced Rotorcraft Configurations*, in *Aeronautical Engineering*1997, University of Glasgow.

140. Doyle, S., Thomson, D., *Modification of a Helicopter Inverse Simulation to Include an Enhanced Rotor Model.* Journal of Aircraft, 2000. **37**(3).

141. Su, Y., Cao, Y., *A Nonlinear Inverse Simulation Technique Applied to Coaxial Rotor Helicopter Maneuvers.* Aircraft Engineering and Aerospace Technology, 2002. **74**(6): p. 525-533.

142. Sentoh, E., Bryson, A., *Inverse and Optimal Control for Desired Outputs.* Journal of Guidance, Control, and Dynamics, 1992. **15**(3): p. 687-691.

143. Kato, O., Sugiura, I., *An Interpretation of Airplane General Motion and Control as Inverse Problem.* Journal of Guidance, 1986. **9**(2): p. 198-204.

144. Thomson, D., Bradley, R., *Inverse Simulation as a Tool for Flight Dynamics Research: Principles and Applications.* Progress in Aerospace Sciences, 2006. **42**: p. 174-210.

145. Cerbe, T., Reichert, G., *Simulation Models for Optimization of Helicopter Takeoff and Landing*, in *13th European Rotorcraft Forum*1987, European Rotorcraft Forum: Arles, France.

146. Thomson, D., Bradley, R., *An Investigation of the Stability of Flight Path Constrained Helicopter Maneuver by Inverse Simulation*, in *13th European Rotorcraft Forum*1987: Arles, France, .

147. Thomson, D., Bradley, R., *Prediction of the Dynamic Characteristics of Helicopters in Constrained Flight.* Aeronaut, 1990.

148. Thomson, D., Bradley, R. *Modelling and Classification of Helicopter Combat Manoeuvres*. in *ICAS Congress*. 1990. Stockholm, Sweden: ICAS.

149. Glad, T., Ljung, I., *Control Theory - Multivariable and Nonlinear Methods*. 2000, London: Taylor and Francis.

150. Murray-Smith, D., *Feedback Methods for Inverse Simulation of Dynamic Models for Engineering Systems Applications.* Mathematical and Computer Modelling of Dynamical Systems, 2011. **17**(5): p. 515-541.

151. Borri, M., Bottasso, C., Montelaghi, F., *Numerical Approach to Inverse Flight Dynamics.* Journal of Guidance, Control, and Dynamics, 1997. **20**(4).

152. Czechowski, P., *Testing Algorithms for Inverse Simulation*, in *International Conference on Control Applications*2006, IEEE: Munich, Germany. p. 2607-2612.

153. Slotine, J., Li, W., *Applied Nonlinear Control*. 1991, Upper Saddle River, NJ: Prentice-Hall.

154. Bajodah, A., Hameduddin, I., *Aircraft Maneuvering Control Using Generalized Dynamic Inversion and Semidefinite Lyapunov Functions*, in *IEEE International Conference on Control Applications: Part of IEEE Multi-Conference on Systems and Control*2010, IEEE: Yokohama, Japan. p. 1825-1831.

155. Avanzini, G., De Matteis, G., *Two-Timescale Inverse Simluation of a Helicopter Model.* Journal of Guidance, Control, and Dynamics, 2001. **24**(2): p. 330-339.

156. Betts, J., *Survey of Numerical Methods for Trajectory Optimization.* Journal of Guidance, Control, and Dynamics, 1998. **21**(2): p. 193-207.

157. MathWorks. *Matlab: The Language of Technical Computing*. 1994-2011 [cited 2011 February 20]; Available from: http://www.mathworks.com/products/matlab/.

158. Montgomery, D.C., *Design and Analysis of Experiements*. 5th Edition. 2000: Wiley. 672.

159. Hodges, D., Bless, R., *Weak Hamiltonian Finite Element Method for Optimal Control Problems.* Journal of Guidance, Control, and Dynamics, 1991. **14**(1): p. 148-156.

160. Prouty, R., *Helicopter Aerodynamics*. 1985, Peoria, IL: PJS Publications Inc.

161. Prouty, R., *More Helicopter Aerodynamics*. 1988, Peoria, IL: PJS Publications, Inc.

162. De Laurentis, D., Mavris, Dimitri N., , *Generating Dynamic Models Including Uncertainty for Use in Aircraft Conceptual Design*, in *AIAA Atmospheric Flight Mechanics Conference*Aug. 11-13, 1997: New Orleans, LA.

163. Etkin, B., *Dynamics of Atmospheric Flight*. 2005, Mineola: Dover Publications, Inc. 580.

164. Hennis, R., McCormick, S., *Computer Model for Predicting Dynamic Behavior of a Helicopter for Application to Weapons Delivery and Subsequent Safe Excape*, in *NSWC TR85-285*1985: Naval Surface Weapons Center.

165. Gray, G.J., *An Investigation of Open-Loop and Inverse Simulation as Nonlinear Model Validation Tools for Helicopter Flight Mechanics.* Mathematical and Computer Modelling of Dynamical Systems: Methods, Tools and Applications in Engineering and Related Sciences, 2007. **4**(1): p. 32-57.

166. Heffley, R., Mnich, M., *Minimum Complexity Helicopter Simulation Math Model*, 1988, NASA.

167. Rutherford, S., Thomson, D., *Helicopter Inverse Simulation Incorporating an Individual Blade Rotor Model.* Journal of Aircraft, 1997. **34**(5): p. 8.

168. Bradley, R., Padfield, G., Murray-Smith, J., Thomson, D., *Validation of Helicopter Mathematical Models.* Transactions of the Institute of Measurement and Control, 1990. **12**(4).

169. Lee, C., Tsai, C., *Nonlinear Adaptive Aggressive Control using Recurrent Neural Networks for a Small Scale Helicopter.* Mechatronics, 2010. **20**(4): p. 474-484.

170. Shim, D., Koo, T., Hofmann, F., Sastry, S, *A Comprehensive Study of Control Design for an Autonomous Helicopter*, in *37th IEEE Conference of Decision and Control*1998, IEEE.

171. Koo, T., Sastry, S., *Output Tracking Control Design of a Helicopter Model Based on Approximate Linearization*, in *37th IEEE Conference on Decision and Control*1998.

172. Van Nieuwstadt, M., Murray, R., *Real-Time Trajectory Generation for Differentially Flat Systems.* International Journal of Robust and Nonlinear Control, 1998. **8**(11): p. 995-1020.

173. Piedmonte, M., Feron, E., *Aggressive Maneuvering of Autonomous Aerial Vehicles: A Human-Centered Approach.* 2005: p. 6.

174. Cao, Y., Gao, Z. *Equations Governing the Helicopter in Maneuvering Flight and the Nonlinear Inverse Solution*. in *China-Japan Symposium on Aerodynamics and Aircraft Design*. 1990.

175. Cao, Y., Gao, Z., *Studies of Helicopter Maneuvering Flight*, in *Aeronautics and Astronautics*1990, Nanjing University.

176. Cox, S., Haftka, R., Baker, C., Grossman, B., Mason, W., Watson, L., *A Comparison of Global Optimization Methods for the Design of a High-Speed Civil Transport.* Journal of Global Optimization, 2001. **21**: p. 415-433.

177. Vanderplaats, G., *Numerical Optimization Techniques for Engineering Design 4th Edition*. 2005, Colorado Springs, CO: Vanderplaats Research and Development, Inc.

178. Femia, N., *A Robust and Fast Convergent Interval Analysis Method for the Calculation of Internally Controlled Switching Instants.* IEEE Transactions on Circuits and Systems I: Fundamental Theory and Applications, 1996. **43**(3): p. 191-199.

179. Haim, D., Giunta, A.A., Holzwarth, M.M., Mason, W.H., Watson, L.T., Haftka, R.T., *Comparison of Optimization Software Packages for an Aircraft Multidisciplinary Design Optimization Problem.* Design Optimization, 1999. **1**: p. 9-23.

180. Lu, L., Murray-Smith, D., Thomson, D., *Issues of Numerical Accuracy and Stability in Inverse Simulation.* Simulation Modelling Practice and Theory, 2008. **16**: p. 1350-1364.

181. Lu, L., Murray-Smith, D., *Sensitivity-Analysis Method for Inverse Simulation Application.* Journal of Guidance, Control, and Dynamics, 2007. **30**(1): p. 8.

182. Lee, S., Kim, Y., *Time-Domain Finite Element Method for Inverse Problem of Aircraft Maneuvers.* Journal of Guidance, Control, and Dynamics, 1997. **20**(1): p. 7.

183. Drury, R., Tsourdos, A., Cooke, A., *Real-Time Trajectory Generation: Improving the Optimality and Speed of an Inverse Dynamics Method*, in *IEEE Aerospace Conference*2010: Big Sky.

184. Yakimenko, O., *Computing Short-Time Aircraft Maneuvers Using Direct Methods*, in *Guidance, Navigation, and Control Conference and Exhibit*2008, AIAA: Honolulu, Hawaii. p. 23.

185. Yakimenko, O., *Direct Method for Rapid Prototyping of Near-Optimal Aircraft Trajectories.* Journal of Guidance, Control, and Dynamics, 2000. **23**(5): p. 865-875.

186. De Marco, A., Duke, E., and Berndt, J. *A General Solution to the Aircraft Trim Problem*. in *AIAA Modeling and Simulation Technologies Conference and Exhibit*. 2007. Hilton Head, South Carolina: AIAA.

187. Kato, O., *Attitude Projection Method for Analyzing Large-Amplitude Airplane Maneuvers.* Journal of Guidance, 1990. **13**(1): p. 22-29.

188. Elgersma, M., Morton, B., *Nonlinear Six-Degree-of-Freedom Aircraft Trim.* Journal of Guidance, COntrol, and Dynamics, 2000. **23**(2): p. 305-311.

189. Nikas, I.A., Grapsa, T.N., *Bounding the Zeros of an Interval Equation.* Applied Mathematics and Computation, 2009. **213**: p. 466-478.

190. Isakov, V., *Inverse Problems in Partial Differential Equations*. 1998, New York: Springer.

191. Hwang, C., *Multiple Objective Decision Making - Methods and Applications: A State of the Art Survey*, 1979: Springer-Verlag, Germany.

192. Cheng, F., *Multiobjective Optimization of Structures with and Without Control.* Journal of Guidance, Control, and Dynamics, 1996. **19**(2): p. 392-397.

193. Garwood, K.R. *The Emerging Requirements for Dual and Variable Cycle Engines*. in *10th International Symposium on Air Breathing Engines*. 1992.

194. Shutler, A.G. *Definition, Design and Implementation of Control Laws for Variable Cycle Gas Turbine Aircraft Engines*. in *The Design and Control of the Next Generation of Civil and Military Engines: Do Variable Cycle Engines Have a Role?* 1995. RAe.

195. Dadd, G.J. *Multivariable Control of Military Engines*. in *Advanced Aero-Engine Concepts and Controls*. 1995. AGARD.

196. Serr, C., et al., *Rotorcraft Efficient and Safe Procedures for Critical Trajectories (RESPECT).* Air and Space Europe, 2001. **3**(3): p. 266-270.

197. Brannen, K. *U.S. Army Eyes Joint Multirole Helo*. 2010 [cited 2011 June 20]; Available from: http://www.defensenews.com/story.php?i=4713228.

198. Anon, *Aeronautical Design Standard.* Handling Qualities Requirements for Military Rotorcraft, 1994. **ADS-33D**.

199. Thomson, D., Bradley, R., *Mathematical Definition of Helicopter Maneuvers.* American Helicopter Society, 1997: p. 3.

200. Chudoba, B., Cook, M., *Identification of Design-Constraining Flight Conditions for Conceptual Sizing of Aircraft Control Effectors*, in *AIAA Atmospheric Flight Mechanics Conference and Exhibit*Aug. 11-14, 2003: Austin, Texas.

201. Chudoba, B., Cook, M., *Trim Equations of Motion for Aircraft Design: Steady State Straight-Line Flight*, in *Atmospheric Flight Mechanics Conference and Exhibit*2003, AIAA: Austin, Texas. p. 11.

202. Chudoba, B., Cook, M., *Trim Equations of Motion for Aircraft Design: Turning Flight, Pull-Up, and Push-Over*, in *Atmospheric Flight Mechanics Conference and Exhibit*2003, AIAA: Austin, Texas

203. Chudoba, B., Cook, M., *Trim Equations of Motion for Aircraft Design: Rolling Performance and Take-Off Rotation*, in *Atmospheric Flight Mechanics Conference and Exhibit*2003, AIAA: Austin, Texas. p. 11.

204. Chudoba, B., *Stability and Control of Conventional and Unconventional Aircraft configurations: A Generic Approach*. 2001, Germany: Books-on-Demand GmbH. 258.

205. Pandita, R., Chakraborty, A., Seiler, P., Balas, G., *Reachability and Region of Attraction Analysis Applied to GTM Dynamic Flight Envelope Assessment*, in *Guidance, Navigation, and Control Conference*2009, AIAA: Chicago, Illinois. p. 21.

206. Goman, M., Demenkov, M., *Computation of Controllability Regions for Unstable Aircraft Dynamics.* Journal of Guidance, Control, and Dynamics, 2004. **27**(4): p. 647-656.

207. Goman, M., Khramtsovsky, A., Kolesnikov, E., *Evaluation of Aircraft Performance and Maneuverability by Computation of Attainable Equilibrium Sets.* Journal of Guidance, Control, and Dynamics, 2008. **31**(2): p. 329-339.

208. Zagaynov, G.I. *Bifurcation Analysis of Critical Aircraft Flight Regimes*. in *ICAS*. 1984.

209. Frazzoli, E., Dahleh, M., Feron, E., *Real-TIme Motion Planning for Agile Autonomous Vehicles.* Journal of Guidance, Control, and Dynamics, 2002. **25**(1): p. 14.

210. Petersen, F., *A Two-Level Trajectory Decomposition Algorithm Featuring Optimal Intermediate Target Selection.* Journal of Spacecraft and Rockets, 1977. **14**(11): p. 676-682.

211. Rahn, M., and Schoettle, U., *Decomposition Algorithm for Perfromance Optimization of a Launch Vehicle.* Journal of Spacecraft and Rockets, 1996. **33**(2): p. 214-221.

212. Braun, R., Kroo, I., *Development and Application of the Collaborative Optimization Architecture in a Multidisciplinary Design Environment.* Multidisciplinary Design Optimization: State of the Art, 1996. **SIAM**: p. 98-116.

213. Braun, R., Moore, A, and Kroo, I., *Use of the Collaborative Optimization Architecture for Launch Vehicle Design*, in *6th NASA, and ISSMO, Symposium on Multidisciplinary Analysis and Optimization*1996, AIAA: Bellevue, Washington.

214. Braun, R., Moore, A, and Kroo, I., *Collaborative Approach to Launch Vehicle Design.* Journal of Spacecraft and Rockets, 1997. **34**(4): p. 478-486.

215. Frazzoli, E., *Robust Hybrid Control for Autonomous Vehicle Motion Planning*, in *Aeronautics and Astronautics*2001, Massachusetss Institute of Technology: Cambridge, MA.

216. Zhao, Y., Tsiotras, P., *Time-Optimal Parameterization of Gerometric Paths for Fixed-wing Aircraft*, in *Infotech at Aerospace*2010, AIAA: Atlanta, GA. p. 21.

217. Likhachev, M., Ferguson, D., *Planning Long Dynamically Feasible Maneuvers for Autonomous Vehicles.* International Journal of Robotics Research, 2009. **28**(8): p. 933-945.

218. *The Army Aviator's Handbook for Maneuvering Flight and Power Management*, in *USAAVNC*2005. p. 28.

219. *Operational Availability Handbook*, 2003: Navy. p. 93.

220. Bagai, *Aerodynamic Analysis of a Helicopter in Steady Maneuvering Flight Using a Free-Vortex Rotor Wake Model*, in *Technical Specialists' Meeting on Rotorcraft Acoustics and Aerodynamics*1999, AHS: Williamsburg, VA. p. 109-120.

221. Kufeld, R.M., *High Load Conditions Measured on a UH-60A in Maneuvering Flight*, in *51th Annual Forum*1998, AHS: Forth Worth, TX. p. 202-211.

222. Zhao, J., *Dynamic Wake Distortion Model for Helicopter Maneuvering Flight*, in *Aerospace Engineering*2005, Georgia Institute of Technology. p. 156.

223. Hennes, C.C., *Influence of Transient Flight Maneuvers on Rotor Wake Dynamics and Noise Radiation*, in *Specialist's Conference on Aeromechanics*2004, AHS: San Francisco, CA. p. 18.

224. Krothapalli, K.R., *Helicopter Rotor Dynamic Inflow Modeling for Maneuvering Flight.* American Helicopter Society, 2001: p. 129-139.

225. Ribera, M., *Simulation Modeling in Steady Turning Flight with Refined Aerodynamics*, in *31st European Rotorcraft Forum*2005: Florence, Italy.

226. Bottasso, C., *Unsteady Trim for the Simulation of Maneuvering Rotorcraft with Comprehensive Models.* Journal of the American Helicopter Society, .

227. Ribera, M., *Simulation Modeling of Unsteady Maneuvers Using a Time Accurate Free Wake*, in *60th Annual Forum*2004, AHS: Baltimore, MD.

228. Cao, Y., *Modeling the Unsteady Aerodynamic Forces of a Maneuvering Rotor.* Aircraft Engineering and Aerospace Technology, 1999. **71**(5): p. 444-450.

229. Gillula, J.H., *Design of Guaranteed Safe Maneuvers Using Reachable Sets: Autonomous Quadrotor Aerobatics in Theory and Practice*, in *IEEE International Conference on Robotics and Automation*2010, IEEE: Anchorage, Alaska.

230. Dever, C., *Nonlinear Trajectory Generation for Autonomous Vehicles via Parametrized Maneuver Classes.* Journal of Guidance, Control, and Dynamics, 2006. **29**(2): p. 289-302.